ANATOMICAL EVIDENCE FOR VOLUME TRANSMISSION IN THE DORSAL VAGAL COMPLEX OF THE RAT

by

LANCE ANTHONY LADIC

B.Sc., University of British Columbia, 1991

A THESIS SUBMITTED IN PARTIAL FULFILLMENT OF

THE REQUIREMENTS FOR THE DEGREE OF

DOCTOR OF PHILOSOPHY

in

THE FACULTY OF GRADUATE STUDIES

(DEPARTMENT OF PHYSIOLOGY)

UNIVERSITY OF BRITISH COLUMBIA

We accept this thesis as conforming
to the required standard

THE UNIVERSITY OF BRITISH COLUMBIA

In presenting this thesis in partial fulfilment of the requirements for an advanced degree at the University of British Columbia, I agree that the Library shall make it freely available for reference and study. I further agree that permission for extensive copying of this thesis for scholarly purposes may be granted by the head of my department or by his or her representatives. It is understood that copying or publication of this thesis for financial gain shall not be allowed without my written permission.

Department of PHYSIOLOGY

The University of British Columbia
Vancouver, Canada

Date JULY 14, 1997.

ABSTRACT

Injection of either calcitonin gene-related peptide (CGRP) or substance P (SP) into the cerebrospinal fluid or dorsal vagal complex (DVC) of the rat has an effect on gastric function via a vagally-dependent mechanism. These effects are both slow in onset and of prolonged duration, characteristics of non-synaptic events. Although these peptides have been previously detected within the DVC, the anatomical basis for their effects has remained unclear.

In order to examine the possibility that these peptides act via a non-synaptic, volume transmission mechanism within the rat DVC, a combination of retrograde tracing, immunocytochemistry, confocal microscopy and 3-D reconstruction techniques were used to investigate the spatial association between nerve fibres immunoreactive for both CGRP and SP, the substance P receptor (NK-1r) and identified gastric efferent neurons within this region.

In 3-D reconstructions, it was found that the majority of nerve fibres containing either SP- or CGRP-IR surrounded identified gastric efferent neurons without making contact with the membrane of these cells. While most of the CGRP-IR fibres were preferentially associated with the dendrites of retrogradely-labelled neurons around the level of the obex, SP-IR fibres surrounded all surfaces of these cells at all levels of the DVC.

The somatic membrane of a subpopulation of gastric efferent neurons (7%) was labelled with NK-1r-IR. In addition, NK-1r-IR was localized to nerve fibres, mainly in

the rostral DVC. NK-1r-IR covered almost the entire membrane of some DMV neurons, with the highest density of receptors localized to the dendrites.

The distribution of neutral endopeptidase 24.11 (NEP), the principle cleavage enzyme for SP within the CNS, was compared to that of SP-IR, NK-1r-IR and retrogradely-labelled gastric efferent neurons within this region. The enzyme was not associated with vagal neurons or fibres at any level of the DVC, but rather was localized to components of the blood-brain barrier.

In conclusion, the small proportion of neuropeptide-IR nerve fibres that made direct contact with identified neurons, the non-synaptic localization of NK-1r-IR and the absence of NEP-IR associated with identified neurons provide anatomical evidence in support of neural communication via volume transmission within the rat DVC.

TABLE OF CONTENTS

Page

ABSTRACT.....ii

TABLE OF CONTENTS.....iv

LIST OF TABLES.....ix

LIST OF FIGURES.....x

LIST OF ABBREVIATIONS.....xiii

ACKNOWLEDGEMENTS.....xv

1. INTRODUCTION.....1

1.1. Foreword.....1

1.2. Basic Anatomy of the Vagus Nerve.....1

1.3. Functional Anatomy of the Stomach.....4

1.4. Historical Perspective on the Vagal Control of Gastric Function.....9

1.5. Innervation of the Stomach.....11

1.6. Anatomy of Vagal Efferents that Supply the Stomach.....13

1.7. Representation of the Gastrointestinal Tract in the Dorsal Vagal Complex in the Rat Medulla.....16

1.7.1. Nucleus Ambiguus.....16

1.7.2. Dorsal Motor Nucleus of the Vagus.....17

1.7.3. Nucleus of the Solitary Tract.....22

1.7.4. Area Postrema.....25

1.7.5. Connections between the DMV and NTS.....25

1.8. Central Connections of the Vagus Nerve: Regulation of Gastric Function.....26

1.9. Neuropeptides present in the DVC 31

1.10. The Concept of Non-Synaptic Transmission 37

1.11. Metabolism and Inactivation of Neuropeptides 45

1.12. Calcitonin Gene Related Peptide 47

1.13. Substance P and the NK-1 Receptor 52

1.14. Thesis Investigation 57

2. GENERAL METHODS 59

2.1. Animals 59

2.2. Retrograde tracing 59

2.2.1. Fluoro-Gold 61

2.2.2. Cholera Toxin B-subunit 65

2.2.3. Strategies to prevent the leakage and spread of tracers from the injection sites 68

2.3. Perfusion/Fixation 70

2.4. Histology 70

2.5. Immunocytochemistry 71

2.5.1. Basic Principles 71

2.5.2. Immunofluorescence 72

2.5.3. Immunoperoxidase 75

2.5.4. Controls for Immunocytochemistry 75

2.6. Laser Scanning Confocal Microscopy 76

2.7. Segmentation of Image Data 79

2.8. Volume Rendering 81

3. ESTABLISHMENT OF TECHNIQUES FOR THE 3-D RECONSTRUCTION OF NEURONS AND NERVE FIBRES: ASSOCIATION OF CGRP WITH GASTRIC EFFERENT NEURONS IN THE DMV OF THE RAT 83

3.1. Introduction 83

3.2. Methods 84

3.2.1. Preliminary Examination of CGRP with Conventional Epifluorescence Microscopy 84

3.2.2. Laser Scanning Confocal Microscopy 86

3.2.3. Extracting objects of interest from background for 3-D reconstruction 87

3.2.4. Volume Rendering 94

3.2.5. Colour Quantization 96

3.2.6. Measurement of the Distance Between CGRP-IR Fibres and Identified Gastric Efferent Neurons 97

3.2.7. Animations of 3-D Reconstructions 98

3.3. Results 98

3.3.1. Controls 98

3.3.2. Retrograde Labelling 99

3.3.3. Location of CGRP-IR within the DVC using conventional epifluorescence microscopy 102

3.3.4. Association of CGRP-IR fibres with identified gastric efferent neurons observed using confocal microscopy and 3-D reconstruction techniques 104

3.3.5. Distance Measurements Between CGRP-IR Fibres and FG-IR Neurons in the DMV 108

3.4. Discussion 112

4. ASSOCIATION OF SUBSTANCE P AND ITS RECEPTOR WITH GASTRIC EFFERENT NEURONS IN THE DMV OF THE RAT 119

4.1. Introduction 119

4.2. Methods 120

4.2.1. Mapping the Distribution of SP-IR, NK-1r-IR and Identified Gastric Efferent Neurons in the DMV of the Rat 120

4.2.2. Examination of SP, NK-1r and Identified Gastric Efferent Neurons in the DMV using 3-D Reconstruction Techniques 123

4.3. Results 131

4.3.1. Mapping the Distribution of SP-IR, NK-1r-IR and Identified Gastric Efferent Neurons in the DMV of the Rat 131

4.3.1.1. Controls 131

4.3.1.2. Retrograde Labelling 132

4.3.1.3. Location of NK-1r/SP in the DVC 132

4.3.2. Examination of SP, NK-1r and Identified Gastric Efferent Neurons in the DMV using 3-D Reconstruction Techniques 142

4.3.2.1. Association of SP and NK-1r at the single neuron level 149

4.4. Discussion 155

5. COMPARISON OF THE SPATIAL DISTRIBUTION OF ENDOPEPTIDASE-24.11 WITH SUBSTANCE P, SUBSTANCE P RECEPTOR (NK-1r) AND GASTRIC EFFERENT NEURONS IN THE DORSAL VAGAL COMPLEX OF THE RAT 159

5.1. Introduction 159

5.2. Methods 164

5.3. Results 165

5.4. Discussion 171

6. GENERAL DISCUSSION 174

6.1. Differential Distribution of SP and CGRP within the DVC 174

6.2. Evidence for Volume Transmission Within the DVC 178

6.3. Implications of Neutral Endopeptidase 24.11 Localization Within the DVC..... 182

7. SUMMARY AND FUTURE DIRECTIONS 184

7.1. Summary..... 184

7.2. Future Studies..... 185

References..... 191

Appendix I: Absorption and Emission Spectra of Different Fluorophore-Conjugated, Affinity-Purified Antibodies.....212

Appendix II: Spectral Characteristics of the Light Path and Filter Blocks used with the Bio-Rad MRC 600 Confocal Microscope..... 213

LIST OF TABLES

Table 1. Some of the peptides that affect gastric function via a vagally-dependent mechanism. 35

Table 2. Different types of intercellular communication in the central nervous system. 40

Table 3. Summary of the strategies employed for the injection of retrograde tracers. 64

Table 4. Quantification of neurons labelled with FG and NK-1r-IR in the DMV 135

Table 5. Percentage of neurons that were co-labelled with FG and NK-1r-IR in the DMV 136

Table 6. Sites of SP hydrolysis by a variety of enzymatic activities. 163

LIST OF FIGURES

Figure 1. Vagal innervation of visceral structures 3

Figure 2. Diagrammatic representation of the enteric plexuses and muscle layers that comprise the stomach wall. 5

Figure 3. Functional anatomy of the rat stomach. 8

Figure 4. Schematic diagram of subdiaphragmatic vagal branches in the rat. 14

Figure 5. Summary of the motor viscerotopic representation of the alimentary tract in the DMV as projected in the transverse plane 20

Figure 6. Summary of the sensory viscerotopic representation (afferent terminal fields) of the alimentary tract within the NTS as projected in the horizontal plane. 24

Figure 7. Some of the major CNS inputs to the DVC and neuropeptides present in this region. 28

Figure 8. Model of tissue-specific production of CGRP by alternative splicing of the calcitonin gene. 48

Figure 9. Mammalian tachykinins and the NK-1 Receptor. 54

Figure 10. Placement that was used for the injection of retrograde tracer along the greater curvature of the rat stomach.. 60

Figure 11. Basic principles of immunocytochemistry 73

Figure 12. LSCM optics and system configuration. 78

Figure 13. Flowchart summarizing the steps used in the generation of 3-D reconstructions of a double-labelled specimen using image data acquired from a LSCM 90

Figure 14. Screen layout of BOB volume rendering software and companion icol editor 91

Figure 15. Generation of an image mask used to segment an object in a 3-D volume. 93

Figure 16. Characteristic appearance and distribution of retrogradely-labelled neurons in coronal sections through the rat DMV following injection of FG along the greater curcature of the stomach. 101

Figure 17. Epifluorescence micrograph of a section through the medial brainstem illustrating the relationship of CGRP-IR nerve fibres to FG-labelled gastric efferent neurons in the DVC. 104

Figure 18. Maximum intensity projections generated from confocal microscopy data demonstrating a close spatial relationship between CGRP-IR nerve fibres and FG-labelled gastric efferent neurons within the DMV. 107

Figure 19. "Specimen 1": Volume renderings of a neuron in the DMV that was labelled for FG-IR and CGRP-IR that was generated from two 25 μm thick serial sections at positions -350 μm and -325 μm relative to the obex. 109

Figure 20. "Specimen 2": Volume renderings of a neuron in the DMV that was labelled for FG-IR and CGRP-IR that was generated from a single 50 μm section at position +100 μm relative to the DMV. 110

Figure 21. "Specimen 3": Volume renderings of a FG-labelled neuron generated from a single 50 μm thick section at position +650 μm relative to the obex.. 111

Figure 22. Improved segmentation of 3-D objects from brainstem sections using histogram data of control sections. 127

Figure 23. Schematic illustration of FG-labelled neurons compared to NK-1r-IR fibres in coronal sections at various rostrocaudal levels of the DVC..... 137

Figure 24. Schematic illustration of FG-labelled neurons compared to NK-1r-IR fibre distribution in sagittal sections at various rostrocaudal levels of the DVC..... 138

Figure 25. Bar charts representing the distribution of FG-, NK-1r- and FG+NK-1r-IR somata within the DMV. 138

Figure 26. Sections through the DVC illustrating NK-1r-IR distribution using the avidin-biotin-peroxidase technique. 140

Figure 27. Demonstration of a FG+NK-1r co-labelled cell body associated with SP-IR fibres within the DMV as viewed with a conventional epifluorescence microscope at high magnification.. 141

Figure 28. Maximum intensity projections of NK-1r-IR generated from coronal sections at various rostrocaudal levels of the DVC..... 143

Figure 29. Montage of 4 overlapping maximum intensity projection images in a horizontal section through the DMV showing NK-1r-IR and gastric efferent neurons labelled with CT-B in this region, and a 3-D scatter plot of identified somata within this region.. 144

Figure 30. A combined montage view of NK-1r and gastric efferent neurons in a horizontal brainstem section through the DMV generated using Figure 29a,b. 145

Figure 31. Volume renderings of NK-1r-IR on the cell membrane of selected gastric efferent neurons that were extracted from the volumes represented by the montage view in Figure 30.. 146

Figure 32. Volume rendering of a gastric efferent neuron that is co-labelled with NK-1r-IR that was extracted from a horizontal brainstem section through the DMV demonstrating a high density of receptor labelling on dendrites. 147

Figure 33. Volume rendering of a gastric efferent neuron that is co-labelled with NK-1r-IR and surrounded by SP-IR nerve terminals generated from a coronal brainstem section at position +600 μm relative to the obex. 150

Figure 34. Volume rendering of SP-IR and NK-1r-IR in relation to an isolated gastric efferent neuron (labelled with CT-B, blue) generated from a horizontal brainstem section through the DMV 153

Figure 35. Cross sections through the volume shown in Figure 34 demonstrating the relationship between SP-IR nerve fibres and NK-1r-IR on the cell membrane of the gastric efferent neuron. 154

Figure 36. Distribution of NEP-IR, SP-IR and NK-1r-IR at different rostrocaudal levels of the DVC. 167

Figure 37. Comparison of FG-labelled gastric efferent neurons to NEP-IR distribution in the DVC. 168

Figure 38. Demonstration of NEP-IR in the ependymal lining of central canal, endothelial cells of a blood vessel and capillaries within the DVC 169

Figure 39. The location of NEP-IR compared to that of FG-labelled gastric efferent neurons, NEP-IR and SP-IR in a coronal brainstem section at +700 μm relative to the obex. 170

LIST OF ABBREVIATIONS

3-D = three dimensional
5-HT = 5-hydroxytryptamine (serotonin)
AP = area postrema
BN = bombesin
BST = bed nucleus of the stria terminalis
BV = blood vessel
CC = central canal
CCK = cholecystokinin
CGRP = calcitonin gene-related peptide
CNA = central nucleus of the amygdala
CNS = central nervous system
CRF = cortical releasing factor
CSF = cerebrospinal fluid
CT-B = cholera toxin B-subunit
CT-HRP = cholera toxin horseradish peroxidase
DAB = diaminobenzidine
DMV = dorsal motor nucleus of the vagus
DVC = dorsal vagal complex
ECF = extracellular fluid
FG = Fluoro-Gold
FITC = fluorescein isothiocyanate
H_2O_2 = hydrogen peroxide.
HYP = hypoglossal nucleus
IR = immunoreactivity
IV = fourth ventricle
LSCM = laser scanning confocal microscopy
MIP = maximum intensity projection image
mRNA = messenger RNA
NA =nucleus ambiguus
NEP = neutral endopeptidase 24.11
NK-1r = NK-1 receptor
NKA = neurokinin A
NKB = neurokinin B
NPY = neuropeptide Y
nRA = raphe pallidus
nRO = raphe obscurus
NTS = nucleus of the solitary tract
PBS = phosphate buffered saline
PBSHST = phosphate buffered saline plus horse serum and Triton X-100
PBST = phosphate buffered saline plus Triton X-100
PP = pancreatic polypeptide

PVH = paraventricular nucleus of the hypothalamus
RGB = red-green-blue
SP = substance P
SS = somatostatin
TRH = thyrotropin releasing hormone
VT = volume (non-synaptic) transmission
WT = wiring (synaptic) transmission

ACKNOWLEDGEMENTS

I would like to express my appreciation to my supervisor, Dr. A.M.J. Buchan, for her support and encouragement during my stay in her lab. I am grateful to her for giving me the opportunity to pursue a project that allowed me to explore my interests in both Physiology and Computer Science.

I would also like to acknowledge the support I have received from the Dept. of Computer Science at U.B.C., in particular the Imager group (computer graphics laboratory). Specifically, I would like to thank Dr. A. Fournier, Dr. K. Booth and Dr. F. Forsey for allowing me to utilize the Department's facilities during the course of my graduate programme. Without their assistance, the work presented in this dissertation would not have been possible. I would also like to single out Dr. P. Cahoon for his help and encouragement over these past few years.

I wish to thank the technicians and laboratory assistants who provided help with various aspects of my research. I would like to thank J. Sanker and J. Tay for their help with slides and posters. My thanks to S. Shinn, N. Dhatt, and S. Atmadja for their expertise and advice related to histology, immunocytochemistry and handling of laboratory animals. Thanks to M. Weiss and E. Humphrey for their invaluable and top-notch help with confocal microscopy, and for the use of the BioSciences Facility in the Dept. of Zoology.

I am also grateful to my supervisory committee, Dr. T. Pearson, Dr. K. Baimbridge, Dr. E. Moore, Dr. S. Vincent and Dr. A. Fournier for their suggestions and interest at every stage of my research. Thanks also to Dr. R. Pederson for his support as graduate advisor and for organizing many memorable Physiology Graduate Student Retreats.

Finally, and most importantly, I would like to express heartfelt thanks to my mother and father who provided endless support and encouragement during my studies.

1. INTRODUCTION

1.1. Foreword

Since the focus of this dissertation will be to examine the neuropeptide inputs to gastric vagal efferent neurons in the brainstem of the rat and NK-1 receptors, certain topic areas that are pertinent to understanding the significance of the results will be reviewed. First, the basic anatomy of the vagus nerve and the stomach will be considered. Next, highlights of various historical contributions which aided the understanding of vagal control of gastric function will be presented. A description of the general innervation of the stomach and the neuroanatomy of gastric vagal efferent nerves will then be provided. This will be followed by an overview of the central nervous system regulation of vagal function. The final series of topics covered will include a summary of the neuropeptides present in the brainstem nuclei of the vagus nerve, the concept of non-synaptic transmission and neuropeptide inactivation, and finally an introduction to the two neuropeptides, substance P and calcitonin gene-related peptide, which were the subjects of investigation in this dissertation.

1.2. Basic Anatomy of the Vagus Nerve

The vagus nerve (cranial nerve X) is one of the most complex nerves in the body. It is involved in conveying information to and from most of the viscera of the thorax and abdomen as well as many structures of the head and neck. In vertebrates, it is a mixed

nerve in that it consists of both visceral and somatic afferent fibers and visceral and branchial efferents (Finger, 1992).

In the rat and other mammals, the site of origin of the vagus nerve is the medulla oblongata where the preganglionic vagal efferent cell bodies are located (see Mitchell and Warwick, 1955; Lewis et al., 1970 for reviews). From this location, it passes below the cerebellum in the company of the glossopharyngeal (XI) and cranial accessory nerves to the jugular foramen at the base of the skull. After passing through this region, the nerve exhibits ganglia which contain the vagal afferent cell bodies. Unlike the human, which contains two distinct ganglia, the jugular (superior) and the nodose (inferior), the rat has a fused ganglionic mass containing the cell bodies of both vagal (nodose) and glossopharyngeal nerves (Altschuler et al., 1992). Within this fused mass, the nodose ganglion is located at the base of the ganglion, and contains vagal afferent neurons that project to the abdominal viscera, including the stomach. These afferent cell bodies are often referred to as "psuedo-unipolar" since they send afferent fibres both to the brainstem and to peripheral target organs (Craigmyle, 1985). As the vagus passes from the jugular foramen along the neck to the thorax and the abdomen, it divides into several branches at each of these levels. These branches in turn innervate a large number of target organs, as illustrated in Figure 1.

The vagus nerve consists primarily of afferent fibres characterized by slow conduction velocities (i.e. C-type fibres; 0.5-2 m/s) (Ganong, 1989). In many species, vagal afferent fibres constitute up to 80-90% of the nerve (Asala and Bower, 1986). In the rat, afferent fibres compose 70-80% of all fibres in subdiaphragmatic vagus which supplies the abdomnial viscera (Prechtl and Powley, 1990).

Figure 1. Vagal innervation of visceral structures (modified from Ganong, 1991).

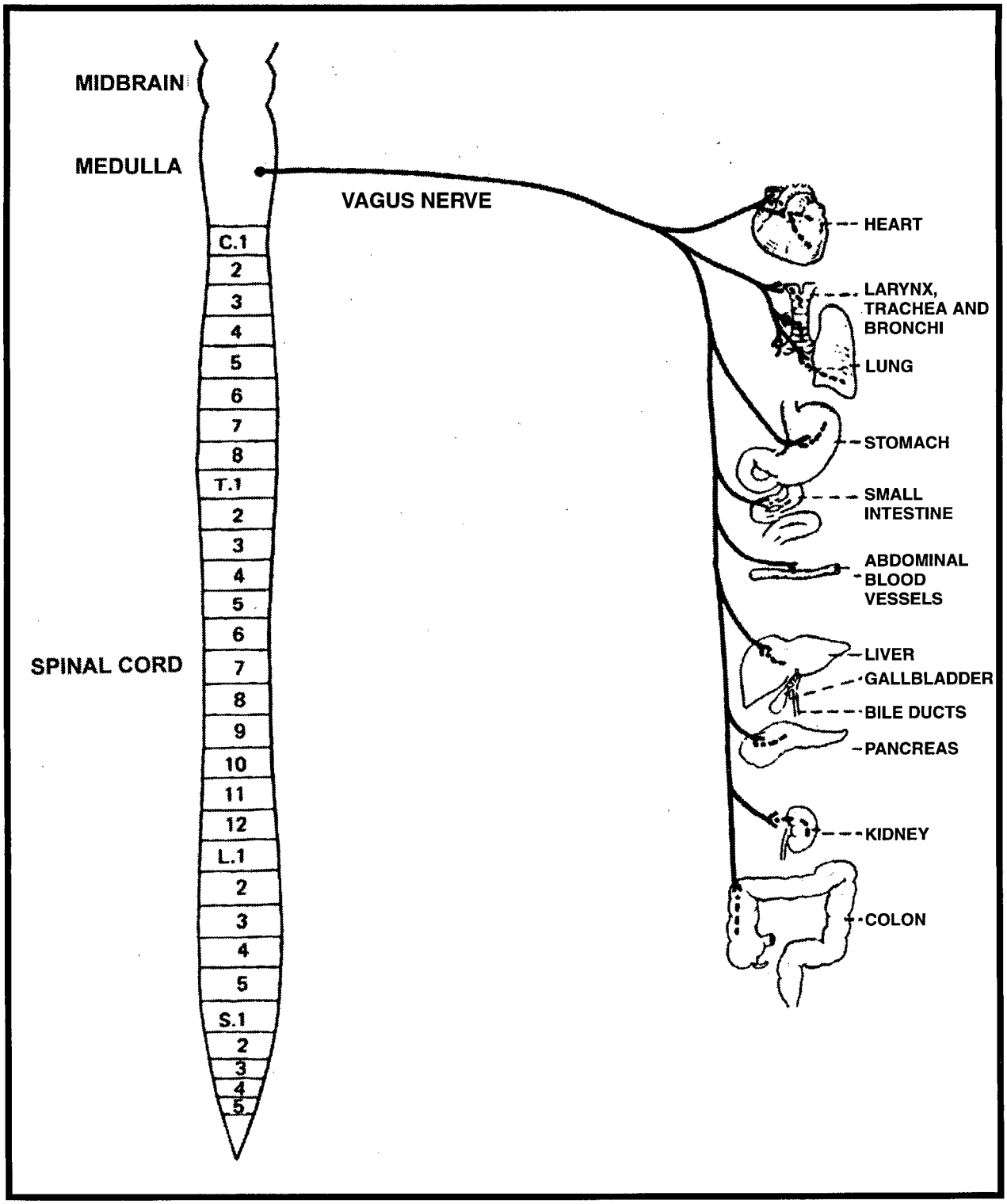
MIDBRAIN
MEDULLA
VAGUS NERVE
C.1
2
3
4
5
6
7
8
T.1
2
3
4
5
6
7
8
9
10
11
12
L.1
2
3
4
5
S.1
2
3
4
5
SPINAL CORD
HEART
LARYNX, TRACHEA AND BRONCHI
LUNG
STOMACH
SMALL INTESTINE
ABDOMINAL BLOOD VESSELS
LIVER
GALLBLADDER
BILE DUCTS
PANCREAS
KIDNEY
COLON

Together with the occulomotor, facial and glossopharyngeal nerves, the vagus comprises the cranial outflow of the parasympathetic division of the autonomic nervous system. The vagus shares some common features with other parasympathetic nerves. These include being part of reflex pathways consisting of preganglionic neurons (located in the brainstem of the rat) with long axonal connections which synapse on postganglionic neurons within the organ being innervated (i.e. post-ganglionic connections). Furthermore, like other parasympathetic nerves, the neurotransmitter that is released from the vagus at pre-ganglionic synapses is acetylcholine (Ganong, 1989). While this neurotransmitter is contained in postganglionic efferent fibres, the final effector released from the target ganglion (e.g. myenteric plexus) may be any of a number of substances (see section 1.5).

1.3. Functional Anatomy of the Stomach

The stomach is a specialized portion of the digestive tract that is located between the esophagus and duodenum. It is composed of an inner secretory surface (the mucosa) that is surrounded by opposing smooth muscle layers that are separated by ganglionated nerve plexuses (Figure 2). The main functions of the stomach are to store and process food for absorption by the intestine.

Figure 2. Diagrammatic representation of the enteric plexuses and muscle layers that comprise the stomach wall (modified from Furness and Costa, 1987).

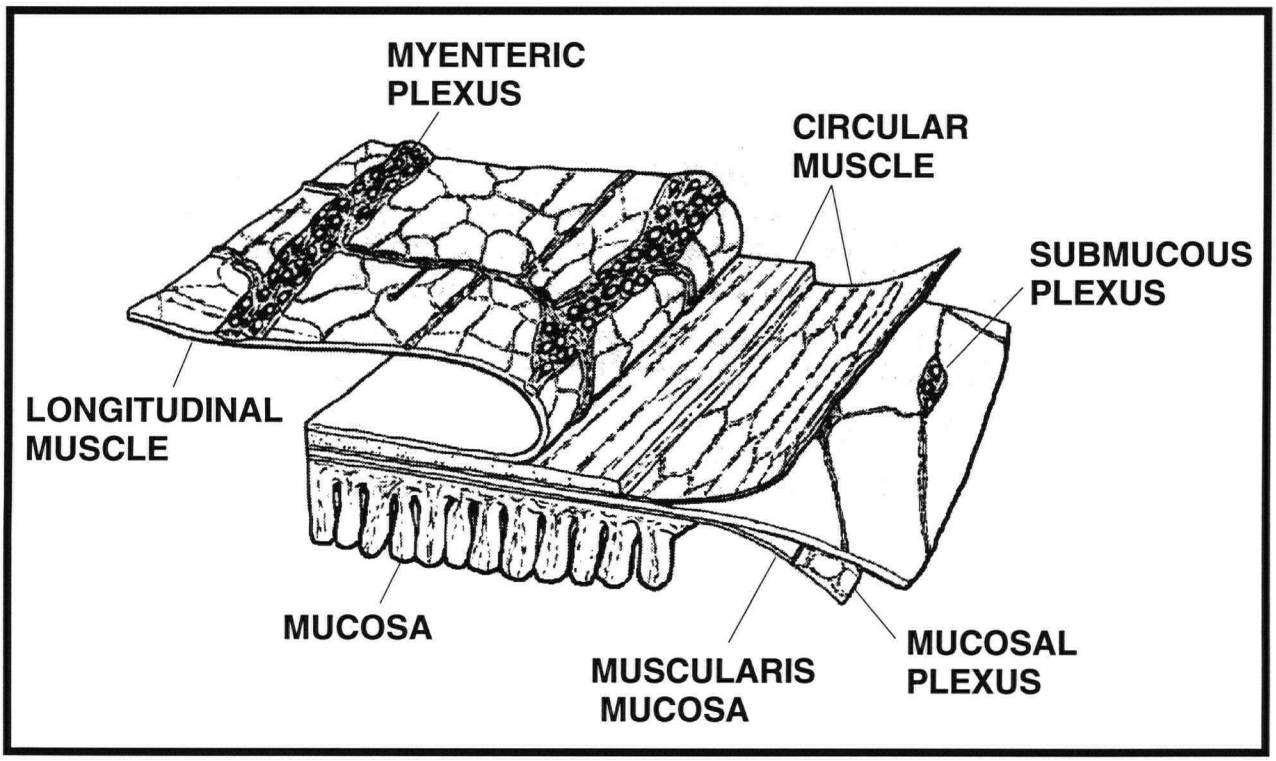
MYENTERIC
PLEXUS
CIRCULAR
MUSCLE
SUBMUCOUS
PLEXUS
LONGITUDINAL
MUSCLE
MUCOSA
MUSCULARIS
MUCOSA
MUCOSAL
PLEXUS

Although the vertebrate stomach shares a number of common structural features, the gross morphology can vary greatly. Species variations are related to differences in body size and shape, the need for food storage, the nature of the diet and the frequency of food intake (Ito, 1987). The anatomy of the rat stomach is unique, and nomenclature has been proposed that reflects the similarities and differences between it and the human stomach, to which it is most frequently compared (Robert, 1971). The rat stomach can be divided into functional regions on the basis of secretion (i.e. glandular and non-glandular areas) and motility.

In terms of secretion, the stomach is divided into the forestomach, corpus and antrum (Figure 3). The forestomach is the portion of the stomach located immediately adjacent to the esophagus. Unlike the fundus of the human stomach which is glandular, the rat forestomach is non-glandular and consists of squamous epithelium. In the rat, the corpus is the area containing oxyntic glands. These glands contain parietal cells which secrete hydrochloric acid, chief cells which secrete pepsinogen and intrinsic factor and enterochromaffin-like cells that secrete histamine. In addition, the oxyntic glands contain mucous cells which secrete a glycoprotein mucus that forms a protective layer on the inner surface of the stomach. The antrum, which adjoins the duodenum, is sharply delimited from the corpus in the rat by its thinner mucosa. The antrum contains the pyloric glands which contain gastrin, somatostatin, enterochromaffin and mucous cells.

In terms of motility functions, the rat stomach like that of the human, can be divided into two major regions, orad and caudad. The forestomach comprises the orad portion of the stomach, and exhibits little contractile activity. It is mainly involved with accommodation of ingested material, and the eventual movement of this material to the

caudad region. In contrast to the orad stomach, the caudad stomach is characterized by marked activity. Waves of peristaltic contractions originate from a 'pacemaker' region in the mid stomach and move toward the gastro-duodenal junction. These waves, referred to as gastric slow waves, serve to mix (via retropulsion) and propel gastric contents into the intestine, where absorption occurs (Ganong, 1989).

Figure 3. Functional anatomy of the rat stomach (modified from Berthoud and Powley, 1992).

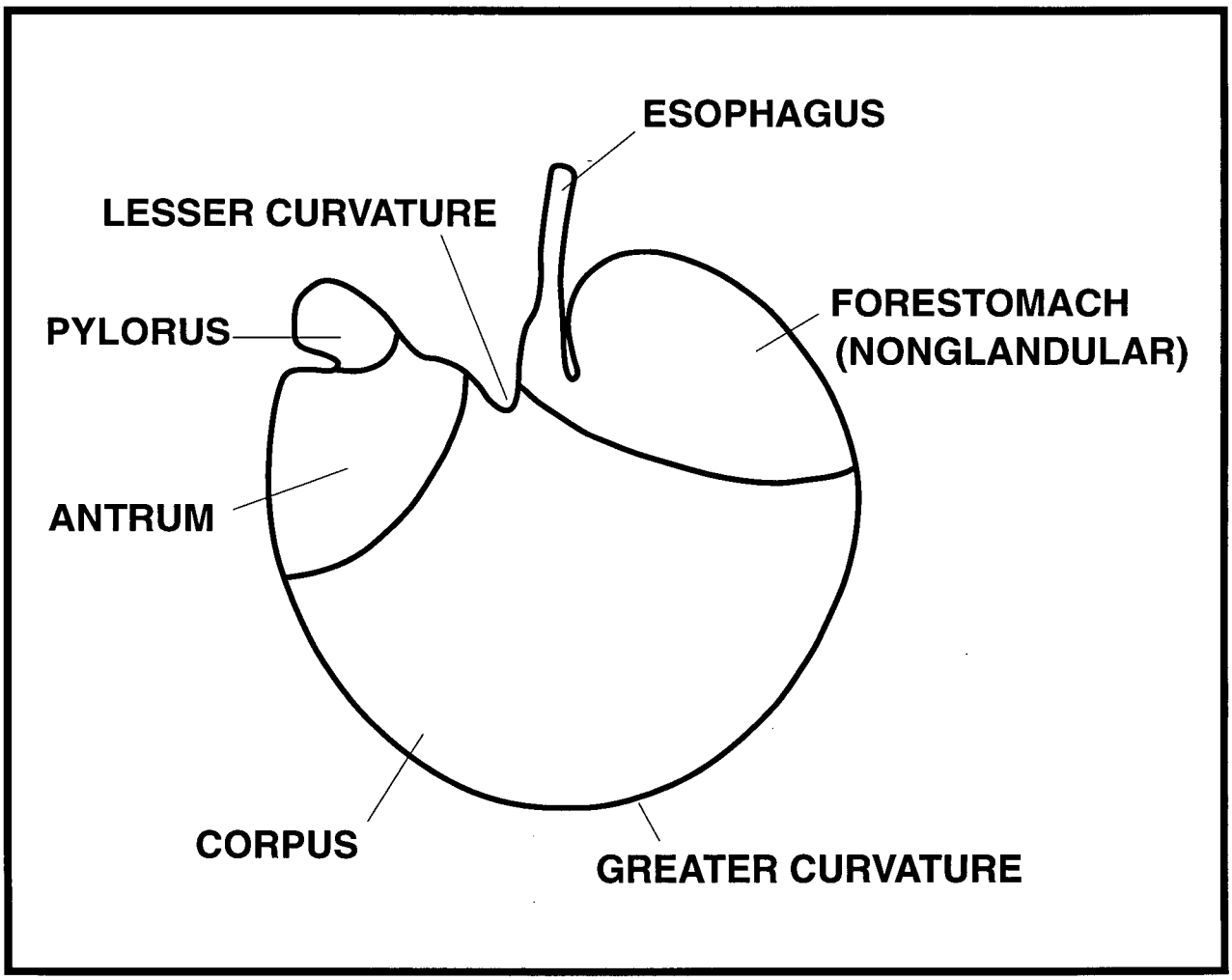
ESOPHAGUS
LESSER CURVATURE
PYLORUS
FORESTOMACH
(NONGLANDULAR)
ANTRUM
CORPUS
GREATER CURVATURE

1.4. Historical Perspective on the Vagal Control of Gastric Function

In the mid-nineteenth century, physiologists found that electrical stimulation of vagal nerves to the stomach resulted in gastric secretion. However, because such stimulation also increased gastric blood flow, it was uncertain if the secretion was due to hyperemia or a direct effect of the nerves upon the secreting cells. In the 1890s, Pavlov provided the first complete demonstration of vagal control of gastric secretion (Davenport, 1992). Dogs were prepared with a vagally-innervated pouch of the corpus region of the stomach and a fistula in the esophagus. When these dogs ate, food would fall through the fistula in the esophagus without reaching the stomach. These animals continued to eat indefinitely, and Pavlov called the process sham feeding. During this type of feeding, acid continued to be produced in the corpus pouch, but terminated after vagotomy. Thus, Pavlov proved that the efferent pathway is in the vagus, and because the afferent pathways are in the head and not the stomach, he termed the response the cephalic phase of digestion. These findings were consistent with Pavlov's "nervism" concept in which he believed that "the nervous system controls the greatest possible number of bodily activities." The repeatability of these experiments led Pavlov to the discovery of conditioned reflexes (Davenport, 1992).

At the start of the 20th century, the vagus nerve was still considered to serve a primarily visceromotor function. At this time, Langley classified the vagus as part of the parasympathetic division of the autonomic nervous system, and described it in terms of its motor effects (Koizumi and Brooks, 1980). Although it was well understood that the motor activity of the stomach could function in the absence of external innervation, it was realized that gastric tone and contractions could be modified by the vagus.

In 1904, Page May demonstrated that electrical stimulation of the central cut end of the vagus nerve inhibited spontaneous gastric contractions in several species (Raybould, 1992). In contrast, Rogers in 1917 demonstrated that in decerebrate dogs, the same electrical stimulation of the vagus caused contraction of the entire stomach (Raybould, 1992). Around this time, studies by Carlson found that stimulation of the gastric mucosa by acid, alcohol and alkali inhibited both gastric tone and contractions in dog and man only if the vagus was intact (Raybould, 1992). Thus, these early studies demonstrated that both excitatory and inhibitory effects of vagal efferents on the stomach could be activated by vagal afferent stimulation.

In 1911, during his studies on the peristaltic activity of the stomach in cats, Cannon recognized that the stomach acted as a reservoir (Raybould, 1992). Using animals prepared with esophageal fistulas, he placed a balloon in the stomach to measure gastric volume. When these animals ate a piece of meat, it would fall through the fistula without entering the stomach. However, the volume of the balloon in the stomach increased during this event, representing relaxation of the stomach. The response was rapid, and did not occur when the vagus nerve was cut bilaterally. Thus, Cannon demonstrated that this "receptive relaxation" was mediated by a vago-vagal reflex involving both vagal afferents and efferent nerves (Raybould, 1992).

Although the discovery of gastrin in 1905 had established a hormonal basis for gastric regulation and challenged Pavlov's nervism concept, it was not until the late 1950's that definitive proof was presented for the vagal release of gastrin. In 1959, Schofield and coworkers constructed a vagally-innervated pouch out of the pyloric gland region of the stomach, thus removing it from the path of gastric acid. The results

demonstrated that vagal stimulation released gastrin and that this could be attenuated by infusion of acid into the pouch (Davenport, 1992).

Within the past 25 years, additional vagal reflexes influencing gastric function have been elucidated. In 1973, Abrahamson demonstrated that stimulation of gastric mechanoreceptors by transient, graded distention produced a long lasting gastric relaxation, which he termed "gastric accommodation" (Raybould, 1992). In the mid 1980s, Malagelada provided evidence for the existence of an enterogastric reflex involving the vagus, whereby duodenal distention decreases proximal gastric motility (Raybould, 1992).

The study of vagal reflexes controlling gastric acid secretion and motility have largely been overshadowed within the past few decades in favour of studying the humoral and hormonal mechanisms of gastric control. The development of immunological, biochemical and molecular biological approaches has resulted in the demonstration of many peptides within nerves and endocrine cells that can influence the actions of the vagus on the stomach. In addition, the use of refined neuroanatomical tracing techniques and immunocytochemical procedures have begun to provide a detailed structural basis for the vagal regulation of gastric function.

1.5. Innervation of the Stomach

The nerve supply to the stomach can be divided into intrinsic and extrinsic components. The intrinsic innervation of the stomach is a complex neural network, commonly referred to as the gastro-enteric nervous system. It consists of a large number of neurons that are organized into two major ganglionated plexuses. The myenteric

plexus (also known as Auerbach's plexus) is situated between the longitudinal and circular muscle layers, whereas the submucosal plexus (Meissner's plexus) is located within the submucosa between the mucosa and circular muscle. Neurons within each plexus are connected, and the separate plexuses are also interconnected. Nerve fibres from the plexuses innervate the different layers of the stomach, including smooth muscle, secretory cells and blood vessels. The majority of axons within the stomach wall originate from intrinsic neurons, and these represent the major neural component controlling gastric functions. The observation that spontaneous and reflex activities can persist in the absence of extrinsic input provides strong evidence for the existence of sensory receptors, intrinsic primary afferent neurons, interneurons and motor neurons within the enteric nervous system.

The extrinsic innervation of the stomach is comprised of both efferent as well as afferent inputs. These inputs contribute to the fibre network of the enteric nervous system, and serve to integrate the activity of the intrinsic neurons. The autonomic input to the stomach is supplied by both the sympathetic and parasympathetic nerves.

The parasympathetic supply to the stomach is provided solely through the vagus nerve. The sympathetic nerves that supply the stomach originate in the lower thoracic and upper lumbar regions (T_5-L_1/L_2) of the spinal cord. It is important to note that the enteric neurons within the stomach can either be excitatory or inhibitory (Jass, 1983). These neurons can either be acted upon directly by the extrinsic nerves or via interneurons (Jass, 1983). Furthermore, it is now well established that acetylcholine and norepinephrine are not the only neurotransmitters released within the gut. There is a

significant component derived from non-adrenergic, non-cholinergic neurons which includes peptides and other substances (Furness and Costa, 1987).

1.6. Anatomy of Vagal Efferents that Supply the Stomach

In the rat, the subdiaphragmatic vagus consists of five branches: the left and right gastric, the celiac and accessory celiac and the hepatic (Figure 4). As their name implies, the gastric branches contain the vast majority of vagal nerve fibres that supply the stomach. These branches enter the stomach near the gastroesophageal junction or at the lesser curvature where the branches further subdivide to supply the dorsal (left gastric) and ventral (right gastric) surfaces of the stomach. Recent evidence also suggests that some vagal efferent fibres are associated with the gastroepiploic arteries that supply the greater curvature of the rat stomach (Donahue et al., 1988; Yoshida et al., 1988b; Yoshida et al., 1989). It is believed that these may arise from the hepatic branch of the vagus which supplies the duodenum or from the celiac branch.

Until recently, most of the information concerning the structural details of vagal efferents within the digestive tract have come from studies of the small intestine or esophagus. In the rat, studies employing neuronal tracing techniques and immunocytochemistry of wholemount sections have provided structural details of vagal efferents within the wall of the stomach and their association with gastric targets (Kirchgessner and Gershon, 1989; Berthoud et al., 1990; Berthoud and Powley, 1992; Powley et al., 1994). The use of confocal microscopy and 3-D reconstruction techniques in one of these sudies (Powley et al., 1994) provided fine structural details of the vagal innervation.

Figure 4. Schematic diagram of subdiaphragmatic vagal branches in the rat (modified from Norgren and Smith, 1988).

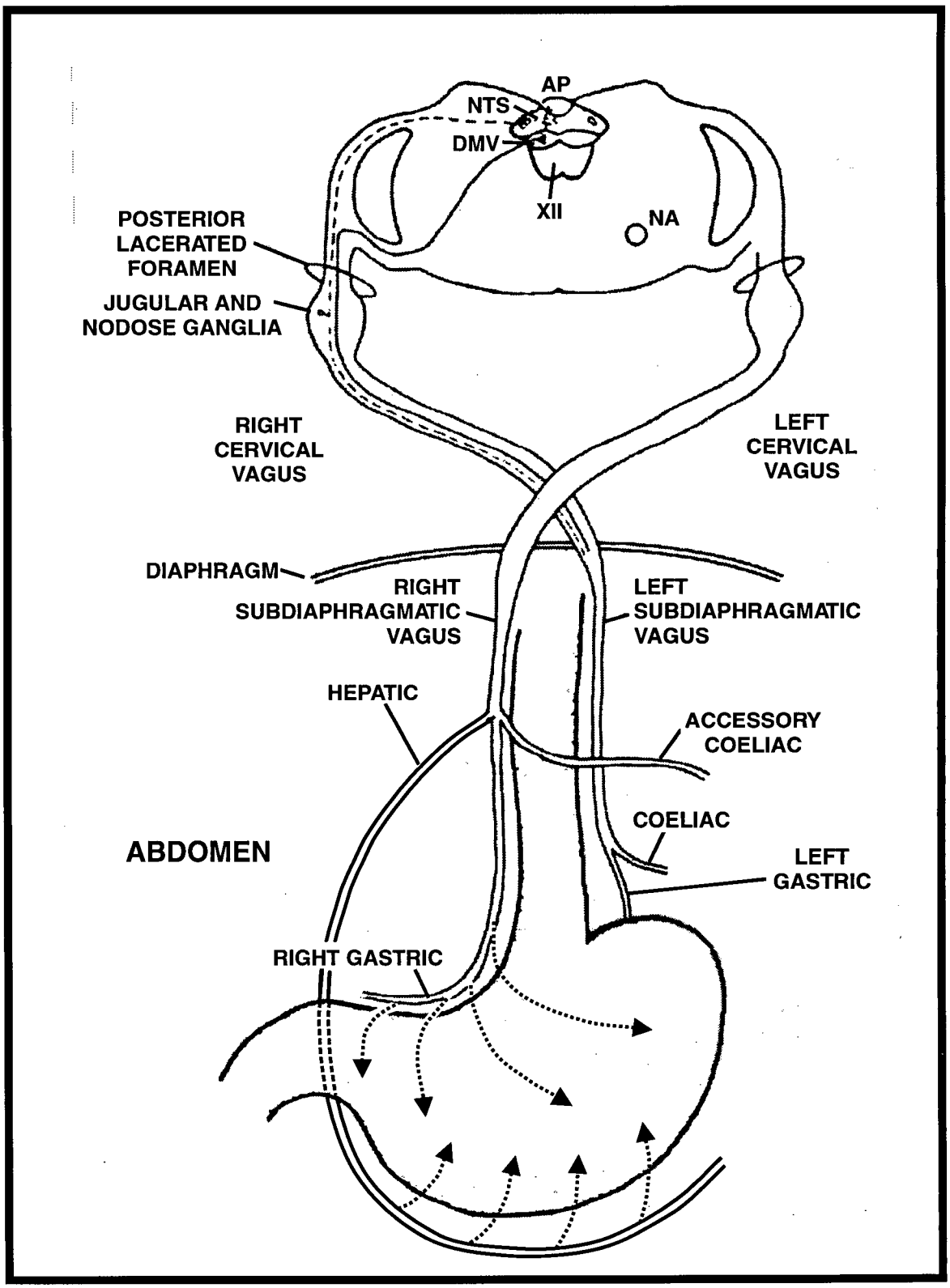
AP
NTS
DMV
XII
NA
POSTERIOR LACERATED FORAMEN
JUGULAR AND NODOSE GANGLIA
RIGHT CERVICAL VAGUS
LEFT CERVICAL VAGUS
DIAPHRAGM
RIGHT SUBDIAPHRAGMATIC VAGUS
LEFT SUBDIAPHRAGMATIC VAGUS
HEPATIC
ACCESSORY COELIAC
COELIAC
LEFT GASTRIC
ABDOMEN
RIGHT GASTRIC

Preganglionic vagal efferent fibers are grouped into slender bundles that enter the stomach in conjunction with blood vessels. The bundles in some instances travel on the surface of the stomach for a short distance then penetrate the longitudinal muscle layer as fascicles and enter the connectives of the enteric nervous system. Within the myenteric ganglia, efferent fibers contain *en passage* and terminal varicosities of varying sizes. Other vagal preganglionic fibers or collaterals travel through the circular muscle layer to the connectives and ganglia of the submucosal plexus, where they also display varicosities. However, compared to the myenteric plexus, the submucous plexus is sparsely innervated by direct vagal preganglionic projections.

The number of neurons within the enteric ganglia of the stomach outnumber the incoming vagal efferent fibres by several thousand to one. In 1922, Langley postulated that a limited subset of myenteric neurons serve as "mother cells" (corresponding to postganglionic neurons) receiving direct vagal efferent projections and then distributing the autonomic outflow within the myenteric ganglia (Wang et al., 1995). In a similar vein, Wood proposed that vagal preganglionic nerve fibres project to "command neurons" within the enteric ganglia (Wood, 1987). Although the recent experiments described above have only begun to address this issue, the current consensus is that the vagal efferent fibre distribution is more extensive and complex than has been appreciated in the past. These studies have demonstrated that the vagal efferents were distributed much more divergently than either the "mother cell" or "command neuron" hypotheses would require.

1.7. Representation of the Gastrointestinal Tract in the Dorsal Vagal Complex in the Rat Medulla

Although the central origin of the vagus nerve in the brainstem was described over 150 years ago (Mitchell and Warwick, 1955), it has only been within the last 20 years that a viscerotopic organization within this region has been elucidated. This has been largely due to the relatively recent introduction of neuroanatomical tracing techniques, which has facilitated the identification of vagal afferent and efferent components within the dorsal vagal complex in the medulla that innervate the gastrointestinal tract (see Shapiro and Miselis, 1985).

The vagal nuclei in the brainstem are divided into motor components which include the dorsal motor nucleus (DMV) and nucleus ambiguus (NA) and sensory nuclei (the nucleus of the solitary tract [NTS] and the area postrema [AP]). Due to the close anatomical relation of the DMV, NTS and AP in the dorsal medulla, they are often referred to collectively as the "dorsal vagal complex" (DVC) (Altchuler et al., 1992). In the following sections, the structure of each of these nuclei will be considered briefly, with emphasis placed on the location and arrangement of gastric afferent and efferent fibres within the DVC.

1.7.1. Nucleus Ambiguus

There is now conclusive evidence that the NA does not provide general visceral efferent innervation to the abdominal viscera (Altschuler et al., 1992). The NA is located in the ventrolateral medulla with the dorsal division providing visceral efferent innervation to the striated muscle of the upper alimentary tract (esophagus, larynx,

pharynx and soft palate) and respiratory tract (branchiomeric musculature). The ventral division is the source of general visceral efferents innervating the thoracic viscera, including the heart.

1.7.2. Dorsal Motor Nucleus of the Vagus

The DMV is considered to be the source of general visceral efferent fibres to the gastrointestinal tract. Efferents in the DMV begin their innervation of visceral targets at the level of the stomach and continue providing inputs as far caudal as the descending colon. Within the gastrointestinal tract, efferent vagal fibres synapse on postganglionic neurons located within the myenteric plexus. No direct contacts between the DMV and smooth muscle cells have been demonstrated.

The DMV lies in register with, and immediately ventral to, the NTS. From a perspective dorsal to the medulla, the DMV appears as a bilaterally symmetrical, longitudinally elongated aggregate of cells located on either side of the midline that form a characteristic "Y" shape. Caudally, the DMV is fused at the midline in a position immediately dorsal and dorsolateral to the central canal. At levels rostral to the obex (where the central canal fuses with the fourth ventricle) each half of the DMV is shifted laterally to maintain a position just ventromedial to the corresponding side of the NTS. In the rat, the DMV spans a distance of >4 mm in the rostrocaudal dimension. In this species, neuronal tracing studies have demonstrated that there are approximately 3000-3500 neurons on each side of the DMV (Fox and Powley, 1985; Berthoud et al., 1991). The largest concentration of efferent neurons occurs around the level of the obex while a smaller number of neurons are located at each pole of the nucleus.

The right and left DMV contribute efferent axons to the right and left cervical vagal nerves, respectively. These nerves cross above the diaphragm and then enter the abdominal cavity where they have been designated as the left and right subdiaphragmatic vagus nerves, respectively. Below the level of the diaphragm in the rat, the vagus divides into five separate branches. The left or dorsal subdiaphragmatic vagus divides into the celiac and left gastric nerves, while the right or ventral subdiaphragmatic vagus divides into the hepatic, accessory celiac and right gastric nerves.

Application of neuroanatomical tracers to the abdominal branches of the vagus or directly to different abdominal viscera have led to the formulation of organizational maps of the DMV (see Altschuler et al., 1992; Hopkins et al., 1996 for a review). These studies have revealed that the DMV is composed of a number of longitudinally (i.e. rostrocaudally) and mediolaterally arranged columnar subnuclei that correspond to the branches of the abdominal vagus. This topology has been studied in a number of species (Powley et al., 1992), and has been delineated in detail in the rat.

In the rat, there are four distinct columns of neurons which together form the general profile of the DMV (Fox and Powley, 1985; Norgren and Smith, 1988). The largest column, comprising 80-90% of all of the neurons within the DMV, is the medial column. This column occupies the medial half or more of the DMV on either side of the brainstem. The medial column in the left DMV corresponds to the ventral gastric branch of the vagus, whereas this column in the right DMV corresponds to the dorsal gastric branch. There are also lateral columns on either side of the DMV, which in the left DMV corresponds to the accessory celiac branch, and the right DMV contains the celiac branch. The fifth column, which contains the fewest efferent neurons (less than 10% as many as

the gastric branch) and is more diffuse than the other columns, is contained within the medial gastric branch column within the left DMV.

Direct intramuscular injection of retrograde tracers into the stomach and pancreas have revealed that vagal efferent neurons projecting to these viscera are located bilaterally in the medial columns of the DMV (Shapiro and Miselis, 1985; Altschuler et al., 1992). The concensus of these tracing studies is that the stomach and cecum dominate the medial and lateral columns, respectively, whereas other areas of the bowel are represented by sparse labelling within the columns (see Altschuler et al., 1992; Hopkins et al., 1996 for a review). The duodenum is supplied by vagal efferents within the medial columns of the DMV, while regions of the gastrointestinal tract from the jejunum to the descending colon are confined to the lateral columns. Figure 5 is a schematic summarizing the viscerotopic organization within the DMV.

The positioning of longitudinal efferent neuron columns within the DMV has also been corroborated by electrophysiological experiments in the rat (Berthoud et al., 1991b). Furthermore, using electrical stimulation, it has been demonstrated that the spatial organization of DMV efferents that control gastric acid, insulin and glucagon secretion in the rat are organized into bilateral longitudinal columns, with some medial to lateral displacement of the "centers of gravity" of the different responses (Laughton and Powley, 1987).

Figure 5. Summary of the motor viscerotopic representation of the alimentary tract in the DMV as projected in the transverse plane (modified from Altschuler, 1992). Orientation: D=dorsal, V=ventral, L=left, R=right. DMV_{med}=medial column of the DMV; DMV_{lat}=lateral column of the DMV. AP=area postrema. TS=tractus solitarius. XII=hypoglossal nucleus.

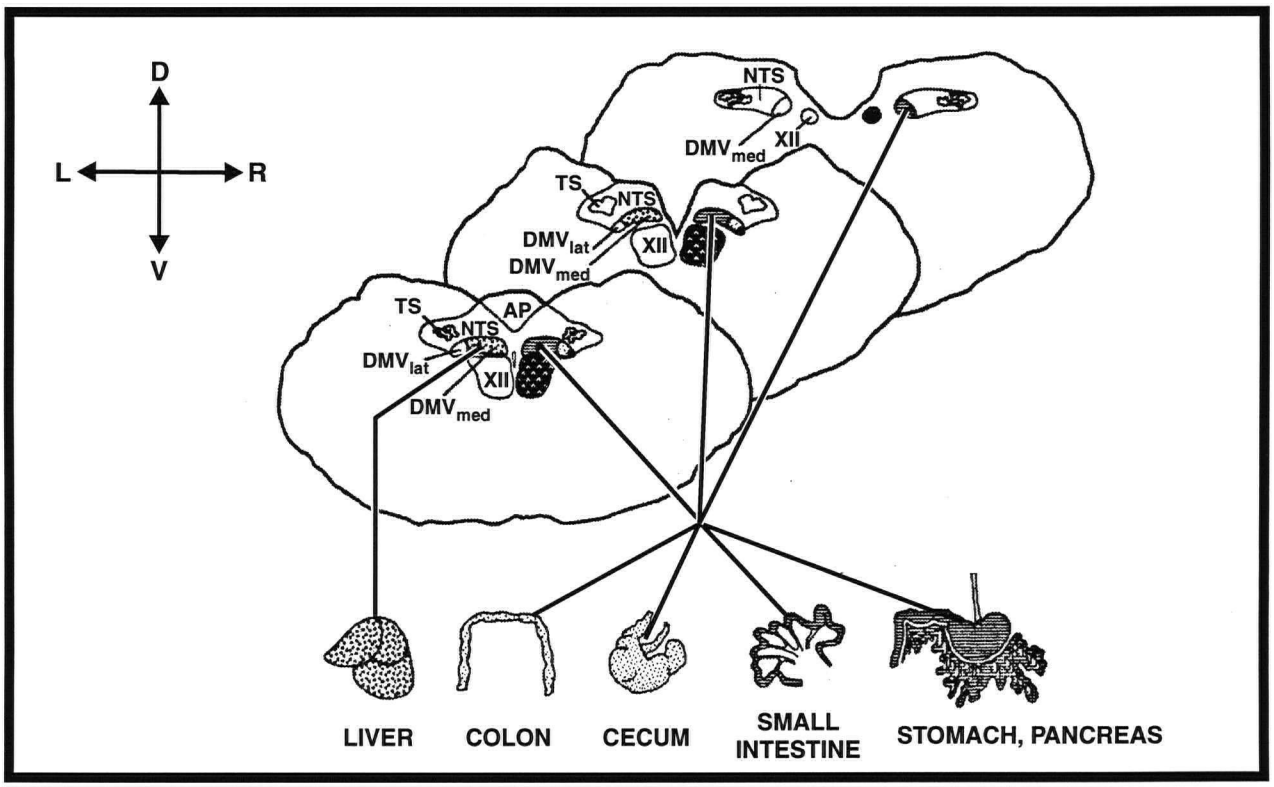
D
L
R
V
NTS
XII
DMV med
TS
NTS
DMV lat
XII
DMV med
TS
AP
NTS
DMV lat
XII
DMV med
LIVER
COLON
CECUM
SMALL INTESTINE
STOMACH, PANCREAS

In addition to the gross level of organization describing the layout of the gastrointestinal tract within the DMV, evidence for a more precise viscerotopic organization of the stomach is now emerging. Application of a retrograde tracer to secondary branches of the gastric vagus nerves (e.g. branches of the anterior gastric branch; Powley et al., 1987) or to discrete regions of the stomach have revealed that the medial gastric column within the DMV is composed of finer, spatially distinct longitudinal columns which occupy the full rostrocaudal extent of the nucleus (Shapiro and Miselis, 1985; Okumura and Namiki, 1990). The consensus is that the antrum/pylorus is represented most medially, the forestomach most laterally and the corpus diffusely within the overall medial gastric column in the DMV.

The use of retrograde tracers such as cholera toxin horseradish peroxidase (CT-HRP) and intracellular neuronal filling techniques (e.g. using the dye Lucifer Yellow) have demonstrated that DMV neurons have both extensive intranuclear and extranuclear dendritic arborizations (Altschuler et al., 1992; Fox and Powley, 1992). Efferent neurons within the medial and lateral columns exhibit similar branching structure. At all levels of the DMV, the majority of gastric and cecal neurons project primarily in a rostrocaudal direction within the confines of their respective columns and, to a lesser extent, between columns (Shapiro and Miselis, 1985). The architecture of DMV dendrites provides a structural arrangement for coordination of efferent activity throughout the rostrocaudal extent of the nucleus as well as between columns (Altschuler et al., 1992).

The major extranuclear site of termination for DMV dendrites is the NTS. Dendrites of gastric and cecal efferent neurons penetrate into the NTS essentially parallel to each other and terminate in areas that overlap the terminal fields of their respective

afferent fibres. This type of arrangement between afferent fibres and efferent dendrites supports the possibility of organ-specific monosynaptic connections. In the case of the stomach, this has been demonstrated at the ultrastructural level in the gelatinosus subnucleus of the NTS where gastric afferent fibres terminate. In further support of contacts between organ specific afferent fibres and corresponding efferent dendrites, it has been shown that the dendrites of gastric and cecal neurons encircle or avoid the afferent fields of other organs within the NTS (Altschuler, 1991).

In summary, the vagal preganglionic efferent supply to the stomach represents the largest number of neurons within the DMV. These neurons are arranged in longitudinal columns which form the medial half or more of the nucleus on either side of the DMV. Each of these columns projects to a different surface of the stomach. There is some indication that there is a more precise representation of the stomach in the DMV, such that the antrum/pylorus and fundus occupy distinct 'subcolumns' within the medial columns. The dendrites of gastric efferent neurons within the DMV project mainly into the NTS, where they form synaptic connections with interneurons (majority) or monosynaptic connections with primary gastric afferents (minority). The morphology (including somata size and dendritic length and degree of arborization) of preganglionic vagal neurons within the DMV varies at different rostrocaudal levels of the nucleus.

1.7.3. Nucleus of the Solitary Tract

The NTS is the first synaptic site for afferent projections from peripheral structures conveyed through cranial nerves V, VII, IX and X (see Altschuler et al., 1992 for a review). The NTS lies immediately dorsal to, and in register with, the DMV and has

the same characteristic "Y" shape when viewed in the horizontal plane. The primary afferent cell bodies that project to the NTS from the viscera are located in the nodose ganglion.

In the rat, the NTS is a complex nucleus that is composed of several subnuclei that have different cell morphology, packing density, intensity of Nissl staining, neuropeptide content and connectivity. Afferents from the gastrointestinal tract project mainly to the medial division of the NTS (area medial to the tractus solitarius). Within the NTS, these fibres travel mainly perpendicular to the rostrocaudal axis and terminate with a viscerotopic organization in distinct subnuclei: gelatinosus, centralis, commissuralis, medialis, interstitialis and intermedialis (Altschuler et al., 1992).

A major organizational feature of the NTS is the rostrocaudal segmentation of afferent terminal fields that roughly corresponds to rostrocaudal positioning along the gastrointesinal tract (Figure 6). With respect to the stomach, the greatest concentration of gastric afferents within the NTS is found within the gelatinosus subnucleus (Shapiro and Miselis, 1985; Altschuler et al., 1992). Some gastric afferents also penetrate into the medial and commisural subnuclei. In contrast, cecal afferents project mainly to the dorsolateral region of the commissural subnucleus. Although both gastric and cecal afferents can be found in the commisural and medial subnuclei, there is no overlap in the distribution of their terminal fields.

Figure 6. Summary of the sensory viscerotopic representation (afferent terminal fields) of the alimentary tract within the NTS as projected in the horizontal plane (modified from Altschuler, 1992). Orientation: R=rostral, C=caudal, L=lateral, M=medial. IV=fourth ventricle. AP=area postrema.

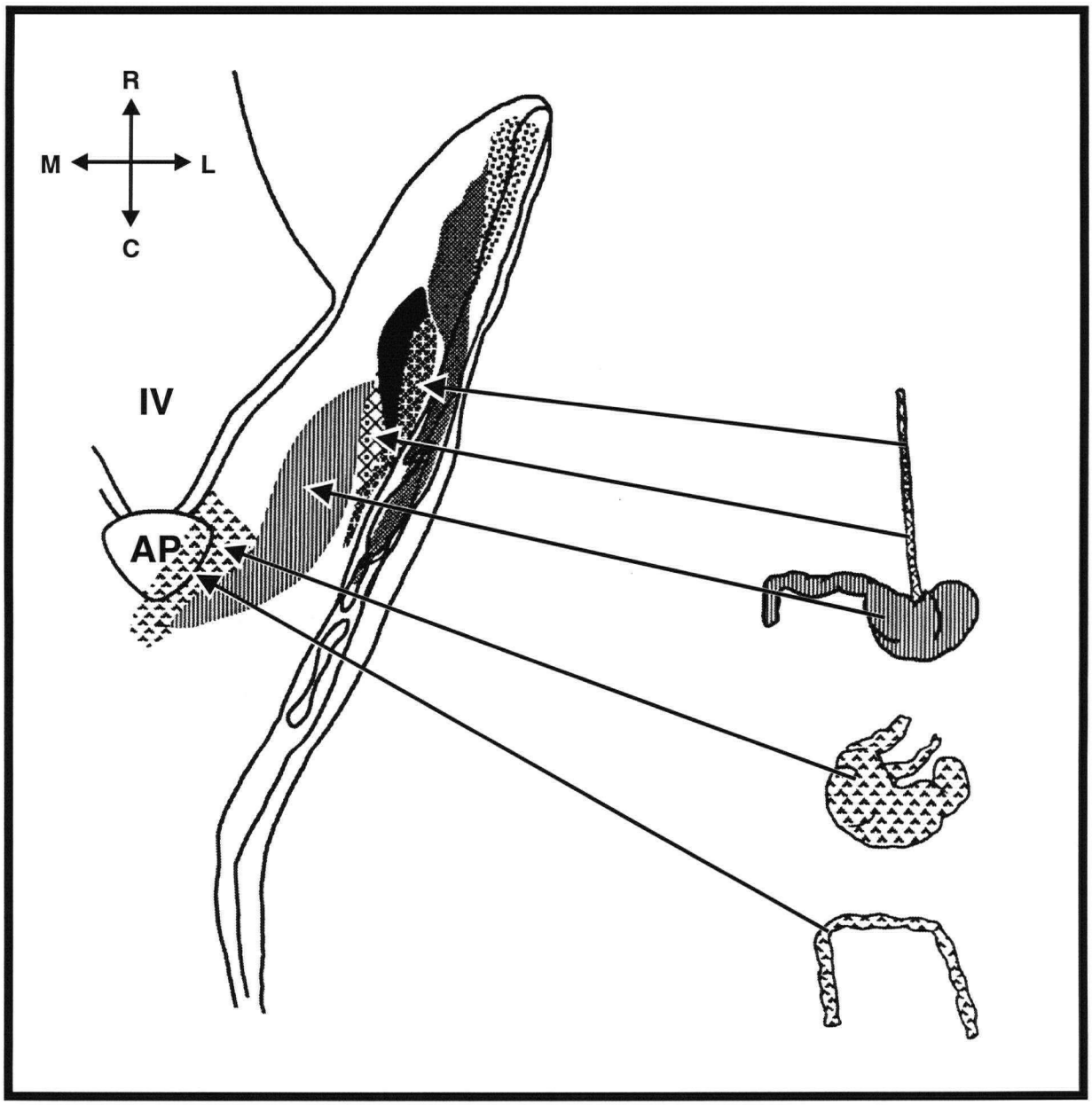
R
M
L
C
IV
AP

1.7.4. Area Postrema

The AP lies immediately caudal to the obex, on the floor of the fourth ventricle. It is sparsely populated with small neurons averaging 12 μm in diameter (Leslie et al., 1992). It receives some vagal afferent fibres of mainly gastric origin (Kalia and Mesulam, 1980). In addition, a small number of dendrites from efferent neurons in the DMV have been shown to terminate in the AP (Shapiro and Miselis, 1985). The distinguishing feature of the AP is that it is one of the circumventricular organs with a weak blood-brain barrier, allowing access of humoral elements to influence both vagal afferent and efferent components.

1.7.5. Connections between the DMV and NTS

Vagal efferent fibres have a continuous low frequency spontaneous discharge that is modulated by sensory inputs (Davison and Grundy, 1978). The cessation of this spontaneous activity after ipsilateral vagotomy demonstrates that the ongoing activity of vagal efferent neurons is dependent on some degree of afferent input.

Ultrastructural studies have identified monosynaptic connections between gastric afferent fibres and efferent dendrites in the gelatinosus subnucleus of the NTS (Neuhuber and Sandoz, 1986; Rinaman, et al., 1989). Furthermore, a subset of primary afferent terminals have been shown to synapse directly onto neurons within the DMV as well as the NTS. Although monosynaptic connections do exist, these are believed to be far less common than di- or poly-synaptic connections via an interneuron in the NTS or DMV itself (Neuhuber and Sandoz, 1986).

Powley et al. 1992 have proposed a "sensory-motor lattice" hypothesis to explain the functional interactions between the NTS and DMV (Powley et al., 1992). This hypothesis is based on two major observations. Firstly, the tight register and extensive interconnections between the NTS and DMV facilitates the operation of these nuclei as a functional unit. Secondly, the transverse arrangement of vagal afferent components in the NTS is at right angles to the longitudinal efferent organization within the DMV, providing an anatomical basis for a lattice-like arrangement with intersecting regions. They contend that this type of arrangement could provide an efficient plan for organizing afferent inputs to different vagal motor responses.

An examination of the results of electrophysiological studies of neurons within the DVC that respond to gastrointestinal stimulation suggests that there may be additional levels of complexity within the proposed lattice model. These studies have shown that neurons within the same column of the DMV and presumably receiving the same afferent input can exhibit different responses to the same visceral stimulus (Zhang et al., 1992; Fogel et al., 1996). For example, distention of the gastric antrum identifies two groups of vagal motor neurons: those that can be excited (the majority) and those that are inhibited (the minority) (Davison and Grundy, 1978; Blackshaw et al., 1987; Blackshaw and Grundy, 1989).

1.8. Central Connections of the Vagus Nerve: Regulation of Gastric Function

Although it is clear that the gastro-enteric nervous system is capable of limited independent regulatory function, it has also been established that vagal efferent input provides the overall co-ordination and control of the stomach. This controlling input

from the central nervous system (CNS) is essential to the rapid changes induced in digestive function by feeding (Diamant et al., 1980).

Neuroanatomical tracing studies have revealed that the sensory and motor components of the gastric vago-vagal reflexes in the DVC receive significant and discrete inputs from several CNS sources (Figure 7). Therefore, although basic gastric functions can be maintained by vago-vagal reflexes that are localized within the brainstem, these reflexes may be modulated by CNS inputs to these basic control circuits (Rogers and Hermann, 1992). These extrinsic inputs are implicated in the co-ordination of gastric function with behaviour. Although there are many CNS areas that have projections to the DVC (see Sawchenko, 1983 and Leslie et al., 1992 for a review), only a subset of these have been examined with respect to their effect on gastric function.

Three structures in the ventral forebrain, the paraventricular nucleus of the hypothalamus (PVH), the central nucleus of the amygdala (CNA) and the bed nucleus of the stria terminalis (BST), all send input directly to the NTS and DMV (Rogers and Hermann, 1992). The PVH, CNA and the BST together form a continuous interconnected band of "pre-vagal" neurons that extends laterally from the PVH through the dorsal part of the lateral hypothalamus. Anatomical observations indicate that the entire dorsal half of the lateral hypothalamus may belong to this band of pre-vagal neurons. Through synaptic connections with the DMV and NTS, this band of ventral forebrain projections has been implicated in the control of gastric function via a direct effect, or through modulating the gain of gastric vago-vagal reflexes.

Figure 7. Some of the major CNS inputs to the DVC. Inset: list of some of the neuropeptides that have been detected within the DVC. (compiled from Rogers and Herman, 1992, Leslie, 1985 and Diz et al., 1987). PVH=paraventricular nucleus of the hypothalamus; CNA=central nucleus of the amygdala, BNST=bed nucleus of the stria terminalis; nRO=raphe obscurus.

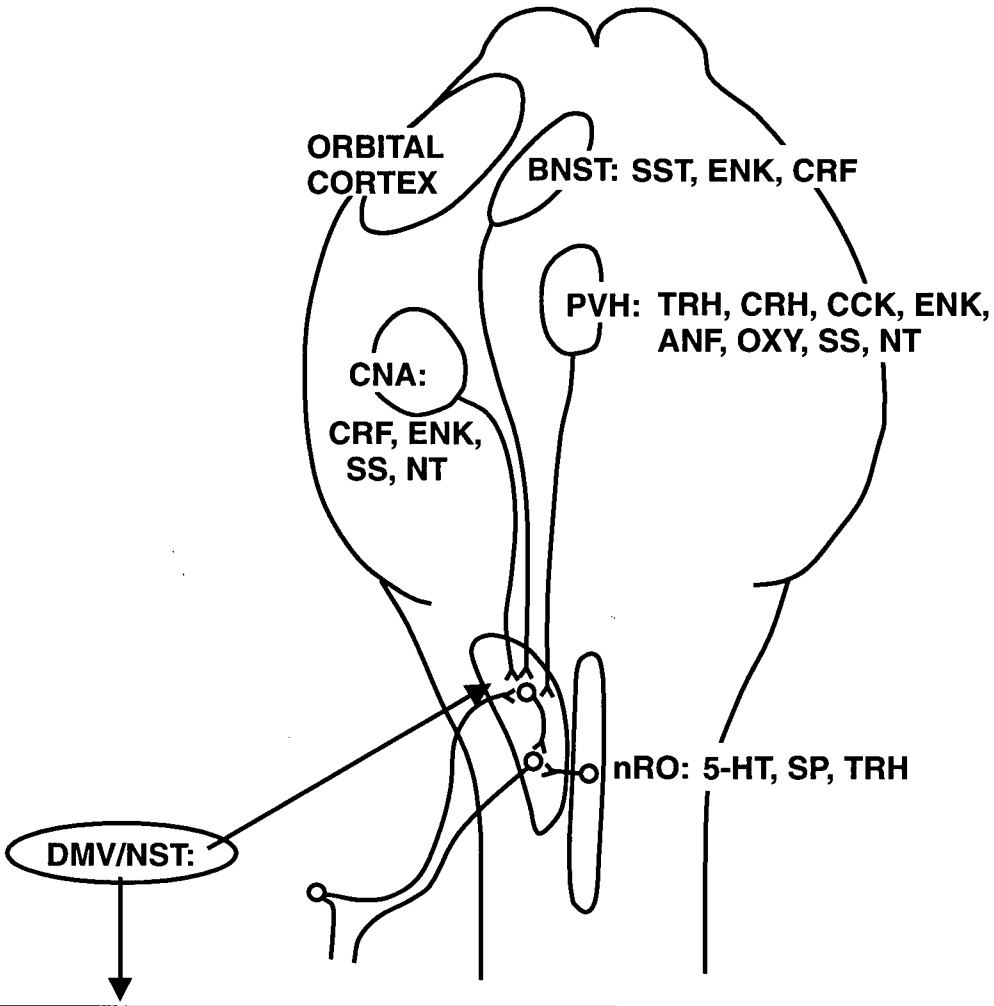

Adrenocorticotropin ACTH
α- and γ-melanocyte-stimulating hormone (MSH)
Angiotensin II
β-Endorphin
Bombesin (BN)
Calcitonin Gene-Related Peptide (CGRP)
Cholecystokinin (CCK)
Corticotropin-releasing hormone (CRH)
Dynorphins
Enkephalins
Galanin
Luteinizing hormone-releasing hormone (LHRH)
Neuropeptide Y (NPY)
Neurotensin
Oxytocin
Opioids
Phe-Met-Arg-Phe
Somatostatin (SS)
Substance P (SP)
Thyrotropin-releasing hormone (TRH)
Vasopressin
Vasoactive Intestinal Polypeptide (VIP)

Injection of endogenous neuropeptides into specific cerebral nuclei or the ventricular system can greatly affect gastric function (see Taché, 1987, Gillis et al., 1988 for a review). As a result of such studies, it is now believed that the CNS regulation of gastric function involves a delicate balance of interacting neuropeptides within the sensory and motor components of the DVC. Since a large number of neuropeptides can be found within the limbic and hypothalamic areas that are involved with gastrointestinal function, the possibility exists that specific gastrointestinal responses may be encoded by peptidergic projections from these and other CNS regions to the DVC.

Although peptide containing neural pathways from the aforementioned forebrain structures may modulate vagal control of the stomach either directly or indirectly, the mechanism by which the brain converts perceptions of the outside world into appropriate autonomic functions is poorly understood. However, using data from neuroanatomical tracing studies, a rough outline of how the brain may control gastric function by making appropriate autonomic changes to environmental cues is emerging. The orbital cortex, PVH, CNA and BST all receive a substantial amount of information from complex cortical sensory processing regions and from limbic structures associated with interpreting sensory inputs (Price, 1987). These areas also receive afferent input from visceral sensory relays in the NTS and parabrachial nuclei, and project efferents to the NTS and DMV. It has been proposed that the orbital cortex, PVH, CNA and BST thus form "executive" nuclei which monitor the state of the *milieu interieur* and perceived status of the organism in the environment and modify the autonomic responses that control gastric function accordingly (Rogers and Hermann, 1992).

In addition to the forebrain, the DVC also receives connections from several brainstem nuclei (Leslie et al., 1992). Neuroanatomical tracing studies have revealed that the caudal raphe nuclei and neurons in the adjacent reticular formation are sources of a significant amount of afferent input to the DMV and NTS (Taché et al., 1995). Although the role of the reticular formation in controlling gastric function is poorly understood at present, two raphe nuclei, the raphe obscurus (nRO) and raphe pallidus (nRPA), are emerging as important modulators of vagal gastrointestinal control circuits (Taché et al., 1995). Electrical stimulation of the nRO or nRPA causes a significant increase in gastric motility and secretion in rats (McCann et al., 1989; Yang et al., 1993). These effects are believed to be mediated via vagal pathways since they can be blocked by application of a peripheral muscarinic antagonist and by vagotomy (McCann et al., 1989; Yang et al., 1993). Futhermore, the electrical stimulation of the nRO and nRPA results in inhibition of neurons in the NTS (Rogers and Hermann, 1992). This would suggest that the nRO, like the PVH, may alter gastric functions by changing the excitability of NTS neurons which form the afferent limb of vago-vagal reflexes.

The neuropeptides thyrotropin-releasing hormone (TRH) and substance P (SP), as well as serotonin (5-HT), are colocalized within nRO and nRPA neurons that project to the DVC (Leslie and Hermann, 1992; Taché et al., 1995). Injection of TRH into the DMV has been shown to produce a significant increase in both motility and secretion (McCann et al., 1988). Electrophysiological experiments that have examined the effects of TRH on the DMV and NST have revealed that the peptide has opposing effects dependent on its site of action (Rogers et al., 1988). In the DMV, approximately 50% of neurons tested were stimulated by TRH and none were inhibited, whereas in the NTS,

50% were inhibited and none were stimulated. These differential effects on the DMN and NTS may be important to a general understanding of the central regulation of gastric functions.

Pharmacological studies indicate that injection of the SP antagonist CP-96,345 into the DMN potentiates gastric acid secretion induced by activation of the nRPA (Yang and Taché, 1992). Conversely, injection of the stable SP analogue, [pGlu^4,MePhe^8,MeGly^9]-SP (5-11), into the DMN decreases this effect (Yang and Taché, 1992). In light of these results, it has been proposed that SP may attenuate the excitatory effects of TRH within the DMV. Thus, the presence of multiple neuropeptides in central pathways that project to the DVC also raises the possibility of one peptide modulating the effect of another.

1.9. Neuropeptides present in the DVC

Over the past 25 years, a large number of neuropeptides have been characterized using immunological, biochemical and molecular biological techniques. The combination of these techniques with neuroanatomical tract tracing studies have revealed that brain nuclei that influence gastric function contain a variety of peptides. Furthermore, the use of pharmacological methods involving injection of peptides into various brain nuclei or the ventricular system have demonstrated that many of these have the potential to alter gastric function.

The DVC contains many peptides of intrinsic and extrinsic origin. Those found intrinsically are located in the somata and projections of NTS, AP and DMV neurons, while those that are extrinsic include afferent and efferent fibres terminating in the DVC

from other brain areas. Figure 7 provides a summary of the neuropeptides that have been identified within the DVC as well as in other brain areas that project to this region. Rather than attempting a comprehensive review of each, a brief overview will be provided that describes how peptides can influence gastric function by acting upon vagal components within the DVC. For detailed reviews of the distribution of neuropeptides within the DVC and associated references, please refer to Leslie, 1985 and Diz et al., 1987. Additionally, for reviews on the CNS actions of various peptides on gastric function, please refer to Taché, 1987 and Taché et al., 1990.

Peptides within the DVC can modify gastric vago-vagal reflexes by altering the excitability of interneurons within NTS or exert a direct effect on vagal efferent neurons within the DMV (Rogers et al., 1996). This can occur through synaptic interaction, local release or diffusion of peptides from remote sites (this concept of "nonsynaptic" transmission will be more thoroughly addressed in section 1.10). The proximity of the NTS and DMV to the cerebrospinal fluid bathing the fourth ventricle and their close association with the AP, provide routes through which circulating ligands (including peptides) can have access to receptors within the DVC.

Since the NTS is a relay station for a large number of sensory afferents from the periphery, and because it shares reciprocal connections with many brain locations, it is a primary target for control of vagal function via neuropeptide mechanisms. Many peptides of both intrinsic and extrinsic origin are found within the different subnuclei of the NTS in varying degrees of density. Vagal afferents projecting to the NTS have been found to contain substance P (SP), corticotropin releasing hormone and cholecystokinin (CCK) (Diz et al., 1987). As mentioned in section 1.8, central brain locations such as the PVH,

CNA and BST, as well as brainstem locations such as the nRO can contribute efferent inputs to the NTS which contain a number of different peptides, some of which can affect gastric function.

Kalia et al.. 1984 have demonstrated that distinct patterns of neuropeptide immunoreactivity exist for substance P, somatostatin, neurophysin II and enkephalins within the various subnuclei of the NTS, DMV and AP (Kalia et al., 1984). Within each subnucleus of the NTS, the neuropeptides located in the perikaryal region were different from those found in the corresponding dendritic zone. For example, within the ventrolateral subnucleus of the NTS, somatostatin is localised to the perikaryal region whereas SP and enkephalin are associated with dendrites in the adjacent ventral parasolitarius region. These results would indicate that different neuropeptides could serve independent functional effects on the soma and dendrites of neurons within different subnuclei of the NTS.

Although nerve fibres terminating in the DMV exhibit immunoreactivity for many neuropeptides, a more limited number have been found within the cell bodies within this nucleus. These include neurotensin, adrenocorticotropin (ACTH), Phe-Met-Arg-Phe (FMRF) and the enkephalins (Diz et al., 1987). Like the NTS, the DMV receives input from many brain locations (Leslie et al., 1992). Neuropeptide-containing fibres within the DMV could originate from these areas, or from interneurons within the NTS. The chemical coding of these fibres (i.e. diversity of neuropeptide content) could provide a mechanism for the central modulation of gastric motor outflow that is co-ordinated with environmental cues and behaviors, or could represent the communication of different vago-vagal reflexes.

The AP, which contains only a small number of cell bodies and fibres, is sparsely populated with neuropeptides. Some of the neuropeptides found within fibres that project to the AP include somatostatin, ACTH, enkephalins, neuropeptide Y (NPY), vasoactive intestinal polypeptide (VIP), SP and neurotensin (Leslie, 1985; Diz et al., 1987). In contrast, the only neuropeptides that have been identified within somata in the AP are cholecystokinin (CCK) and enkephalins (Diz et al., 1987).

Perhaps the most physiologically significant attribute of the AP is the presence of fenestrated capillaries within this region and a weak blood-brain barrier that permits peptides and other neuroactive substances in the blood and CSF to enter the DVC (i.e. via a "neuroendocrine" mechanism). Many of the substances injected intravenously or into the ventricular system in the brain act on vagal components within the NTS and DMV by entering these regions via the AP.

It has been demonstrated that many vagal functions involve more than one transmitter, and each transmitter is involved in more than one function. As illustrated in Table 1, several peptides can act centrally via vagally-dependent mechanisms to affect gastric secretion, motility and transit, and peptides such as TRH can participate in all of these functions. However, since some of these data come from the injection of peptides into the ventricular system, the precise site(s) of action for each of these peptides may not necessarily be within the DVC, but rather within other brain areas that project to this region.

Table 1. Some of the peptides that affect gastric function via a vagally-dependent mechanism. Results were obtained by monitoring gastric function following intracerebroventricular injection of each peptide, or injections into the DVC. (+) = stimulate; (-) = inhibit. Adapted from Taché, 1990.

SECRETION	MOTILITY	TRANSIT
TRH (+)	TRH (+)	TRH (+)
SS (+)	SS (+)	
BN (-)	BN (+)	BN (-)
CRF (-)	CRF (-)	CRF (-)
CGRP (-)		CGRP (-)
	CCK (-)	CCK (-)
oxytocin (+)	oxytocin (-)	
	neurotensin (-)	neurotensin (-)
	SP (-)	
opioids (-)		opioids (-)

Double-labelling experiments which combine neuroanatomical tracing and immunohistochemistry have provided information about the sources of peptidergic inputs to the DVC as well as the association of peptidergic nerve fibres with identified neurons. As described in section 1.8, the neuropeptide content of inputs from forebrain and brainstem regions that project to the DVC have been characterized using these techniques. Furthermore, the association of neuropeptides with gastric efferent neurons in the DMV have also been examined in this way. Buchan et al., 1991 demonstrated that gastric efferent neurons are surrounded by a high density of substance P immunoreactive fibres, and to a lesser extent, neuropeptide Y and CGRP immunoreactive fibres at the boundary of the DMV and NTS (Buchan et al., 1991). Similarly, the results presented in this thesis provide a detailed examination of the association of CGRP- and SP-immunoreactive nerve terminals with respect to identified gastric efferent neurons within the DMV.

The action of peptides within the DVC is dependent upon the presence and distribution of corresponding receptors within this region. Consistent with the immunohistochemical localization of various peptides within the DVC and the pharmacological effects produced by their injection into this region, binding sites for many of the peptides have been identified using a variety of techniques (Herkenham and McLean, 1986).

Many studies have used radiolabelled peptides to identify binding sites using autoradiographic techniques following ablation of afferent input to the NTS, retrograde degeneration of the DMV after cervical vagotomy or removal of both afferent and efferent DVC systems by nodose ganglionectomy (Diz et al., 1987). More recently, the

use of *in-situ* hybridization to detect the receptor mRNA and the availability of specific antisera against some of the peptide receptors has also facilitated their identification within the DVC. Using these techniques, it has been demonstrated that receptors or binding sites for numerous peptides including SP, TRH, CCK, insulin, PP, angiotensin II and NPY are localized within the DVC and that the action of the respective peptides binding to these receptors requires an intact vagal system (Palkovits, 1982; Diz et al., 1987; Elde et al., 1990; Manaker and Zucchi, 1993).

The presence of multiple receptor subtypes within the DVC could provide a further degree of functional specificity mediated by peptides within this region. This specificity could be achieved by a varied distribution of receptor subtypes and differential binding affinities for particular peptide ligands. Although multiple receptors for opiates, 5-HT, CCK and SP have been identified within the DVC, the potential for each of these to participate in specific gastric functions has not been examined in detail.

1.10. The Concept of Non-Synaptic Transmission

In 1906, Sherrington coined the term 'synapse' to describe the 'surface of separation' between neurons (Vizi, 1984). Since this time, it has become a statement of neurophysiology that this is the primary site for processing of neuronal information. Synapses are viewed as specialized structures for communication, consisting of a presynaptic axon terminal of the source neuron and a postsynaptic receptive region of a target neuron.

The concept of intercellular communication within the CNS has evolved in recent years. Since the mid-1960's, a growing body of evidence obtained from neurochemical,

morphological and pharmacological studies has led to the proposal that modes of communication other than those mediated by classical synaptic connections can occur within the CNS (see Vizi, 1984; Bach-y-Rita, 1993, 1995; and Zoli and Aganti, 1996 for reviews).

In light of the discovery and acceptance of new modes of neural communication, the precise definition of 'neurotransmitter' has also been the subject of debate and confusion (see Bach-y-Rita, 1993 for a review). The classical definition is very narrow, being restricted to a substance that participates in synaptic transmission. Schmitt, 1986 proposed that the term 'informational substances' should be used as it encompasses all neurochemicals capable of acting as intercellular messengers. Hoyle, 1979 preferred the term 'neuroactive substance' since this can be applied to any substance that is responsible for the transmission of information between neural components. Other authors have extended the term 'neurotransmitter' (or simply 'transmitter') to include substances that can be released by non-synaptic mechanisms, including peptides, amino acids and biogenic amines. It should be noted that some transmitters, such as peptides, are further classified as 'neuromodulators' based on their mode of action (Vizi, 1984; Bach-y-Rita, 1995).

Although many authors have suggested different names to describe the alternative modes of communication within the CNS (Bach-y-Rita, 1995; Zoli and Agnati, 1996), the terms "wiring transmission" (WT) and "volume" transmission (VT) proposed by Fuxe, Agnati and coworkers are those generally accepted to describe the primary conceptual categories for intercellular communication (see Fuxe and Agnati, 1991; Zoli and Agnati, 1996 for a review). Both WT and VT are complementary, and it is believed that most

neural systems use both mechanisms to achieve a wide array of functions. It is important to note that WT and VT are defined with respect to the modality of transmission and are neutral in terms of the source and target(s) of transmission and the informational substance that is transmitted. Some of the differences between WT and VT are presented in Table 2.

Table 2. Different types of Intercellular Communication in the Central Nervous System. WT=wiring transmission; VT=volume transmission; CSF=cerebrospinal fluid. Adapted from Zoli and Aganti, 1996.

Transmission type	Mode	Source:Target ratio	Source:Target distance	Source:Target delay
1. Gap junction	WT	1:1	2-3 nm	msec
2. Membrane juxtaposition (ephapsis)	WT	1:1	10 nm	msec
3. Closed synaptic transmission	WT	1:1	20-50 nm	msec
4. Paracrine transmission	VT			
A. Open synaptic transmission	VT	1:n, n>1-n>>1	100 nm-mm	msec-min
B. Non-synaptic source	VT	1:n, n>>1	1 μm-mm	sec-min
5. Endocrine-like transmission	VT			
A. Nerve-bundle-associated	VT	1:n, n>>1	mm	min
B. Paravascular fluid circulation	VT	1:n, n>>1	mm	min
C. Transmission in CSF	VT	1:n, n>>1	mm-cm	min

Wiring transmission refers to the cellular circuits based on classical synaptic transmission. In this scenario, intercellular communication is characterized by a single transmission channel made by cellular (neuronal or glial) structures with a region of discontinuity not larger than a synaptic cleft. This morphological arrangement provides a relatively stable connection for rapid communication of information between cellular components. Included in the WT framework are chemical synaptic-, gap junction- and membrane juxtaposition-mediated transmission (Zoli and Agnati, 1996).

In contrast, VT is characterized by the diffusion of chemical and electrical signals in a three-dimensional fashion in the extracellular fluid (ECF). Unlike the synaptic junctions in WT, the "transmission channels" in VT are generally not well-characterized. Volume transmission is a relatively slow mode for intercellular communication, but it allows for wider diffusion of signals and, in some cases, long lasting effects on large numbers of target cells (Fuxe and Agnati, 1991; Zoli and Agnati, 1996). Both paracrine- and endocrine-type communication have been classified as types of VT. Volume transmission may be the primary information transmission mechanism in certain mass, sustained functions, such as sleep, vigilance, hunger, brain tone and mood as well as in neuromodulation and plasticity mechanisms such as long-term potentiation (Bach-y-Rita, 1993).

The concept of "closed" and "open" synapses has been presented to further clarify the differences between WT and VT (Zoli and Agnati, 1996). Closed synapses are those that restrict the diffusion of transmitters, whereas open synapses favor diffusion. These two categories of synapses can be distinguished based on anatomical and functional criteria. Anatomically, three types of release sites can be found in presynaptic terminals:

synaptic, para-synaptic and non- (or extra-) synaptic (Golding, 1994; Zoli and Agnati, 1996). Synaptic terminals are identified by thickenings at the synaptic site. Para-synaptic terminals correspond to undifferentiated regions of the pre-synaptic membrane that lie adjacent to the postsynaptic cell. Non-synaptic terminals are characterized by areas of the terminal membrane that are in contact with elements (e.g. glia) that have no conventional synaptic relationship with the postsynaptic cell.

Functionally, mechanisms affecting transmitter diffusion from each of these types of presynaptic terminals are related to the characteristics of transmitter receptors, re-uptake sites and metabolic enzymes (this last point will be addressed more thoroughly in section 1.11). The extent to which transmitter diffusion can be restricted by each of these is based on their anatomical location and affinities for the transmitter. It has been demonstrated that some neurotransmitters can diffuse for long distances. For example, NPY (10 fmol/0.5 μl) can diffuse for more than 1 mm when injected into the striatum and hypothalamus of the rat (Fuxe and Agnati, 1991). In this case, the diffusion was anisotropic, revealing that properties of the ECF matrix may also control the spreading of transmitters after their release.

In order for chemical transmission to be fulfilled, the concentration of the transmitter in the vicinity of the receptor must be high enough in order to activate the receptor. In this regard, the amount of transmitter that is released and the location and affinity of corresponding receptor(s) are of major importance. Synapses containing multiple transmitters can act as an open synapse for one transmitter and a closed synapse for another. Thus, the prevalence of open vs. closed synapses within a given anatomical

framework depends on the affinity and density of intra- vs. extra-synaptic receptor populations.

Although peptidergic synapses are not as well characterized as synapses associated with classical transmitters, several lines of evidence suggest that in most instances, anatomical arrangements and functional mechanisms favour the release of peptides via open synapses. Neuropeptide receptors, which are typically linked to G-proteins and are of very high affinity, are mainly located in non-synaptic regions (Dana et al., 1989; Liu et al., 1994; Shigemoto et al., 1993). Within varicosities of nerve terminals, peptides are stored in large dense-core vesicles typically located in para- or non-synaptic areas from which they can easily reach the extracellular space (Thureson-Klein et al., 1986; Matteoli, 1991; Golding, 1994).

The potential for peptides to be released from open synapses is consistent with their role as 'neuromodulators' (Vizi, 1984; Bach-y-Rita, 1995). Unlike neurotransmitters (such as Ach and catecholamines) which act locally within the synaptic cleft to affect the excitability of the postsynaptic cell or presynaptic membrane, neuromodulators are transmitters that can be released from either synaptic or non-synaptic sites to modify synaptic transmission, conduction of nerve impulses or cellular excitability (Florey, 1979). In many cases, neuromodulators are co-released with classical transmitters from the same nerve terminals (Nicoll, 1988; Lundberg, 1991).

Like classical neurotransmitters, neuromodulators depend on the presence of pre- or postsynaptic receptors to exert their effect. Neuromodulators usually produce a long lasting effect (as described above for peptides) as compared to the short, phasic nature of neurotransmitters acting within closed synapses. There are, however, situations in which

classical synaptic transmitters can act as neuromodulators (e.g. noradrenaline in the coerulean system of the rat; Bach-y-Rita and Smith, 1993) and where substances such as peptides, amino acids and amines can act as synaptic transmitters (e.g. Substance P in the prevertebral ganglia of the guinea pig; Konishi et al., 1985, and 5-HT in the raphe nuclei, Cooper et al., 1986).

In light of the structural and functional organization of the DVC, it is likely that the vagal control of gastric function within this region consists of both WT and VT mechanisms. As mentioned in section 1.9, a large number of peptides and other transmitter substances have been identified with the DVC that originate from peripheral, brainstem and forebrain inputs, as well as intrinsic components such as interneurons in the NTS. Detailed structural analyses have revealed the presence of both synaptic structures as well as unspecialized terminal endings such as peptide-containing varicosities within the DVC. Recent data (such as that presented in this dissertation) have identified mismatches between transmitters and receptors within this region. Furthermore, it has been shown that some receptors can be located in both synaptic and non-synaptic regions on DVC neurons and nerve fibres. As mentioned in section 1.7.4, the absence of a blood-brain barrier in the AP permits transmitter substances from the blood and ECF to penetrate into the DVC where they can exert an effect on vagal afferent and efferent components. Therefore, vagal regulation of gastric function within the DVC could be influenced by classical synaptic transmission as well as by the non-synaptic action of neuromodulators.

1.11. Metabolism and Inactivation of Neuropeptides

As described above, neuropeptide transmission within the CNS is characteristically of slower onset and longer duration than the effects elicited by classical neurotransmitters. Furthermore, neuropeptides are typically released from open synapses and can diffuse over large distances to bind to target receptors. Because of these spatial and temporal characteristics, peptidergic signals may be largely governed by the distance travelled before being inactivated.

The mechanisms responsible for inactivation of neuropeptides include cleavage within the extracellular fluid by serum proteases, diffusion away from the receptor, extra- or intracellular enzymatic degradation or covalent modification once bound to the receptor and receptor internalization and recycling (Krause, 1985; McKelvy and Blumberg, 1986).

Since most studies to date have examined the inactivation and metabolism of neuropeptides that are released within the framework of closed synapses, membrane-bound peptidases have been the focus of much study. However, several peptidases have been identified within the ECF (including blood and CSF) that could potentially act on neuropeptides. These include serum cholinesterase (EC 3.1.1.8), angiotensin-converting enzyme, dynorphin-converting enzyme, substance P endopeptidase, endopeptidase-24.11 (EC 3.4.24.11) (Krause, 1985; Terenius and Nyberg, 1991). The importance of these peptidases depends on whether peptide concentrations within the ECF are within the affinity range of the enzymes. Since the affinity of most of these enzymes for substrates is low (Terenius and Nyberg, 1991), it is likely that at physiological levels, neuropeptides

would not be degraded. Thus, although a serum peptidase may be able to cleave a particular peptide *in vitro*, this cannot be taken as evidence for a role *in vivo*.

As is evident in the names of some of the CSF enzymes listed above, some of these are known to have a "converting" role whereby they can cleave peptides into fragments that have altered biologic activity. These enzymes are also responsible for the conversion of some peptides from an inactive to an active form. It has been hypothesized that these enzymes (and others that are found in the CSF) are stored along with neuropeptides or their precursors in large dense-core vesicles (LDVs) and all of these are released into the ECF on nerve activation (Terenius and Nyberg, 1991). Therefore, in addition to their possible function of degrading peptides, enzymes present in the ECF may also act as modifiers of peptide transmission by increasing bioactivity.

Most enzymes that have been implicated in the degradation of neuropeptides have a wide substrate specificity (McKelvy and Blumberg, 1986; Schwartz et al., 1991). A current view is that there exists only a small number of enzymes that are able to act on a wide variety of peptidergic signals, perhaps on the basis of quantitative differences in activity due to the different "chemistries" of the signals (Loh, 1984; McKelvy and Blumberg, 1986). For example, it has been demonstrated that conformational factors, especially those directed by hydrophobicity forces, greatly affects the susceptibility of peptides to hydrolysis by peptidases (Hersh, 1980; Hui et al., 1983) When assessing whether or not a particular peptidase is involved in the physiological inactivation of a particular neuropeptide, the substrate specificity and, more importantly, the localization of the enzyme with respect to peptide-releasing nerve regions must be considered (Schwartz et al., 1991).

Although much has been published concerning the enzymatic hydrolysis of neuropeptides in a variety of preparations, including crude brain homogenates and purified enzymes, the relevance of these results to the *in vivo* state remains unclear.

1.12. Calcitonin Gene Related Peptide

Calcitonin gene-related peptide (CGRP) is a 37 amino acid peptide that is a product of tissue-specific, alternative splicing of RNA encoded by the calcitonin gene (Figure 8). In thyroidal "C" cells, the primary gene transcript is spliced into mRNA encoding the precursor protein of the peptide hormone calcitonin, whereas in neural systems, the transcript is spliced into mRNA encoding the CGRP precursor protein (α-CGRP) (Amara et al., 1982).

CGRP is expressed in a variety of neuronal structures in both the central and peripheral nervous systems, as well as in endocrine cells (Rosenfeld et al., 1983; Goodman and Iversen, 1986). This wide distribution provides a morphological basis for a number of biological effects. CGRP is a powerful vasodilator and has been implicated in neurogenic inflammation and nociception (Goodman and Iversen, 1986). Other biological effects include the modulation of nicotinic receptor activity at the neuromuscular junction, a reduction of gastric acid secretion, cardiac acceleration, regulation of calcium metabolism and insulin secretion, an increase in body temperature and a decrease in food intake (see Quirion et al., 1992 for refs.).

Figure 8. Model of tissue-specific production of CGRP by alternative splicing of the calcitonin gene (from Rosenfeld et al., 1992).

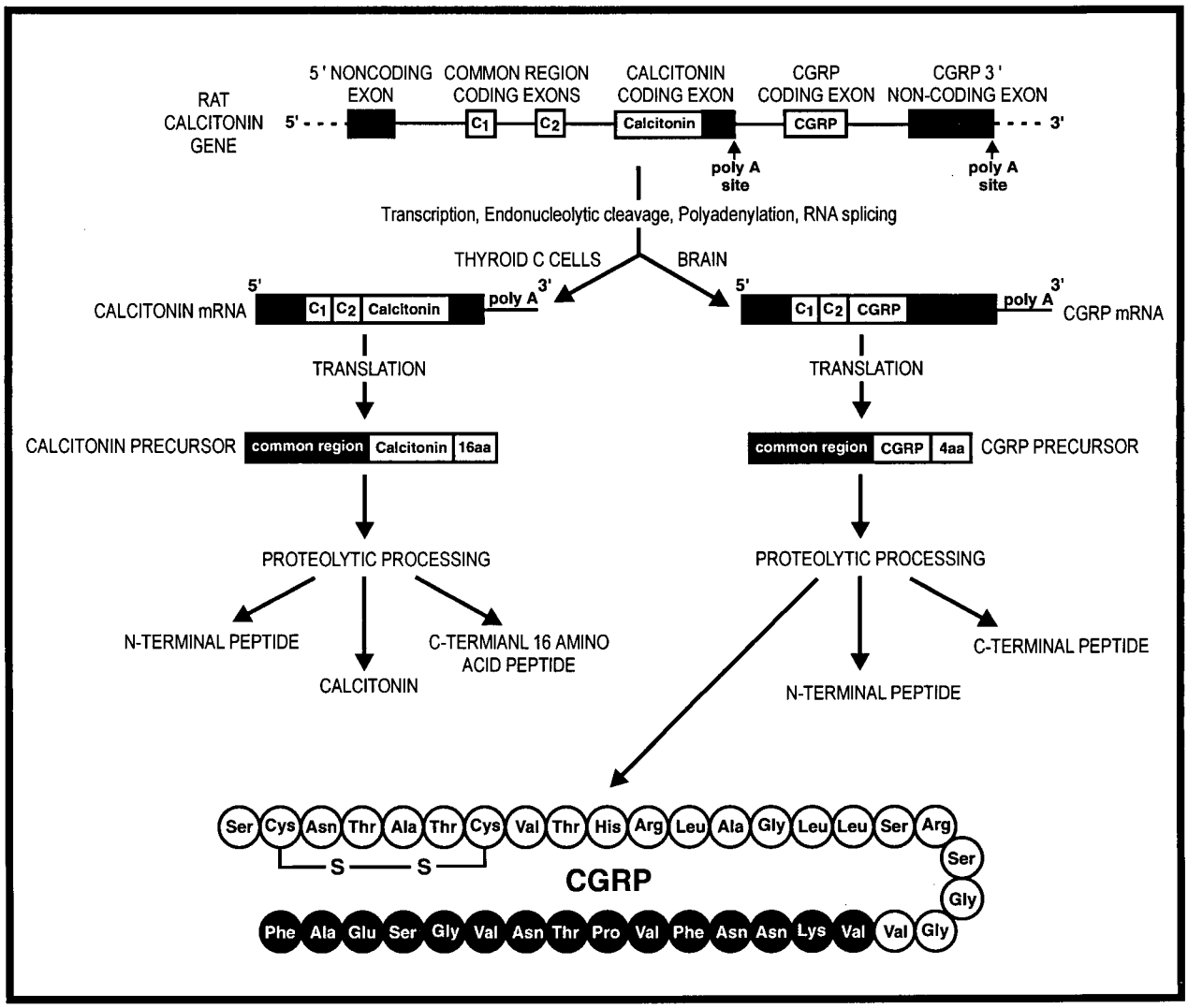
RAT CALCITONIN GENE
5' NONCODING EXON
COMMON REGION CODING EXONS
CALCITONIN CODING EXON
CGRP CODING EXON
CGRP 3' NON-CODING EXON
5'
C1
C2
Calcitonin
CGRP
3'
poly A site
poly A site
Transcription, Endonucleolytic cleavage, Polyadenylation, RNA splicing
THYROID C CELLS
BRAIN
CALCITONIN mRNA
poly A
CGRP mRNA
TRANSLATION
TRANSLATION
CALCITONIN PRECURSOR
common region
16aa
CGRP PRECURSOR
4aa
PROTEOLYTIC PROCESSING
PROTEOLYTIC PROCESSING
N-TERMINAL PEPTIDE
C-TERMIANL 16 AMINO ACID PEPTIDE
CALCITONIN
N-TERMINAL PEPTIDE
C-TERMINAL PEPTIDE
Ser Cys Asn Thr Ala Thr Cys Val Thr His Arg Leu Ala Gly Leu Leu Ser Arg
S S
CGRP
Ser
Gly
Phe Ala Glu Ser Gly Val Asn Thr Pro Val Phe Asn Asn Lys Val Val Gly

CGRP has a widespread distribution in the rat brain where it has been localized to both neuronal cell bodies and fibres using immunohistochemistry (Kawai et al., 1985 and Skofitsch and Jacobowitz, 1985). In the DVC, CGRP-IR cell bodies have been identified within the NTS. In addition, CGRP-IR has been reported within motoneurons of all of the cranial nerves (including the occulomotor, trochlear, trigeminal, facial, hypoglossal and nucleus ambiguus), with the exception of the DMV.

The density of CGRP-IR fibres differs in various areas of the rat brain (Kawai et al., 1985; Skofitsch and Jacobowitz, 1985). In the lower brain stem, a high concentration of CGRP-IR fibres has been reported in many regions including the sensory trigeminal areas, the parabrachial nucleus, the superior olive and parts of the vestibular nuclei. CGRP-IR nerve fibres have also been reported within the NTS and DMV (this will be discussed in more detail below).

It is now well established that CGRP is colocalized with SP in sensory neurons (see Hökfelt et al., 1992 for refs.) At the ultrastructural level, it has been demonstrated that CGRP and SP are present within the same large, dense-core vesicles in peripheral and central nerve endings of primary sensory neurons and in their cell bodies in the dorsal root ganglia (Gulbenkian et al., 1986; Merighi et al., 1988). There is evidence to suggest that CGRP may have an inhibitory effect on a substance P endopeptidase, and thus may prolong the actions of SP in nociceptive responses by preventing its breakdown (Le Greves et al., 1985).

Two receptor subtypes have been identified for CGRP, designated $CGRP_1$ and $CGRP_2$ (Quirion et al., 1992). These receptors are distinct from those for calcitonin, and

are differentiated in terms of their binding affinities for CGRP analogues and C-terminal fragments of the peptide.

Within the rat forebrain, high densities of CGRP receptors have been found in several regions including the cerebellum, hypothalamic nuclei, central gray matter, nucleus accumbens, amygdala, caudal stiatum, substantia nigra and ventral tegmental area (Kawai et al., 1985; Skofitsch and Jacobowitz, 1985b). In the DVC, CGRP-IR nerve fibres have been detected within the NTS of several species, including cat (Torrealba, 1992), pigeon (Berk et al., 1993), monkey (Christopolous et al., 1995), human (Fodor et al., 1994) and rat (Rosenfeld et al., 1983; Kawai et al., 1985; Buchan et al., 1991, Sykes et al., 1994).

CGRP-IR cell bodies have also been detected within the rat NTS, but only in studies that have used colchicine (e.g. Kawai et al., 1985 and Skofitsch and Jacobowitz, 1985). Since this compound is known to disrupt microtubules, it inhibits the axoplasmic transport of neuropeptides from the nucleus to the nerve terminals (Boyer et al., 1992). This permits the consequent rise in neuropeptide concentration in the cell body to be detected using a method such as immunocytochemistry. Interestingly, in other studies which did not use colchicine, no CGRP-IR somata were observed within the NTS although they were detected in the nearby hypoglossal nuclei (Buchan et al., 1991, Sykes et al., 1994). This may suggest that, if present within interneurons in the NTS, CGRP is normally expressed at very low levels. No projections from the hypoglossal nuclei to the NTS were observed in these latter studies.

Data from studies employing pharmacological, electrophysiological and surgical techniques in the rat suggest that the central action of CGRP to inhibit gastric acid

secretion is mediated through vagal pathways. Microinjection of picomole quantities of CGRP into the DVC inhibits gastric acid secretion that is stimulated by pentagastrin or by the vagal stimulant baclofen (Goto et al., 1985; Ishikawa and Taché, 1989). Furthermore, the inhibition of pentagastrin-stimulated acid secretion induced by CGRP injection into the CSF is abolished after vagotomy (Taché et al., 1984; Lenz et al., 1985). Additionally, intracisternal injection of CGRP has been demonstrated to induce dose-related inhibition of unit efferent discharges recorded from the gastric branch of the vagus nerve (Wei and Taché, 1990). It has been speculated that the antisecretory effect of centrally administered CGRP is due to a diminished cholinergic and histaminergic input to the parietal cells in the stomach, since gastric vagal outflow is decreased.

It should be noted that peripheral adminstration of CGRP by intravenous injection also results in an inhibition of gastric acid secretion in rat. However, the mechanism by which this occurs is completely separate from the centrally mediated effect. CGRP antiserum injected intravenously at a concentration that prevented the antisecretory effect of peripheral intravenous administration of CGRP did not alter the inhibitory effect on the same dose injected into the CSF (Lenz et al., 1984). Furthermore, the antisecretory effect of intravenously administered CGRP is not vagally mediated or related to changes in prostaglandin synthesis, gastrin secretion or mucosal blood flow. Instead, there is convincing evidence that part of the antisecretory effect attributable to peripheral CGRP administration is mediated through somatostatin release from the stomach, and by a decrease in cholinergic input through an action on the enteric nervous system (Helton et al., 1989; Ren et al., 1992).

1.13. Substance P and the NK-1 Receptor

Of all neuropeptides, substance P (SP) has the longest history. It was originally detected in 1931 by von Euler and Gaddum in the gut as a hypotensive factor that was distinct from acetylcholine and resistant to atropine (Turner, 1986). It was named 'substance P' by Gaddum simply on the basis of being isolated as a white powder ('P' for 'Pulver'), and the name has remained unchanged to this day.

Although SP was identified as a sensory transmitter in 1953 by Lembeck, relatively little work was done on this peptide until it was isolated and characterized by Chang and Leeman in 1971 (Leeman, 1991). These studies revealed that SP is a polypeptide of 11 amino acids (Figure 9a). It has since been demonstrated that SP has a similar structure to the molluscan salivary gland peptide eledoisin and amphibian skin peptides such as kassinin and physalaemin, a group of peptides generically referred to as tachykinins. These peptides share a common C-terminal sequence, and exhibit similar biological activities including reduction of blood pressure (i.e. via vasodilation), smooth muscle contraction, salivation and stimulation of glandular secretion (Turner, 1986).

In the 1980's, four additional mammalian tachykinins were discovered. The first two novel tachykins were given various names, but are now unambiguously termed neurokinin A (NKA, formerly: substance K, neuromedin L and neurokinin α; Minamino et al., 1984; Nawa et al., 1984) and neurokinin B (NKB, formerly: neuromedin K and neurokinin β; Maggio and Hunter, 1984). The two most recent tachykinins to be discovered are neuropeptide K and neuropeptide-γ (Kage et al., 1988; Maggio, 1988). These peptides are both N-terminally extended forms of NKA. The five known mammalian tachykinins are derived from two peptide precursor genes: the

preprotachykinin A and B (PPT-A and PPT-B) (Krause et al., 1987). The PPT-A gene encodes the precursors common to SP and NKA, whereas the precursor for NKB is produced by the PPT-B gene. The expression of both genes is closely associated with alternative RNA processing, which is responsible for the formation of multiple species of mRNAs in a tissue-specific manner (Nawa et al., 1984; Kotani et al., 1986).

Three general types of tachykinin receptors have been described based upon current pharmacological, biochemical and molecular characterization techniques (Regoli et al., 1987; Ohkubo and Nakanashi, 1991; Burcher et al., 1991; Mussap et al., 1993). These receptors have been named NK-1, NK-2 and NK-3 (where "NK" designates neurokinin; "r" will be appended to these abbreviations to designate "receptor"). The assumed endogenous ligands for these receptors are SP, NKA and NKB, respectively. In the absence of selective antagonists, the classification of tachykinin receptors was based upon the rank order of potency of tachykinins; that is, at the NK-1r, SP>NKA>NKB, at the NK-2r, NKA>NKB>SP, and at the NK-3r, NKB>NKA>SP.

Cloning and sequencing of the tachykinin receptors revealed that they are single polypeptide chains consisting of seven hydrophobic transmembrane-spanning domains with an extracellular amino terminus and intracellular carboxy terminus (Figure 9), structural features that are characteristic of the G protein-coupled receptor superfamily (see Trumpp-Kallmeyer et al., 1994 for refs.). In the case of the NK-1r, evidence suggests that this receptor is coupled to a pertussis toxin-insensitive G protein (either Gq or G_{11}) which is positively coupled to phospholipase C (MacDonald et al., 1996). Activation of this enzyme catalyzes the hydrolysis of inositol phospholipids into

Figure 9. (A) Chart of known mammalian tachykinins (from Burcher et al., 1992).
(B) Schematic of the rat NK-1 receptor (adapted from Hershey et al., 1992).

A

Substance P	Arg-Pro-Lys-Pro-Gln-Gln-Phe-Phe-Gly-Leu-Met-NH_2
Neurokinin A	His-Lys-Thr-Asp-Ser-Phe-Val-Gly-Leu-Met-NH_2
Neurokinin B	Asp-Met-His-Asp-Phe-Phe-Val-Gly-Leu-Met-NH_2
Neuropeptide K	Asp-Ala-Gly-His-Gly-Gln-Ile-Ser-His-Lys-Arg-His-Lys-Thr-Asp-Ser-Phe-Val-Gly-Leu-Met-NH_2
Neuropeptide γ	Asp-Ala-Asp-Ser-Ser-Ile-Glu-Lys-Gln-Val-Ala-Leu-Leu-Lys-Ala-Leu-Tyr-Gly-His-Gly-Gln-Ile-Ser-His-Lys-Arg-His-Lys-Thr-Asp-Ser-Phe-Val-Gly-Leu-Met-NH_2

B

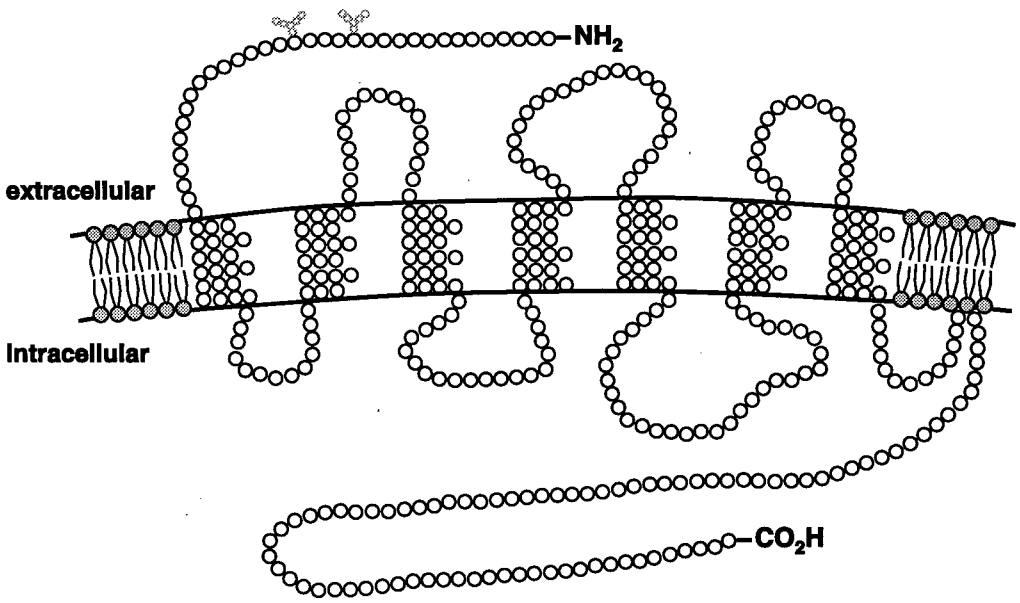

diacylglycerol and inositol phosphates, with a resulting mobilization of intracellular calcium (Abdel-Latif, 1986; Sugiya et al., 1988).

Substance P is widely expressed in the central and peripheral nervous systems where it elicits excitatory effects as a neurotransmitter or neuromodulator (see Otsuka and Yoshioka, 1993 for a review). In the periphery, SP has been colocalized with CGRP within the same large, dense core secretory vesicles in primary sensory neurons (see section 1.12). Some of the biological actions of SP include sensory perception (e.g. olfaction, vision, audition and nociception), movement control, gastric motility, vasodilation, salivation and micturation (Pernow, 1983; Maggi et al., 1987). These diverse effects can be attributed to the activation of NK-1 receptors that are widely distributed throughout the nervous system and peripheral tissues (Hershey et al., 1992).

Within the rat CNS, SP has been localized to both neuronal cell bodies and fibres using immunohistochemistry (Cuello and Kanazaw, 1978; Ljungdahl et al., 1978; Shults et al., 1984). These studies reported high densities of SP-IR nerve terminals in sensory nuclei and other non-sensory structures such as thalamus, hypothalamus and extrapyramidal system. The highest density of SP-IR fibres and nerve terminals was reported in the substantia nigra. Cell bodies that were immunoreactive for SP were found in regions such as the amygdala, septal nuclei, nucleus accumbens and raphe nuclei.

Substance P-IR has also been reported in the rat DVC, where it was localized to axonal fibres and bouton-like swellings using immunocytochemistry (Kalia et al., 1984; Kawano and Chiba, 1984; Thor et al., 1988; Buchan et al., 1991; Tallaksen-Greene et al., 1993; Sykes et al., 1994). Most studies reported at least a moderate density of SP-IR nerve fibres at all levels of the DVC, with the majority of these confined to the NTS and

DMV. Few SP-IR fibres have been reported in the AP. SP-IR cell bodies have been reported in the NTS, but only when colchicine was used (e.g. Shults et al., 1984). SP-IR has also been detected within the DVC of many other species, including cat (Baude et al., 1989; Baude et al., 1992), dog (Block et al., 1987), human (Rikard-Bell et al., 1990; Huang et al., 1993; Fodor et al., 1994) and pigeon (Berk et al., 1993).

The results of previous studies would suggest that all three tachykinin receptors types are present within the rat DVC. Surveys of the general distribution of NK-1r within the rat brain using *in situ* hybridization have reported this receptor within the DMV and NTS (Elde et al., 1990; Kiyama et al., 1990; Maeno et al., 1993). The presence of NK-1r and NK-2r within the DMV has also been implied using specific pharmacological agonists for these receptor subtypes (Martini-Luccarini et al., 1996). Finally, the distribution of NK-3r within the DVC was recently reported using an antibody to this receptor (Carpentier and Baude, 1996).

Within the CNS of the rat, there appears to be no consistent correlation between the density and distribution of SP innervation (as revealed by immunocytochemistry) and SP-binding sites (as revealed by autoradiography) (Shults et al., 1984; Mantyh et al., 1984). These studies revealed that there were some regions which had a striking mismatch between distribution of SP-IR and SP-binding sites. For example, the substantia nigra, which contains the highest density of SP in the rat brain possessed few SP-binding sites, whereas the cerebral cortex, which contains a very low density of SP contains a very high density of SP-binding sites. Similar results were obtained when the distribution of SP-IR was compared to that of the NK-1r as identified by *in situ* hybridization (Kiyama et al., 1993; Maeno et al., 1993).

In addition to the mismatch between SP and its receptor in terms of general distribution within various brain regions, there is now evidence to suggest that there is a discrepancy between the distribution of these structures at the cellular and subcellular levels. Using immunocytochemistry, the NK-1r has been detected on most of the surface membrane of neurons in areas such as the spinal cord, cortex and striatum, even in cellular regions that are not directly apposed by SP-containing terminals (i.e. non-synaptic localization of receptor) (Liu et al., 1994). These results indicate a distinct distribution of peptide/receptor that differs from "classical" synapses where receptors are situated in direct apposition to the site of neurotransmitter storage and release.

1.14. Thesis Investigation

The hypothesis investigated by the studies described in this thesis was that SP and CGRP can act on gastric efferent neurons within the DVC via a nonsynaptic, volume transmission mechanism.

Chapter 2 provides an overview of the experimental procedures that were used, including retrograde tracing, immunocytochemistry and confocal microscopy.

Chapter 3 describes experiments which established a general procedure for the three-dimensional (3-D) reconstruction of neuropeptide-immunoreactive (IR) nerve terminals and identified neurons. These techniques were used to examine the spatial relationship of CGPR-IR nerve fibres to retrogradely-labelled gastric efferent neurons in the DVC of the rat.

Chapter 4 deals with the spatial relationship of SP, NK-1r and identified gastric efferent neurons within the DVC. Initial studies examined the gross distribution of SP

and the NK-1r with respect to identified neurons at different rostrocaudal levels of the DVC. Later studies built upon the methodology established in Chapter3, and examined the 3-D spatial relationship of peptide and receptor with respect to individual identified neurons.

Chapter 5 describes studies which examined the spatial relationship of the enzyme neutral endopeptidase-24.11 with respect to SP, NK-1r and identified gastric efferent neurons in the DVC. These studies were undertaken to determine if the endopeptidase was expressed on the cell membrane of the NK-1r-IR neurons.

Chapter 6 discusses the results of Chapters 3, 4 and 5 and relates the findings to the potential for volume transmission within the DVC of the rat.

Chapter 7 summarizes the findings of this dissertation and suggests possible lines of future research.

2. GENERAL METHODS

2.1. Animals

All experimental procedures were performed on male Wistar rats with an initial weight of 175-250g. Treatment of rats was in accordance with The Guide to Animal Care and Use of Experimental Animals, Vol. 1-2, Canadian Council of Animal Care, 1980. The animals were obtained from the breeding colony at the Animal Facility, University of British Columbia. The rats were maintained in the Department of Physiology Animal Facility with a 12 h light/dark cycle.

2.2. Retrograde tracing

Rats were anesthetized using an intraperitoneal injection of sodium pentobarbital (60 mg/kg). Under anesthesia, the abdominal cavity was opened by a 1 inch midline incision. The stomach was located and gently exteriorized using blunt-ended forceps. The retrograde tracer to be used was injected directly under the serosal surface along the length of the greater curvature of the stomach (corpus) using a 10 µl Hamilton syringe. The preparation and volumes used varied between tracers (Table 3). The injections were located between the epiploic veins and were spaced such that all incoming efferents would be labelled (Donahue et al., 1988, Okumura and Namiki, 1990). The placements of the injections is diagrammed in Figure 10.

Figure 10. Placement that was used for the injection of retrograde tracer along the greater curvature of the rat stomach. Dotted lines indicate the approximate position of gastroepiploic arteries.

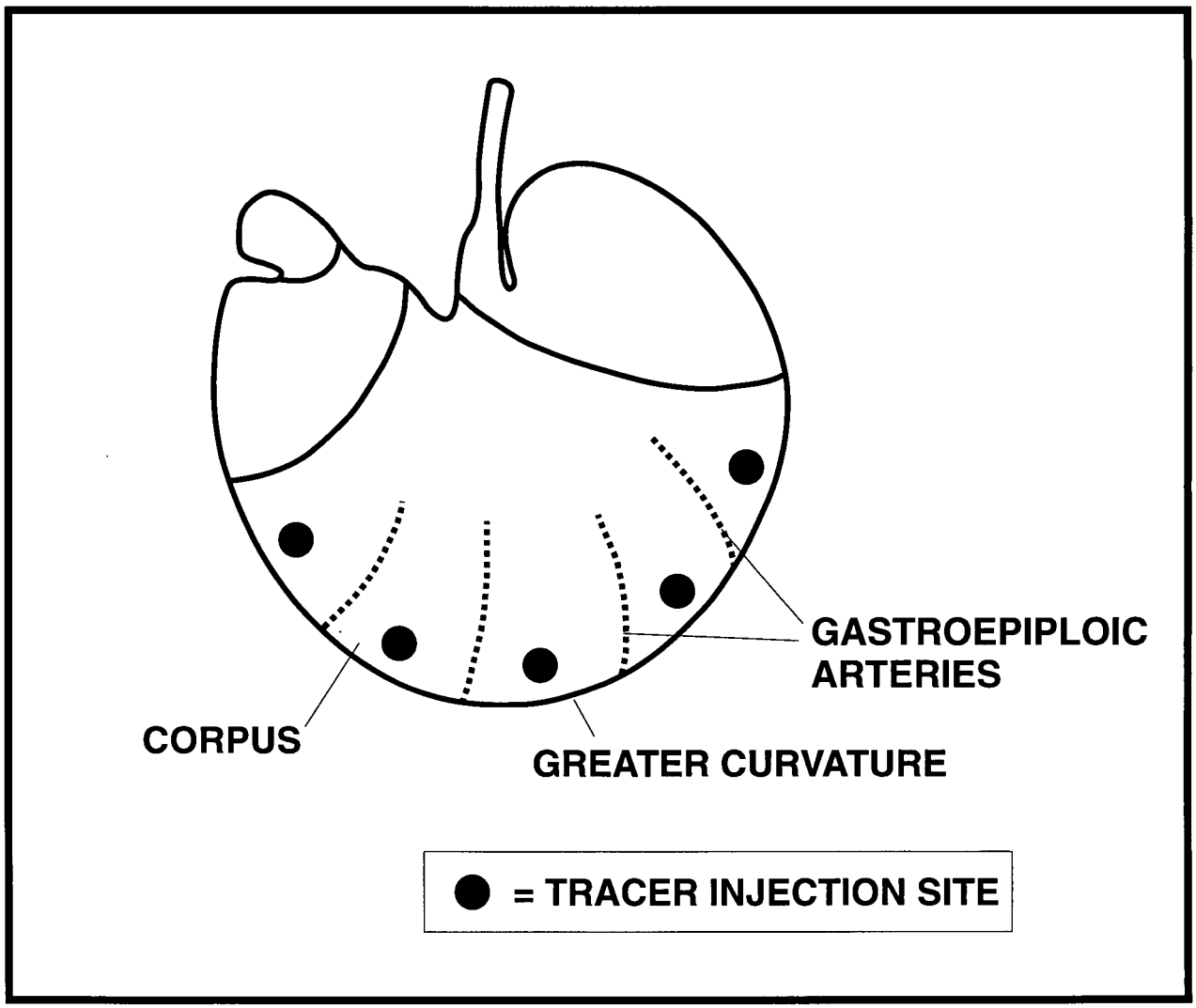
GASTROEPIPLOIC
ARTERIES
CORPUS
GREATER CURVATURE
= TRACER INJECTION SITE

Following the injections of the tracer, the stomach was carefully placed back into the abdominal cavity through the small incision. The muscle layer of the midline incision was closed using 3-0 suture thread. Finally, the skin layer was held together using steel sutures, and the animals were allowed to recover under heat lamps. The animals were maintained for a few days to one week, depending on the neuronal tracer used, (Table 3) to permit time for transport of the tracer from the injection sites to the vagal efferent perikarya in the brainstem. A number of precautions were taken to prevent and assess the amount of leakage of tracer from the injection sites, and this is addressed in a separate section below.

Two retrograde tracers were tested for use in the experiments described: Fluoro-Gold and cholera toxin B-subunit (CT-B). Each of these compounds achieve uptake and transport via different mechanisms. Furthermore, the type and extent of labelling of identified neurons also differed for each tracer.

2.2.1. Fluoro-Gold

Fluoro-Gold (FG) has gained widespread acceptance and use as a retrograde tracer due to its high resistance to fading, lack of diffusion from labeled cells and its compatibility with immunocytochemistry (Schmued and Fallon, 1986). The spectral properties of FG have been previously characterized in detail (Wessendorf, 1991). Briefly, FG contains at least two major fluorescent components, both being maximally excited within the ultraviolet range. One has a maximal excitation wavelength of 365 nm and emits with maxima at 448 nm and 582 nm. The second component is maximally excited at around 312 nm and emits maximally at 407 nm.

It is now known that the compound in FG that is responsible for its retrograde labelling of cells is hydroxystilbamidine (Wessendorf, 1991). Chemically, this compound is a weak base, and diffuses across cell membranes in an uncharged form and is trapped in lysosomes and endosomes by the pH gradient (Wessendorf, 1991). This diffusion mechanism would suggest that FG could be taken up by undamaged axons of passage, however, the amount of uptake appears to be system dependent (Schmued and Fallon, 1986; Dado et al., 1990).

In the context of the current experiments, injection of FG under the serosal surface along the greater curvature of the stomach produced bilateral labelling of neurons within the DMV in the rat brain stem. Other studies have demonstrated that FG injected into the stomach using similar strategies produced comparable results (Yoshida et al., 1988a,b; Sugitani et al., 1991; Buchan et al., 1991). Since vagal efferents are the only fibres within the stomach wall that project retrogradely to the DMV, labelling of other nerve fibres in the immediate vicinity of the injection sites was not of consequence. The potential for non-specific labelling due to uptake by fibres of passage was more related to leakage of the tracer and uptake by surrounding organs that are innervated by the vagus.

The concentration and volume of FG that was injected into the stomach, as well as the survival time following injection of the tracer (Table 3) are in accordance with established protocols (Yoshida et al., 1988a,b; Sugitani et al., 1991; Buchan et al., 1991; Bentivoglio and Chen, 1993). Initial trials that varied the allowed transport time (7, 14 or 21 days) for FG revealed no differences in the number or brightness of labelled somata within the DMV. This provided some flexibility when scheduling perfusion/fixation of animals used in these studies. These results are in accordance with previous studies that

found that increasing survival time and/or concentration of FG used had little effect on the brightness of labelled neurons (Skirboll et al., 1989).

Contrary to previous reports, FG rarely produced good filling of the dendritic processes of retrogradely labelled neurons. Most frequently, only the primary projections of the labelled neurons could be observed, with fluorescence decreasing with increasing distance from the soma. When an antiserum to FG was used (Freedman and Yi, 1993; obtained from Chemicon, Temecula, CA) in combination with a secondary biotinylated antibody followed by avidin-fluorescein, greater morphological detail of the dendrites could be observed (for details, see section 3.3.2). Even in these instances, however, no better than second order dendrites of the retrogradely labelled neurons could be resolved.

Although FG produced reliable retrograde labelling of gastric efferent neurons in the DMV following its injection into the stomach, some problems were encountered when screening the brainstem sections. For example, neurons that were intensely labelled with FG could be observed in the fluorescein isothiocyanate (FITC) emission wavelength. Furthermore, for experiments using confocal microscopy, FG could not be detected directly due to the lack of a laser capable of exciting within the ultraviolet wavelength range. Although a rabbit antiserum to FG could be used in combination with an alternative fluorophore to circumvent this limitation in the initial studies with CGRP (see Chapter 3), this was not possible for studies involving NK-1r, since the antiserum to this receptor was also raised in rabbit. Therefore, although FG was used initially, later experiments made use of unconjugated cholera toxin B-subunit, which was found to provide better dendritic labelling and more flexibility when used in multilabelling experiments.

Table 3. Summary of the strategies employed for the injection of retrograde tracers that were used in the all of experiments described in this dissertation. Each retrograde tracer was injected into both the dorsal and ventral surfaces of the stomach along the greater curvature (corpus region only) as depicted in Figure 10.

	Fluoro-Gold (FG)	**Cholera Toxin B-subunit (CT-B)**
Concentration of tracer	4%	0.1%
Number of injections per surface of stomach	5	5
Volume per injection	2 µl	2 µl
Total volume injected	20 µl	20 µl
Survival time	7-10 days	3 days

2.2.2. Cholera Toxin B-subunit

Cholera toxin or its B-subunit (CT-B) conjugated to horseradish peroxidase (CT-HRP) has long been used as a neuroanatomical tracer (see Llewellyn-Smith et al., 1990 and Luppi et al., 1990 for references). Indeed, most of the initial tract tracing studies that laid the foundation for the viscerotopic representation of the alimentary tract in the brainstem of the rat were accomplished using CT-HRP (Altschuler et al., 1992). Additionally, unconjugated CT-B, which can be detected by anti-CT-B antibodies, has also been used for pathway mapping studies (Ericson et al., 1985; Ericson and Blomqvist, 1988; Luppi et al., 1990).

Use of the unconjugated form of the toxin offers several advantages over the HRP-conjugated form. Peroxidase enzyme activity is optimal when fixatives containing high concentrations of glutaraldehyde with little or no formaldehyde are used, but these fixatives severely decrease the immunogenicity of many antigens (Mesulam, 1982). Furthermore, detection of the retrogradely transported HRP depends on the chromogen used in the peroxidase reaction. The chromogens most commonly used to visualize HRP are diaminobenzidine (DAB) and tetramethylbenzidine (TMB) (see Luppi et al., 1990 for refs.). While the insoluble precipitates produced using these chromogens are suitable for light and electron microscopical analysis, they are generally incompatible with fluorescence microscopy as they tend to mask or reduce the fluorescence of other markers used in multilabelling experiments (Bentivoglio and Chen, 1993). Another serious drawback of HRP (and its conjugates) is that it is rapidly degraded in retrogradely labelled cells (Trojanowski et al., 1982).

The B-subunit of cholera toxin is easier to handle than the entire molecule itself as it is non-toxic (Sawchenko and Gerfen, 1985). Unconjugated CT-B is taken up and transported both anterogradely and retrogradely, but not trans-synaptically (Ericson and Blomqvist, 1988; Luppi et al., 1990). The ability of CT-B to trace neuronal pathways is due to its ligand affinity for the superficial carbohydrate residues (GM1 gangliosides) on the plasma membranes (Sawchenko and Gerfen, 1985; Robertson and Grant, 1989). After binding these residues, the GM1-CT complex is internalized by endocytosis (Gonatas et al., 1983).

Previous studies have presented conflicting results concerning uptake of CT-B by fibres of passage. Some have demonstrated that CT-B can be taken up and anterogradely as well as retrogradely transported in damaged but not intact fibres of passage (Luppi et al., 1990). These authors compared pressure versus iontophoretic application of the tracer, and claimed that while uptake by fibres of passage was present in cases where pressure injection was used, this was absent when iontophoresis was used. They suggested that mechanical damage of fibres of passage caused by the needle used for pressure injections was responsible for the non-specific uptake and transport of tracer. It was implied that the lack of mechanical injury using iontophoresis prevented this. In contrast to these findings, other studies which employed iontophoretic application of tracer reported uptake and transport by intact fibres of passage (Chen and Aston-Jones, 1995).

Despite a common uptake mechanism for CT-B, the anterograde and retrograde labelling mechanisms of this tracer appear to differ in terms of time course of transport. In studies conducted by Luppi et al., 1990, retrograde transport of CT-B from brainstem to forebrain regions in cat was shown to occur within 24 h of application of the tracer

(Luppi et al., 1990). In contrast, anterograde transport of CT-B was observed to move at an estimated rate of 6-8 mm per day. These results are in agreement with earlier studies that have shown that anterograde and retrograde transport of CT-B occurs by slow and fast axonal transport mechanisms, respectively (Bobillier et al., 1976).

It has been demostrated that transganglionic transport of CT-HRP requires survival times of approximately 48 h or longer in order to obtain significant primary afferent terminal labelling (Mesulam and Brushart, 1979). Previous studies which examined the central organization of the vagus nerve innervating the stomach of the rat (Shapiro and Miselis, 1985) limited the survival time to 24 h following CT-HRP injection into the stomach to confine labelling to retrograde pathways only. However, the total volume of tracer injected (65 μl), the concentration of tracer used (a "total protein" concentration of 1.3 μg/μl or 0.22-0.44%), the location ("total stomach") and number of injections (precise number unknown; 3-5 μl per injection site) and the fact that CT was conjugated to HRP differed from the current experiments. Based on previous findings, a survival time of 3 days was selected for the present experiments that used CT-B as a neuronal tracer. Within this time frame, brainstem labelling was confined to retrograde transport to the vagal efferent somata and dentrites. No characteristic anterograde labelling of afferents within the NTS was observed, although this has been demonstrated previously after a longer transport period (Shapiro and Miselis, 1985; Altschuler et al., 1991; Altschuler et al., 1992).

The injection strategy employed for CT-B is shown in Table 3. While the volume of CT-B administered per injection site may appear large compared to that applied for intracerebral pathways (e.g. 2 μl as compared to 0.05-0.2 μl; see Luppi et al., 1991), the

concentration used is much lower (0.1% compared to 1%). Furthermore, the volumes and number of injections used for peripheral sites such as the abdominal viscera are consistently larger (Shapiro and Miselis, 1985; Altschuler et al., 1991). The injection strategy described here is in accordance with previous experiments in which CT-HRP was injected into the stomach.

2.2.3. Strategies to prevent the leakage and spread of tracers from the injection sites

Viscerotopic maps for vagally innervated structures derived from neuroanatomical tracing experiments have depended in part on the development of injection strategies to control leakage and spread of tracers from the injection site(s) (Altschuler et al., 1992). Previous work by Fox and Powley has indicated that precautions must be taken to prevent leakage following injection of neuronal tracers. Some of the major problems include local diffusion into either adjacent tissues or extracellular fluids within the body cavity, vasculature, lymphatics, or exocrine ducts that can cause the tracer to be transported to inappropriate tissues (Fox and Powley, 1986; Fox and Powley, 1989). In addition, there is the possibility of uptake by fibres of passage (nerve fibre tracts passing through the area of tracer injection) that are not the intended targets of study.

In order to minimize problems due to tracer leakage, various precautions were taken during the injection procedure. When the stomach was exteriorized for injection, a gauze pad moistened with distilled water was placed under it to prevent accidental spillage of the tracer into the abdominal cavity during injection. Following each injection of tracer, the tip of the syringe was left in place for 1-2 min to equilibrate pressure and

minimize backflow along the needle tract. Furthermore, a cotton swab (Q-tip) was held over the needle tip as it was slowly removed from each injection site, and this was held in place with light pressure for a further 1-2 min. Once the injections had been completed, the stomach was left exteriorized for approx. 5 min to allow for any passive leakage of the tracer from each of the injection sites. This was usually very minimal; any tracer that did leak out was mopped up with cotton swabs. Before returning the stomach to the abdominal cavity following the injection, it was washed with sterile saline in order to remove any tracer that may have leaked out. Care was taken to ensure that the wash solution did not leak into the exposed abdominal cavity.

The spread of tracer at the injection site was also monitored using histological methods. The extent of labelling of the AP was assessed in coronal sections of brain stem from animals injected with the tracers. The amount of labelling in this region has been shown to be a proportional measure of tracer leakage into the vasculature (Fox and Powley, 1985). In addition, the labelling of the nucleus ambiguus within these sections was also checked, as this would also give an indication of tracer leakage into the abdomen (Fox and Powley, 1985). Previous experiments in our laboratory that employed FG injections into the stomach using the same methods described in this chapter demonstrated labelling of neurons within the myenteric plexus surrounding the immediate region of each injection and up to 2-4 mm away from these sites (Buchan et al., 1991). The size of injections chosen in these studies (3 μl) produced localized diffuse labelling in the myenteric plexus and longitudinal muscle layer. Sections of the stomach taken from areas >1cm away from each injection site did not contain any labelled structures.

2.3. Perfusion/Fixation

After the required time for retrograde tracer transport had elapsed, the animals were reanesthetized with sodium pentobarbital (60 mg/kg), and perfused through the ascending aorta with 500 ml of 0.9% saline followed by 500 ml of freshly prepared 4% paraformaldehyde in 0.1 M phosphate buffer (PB, pH 7.4.) This fixative was selected because of its compatibility with the retrograde tracers used and immunocytochemistry. These solutions were delivered into the animal using a peristaltic pump (MasterFlex, catalogue #7553-20, Cole-Parmer Instrument Co., Chigago, IL). Once the perfusion had been completed, the brains were removed and post-fixed in 4% paraformaldehyde overnight, followed by cryoprotection in 20% sucrose in 0.1 M PB for 24h.

2.4. Histology

After perfusion/fixation and cryoprotection, the brainstem was dissected from the forebrain, and a small portion from the left side was removed for future orientation. Each brainstem was mounted on a piece of cork board in a manner corresponding to the desired orientation of sectioning (i.e. coronal, sagittal or horizontal), covered with OCT embedding medium (Tissutek) and then frozen in isopentane cooled in liquid nitrogen to -60^{o}C for 1 min. Immediately after freezing, the brainstems were placed in a cryostat (Fisher, model HM500) cooled to -20^{o}C, and left there for 10 min to equilibrate to that temperature. The frozen brainstems were mounted and aligned on cutting blocks, and sections of the desired thickness (typically 25 or 50 μm; see the methods sections of Chapters 3-5) were cut. Serial sections through the medulla were collected and stored in

0.1 M phosphate-buffered saline (PBS, pH 7.4) in individual wells of Falcon 48-well plates.

2.5. Immunocytochemistry

2.5.1. Basic Principles

All of the immunocytochemical procedures described in this chapter use more than one antibody solution in sequence and are referred to as 'indirect' methods (Hrapchak, 1980). In this method, the different antibody solutions are referred to as "primary", "secondary" etc. based on the order they are applied to the test specimen. Primary antibodies bind to the antigen being investigated, and must be raised in a species that is different to that in which the antibody is being used. Secondary antibodies are raised against the IgG molecule of the species that was used to produce the primary antibody. In these studies, the secondary antibodies were conjugated to either a fluorophore (for immunoflurescence) or to biotin (for immunoperoxidase). Both of these methods are depicted in Figure 11.

In addition to a biotinylated secondary antibody, the immunoperoxidase technique employed in these studies relied on a "tertiary" molecule that consisted of a complex of peroxidase conjugated to biotin and the egg-white glycoprotein avidin (Hrapchak, 1980). Avidin has a very high affinity for biotin, so this complex binds to the secondary antibody. The original antigen was revealed by reacting the complex with the chromagen diaminobenzidine (DAB) which served as an electron donor, and hydrogen peroxide, which served as a substrate for the enzyme. The staining was further intensified by

adding nickel ammonium sulphate to the reaction mixture, which co-precipitates with DAB.

All immunocytochemical methods were carried out in 48 or 96 well plastic plates, with one section of brainstem tissue per well. Processing of free-floating sections rather than sections affixed to slides was selected due to the increased penetration of antisera that can be achieved using this method. This consideration was especially important for thick sections (i.e. >50 μm) that were used for confocal microscopy.

2.5.2. Immunofluorescence

Before application of primary antibodies, all sections were incubated in normal horse serum in PBS (1:10) containing 0.1-0.5% Triton X-100 (PBSHST) for 30 min at room temperature. The amount of detergent used was proportional to the thickness of the tissue. For sections of 25 μm thickness, 0.1% Triton X-100 was used, whereas 0.3-0.5% Triton X-100 was used with 75 μm sections. Triton X-100 was used to increase the permeability of the tissue for increased antibody penetration, which was especially important for sections > 50 μm thick. The preliminary incubation of tissue sections in PBSHST was performed to reduce non-specific binding of antisera.

Figure 11. Basic principles of immunocytochemistry. (A) Immunofluorescence. (B) Immunoperoxidase. ABC complex = complex of avidin, biotin and peroxidase molecules.

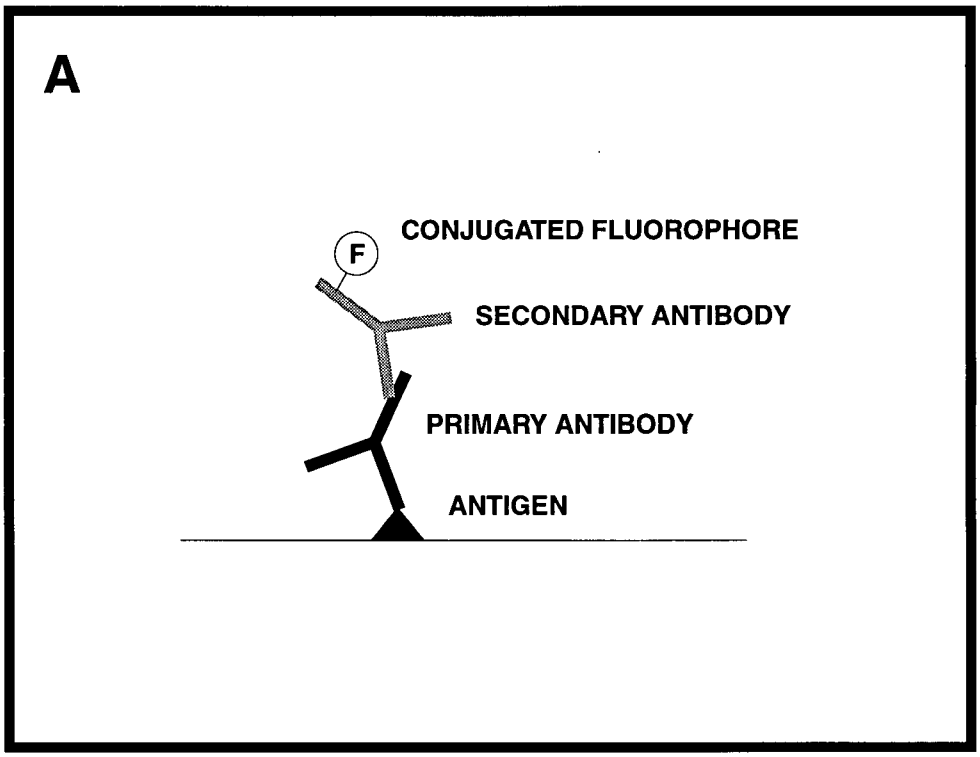
A
F
CONJUGATED FLUOROPHORE
SECONDARY ANTIBODY
PRIMARY ANTIBODY
ANTIGEN

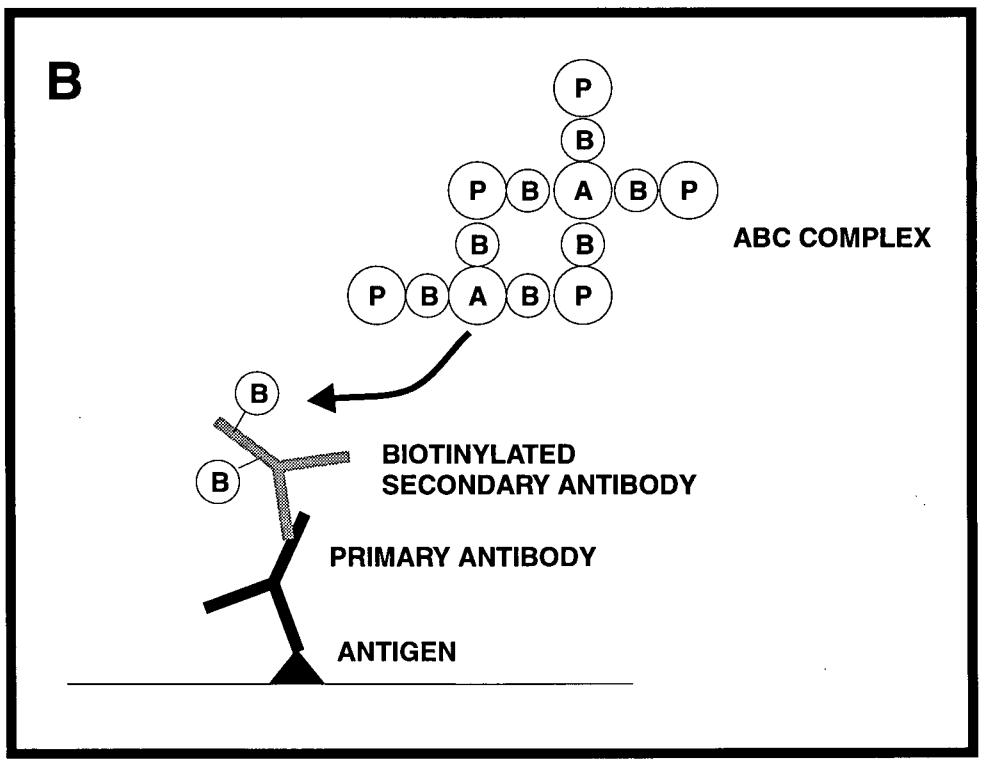
B
P
B
P B A B P
B B
P B A B P
ABC COMPLEX
B
B
BIOTINYLATED
SECONDARY ANTIBODY
PRIMARY ANTIBODY
ANTIGEN

After this initial blocking step, sections were incubated with a combination of primary antisera in PBSHST for 2-3 days at 4°C. In between incubation steps, the sections were washed 3 times in PBS + Triton X-100 (the concentration of detergent used in the wash solution was either 0.1% or 0.3%, depending on the thickness of the tissue sections being processed; see above in this section). All subsequent steps were performed at room temperature. Secondary antibodies, each conjugated to a different fluorophore, were prepared in PBSHST and incubated with tissue sections for 2 h. After this time, the sections were washed three times in PBST, placed on glass slides and coverslips were applied using PBS/glycerine (1:9) adjusted to pH 8.6, which has been shown to be optimal for the fluorophores used in these studies (Johnson et al., 1982). To preserve fluorescence, 9 mM of the antifade reagent p-phenylenediamine was added to the mounting media (Krenik et al., 1989). The coverslips were sealed to the slides using nail polish to prevent movement of the sections and to reduce their exposure to air, which decreases the fluorescence of the fluorophores by oxidation. The sections were screened using a Zeiss Axiophot microscope equipped for epifluorescence. Sections exhibiting bright fluorescence and relatively low background were selected for screening by a Bio-Rad MRC 600 confocal microscope system. The excitation/emission wavelengths of all fluorophores used can be found in Appendix I. A description of the spectral characteristics of the filter sets used with both the epifluorescence microscope and the confocal microscope used in these studies can be found in Appendix II.

2.5.3. Immunoperoxidase

Prior to incubation with the primary antibodies, intrinsic peroxidase activity was blocked by immersing the sections in 0.3% H_2O_2 in PBS for 30 min, followed by a 30 min incubation in PBSHST to block non-specific binding (as described above for immunofluorescence). The sections were then incubated with the primary antibody for 2-3 days at 4 ^{o}C. As with the sections processed for fluorescence microscopy, 3 washes in PBST were performed between all steps. Following incubation with the primary antibody, the sections were transferred into wells containing a biotinylated secondary antibody for 1 h. The sections were then incubated with avidin-biotin-peroxidase complex (1:1000; Vector Elite Kit, Vector Labs) for 1 h. Finally, the sections were developed in a solution ("DAB/Ni") containing 10 ml of 0.05 M Tris-HCl buffer (pH 7.5), 30 mM nickel ammonium sulfate, 2 mg 3,4,3',4'-tetra-aminobiphenyl hydrochloride (DAB; BDH), and 5 µl of 30% H_20_2, which was dispensed into wells. After approximately 10 min., the reaction was terminated by placing the sections in 0.05M Tris-HCl buffer.

2.5.4. Controls for Immunocytochemistry

All antisera used were prescreened to ensure minimal crossreactivity. Initial experiments were performed whereby each individual primary antibody was developed separately, and the results were compared to when solutions containing multiple primary antibodies were used. Furthermore, all primary antisera that were used have been characterized previously to ensure their specificity (see immunocytochemistry section of

Chapters 3, 4 and 5 for details). The secondary antisera used for immunofluorescence studies were purchased from Jackson ImmunoResearch Laboratories, Inc. and were designated as suitable for multi-labelling experiments. These antibodies were all affinity-purified and were derived from the same host species so that they did not recognize one another. They were screened for cross-reactivity with other species so that they did not recognize other primary antibodies that were present or bind to the tissues or cells under investigation.

Control incubations were performed by either omitting the primary antibodies or by using only normal serum solutions obtained from the same host species from which the primary antisera originated. For immunoperoxidase staining, some sections were developed in the DAB/Ni solution with the primary and/or secondary antibody incubations omitted. All control incubations were performed in parallel with the test sections, using the same solutions (minus the appropriate antisera) in order to reduce variations in antibody/fluorophore concentration and other variables (e.g. precise timing and temperature of incubations).

2.6. Laser Scanning Confocal Microscopy

Laser-scanning confocal microscopy (LSCM) provides a means of examining thick specimens with increased resolution when compared to traditional epifluorescence microscopy (see Inoué, 1995 for a review). This is mainly due to the ability to perform "optical sectioning" (precisely control the focus in the Z-plane within a specimen) in sub-micron increments and reduce the glare from out-of-focus layers. Furthermore, the

optical sections obtained from a confocal microscope facilitate the generation of three-dimensional (3-D) reconstructions using an approach such as volume rendering.

In LSCM, a laser beam is focused to a small spot by an objective lens onto a fluorescent specimen. Through a X-Y deflection mechanism, the beam is scanned across the specimen in a raster sweep pattern, providing excitatory illumination one point at a time. The mixture of reflected light and emitted fluorescent light for each point hit by the laser is captured by the same objective and is focused onto a photodetector (photomultiplier) via a dichroic mirror (beam splitter). The reflected light is deviated by the dichroic mirror while the emitted fluorescent light passes through in the direction of the photomultiplier. A confocal aperture (commonly referred to as a "pinhole") is placed in front of the photodetector, such that the fluorescent light from points on the specimen that are not within the focal plane (the so called "out-of-focus light") where the laser beam was focused will be largely obstructed by the pinhole. In this way, out-of-focus information (both above and below the focal plane) is greatly reduced. This becomes especially important when dealing with thick specimens. The spot that is focussed on the center of the pinhole is often referred to as the "confocal spot." A simple arrangement of a LSCM illustrating the confocal principle and a schematic of a typical confocal system is illustrated in Figure 12.

Figure 12. (A) A simple arrangement of a LSCM illustrating the confocal priciple. (B) A typical arrangement of an entire LSCM system.

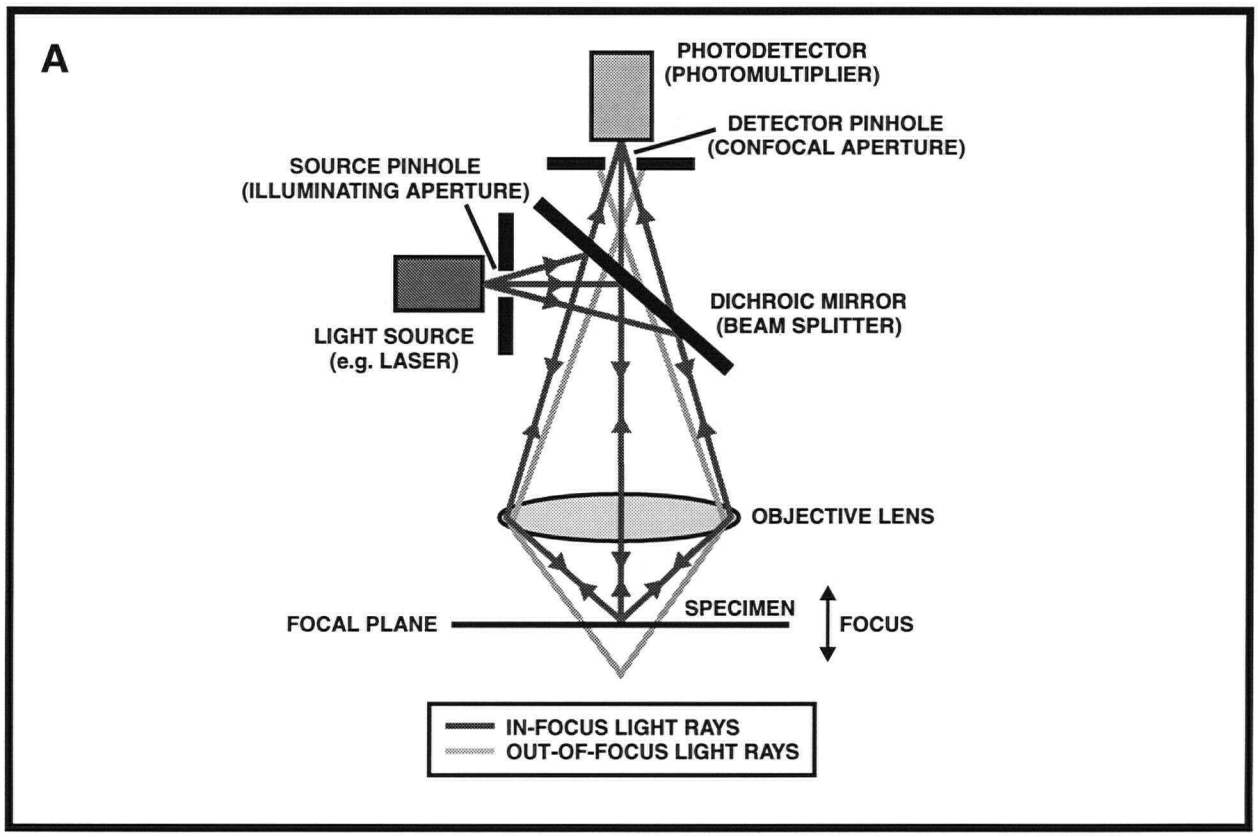
A
PHOTODETECTOR
(PHOTOMULTIPLIER)
DETECTOR PINHOLE
(CONFOCAL APERTURE)
SOURCE PINHOLE
(ILLUMINATING APERTURE)
DICHROIC MIRROR
(BEAM SPLITTER)
LIGHT SOURCE
(e.g. LASER)
OBJECTIVE LENS
FOCAL PLANE
SPECIMEN
FOCUS
IN-FOCUS LIGHT RAYS
OUT-OF-FOCUS LIGHT RAYS

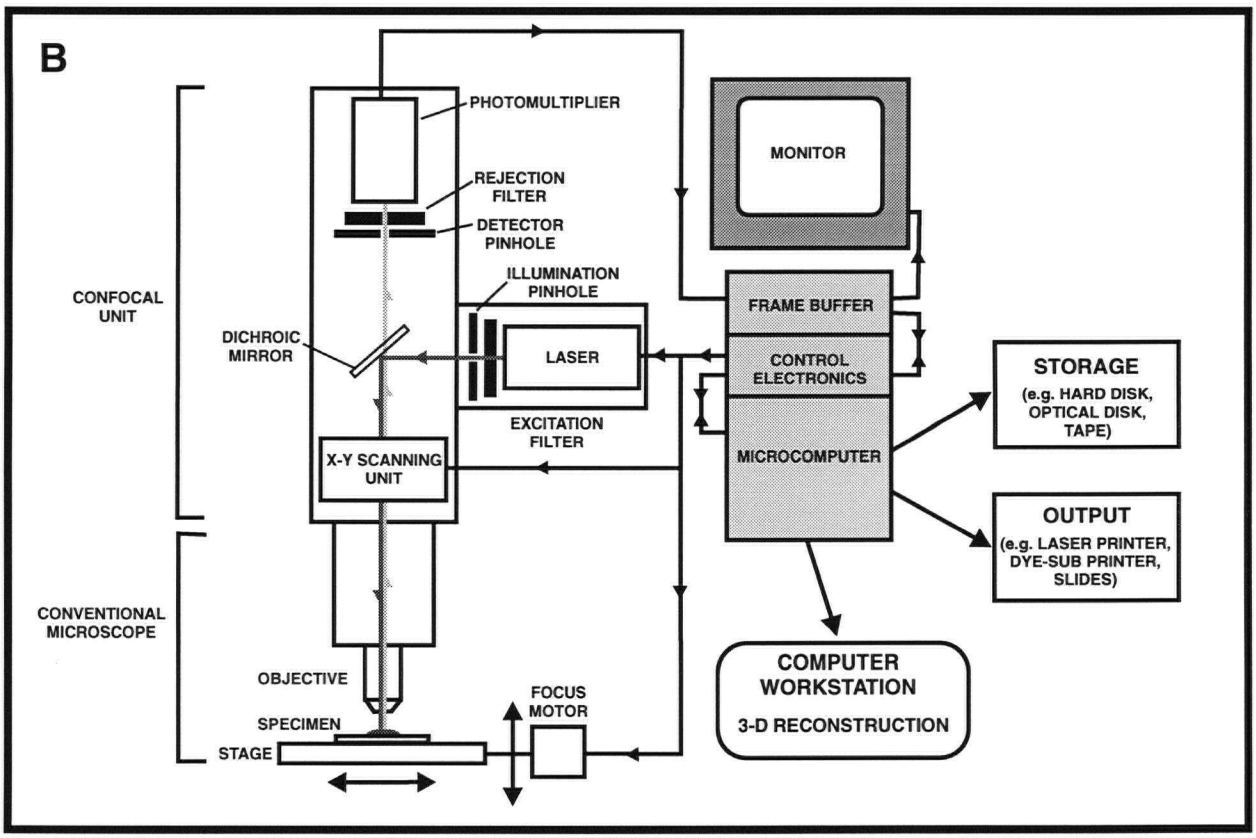
B
PHOTOMULTIPLIER
REJECTION
FILTER
DETECTOR
PINHOLE
ILLUMINATION
PINHOLE
CONFOCAL
UNIT
DICHROIC
MIRROR
LASER
EXCITATION
FILTER
X-Y SCANNING
UNIT
CONVENTIONAL
MICROSCOPE
OBJECTIVE
SPECIMEN
STAGE
FOCUS
MOTOR
MONITOR
FRAME BUFFER
CONTROL
ELECTRONICS
MICROCOMPUTER
STORAGE
(e.g. HARD DISK,
OPTICAL DISK,
TAPE)
OUTPUT
(e.g. LASER PRINTER,
DYE-SUB PRINTER,
SLIDES)
COMPUTER
WORKSTATION
3-D RECONSTRUCTION

A 2-D image of a small partial volume of the specimen centered around the focal plane (referred to as an "optical section") is generated by performing a raster sweep of the specimen at that focal plane. As the laser scans across the specimen, the analog light signal, detected by the photomultiplier, is converted into a digital signal. This contributes to a pixel-based image displayed on a computer monitor attached to the LSCM. The relative intensity of the fluorescent light, emitted from the laserhit point, corresponds to the intensity of the resulting pixel in the image (typically 8-bit greyscale). The plane of focus (Z-plane) is selected by a computer-controlled fine-stepping motor which moves the microscope stage up and down. Typical focus motors can adjust the focal plane in as little as 0.1 micron increments. A 3-D reconstruction of a specimen can be generated from 2-D optical sections collected in series (commonly referred to as an "image stack") using a computer graphics technique such as volume rendering.

2.7. Segmentation of Image Data

Segmentation refers to the process of extracting the desired object (or objects) of interest from the background in a digital image or data volume using computer graphics techniques. It is often a necessary step before attempting a 3-D reconstruction using confocal microscopy data, especially when an object of interest is occluded by other structures (e.g. a labelled neuron embedded inside a thick slice of tissue which has some background labelling). Segmentation can be aided through manual intervention (i.e. interactive manipulation of segmentation parameters) or handled automatically through software algorithms. Although many segmentation techniques have been devised, two of

the most commonly used methods applied to confocal microscopy data are thresholding and masking (White, 1995; Ladic, 1997).

Thresholding typically involves selecting an intensity level that is at the interface between two "materials" in a dataset, and rejecting all intensity values above or below that value. The resulting dataset can be represented in binary (black and white) format where rejected and retained regions are each displayed in one of the two possible colours. Alternately, grayscale intensities above the threshold (corresponding to desired signal) can be kept unaltered, while intensities below the threshold (corresponding to "background" or noise) are set to a uniform colour (usually black).

Masking is a procedure whereby an enclosed region(s) of an image (or of the image stack) are defined for processing. This can be done either by manually tracing around the regions of interest (e.g. with a mouse in a graphics application) or by an automated routine. An easy (and useful) application of this is to use a maximum intensity projection (MIP) to define the mask. A MIP is a single image that is generated from a sequential series of images representing a 3-D volume (such as an image stack obtained from a confocal microscope) (White, 1995). A computer algorithm examines each image sequentially, and compares the intensity of a pixel in one image with the corresponding pixel at the same X and Y co-ordinates in the image before it in the series. The pixel with the greatest intensity is retained and used as the basis for comparison with the next image in the series. This procedure is repeated for all X,Y co-ordinates comprising each image and for all images in the series. At the end of this process, the MIP represents the cumulative result of the maximum intensities from all images in the 3-D volume. If an object of interest has a closed, continuous surface (such as that of a neuron) the MIP

defines the absolute boundaries of the object in 2-D. A mask can be formed by either manually tracing around the boundaries of the object(s) of interest in the maximum intensity projection or by thresholding to produce a binary (black and white) image. The mask can then be applied to the entire image stack, such that regions falling within the mask selection area are preserved, whereas areas outside this region are eliminated (e.g. set to 0 [black].)

Once objects have been identified by segmentation, they can be further classified by assigning properties such as colour and opacity, the latter criterion being particularly important during volume rendering (see section 2.8 below). The selection of opacity values that are assigned to each intensity value during volume rendering can also be useful for further segmentation of the data. For example, areas of a volume that have been set to black after a preliminary masking or thresholding operation can be made fully transparent, effectively eliminating them from view.

2.8. Volume Rendering

Volume rendering is a computer graphics technique for the display of 3-D volumetric data (see Kaufman, 1991 for a review). Using this method, the object to be reconstructed is subdivided into many cubic building blocks, called "voxels" (or volume elements). A voxel is the 3-D counterpart of the 2-D pixel and is a measure of unit volume. Each voxel carries one or more values for some measured property of the volume, such as intensity, colour or transparency. The 3-D voxel sets are typically assembled from multiple 2-D images (such as a series of optical section images from a

confocal microscope), and are displayed by projecting these images into 2-D pixel space where they are stored in a frame buffer.

The volume rendering technique has both advantages and pitfalls. A major advantage is that a 3-D volume can be displayed without any knowledge of the geometry of the dataset. However, since all of 3-D image data is used for volume rendering, computers with large amounts of memory and processing power are required to handle volumes rendered in this manner. Finally, because the entire dataset is preserved in volume rendering, any part, including internal structures and details may be viewed.

3. ESTABLISHMENT OF TECHNIQUES FOR THE 3-D RECONSTRUCTION OF NEURONS AND NERVE FIBRES: ASSOCIATION OF CGRP WITH GASTRIC EFFERENT NEURONS IN THE DMV OF THE RAT

3.1. Introduction

Pilot studies in our laboratory have detected the presence of calcitonin gene-related peptide (CGRP) immunoreactive (IR) nerve fibres in the vicinity of retrogradely-labelled gastric efferent neurons within the DMV of the rat (Buchan et al., 1991). In these studies, which employed conventional epifluorescence microscopy, it was found that although few CGRP-IR nerve fibres came into close association with the somata of identified gastric efferent neurons in the DMV, a possible relationship between these fibres and the dendrites of gastric efferent neurons within the NTS could not be ruled out. Furthermore, the precise spatial relationship of immunoreactive fibres and identified neurons could not be determined.

Previous studies have demonstrated that injection of CGRP into the CSF or directly into the DVC of the rat inhibits gastric acid secretion by a vagally-dependent mechanism (Taché et al., 1984; Taché, 1992). In these studies, it was found that intracerebroventricular injection of as little as 1 pmol of CGRP could produce an antisecretory effect lasting over 2 hrs (Lenz et al., 1985). This prolonged time course of action raises the possibility that CGRP exerts its effect via a non-synaptic, volume transmission mechanism. Finally, the fact that binding sites for CGRP have been

detected in the NTS would suggest that the vagal centers within the DVC are a target for this peptide (Sexton et al., 1986; Inagaki et al., 1986).

In light of this preliminary neuroanatomical and pharmacological data, the underlying hypothesis for this study was that if CGRP was acting via a volume transmission mechanism, CGRP-IR nerve fibres should come into close spatial association with identified gastric efferent neurons within the DVC of the rat. In order to test this hypothesis, the primary aim was to develop a method which would permit the 3-D reconstruction of identified gastric efferent neurons and surrounding nerve fibres in the DVC of the rat, using a combination of retrograde tracing, immunocytochemistry, confocal microscopy, image processing and volume rendering techniques. The precise association of CGRP-IR fibres to efferent cell bodies was achieved by identifying the proportion of these fibres that directly apposed the identified neurons versus those that terminated in the vicinity of these neurons without making contact.

3.2. Methods

3.2.1. Preliminary Examination of CGRP with Conventional Epifluorescence Microscopy

A group of 5 rats were injected with a solution of 4% Fluoro-Gold along the greater curvature of the stomach as described in Chapter 2. After allowing time for retrograde transport of the tracer, the rats were perfused and fixed, and either 25 μm or 50 μm thick serial sections were cut in the coronal plane using a cryostat. While cutting, the section at the position of the obex was noted and all other sections were referenced as

being either rostral (+) or caudal (-) to this landmark. Distances between sections were expressed in microns.

Brain stem sections at positions both rostral (up to +1000 μm) and caudal (up to -1000 μm) were processed for immunocytochemistry in 48 well plastic plates following the protocols for immunofluorescence outlined in Chapter 2. To localize CGRP, a monoclonal mouse anti-CGRP antibody (provided by Dr. Sternini, Centre for Ulcer Research and Education, UCLA) was used at a concentration of 1:1000. A donkey anti-mouse antibody conjugated to Texas Red used at a concentration of 1:750 was used to visualize the CGRP-IR.

Sections destined for examination with the confocal microscope were also processed according to the protocols outlined for immunofluorescence in Chapter 2, with a few exceptions. Brain stem slices were incubated initially with mouse anti-CGRP and rabbit anti-FG, both at a dilution of 1:1000. After incubation for 3 days at 4°C, the sections were washed and placed into wells containing a solution of Texas Red conjugated donkey anti-mouse IgG (1:750) and biotinylated donkey anti-rabbit IgG (1:1000) for 1 hr. After washing, the sections were then placed into wells containing Texas Red conjugated donkey anti-mouse IgG (1:750) plus avidin conjugated FITC at 1:750 to label FG. Therefore, the total incubation time for the Texas Red-conjugated secondary antibody used to visualize CGRP was 2 hrs. Sections were mounted on slides as described in Chapter 2. Appropriate control sections were developed in parallel to the test sections, as described in Chapter 2. In addition, control sections consisting of only FG-IR (FITC) or CGRP-IR (Texas Red) were prepared to test for possible "bleed through" effects during confocal microscopy.

3.2.2. Laser Scanning Confocal Microscopy

The "dual acquisition" mode of the confocal microscope was used to capture double-labelled specimens, whereby both FG-IR (FITC) and CGRP-IR (Texas Red) could be detected simultaneously. This was accomplished using the 488 and 568 nm laser lines in conjunction with a combined K1/K2 filter block (to excite and detect FITC and Texas Red, respectively; see Appendix II). Specimen 1 was scanned from two serial sections of brain stem, each 25 μm, spanning brain stem positions of -350 to -325 μm. Two serial sections were used since the identified gastric efferent neuron of interest was not confined to a single section. This specimen was captured with the dual acquisition mode in conjunction with a 40x oil objective lens (1.0 NA). The acquisition parameters were selected such that the dimensions in X, Y and Z for each point sampled was 0.4 μm (i.e. 0.4 μm^3/voxel). A total of 100 optical section images (each 768x512 pixels) were captured, 50 images for each of the two brain stem sections. Additional images were captured above and below the actual region of interest within a brain stem slice to prevent possible structures of interest being truncated.

The series of optical section images acquired for each brain stem slice was referred to as the "image stack" for that slice for simplicity. Each half of every optical section image (384x512 pixels) captured using the dual acquisition mode represented the data of a different fluorophore, with FITC constituting the left half of the image and Texas Red the right half. A MIP was also saved for each image stack using the software supplied with the LCSM. Control sections that contained only one fluorophore (FITC or Texas Red) were also scanned to determine if any FITC signal could be detected during acquisition of Texas Red fluorescence, and vice versa, using the dual scanning mode.

In a similar manner to Specimen 1, Specimen 2 was obtained from a 50 μm double-labelled (CGRP and FG) section taken from location +100 μm within the brain stem. This section was also scanned using the dual acquisition mode of the confocal, and a 768x325x233 stack was captured using the K1/K2 filter block in conjunction with a 63x oil (1.4 NA) objective with voxel dimensions of 0.2 μm^3. Specimen 3 was obtained from a 50 μm section that was only labelled with antisera to FG, and was from position +650 μm within the brain stem. This section was scanned using only the 488 nm laser line of the confocal, and a 768x512x50 stack was captured using the BHS filter block (see Appendix II for the spectral characteristics of this filter). The same 63x oil objective was used (as above) except the dimensions were 1.0 μm^3/voxel.

After acquiring the image stacks with the confocal microscope, the data was transferred to a Silicon Graphics VGX workstation with 128 MB of RAM for further processing.

3.2.3. Extracting objects of interest from background for 3-D reconstruction

In order to produce 3-D reconstructions of individual FG-labelled neurons and surrounding CGRP-IR fibres, these structures had to be extracted from the 3-D volumes. This procedure was achieved with a combination of masking and thresholding techniques using computer graphics software. Several algorithms, formulated using the C programming language, were also used (these will be referred to as "custom algorithms"). Each of these consisted of less than 100 lines of program code, and included subroutines for basic file/image manipulation and related operations that were not available with the pre-made graphics software packages that were used. The methods described in the

following sections refer to those used in the reconstruction of specimen 1, since this dataset required the most complex processing of the 3 specimens presented here. Reconstructions of the other specimens were carried out using a subset of these methods, and these will be mentioned briefly at the end of each section. A flowchart summarizing the procedures used is presented in Figure 13.

First, the combined images stacks (which had a dimension of 768x512x50 voxels) were separated into individual stacks with a dimension of 384x512x50 voxels using a custom algorithm. This was completed so that each fluorophore could be treated as a separate data volume. In addition to separating the stacks, this algorithm removed the proprietary Bio-Rad file header and footer information that was automatically added during acquisition by the software supplied with the LSCM. This procedure generated 4 image stacks, 2 representing FG-IR and 2 for CGRP-IR, consisting of raw, 8-bit pixel data (X*Y*Z).

At this stage, each image stack was loaded into the volume rendering software ("BOB", part of the freeware "GVLware" volume visualization package from the Army High Performance Research Center, Minnesota, USA) for preliminary visualization. To ascertain if the initial volume could be truncated to a smaller subvolume and to determine the amount of masking that would be required to extract the objects of interest.

Subvolumes of interest could be selected by moving a series of slider controls in the BOB software that corresponded to "size" and "center" parameters for the X, Y and Z dimensions (Figure 14a,b). Once a subvolume had been selected, the values of the above parameters were recorded for later application (see below). In the case of specimen 1, although the original X and Y dimensions for each image stack were preserved, the Z-

dimension of each stack was reduced to eliminate out of focus images that were observed at the "top" and "bottom" of each stack. It is important to note that the same Z dimensions were used for each corresponding pair of stacks to preserve alignment in this axis.

Next, the level of background fluorescence and position of all objects within the volume was established. Using the "icol" utility supplied with the GVLware package, a consecutive series of low intensities (starting at intensity 0) were set to "100% transparent" (Figure 14c). The changes made here were dynamically updated in the BOB software so that the effect on the volume could be observed interactively. Making these low intensities transparent served to eliminate much of the non-specific background noise from the volume, revealing objects comprised of higher intensities (i.e. neurons and surrounding fibres). The volumes were rotated in 3-D space revealing the amount of background and the presence of undesired structures that obscured the surfaces of objects of interest. With this knowledge, images to be used for masking the volumes were then generated.

Maximum intensity projections for each separate fluorophore image stack (which delineate the absolute boundaries of neurons and fibres) were used to produce "mask" images in binary (black and white only) format. The original MIP obtained using the software supplied with the LSCM was generated for the "X-Y" face of the image stack. Additional MIP images were generated (as needed) for the "Y-Z" and/or "X-Z" faces using a custom algorithm. This algorithm could generate masks for specific subvolumes within an image stack, which was necessary for all three specimens presented in this chapter.

Figure 13. Flowchart summarizing the steps used in the generation of 3-D reconstructions of a double-labelled specimen using image data acquired from a LSCM.

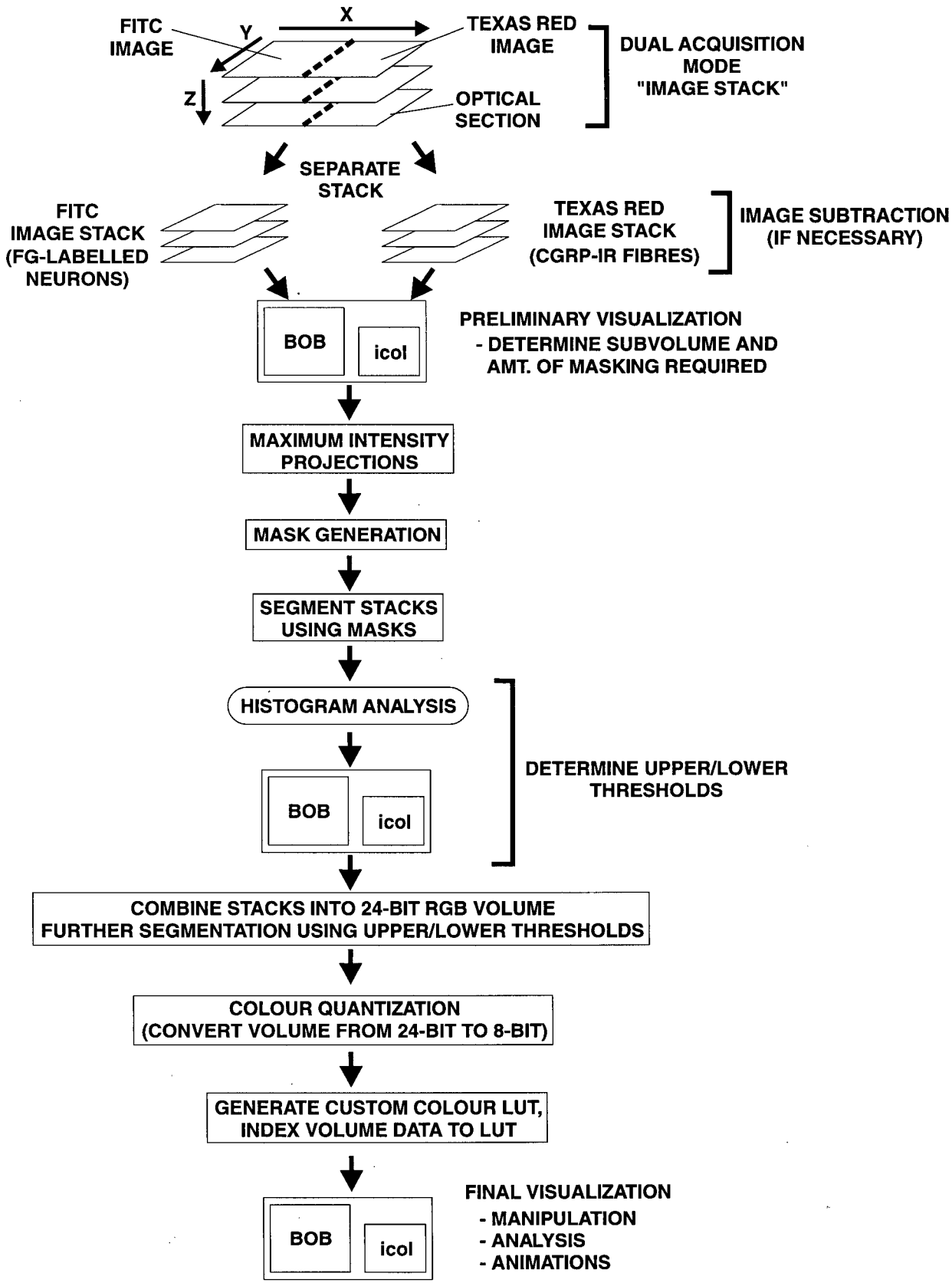
FITC IMAGE
X
Y
Z
TEXAS RED IMAGE
OPTICAL SECTION
DUAL ACQUISITION MODE "IMAGE STACK"
SEPARATE STACK
FITC IMAGE STACK (FG-LABELLED NEURONS)
TEXAS RED IMAGE STACK (CGRP-IR FIBRES)
IMAGE SUBTRACTION (IF NECESSARY)
BOB
icol
PRELIMINARY VISUALIZATION
- DETERMINE SUBVOLUME AND AMT. OF MASKING REQUIRED
MAXIMUM INTENSITY PROJECTIONS
MASK GENERATION
SEGMENT STACKS USING MASKS
HISTOGRAM ANALYSIS
BOB
icol
DETERMINE UPPER/LOWER THRESHOLDS
COMBINE STACKS INTO 24-BIT RGB VOLUME
FURTHER SEGMENTATION USING UPPER/LOWER THRESHOLDS
COLOUR QUANTIZATION
(CONVERT VOLUME FROM 24-BIT TO 8-BIT)
GENERATE CUSTOM COLOUR LUT,
INDEX VOLUME DATA TO LUT
BOB
icol
FINAL VISUALIZATION
- MANIPULATION
- ANALYSIS
- ANIMATIONS

Figure 14. Screen layout of BOB volume rendering software and companion icol editor. (A) Viewport in BOB where volumes are observed and manipulated. (B) Slider bars in BOB that control dimensions of the observed volume. (C) icol colour/transparency editor.

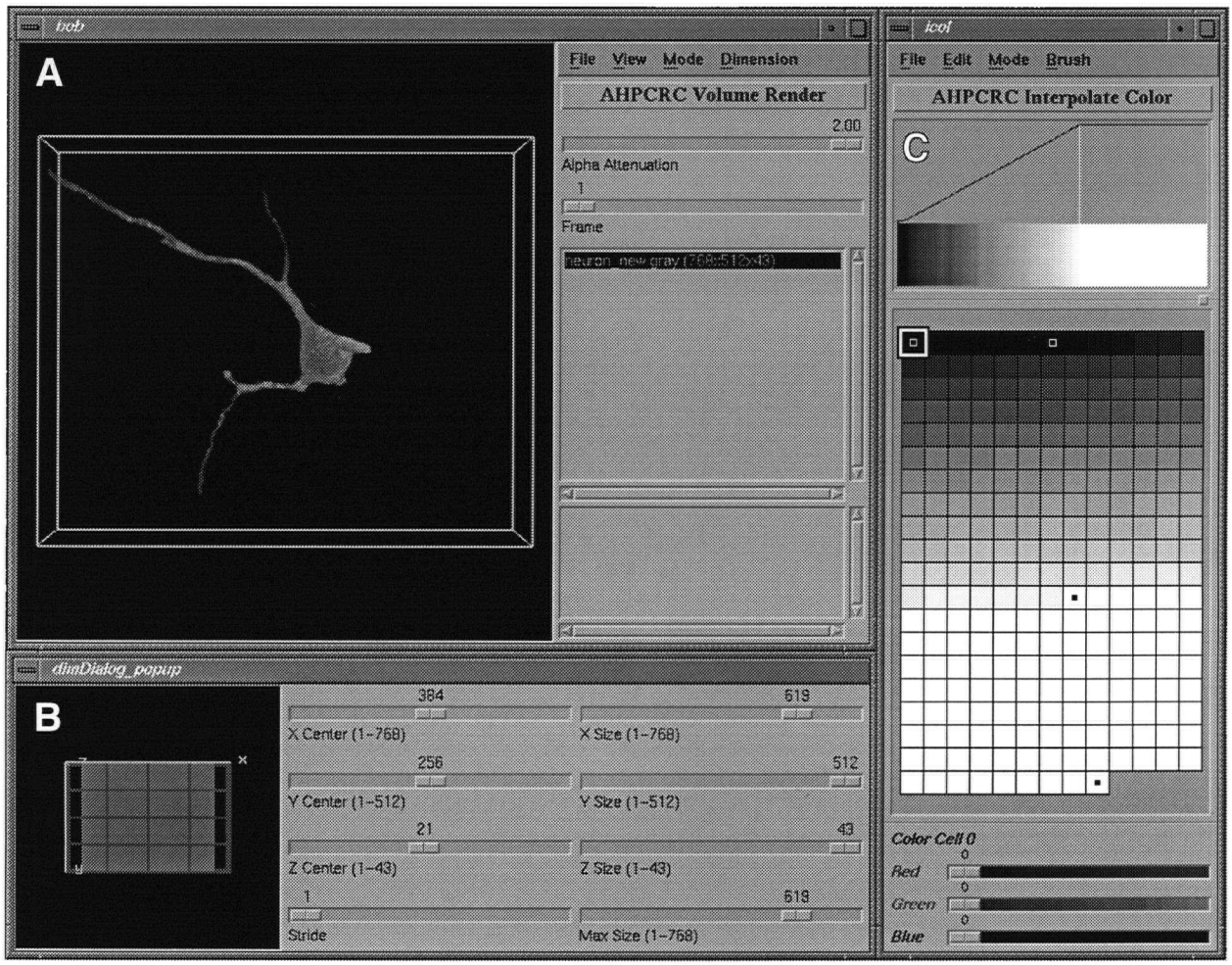
bob
A
File View Mode Dimension
AHPCRC Volume Render
2.00
Alpha Attenuation
1
Frame
dimDialog_popup
B
384
X Center (1-768)
519
X Size (1-768)
256
Y Center (1-512)
512
Y Size (1-512)
21
Z Center (1-43)
43
Z Size (1-43)
1
Stride
519
Max Size (1-768)
icol
File Edit Mode Brush
AHPCRC Interpolate Color
C
Color Cell 0
Red
Green
Blue

First, the objects of interest were selected by loosely tracing around their outlines in the MIP selected for masking. This was done manually using the "lasso tool" in Adobe PhotoShop graphics software (Adobe Systems, Inc.) in a mode that permitted straight-edge selection borders to be generated. None of the built-in filters or other automated selection tools of this software were used. The region outside of the outlined area (comprising undesired "background" labelling) was set to black, and the area within the selection was thresholded (all intensities above a certain cutoff value were set to white). The threshold was determined interactively, and typically >95% of all intensity values in the data were retained. The resulting mask image was then applied to all images in the respective fluorophore image stack whereby all areas for each optical section image that fell within the white area of the mask were retained whereas those that were in the black area were discarded. Unique masks were generated separately for each of the 4 image stacks and were applied using a custom algorithm. This algorithm also cropped the entire subvolume given the appropriate parameters. For this specimen, only masks obtained for the "X-Y" face of both the FG-IR and CGRP-IR stacks were required. Once the individual stacks were masked, the two pairs of stacks were joined using another custom algorithm to form two final stacks: one for FG-IR and the other for CGRP-IR.

Figure 15. Generation of an image mask used to segment an object in a 3-D volume. (A) The object of interest in a MIP of the voulme is selected by tracing around its perimeter using Adobe Photoshop software. (B) The area inside the selected outline is set to white, the and the area outside this region is set to black, producing a binary mask.
Scalebar = 50 μm.

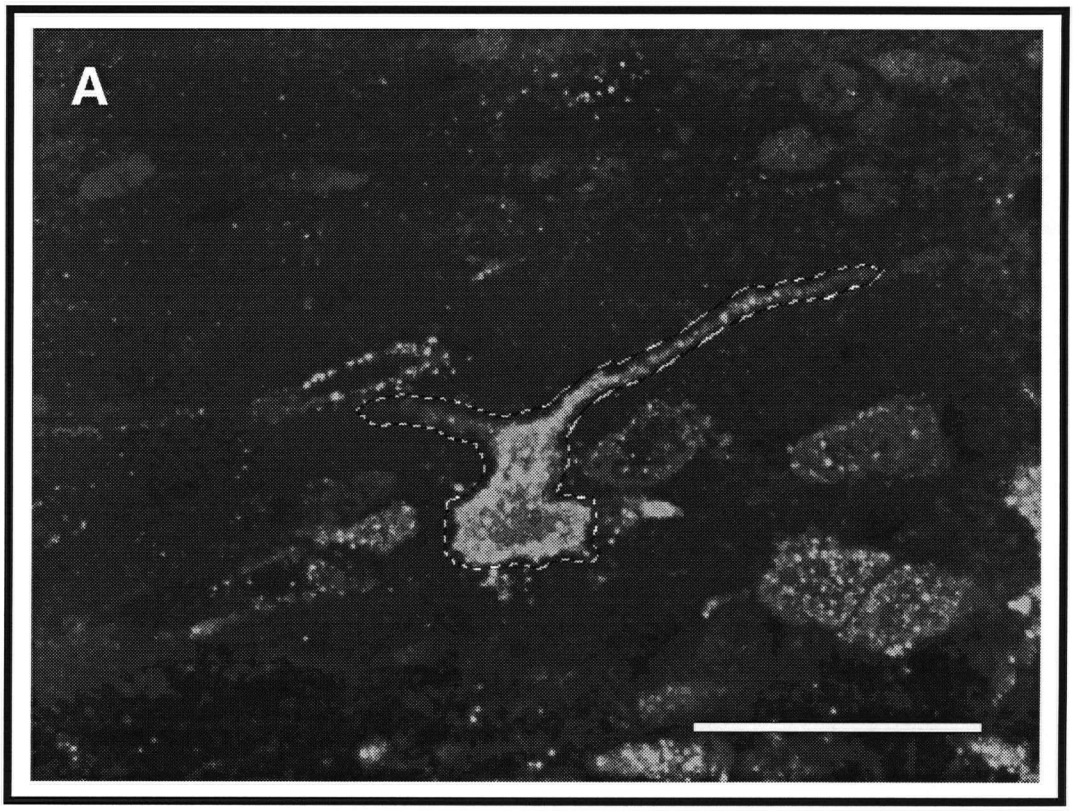
A

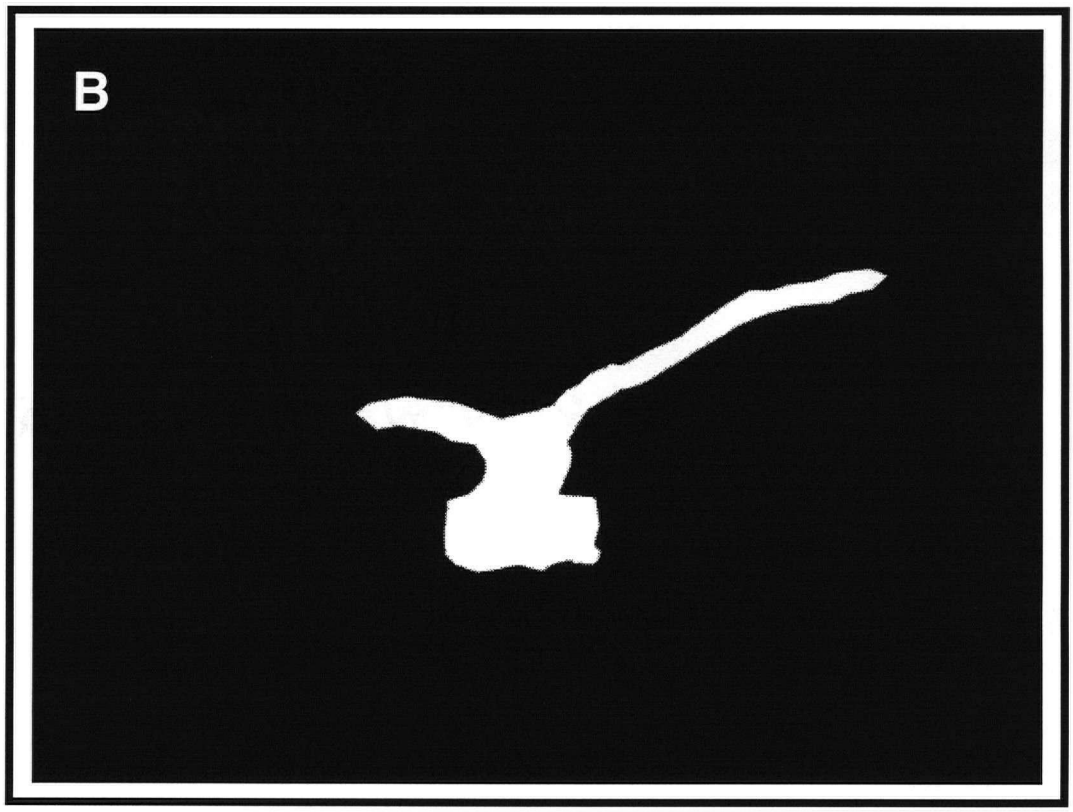
B

Specimen 2 was processed in a similar manner to specimen 1, except the "join" algorithm was not applied since only one image stack was used. For this dataset, two MIP images (for the "X-Y" and "Y-Z" faces) were used to mask the FG-IR stack, while only one was required for the CGRP-IR stack. In the case of the FG-IR stack for this specimen, each mask was applied separately. The file header of specimen 3 (which consisted of only single channel fluorescence) was removed using a custom algorithm. Two MIP images were also used to extract this neuron (obtained for the "X-Y" and "Y-Z" faces). Finally, a custom algorithm for masking single channel image stacks was applied to this specimen. This algorithm cropped the initial volume to the desired subvolume size and position.

3.2.4. Volume Rendering

Once the desired structures had been extracted, the combined FG-IR and CGRP-IR stacks were prepared for volume rendering. The first step in this procedure was to determine upper and lower thresholds for each fluorophore associated with each specimen. These thresholds served to brighten the appearance of dim structures and remove "background" (i.e. non-specific fluorescence and noise), respectively. Each extracted fluorophore stack was loaded into Adobe PhotoShop and its intensity histogram obtained. The intensity value below which 95-99% of all intensities were located was selected as an "upper threshold" and was recorded. Each image stack was then loaded into the volume rendering software for re-examination. While the masking procedure outlined above served to eliminate the majority of background labelling and presence of undesired objects, some artifacts remained immediately surrounding the neuron and fibres

in the X-Y plane for each image, as well as between images (most notably the CGRP-IR fibres) in the Z-plane. Using the "icol" utility, the lower threshold was determined by setting the transparency of all intensities below a certain value to 100% (i.e. invisible). The starting value for the lower threshold was zero. This was slowly increased and the effect on the loaded image stack was observed. This procedure was continued until the majority of remaining undesired background intensities were removed. The intensity value at this point was selected as the "lower threshold".

Once the lower and upper thresholds for each fluorophore image stack had been determined, both were merged into a single data set using a custom algorithm. This was done by combining the individual 8-bit stacks into a single 24-bit RGB (red-green-blue) image, with each fluorophore representing a different channel. In this scenario, CGRP-IR (Texas Red) was loaded into the red channel, FG-IR (FITC) was loaded into the green channel, and the blue channel was left empty since it was unused (i.e. it was filled with black). At the same time, the intensities of both data stacks were recalculated based on the lower and upper thresholds determined for each. The low threshold was set to 0 (full black) and the high threshold was set to 255 (full white), with all other intensities being interpolated linearly between these 2 extremes.

The methods described in the preceding paragraphs were also performed for specimen 2. Since specimen 1 was a single channel data set, it was not necessary to apply the "merge" algorithm on this stack.

3.2.5. Colour Quantization

Due to limitations with the volume rendering software that was used, the resulting 24-bit volume had to be converted back into an 8-bit representation. The conversion was achieved using colour quantization (reduction) software (a feature of the ImageMagick package, developed by John Cristy at DuPont, Inc.). This software uses the octree method of colour quantization (Gervautz and Purgathofer, 1988). Briefly, in the context of the double-labelled datasets that were examined, the colour quantization algorithm calculated the entire number of colours and the corresponding RGB values used in all images within the merged stack. Following this procedure, an optimized set of 256 (i.e. 8-bit) representative colours that best represented the entire original set were selected and these were applied to each image in the stack being processed. Although the merged stack contained only 256 colours, it was still in a 24-bit format following this procedure. A custom algorithm was used to create a colour lookup table (LUT) from this 24-bit dataset consisting of 256 index entries, each referencing a unique RGB triple representing a specific colour chosen by the quantization algorithm. The algorithm converted the 24-bit dataset into an 8-bit representation, replacing each RGB triple in the former with the corresponding LUT index value in the latter. The custom 8-bit LUT generated by this algorithm was saved to a file for subsequent use. Following this, the combined 8-bit data volume was then loaded into the volume rendering software for final visualization. The custom colour LUT was then loaded into the icol utility and was applied to the dataset. The final combined volume could be manipulated and viewed from any angle, such that all surfaces were visible. Furthermore, subvolumes (as described above) and cross sections could be generated and examined in detail.

The merging, colour quantization and 24- to 8-bit colour conversion procedures were also performed for specimen 2. In the case of specimen 1 which consisted of only single channel data, these procedures were not necessary. A custom algorithm was used to apply the selected lower and upper thresholds to this dataset, to interpolate intermediate intensities, and to generate a custom LUT (arbitrarily corresponding to green intensities) for use with the icol utility when the volume was displayed in BOB.

3.2.6. Measurement of the Distance Between CGRP-IR Fibres and Identified Gastric Efferent Neurons

In order to obtain these measurements, the full volume was rotated in 3-D space to locate areas that demonstrated the closest association between CGRP-IR fibres and the surface of the FG-IR neuron. Using the volume rendering software, clipping planes were adjusted to determine the coordinates of these regions. Cross sections through the volume in the X-Y plane were generated by setting the Z dimension to a value of 1 voxel. These images were then loaded into the NIH Image software package for further examination. Using this software, the images were magnified until individual pixels could be seen. Using the "distance" tool, a line was drawn between the closest red and green pixels in each cross section. This tool was calibrated with the the microns/pixel measurement obtained from the confocal software during acquisition, so that measurements would be reported in microns. Cross sections in the X-Y plane were used preferentially when making measurements, rather than cross sections in the X-Z or Y-Z planes (which were generated for visualization purposes only), due to the fact that the lateral resolution (i.e. acquisition resolution in the X-Y plane) of the confocal microscope

is better than the axial resolution (i.e. acquisition resolution in the Z-plane) of this device (Wilson and Sheppard, 1984).

3.2.7. Animations of 3-D Reconstructions

Animations of the 3-D reconstructions were constructed by generating individual images of the entire volume that were rotated at 5 degree increments around a selected axis (i.e. X or Y). These images were saved in the SGI image format and were played back in sequence using the "movieplayer" application that was supplied with the SGI workstation. The frame rate at which the images were displayed was adjusted until the motion appeared fluid, which was typically about 10 frames per second or greater.

3.3. Results

3.3.1. Controls

For immunocytochemisty of CGRP, incubation of brain stem sections with PBSHST or the second layer antisera alone gave no positive staining. The CGRP antiserum used has been characterized previously by preabsorption with CGRP (Buchan et al., 1991). For the studies designed for confocal microscopy which made use of antisera against FG, incubation of sections with avidin-FITC in the presence or absence of the biotinylated secondary antibody produced no staining of FG that could be detected within the FITC range.

Unfortunately, the combination of antisera used to label FG did contribute to a substantial amount of background (i.e. non-specific) staining which was visible within FITC detection wavelengths. This gave the tissue surrounding the FG-IR neurons a

bright green speckled appearance. In spite of this, the background staining could be clearly distinguished from the identified neurons during the preliminary phase of observation. This was done by comparing the appearance of the FG-labelling using the UV and FITC filters of the epifluorescence microscope (i.e. the "speckled" background was only visible in FITC detection wavelengths, while the FG labelling that was confined to neuronal elements was visible using both filters).

When sections containing Texas red-labelled CGRP-IR only were scanned using the dual acquisition mode of the confocal microscope, no fluorescence could be detected using the K1 filter (i.e. within the FITC emission range). In contrast, FITC-labelled FG-IR was found to produce some artifactual "bleed-through" labelling within the Texas red emission range when the K2 filter set was used in this acquisition mode. This only occurred in regions of very intense FG-IR, and not in areas of non-specific FITC labelling as described above. This problem was corrected in double-labelled sections using the "image subtraction" feature in Adobe PhotoShop, where the FITC image was subtracted from the Texas Red image in every optical section.

No FG labelling was observed in either the NA or the AP which would imply minimal leakage and nonspecific uptake of FG (Figure 16a; see Chapter 2). This was also the case when antisera to FG was used. The extent of retrograde labelling was consistent between all animals in the test group.

3.3.2. Retrograde Labelling

Injection of Fluorogold (FG) into the anterior and posterior surfaces along the greater curvature of the stomach (corpus) produced a distinct pattern of labelled neurons

within the DMV (Figure 16). Fluorogold-labelled neurons were observed bilaterally, extending from approximately -2.8 mm to +1.9 mm relative to the obex. The greatest number of FG-labelled cell bodies were observed at and adjacent to the level of the obex, with fewer FG-labelled cell bodies at the rostral and caudal ends of the DMV. The distribution and number of FG-labelled cell bodies were identical on both sides of the DMV.

Using epifluorescence microscopy, FG was visualized as granular labelling within the cytoplasm of labelled neurons. Dendritic labelling was relatively uncommon, and was only seen in a small number of identified neurons at levels rostral to the obex (typically, levels rostral to +500 μm). At levels immediately surrounding the obex where CGRP-IR was most prominent, very few dendrites of gastric efferent neurons could be observed. Use of antisera to FG slightly improved detection of the tracer within the dendrites of these neurons (even after confocal microscopy), as compared to when the tracer was visualized without immunoctyochemical processing. The majority of dendrites that were visible projected dorsally into the NTS, with fewer projecting ventrally.

Figure 16. Characteristic appearance and distribution of retrogradely-labelled neurons in coronal sections through the rat DMV following injection of FG along the greater curvature of the stomach. (A) A coronal section at position -200 μm; note the lack of uptake of FG by the AP. (B) A coronal section rostral to the obex at position +600 μm. Scalebar = 100 μm.

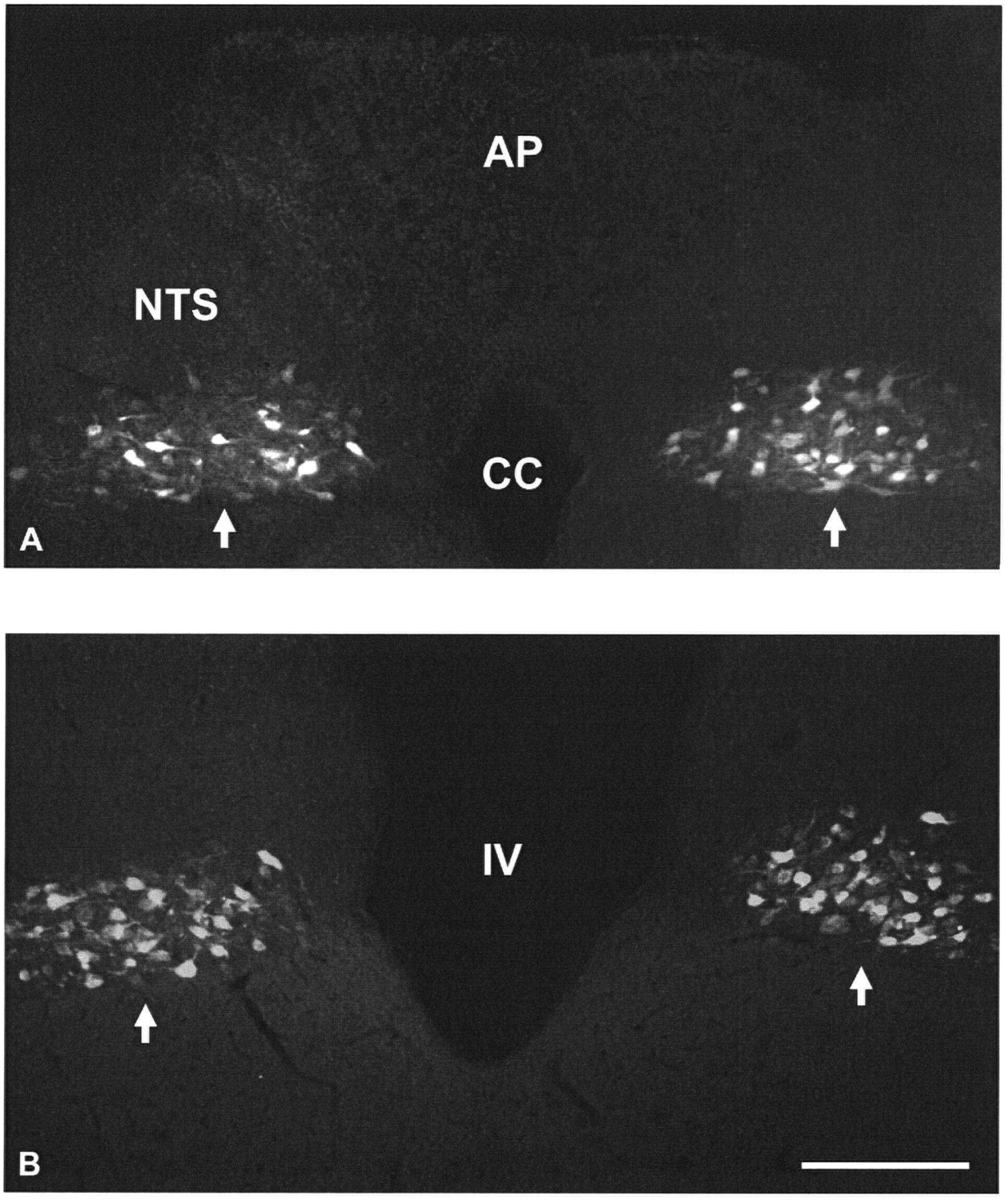
AP
NTS
CC
A
IV
B

The resolution at which the image stacks representing the neurons were acquired using the confocal microscope also affected the appearance of FG in the cytoplasm of these cells. This was especially true when subsequent 3-D reconstructions of the neurons were generated. In the case of Specimen 2, which had the smallest voxel size (0.2 μm^3), the granular appearance was most visible, whereas the use of acquisition parameters that yielded larger voxel sizes (e.g. 1.0 μm^3 for specimen 3) made it appear as if the FG-IR was more uniform. Examination of individual cross sections of most neurons, however, revealed that granular labelling was still present.

The morphology of identified gastric efferent neurons retrogradely-labelled with FG was found to vary somewhat, as can be seen in the 3-D reconstructions of three specimens presented in this chapter (Figures 19-21). Most had a spherical or ovoid soma, with few dendrites visible with the exception of specimen 3. Unfortunately, the 3-D appearance of the FG-IR neuron for specimen 1 was slightly distorted due to the fact that it was mechanically split into two halves (and thus spanned 2 serial sections) when the brain stem slices were cut in the cryostat (Figure 18a,b). Furthermore, some of the structural information for this neuron was lost due to constraints with the imaging procedure using the confocal microscope. This yielded out of focus optical sections at the very top and bottom of the corresponding image stacks that had to be discarded during volume rendering.

3.3.3. Location of CGRP-IR within the DVC using conventional epifluorescence microscopy

Preliminary examination of brain sections using a conventional epifluorescence microscope revealed CGRP-IR fibres within the NTS that penetrated ventrally into the DMV. The majority of CGRP-IR fibres were confined to the medial and gelatinosus subnuclei of the NTS around the level of the obex (Figure 17). The fibres traveled in a lateral direction within the DVC, as revealed by the coronal orientation in which the brain stem sections were cut. Very light CGRP-IR was also detected around the central canal and within the AP. While no CGRP-IR cell bodies were found within either the DMV or NTS, these were observed within the hypoglossal nucleus (Figure 17). Axons from these CGRP-IR cell bodies could not be traced into the vagal complex.

Very few somata of identified gastric efferent neurons within the DMV exhibited a close anatomical relationship with CGRP-IR fibres that projected into this region, and were located at the interface between the DMV and NTS at the level of the obex or immediately caudal to it. Furthermore, the density of CGRP-IR fibres within the DMV proper in this region was sparse (Figure 17). Since the retrograde label was confined to the soma and primary dendrites of most identified gastric efferents at the levels of the DVC where CGRP-IR was highest, few distal dendrites of these neurons could be visualized in the NTS.

Figure 17. Epifluorescence micrograph of a section through the medial brainstem (-200 μm relative to obex) illustrating the relationship of CGRP-IR nerve fibres (red) to FG-labelled gastric efferent neurons (green) in the DVC. The dotted line represents the approximate position of the interface between the DMV and NTS. Note that some neurons in the hypoglossal nucleus are labelled with CGRP-IR (arrows). Regions that appear yellow are due to the double exposure of Texas Red and FITC wavelength emissions, and do not represent co-localization of fluorophores. Scalebar = 50 μm.

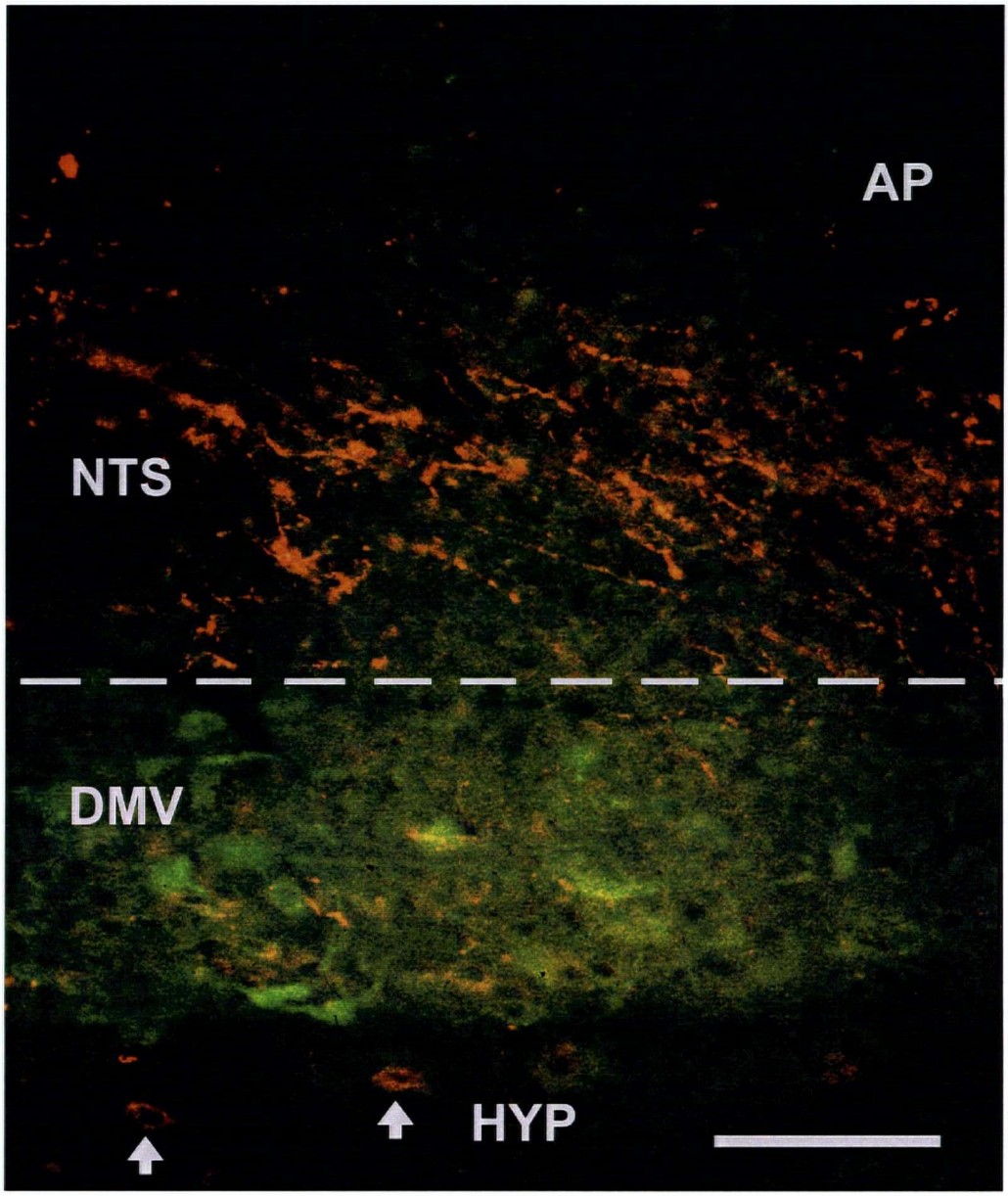
AP
NTS
DMV
HYP

In general, visualization of the precise association of CGRP-IR fibres with retrogradely-labelled neurons in these instances proved to be difficult using conventional epifluorescence microscopy. This was mainly due to background fluorescence from out-of-focus structures and background flare produced by the large number of gastric efferents that were brightly labelled with FG at these levels of the brainstem.

3.3.4. Association of CGRP-IR fibres with identified gastric efferent neurons observed using confocal microscopy and 3-D reconstruction techniques

Imaging of a small region at the interface of the NTS and DMV by confocal microscopy improved the resolution of both CGRP-IR and FG-IR and allowed discrimination of additional features. Maximum intensity projections formed from optical sections acquired in this region confirmed the results obtained using epifluorescence microscopy (Figure 18). These images indicated that CGRP-IR fibres came in close proximity to a small number of identified gastric efferent neurons within the DMV. Only a small number of CGRP-IR fibres were observed within the DMV, and the density of these was low. In most cases where a close spatial relationship between CGRP-IR fibres and identified neurons was apparent, the majority of these fibres were seen in the vicinity of the proximal dendrites of these neurons while fewer were observed near the soma. Unfortunately, despite the improved resolution offered by the confocal microscope, little retrograde label could be detected within the distal dendrites of the identified gastric efferent neurons making it impossible to compare the association between these structures and CGRP-IR fibres within the NTS.

As revealed by MIP images, immunoreactivity for CGRP within labelled nerve fibres was high (Figure 18). Continuous CGRP-IR along the length of the fibres gave them a rope-like appearance. Numerous sites on the fibres were marked by an increased fluorescence intensity typical of varicosities. Using maximum intensity images alone, it was not possible to determine the orientation of the fibres with respect to the neuronal surfaces.

Figure 18. Maximum intensity projections generated from confocal microscopy data demonstrating a close spatial relationship between CGRP-IR nerve fibres (red) and FG-labelled gastric efferent neurons (green) within the DMV. (A) and (B). Specimen 2; scalebar = 50 μm. (C). Specimen 3. Regions that appear yellow are an artifact of merging the MIP projections (green and red) and do not denote colocalization.
Scalebar = 20 μm.

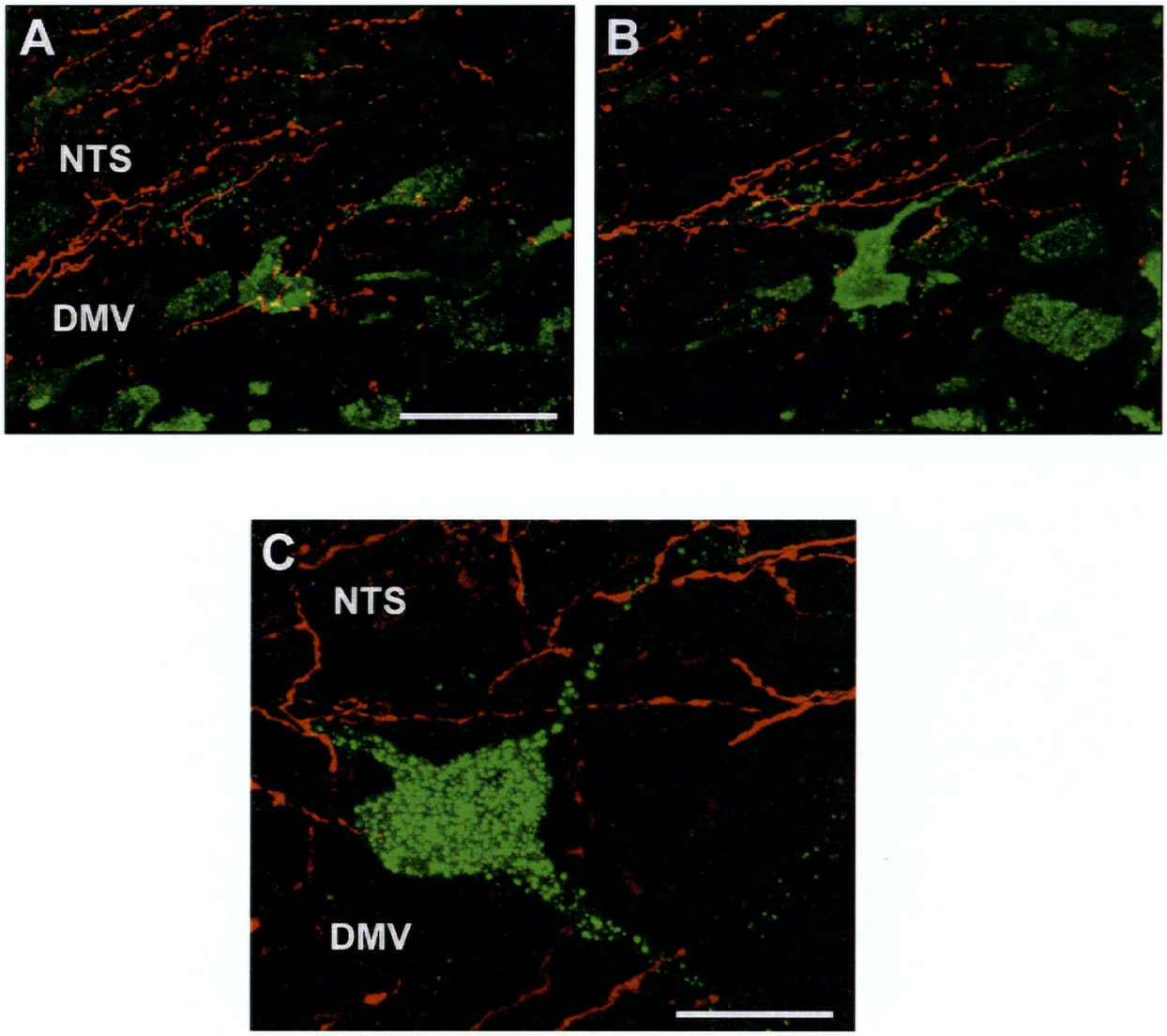
A
NTS
DMV
B
C
NTS
DMV

When 3-D reconstructions were generated using volume rendering software, a more precise spatial relationship between CGRP-IR fibres and an identified gastric efferent neuron could be observed. The volume rendering software that was used permitted the observation of subvolumes (e.g. of the area immediately surrounding the dendrites of an identified gastric efferent neuron) which further enhanced visualization of this relationship. To fully appreciate the 3-D association of CGRP-IR fibres with respect to the identified gastric efferent neurons, animations were generated whereby each reconstruction was rotated about an axis (i.e. X or Y). When viewed at an appropriate speed, the motion appeared fluid and the appearance of depth was accentuated.

3.3.5. Distance Measurements Between CGRP-IR Fibres and FG-IR Neurons in the DMV

Because the size of voxels comprising the 3-D reconstructions was known, spatial measurements could be made. Rather than attempting to count all CGRP-IR fibres that were present, a comparison was made between the proportion of fibres that appeared to directly abut on the cell membrane of isolated FG-labelled neurons versus those that surrounded these neurons without making apparent contact. As can be seen in both of the double-labelled specimens presented in this chapter, most CGRP-IR fibres passed by the proximal dendrites or soma of the identified neurons without terminating on them. The closest these fibres came is within 3-4 μm of the neuronal membrane. The majority of CGRP-IR fibres were 5-10 μm or further away from identified neurons.

Figure 19. "Specimen 1": Volume renderings of a neuron in the DMV that was labelled for FG-IR (green) and CGRP-IR (red) that was generated from two 25 µm thick serial sections at positions -350 and -325 µm relative to the obex. (A) front view; scalebar = 50 µm. (B) back view. (C) left view. (D) right view. (E) tilted view. (F) and (G) cross sections through the volume demonstrating areas where CGRP-IR nerve fibres came into close association with the neuronal membrane of a FG-labelled neuron (arrows). Scalebar = 10 µm.

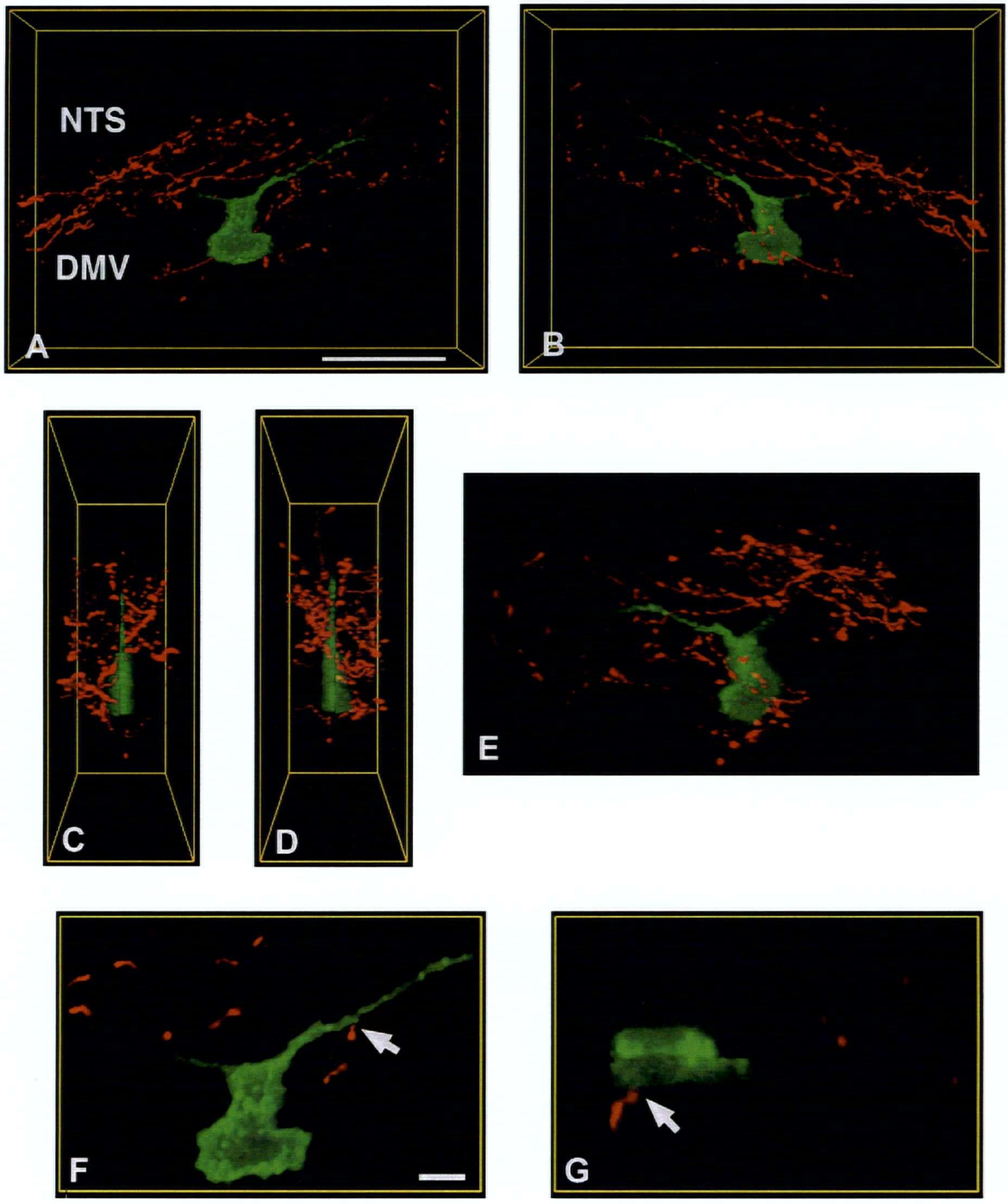
NTS
DMV
A
B
C
D
E
F
G

Figure 20. "Specimen 2": Volume renderings of a neuron in the DMV that was labelled for FG-IR (green) and CGRP-IR (red) that was generated from a single section at position +100 μm relative to the obex. (A) front view; scalebar = 20 μm. (B) back view. (C) right view. (D) left view. (E) tilted view. Note that the CGRP-IR nerve fibres are preferentially associated with the dendrites of the neuron (arrows). (F) and (G) cross sections through the volume demonstrating areas where CGRP-IR nerve fibres came into close association with the neuronal membrane of a FG-labelled neuron (arrows). Scalebar = 20 μm.

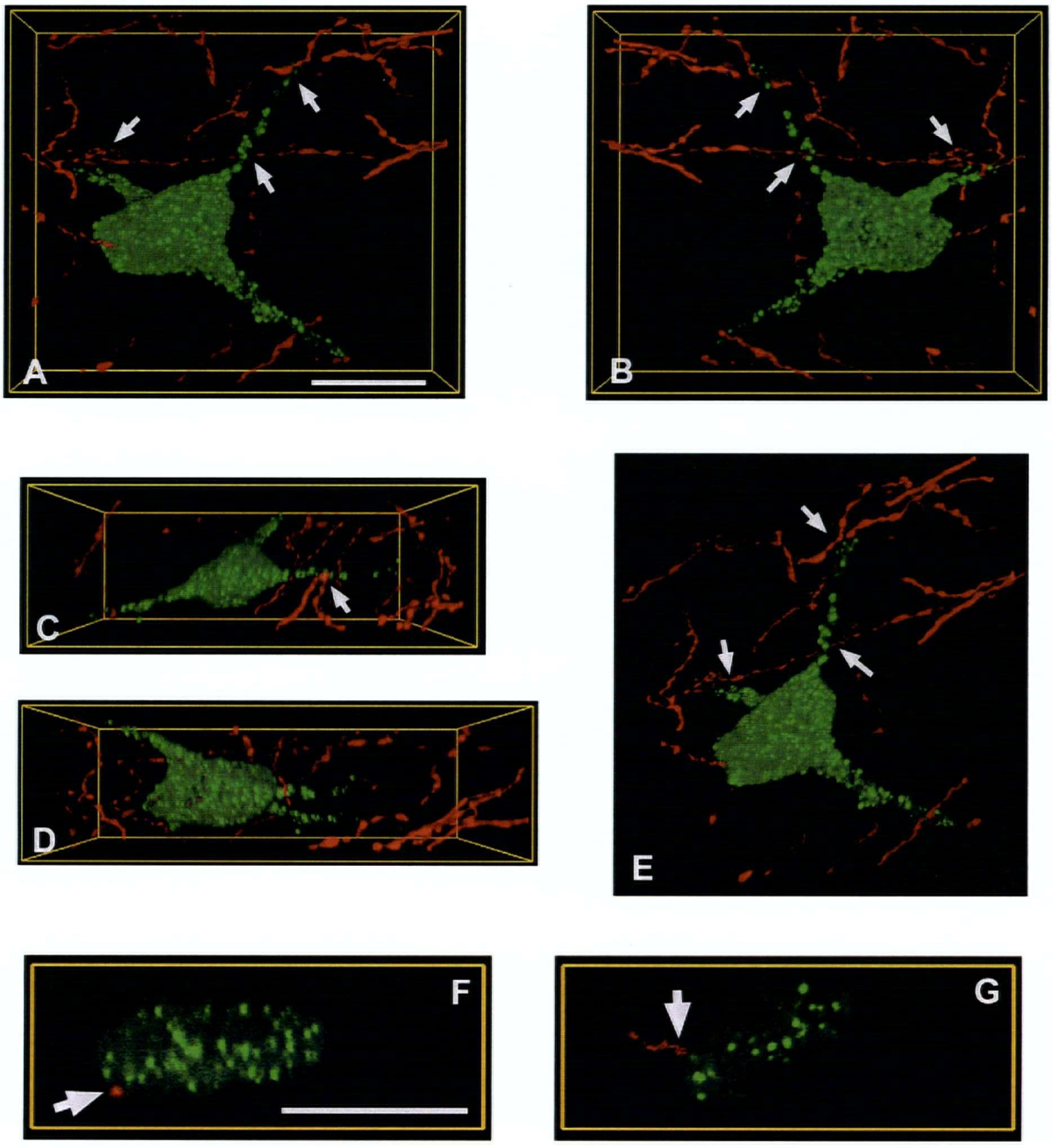
A
B
C
D
E
F
G

Figure 21. "Specimen 3": Volume renderings of a FG-labelled neuron generated from a single 50 μm thick section at position +650 μm relative to the obex. (A) front view of neuron before final segmentation; scalebar = 50 μm. (B) titled view showing portions of other neurons (arrows) which appeared to be part of the neuron in (A). (C) front view after final segmentation which removed these structures. (D) right view. (E) tilted view.

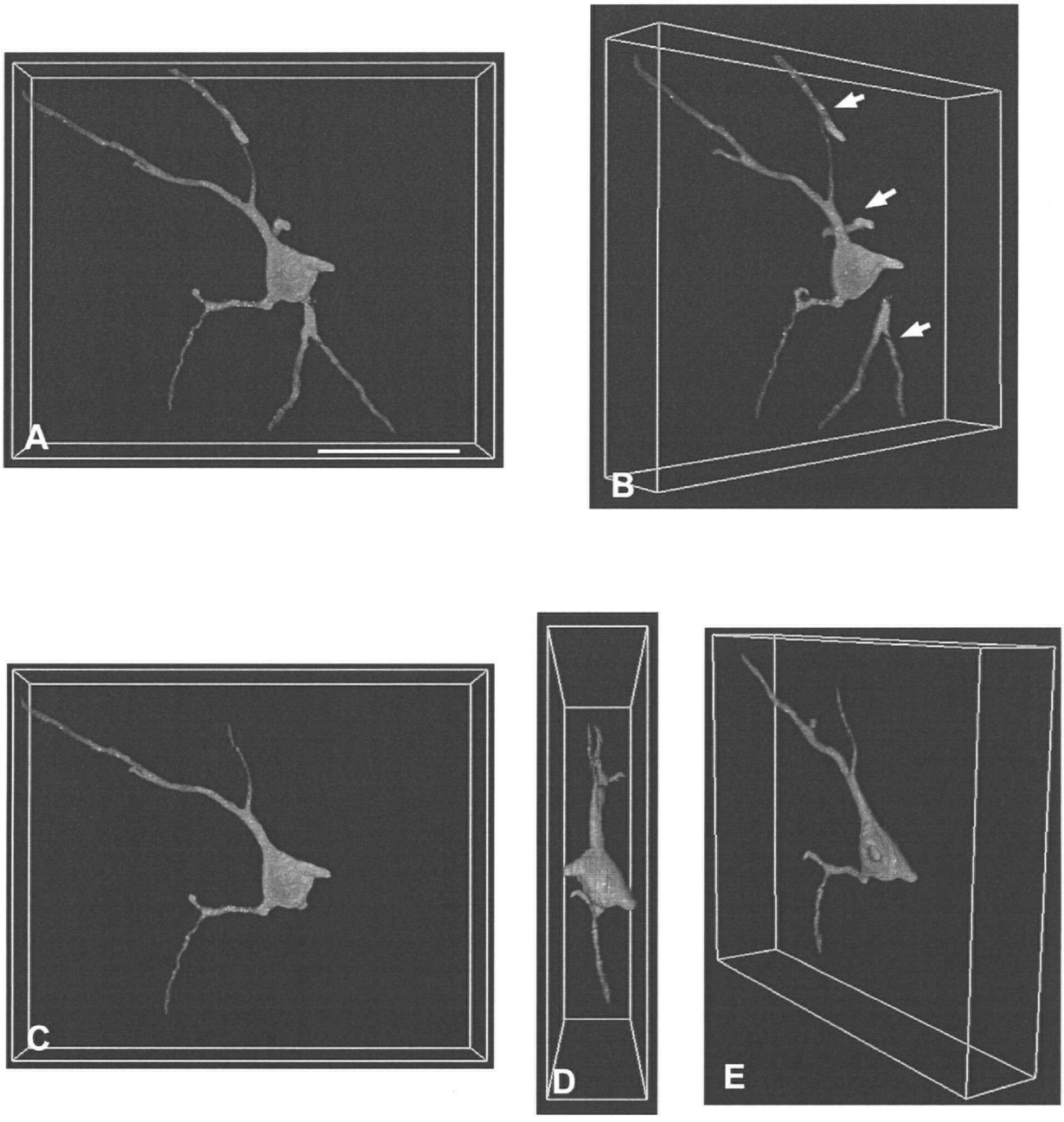
A
B
C
D
E

It was exceedingly rare to find CGRP-IR fibres within a submicron distance from the cell membrane of a FG-IR neuron. Although such sites may indicate the location at which a CGRP-IR nerve fibre comes into contact with the neuronal membrane of a FG-IR neuron, the resolution is not high enough to state this with certainty. Therefore, these locations will be referred to as "presumptive termination sites" to reflect this fact. In the first double labelled reconstruction, two presumptive termination sites could be seen on the cell soma of the neuron. Although the majority of CGRP-IR fibres appeared to run in parallel with the dendrites of this neuron, no such termination sites associated with these structures could be observed. Furthermore, no presumptive termination sites could be observed in specimen 2.

3.4. Discussion

The retrograde tracing results were in accordance with previous reports of the location and distribution of gastric efferent neurons within the DMV that project to the greater curvature of the rat stomach (Donahue et al., 1988; Yoshida et al., 1989; Buchan et al., 1991). Injection of the retrograde tracer into both the posterior and anterior surfaces of the stomach labelled equal numbers of cells on each side of the DMV (Table 4; Figure 25a). The majority of labelled neurons were distributed bilaterally within the medial region of the DMV at all levels of the DVC. Furthermore, no labelling was observed in either the AP or NA. These results would suggest that the tracer was taken up and transported selectively by gastric vagal efferent fibres.

The general staining pattern and distribution of CGRP-IR within the DVC was in general agreement with the results of prior reports (Rosenfeld et al., 1983; Kawai et al., 1985; Buchan et al., 1991, Sykes et al., 1994). In this study, CGRP-IR was confined to nerve fibres located in the NTS, with a few fibres penetrating into the DMV and AP. Although no CGRP-IR cell bodies were observed in the NTS in the current study, they have been reported in this location previously (e.g. Kawai et al., 1985 and Skofitsch and Jacobowitz, 1985). It should be noted however, that these studies used colchicine, which has been shown to increase CGRP mRNA levels in some systems (Rethelyi et al., 1991). Interestingly, in other studies that have not used this substance (e.g. Buchan et al., 1991, Sykes et al., 1994), although CGRP-IR somata were not observed within the NTS, they were observed in the nearby hypoglossal nuclei. This may suggest that, if present within interneurons in the NTS, CGRP is normally expressed at very low levels.

Although the highest density of CGRP-IR nerve fibres was observed around the level of the obex where the greatest number of retrogradely-labelled gastric efferent neurons were located, few identified neurons exhibited a close spatial relationship with CGRP-IR fibres. Those that did were situated at the interface between the DMV and NTS. Distance measurements gathered from cross-sections through 3-D reconstructions of representative gastric efferent neurons in this location revealed that the majority of CGRP-IR fibres were > 5 μm away from the neuronal membrane.

However, since the retrograde tracer used (FG) could only be detected within the soma and proximal dendrites of identified neurons, the possibility that the CGRP-IR fibres within the NTS were in close association with dendrites of gastric efferent neurons in this region could not be clearly examined. Previous studies using alternative neuronal

tracers such as CT-HRP (Shapiro and Miselis, 1985; Altschuler et al., 1992) and intracellular injection of fluorescent dyes (Fox and Powley, 1992) have demonstrated much more extensive arborizations of DMV neurons that project into the NTS at these brainstem levels. It is worthy of note that the few CGRP-IR nerve fibres that were detected in the vicinity of identified gastric efferent neurons in this study did appear to be preferentially distributed to the dendrites rather than the soma of these neurons (Figures 19 and 20).

The fact that a high density of binding sites for CGRP have previously been localized to the NTS would also suggest that this may be the site where the peptide exerts its vagally-mediated inhibitory effect on gastric acid secretion (Sexton et al., 1986, Inagaki et al., 1986). A previous study in which CGRP was injected intracisternally resulted in a dose-dependent inhibition of unit efferent discharges recorded from the gastric branch of the vagus nerve (Wei and Taché, 1990). This result would indicate that the antisecretory effect that is mediated by CGRP occurs via inhibition of vagal efferent neurons in the DMV (Taché, 1992). This inhibition of vagal outflow would result in a diminished cholinergic and histaminergic input to the parietal cells, which in turn would decrease gastric acid secretion. Although the influence of CGRP on neuronal activity within DVC neurons has not been examined, an inhibitory action for this peptide has been reported in rat forebrain where it has been shown to reduce the extracellular activity of single neurons (Twery and Moss, 1985). Taken together, these results would suggest that the vagally-mediated effect of CGRP on gastric acid secretion may involve an inhibitory effect of CGRP released by fibres in the medial NTS on the dendrites of gastric efferent neurons in this region.

The origin of the CGRP-IR fibres within the DVC remains unclear. The distribution and lateral orientation of these fibres is similar to that of primary vagal afferents projecting to the NTS from the viscera (Shapiro and Miselis, 1985; Altschuler, 1992). Specifically, a high density of CGRP-IR fibres was observed in the medialis and gelatinosus subnuclei of the NTS, areas known to contain the highest concentration of gastric vagal afferent fibres (Altchuler, 1992). Although previous studies have localized CGRP within vagal afferent neurons in the nodose ganglion of the rat by immunocytochemistry (Lundberg et al., 1978; Katz and Karten, 1980; Helke and Hill, 1988) and *in situ* hybridization (Czyzyk-Krzeska et al., 1991; Huang et al., 1994), there is little evidence to suggest that vagal afferents projecting to the DVC contribute significantly to the CGRP-IR fibres observed in this region. One study that combined injection of an anterograde tracer into the nodose ganglion with immunocytochemistry to detect CGRP in the DVC found that the nodose only contributes a small proportion of the total number of CGRP-IR axons observed within this brainstem region (Sykes et al, 1994). Conversely, studies which combined the injection of a retrograde tracer into the stomach followed by immunocytochemistry for CGRP in the nodose ganglion have demonstrated that only 2% - 10% of gastric vagal afferent neurons contain CGRP (Green and Dockray, 1987; Sternini, 1992). Furthermore, it has been demonstrated that subdiaphragmatic vagotomy and celiac ganglionectomy have no effect on the CGRP staining observed within the DVC, indicating that a peripheral source of the peptide is unlikely (Buchan et al., 1991).

In addition to the possibility of CGRP-IR interneurons within the NTS, other possible sources of CGRP-IR fibres within the dorsomedial medulla include the petrosal

and trigeminal ganglia, which are known to project to this region and have been shown to contain CGRP-IR cell bodies (Helke and Hill, 1988). Finally, since CGRP-IR cell bodies have been found in several brain regions such as the hypothalamus and amygdala (Kawai et al., 1985; Skofitsch and Jacobowitz, 1985) that are known to project to the NTS (see section 1.12 in Introduction and Leslie et al., 1992), these sources could contribute to the pool of CGRP-IR fibres observed.

Despite limitations with the retrograde tracer that was used (i.e. the inability to effectively label the dendrites of gastric efferent neurons), the data gathered from these studies demonstrated that a combination of retrograde tracing, immunocytochemistry, confocal microscopy, image processing and volume rendering techniques can be used to generate 3-D reconstructions of identified gastric efferent neurons and surrounding nerve fibres in the brainstem of the rat. These reconstructions provided information about the 3-D spatial relationship between CGRP-IR nerve fibres and identified gastric efferent neurons than could not be obtained using conventional techniques such as epifluorescence microscopy alone.

The out-of-focus structures that were present when viewing brainstem slices with an epifluorescence microscope were greatly reduced when using a LSCM. The ability of the confocal to capture optical sections through the depth of a specimen yielded high resolution images with submicron resolution. Although these images could be combined to produce MIP images that provided useful preliminary visualization of the relative positions of the CGRP-IR fibres and retrogradely-labelled neurons, it was not until reconstructions were generated using volume rendering software that the 3-D spatial arrangement of these structures could be observed.

A valuable feature of the 3-D reconstruction process was the ability to merge the data gathered from multiple fluorophores so that different structures (i.e. fibres and neurons) could be viewed simultaneously. Furthermore, the ability to assign an opacity value to individual intensity levels (corresponding to fluorescence intensities), in combination with thresholding and masking techniques, enabled structures of interest to be extracted from the surrounding background. This permitted an unimpaired view of the relationship of CGRP-IR nerve fibres to all surfaces of identified gastric efferent neurons, either by manual manipulation of the volumes with a computer mouse or by viewing animations of simple rotational sequences. The software used also permitted the observation of subvolumes of interest as well as the ability to generate 2-D cross sections at any plane through each volume. Finally, because the voxel sizes comprising each volume were known, measurements could be made between relevant structures of interest.

In summary, the results of these studies confirmed the hypothesis that a combination of retrograde tracing, fluorescence immunocytochemistry, confocal microscopy, image processing and volume rendering techniques can be used to generate 3-D reconstructions of identified gastric efferent neurons and surrounding nerve fibres in the brainstem of the rat. These reconstructions provided information about the morphology and spatial arrangement of identified structures that could not be achieved using conventional techniques such as epifluorescence microscopy alone. The hypothesis that CGRP-IR nerve fibres came into close spatial association with identified gastric efferent neurons could not be tested fully. Although the results revealed that a small number of CGRP-IR fibres came into close spatial association with the somata and

proximal dendrites of identified gastric efferent neurons at the interface between the DMV and NTS, a relationship between the distal dendrites of these neurons and CGRP-IR fibres within the NTS could not be examined due to limitations in the transport of the tracer that was used.

4. ASSOCIATION OF SUBSTANCE P AND ITS RECEPTOR WITH GASTRIC EFFERENT NEURONS IN THE DMV OF THE RAT

4.1. Introduction

Previous studies have identified substance P (SP) immunoreactive nerve fibres throughout the DMV and NTS (Chiba and Murata, 1982; Kalia et al., 1984; Kawano and Chiba, 1984), and a pilot study in our laboratory (Buchan et al., 1991) demonstrated that some of these fibres come into close spatial contact with gastric efferent neurons within the DMV. Although SP receptors within the DVC have not been identified directly, autoradiography was used to locate binding sites for ^{125}I-labelled peptide and demonstrated extensive labelling of the mid-regions of the DMV and NTS with some binding sites also present in the AP (Helke et al., 1984; Manaker and Rizio, 1989; Manaker and Zucchi, 1993). The NK-1r has recently been cloned (NK-1r), and *in situ* hybridization has been undertaken to identify neurons expressing NK-1r mRNA in the brain (Elde et al., 1990; Kiyama et al., 1993; Maeno et al., 1993). Although none of these studies concentrated on the brainstem, labelling of neurons in the DMV and NTS was reported.

The results of previous experiments that employed pharmacological methods have suggested that SP may play a role in the regulation of gastric function. It has been demonstrated that superfusion of SP onto neurons within the DMV induces either depolarization or hyperpolarization via a direct effect on the postsynaptic membrane (Plata-Salaman et al., 1989; Martini-Luccarini et al., 1996). Furthermore, injection of SP

into the medial NTS has been shown to increase gastric pressure and inhibit gastric motility (Spencer and Talman, 1986).

The results of these former studies would suggest that there is an anatomical basis for the direct effect of substance P (SP) acting on identified gastric efferent neurons within the DMV of the rat. In order to verify this, two basic hypotheses must be validated. Firstly, SP-IR nerve fibres should either terminate on, or come in close spatial proximity to, the dendrites and/or soma of these neurons. Secondly, these neurons should express receptors for SP.

In order to test both of these hypotheses, a series of experiments employing an antibody to the NK-1 receptor (NK-1r; Vigna et al., 1994) were conducted. In the first series of experiments, retrograde tracing and fluorescence immunocytochemistry were used in conjunction with conventional epifluorescence microscopy to map the distribution of SP-IR, NK-1r-IR and FG-labelled gastric efferent neurons within the DMV. Building upon the methodology established in Chapter 3, latter experiments made use of 3-D reconstruction techniques to provide a detailed analysis of the anatomical relationship between the peptide, receptor and identified gastric efferent neurons.

4.2. Methods

4.2.1. Mapping the Distribution of SP-IR, NK-1r-IR and Identified Gastric Efferent Neurons in the DMV of the Rat

A group of 11 rats were injected with a solution of 4% Fluoro-Gold along the greater curvature of the stomach as described in Chapter 2. After allowing time for

retrograde transport of the tracer, the rats were perfused and fixed, and 50 μm coronal or sagittal sections were cut. While cutting, the section at the position of the obex was noted and all other sections were referenced as being either rostral (+) or caudal (-) to this landmark. Distances between sections were expressed in microns.

Brainstem sections from -3.0 mm to +3.0 mm were processed for immunocytochemistry in 48 well plastic plates following the protocols outlined in chapter 2. To localize SP, a guinea pig anti-SP antibody ("SP-6"; provided by Dr. Kwok, Department of Physiology, University of British Columbia) was used at a concentration of 1:1000, and visualized using Texas Red conjugated donkey anti-guinea pig IgG (Jackson Labs) at 1:1000. The NK-1 receptor was localized using a rabbit anti-NK-1r antibody which was generated against a synthetic peptide corresponding to a region in the C-terminus of the receptor (residues 393-407) (provided by Dr.Vigna, Duke University Medical Center, NC, USA). This antibody was used at a dilution of 1:5000 and was visualized using a fluorescein conjugated donkey anti-rabbit IgG (Jackson Labs) at 1:1000. Some sections were processed to visualize NK-1r-IR using the immunoperoxidase method. For these studies, the NK-1r antibody was used at a dilution of 1:10,000.

Control incubations were performed by either omitting the primary antibodies and substituting normal rabbit or guinea pig serum, or by pre-absorption of the SP antiserum with SP, NK-B and bombesin (10μM). For avidin-biotin-peroxidase staining, some sections were developed in DAB/Ni solution with the primary and/or secondary antibody incubations omitted. In double labelling experiments, the secondary antibodies had been pre-screened to ensure the absence of cross reactivity. The NK-1r antibody has been

characterized previously (Vigna et al., 1994). Briefly, Western blots of a membrane preparation produced from the homogenization of KNRK cells that were transfected with the NK-1r revealed that the anti-NK-1r antibody reacted only to the band corresponding to purified NK-1r. Furthermore, preabsorption of the anti-NK-1r with the protein fragment used to generate the antibody abolished staining as visualized by immunocytochemistry.

Appropriate controls for retrograde tracing were also conducted. The spread of tracer at the injection site was monitored using the protocols outlined chapter 2 regarding tracer leakage. The extent of labelling in the AP and nucleus ambiguus were checked following histological processing of the brain tissue.

As mentioned above, the obex was used as a point of reference for the relative position of coronal sections within the medulla. In the case of brain stem slices that were cut in the sagittal plane, the position of each section was stated relative to the sagittal section that divided the central canal. As with coronal sections, positions were listed in microns. Schematic illustrations drawn with reference to stereotaxic atlases of the rat brain (Paxinos and Watson, 1986; Barraco et al., 1992).

The initial experiments in this study utilized 50μm sections from brain stem cut either in the coronal (N=5 rats) or saggital (N=3 rats) plane to establish the boundaries of the NK-1r and FG staining. The final series of experiments utilized brain stem sections taken in the coronal plane only for quantitative studies (N=3 rats). Sections were screened at 400x magnification and the number of FG positive, NK-1r positive and co-labelled neurons (FG+NK-1r) from -1.35mm to +2.0mm were counted. The data collected was expressed in terms of mean number of cell bodies per section ± SD. A

visual assessment of labelled nerve fibre density provided a qualitative scale with the highest density being assigned (+++) and sparse staining (+).

4.2.2. Examination of SP, NK-1r and Identified Gastric Efferent Neurons in the DMV using 3-D Reconstruction Techniques

For these experiments, two groups of 4 Male Wistar rats were used. The retrograde tracer selected for these studies was cholera toxin B subunit (CT-B; List Labs, CA). Rats were anesthetized and 20 µl of 0.1% CT-B was injected along the greater curvature of the stomach as described in chapter 2. After allowing time for transport of the tracer, the animals were perfused and fixed and brain sections were cut in a cryostat. For the first group of animals, 50 µm thick sections were cut in the coronal plane, whereas 50 µm thick sections were cut in the horizontal plane for the second group. Coronal sections were referenced with regard to the obex, whereas the position of horizontal sections was obtained using a detailed atlas of the brainstem (Barraco et al., 1992).

Brain stem sections were processed for immunofluorescence as outlined in chapter 2. Sections were incubated with the following antisera: rabbit antiserum to NK-1r (provided by Dr.Vigna, Duke University Medical Center, NC) at a dilution of 1:5,000, guinea pig antiserum to SP ("SP-6"; provided by Dr. Kwok, Dept. of Physiology, U.B.C) at 1:1000 and goat antiserum to CT-B (List Labs., CA) at 1:750. Some sections were incubated with anti-NK-1r alone, with antisera against SP and NK-1r only, or with antisera against NK-1r and CT-B only. The primary antisera were visualized using the following fluorescence-conjugated antibodies: Cy2 conjugated donkey anti-rabbit IgG at

1:1000 (for NK-1r), Texas Red conjugated donkey anti-guinea pig IgG at 1:750 (for SP) and Cy5 conjugated donkey-anti goat IgG at 1:750 (for CT-B). Cy2 was selected as a replacement for FITC in these studies due to it being brighter and more photostable (Hartig et al., 1996). Unfortunately, Cy2 was not readily available when the earlier FG/CGRP studies were conducted (Chapter 3), otherwise it would have been used instead of FITC in those experiments as well. All secondary antisera were obtained from Jackson Labs. After immunocytochemical processing, the sections were mounted on glass slides and coverslips were applied using PBS/glycerine (1:9), pH 8.7, containing 9mM p-phenylenediamine.

Control incubations were performed by either omitting the primary antibodies and substituting normal rabbit, guinea pig or goat serum, or by omitting the secondary antibodies, all of which yielded negative staining. The specificity of the SP and NK-1r antisera have been characterized previously (Buchan et al., 1991; Vigna et al., 1994). The specificity of the CT-B antibodies was assessed by List Labs, CA, prior to shipment.

Selected specimens were scanned with a Bio-Rad MRC-600 laser scanning confocal microscope. Initially, a series of coronal sections from different rostrocaudal levels of the DMV containing labelling for NK-1r-IR (Cy2) only were scanned with the 488 line of the confocal in conjunction with the BHS filter block, using a 10x dry (0.30 NA) objective. For each of these sections, a 512x512x50 image stack was collected (with dimensions of 1.0 μm^3/voxel) and a corresponding MIP image for each was generated. Next, sections (both coronal and horizontal) that were triple labelled for SP, NK-1r and CT-B were scanned using a 2 stage process. First, the dual acquisition mode (488 and 568 nm excitation) and K1/K2 filter block was used to capture NK-1r (Cy2) and SP

(Texas Red) fluorescence. Second, the specimen was re-scanned at the same position (in X and Y, and Z-range) using 647 nm laser line in conjunction with the RHS filter block (see Appendix II for the spectral characteristics of this filter) to capture the CT-B (Cy5) fluorescence. These specimens were scanned using the 63x objective with dimensions of 0.2 μm^3/voxel. Some coronal sections that were double-labelled for NK-1r and SP were also scanned using the dual acquisition mode, also using the 63x objective and dimensions of 0.2 μm^3/voxel. Finally, overlapping fields of view spanning the rostral pole of the left DMV in a representative horizontal section were scanned using a 20x dry objective (0.75 NA) to create a montage view of this region. Separate passes were used to detect NK-1r (488 line/BHS filter block) and CT-B (647 line/RHS filter block). For each field of view, 70 images with dimensions of 768x512x70 (voxel size of 0.7 μm^3) were acquired.

Three dimensional reconstructions were generated using a combination of image processing steps and volume rendering software as described in chapter 3. The addition of a third label (Cy5) in these studies did not result in any significant changes to the methods described in the earlier chapter. When merging three individual channels to produce a combined RGB volume, a modified version of the custom algorithm used to merge the dual-label datasets in Chapter 3 was used. In this case, the Cy5 stack was loaded into the blue channel, which was previously set to black when only two datasets were used.

A significant change was made to the protocol used for the extraction of objects of interest from 3-D volumes that is presented in chapter 2. Instead of using a purely interactive method for determining the lower intensity threshold to be used for removal of

"background" fluorescence, a semi-quantitative method was added to this selection process. Control brain stem sections (N=3) that were cut serial to a test specimen were developed in a solution containing only the secondary antisera conjugated to the fluorophores being used (i.e. Cy2, Texas Red and Cy5). These sections were developed in parallel to the test section using the same secondary antisera solution for consistency. The control sections were scanned using the confocal microscope in the same region (i.e. DMV) on the same day and using the same acquisition parameters as the test specimen. Image stacks of the same size and resolution as the test specimen were gathered.

Figure 22. Improved segmentation of 3-D objects from brainstem sections using histogram data of control sections. (A) Histogram data of 3 brainstem sections labelled only with a Texas-Red conjugated secondary antibody (tall plots) vs. that of a specimen which was incubated with primary antisera against SP and a Texas-Red conjugated secondary antibody (short plot); CM = mean intensity of controls; SD = standard deviation units from mean; SM = mean intensity in specimen data; MAX = maximum intensity in specimen data chosen for histogram stretching (99% of intensity values fell below this value). Inset: mean intensity ± standard deviation (SD) for controls and specimen data. (B-E) Effect of selecting different minimum intensity values for thresholding/opacity assignment when viewing volume renderings of SP-IR: (B) using CM - 1 SD; (C) using CM; (D) using a value >CM and <CM + 2 SD (actual value used); (E) CM + 2 SD. Scalebar = 20 μm.

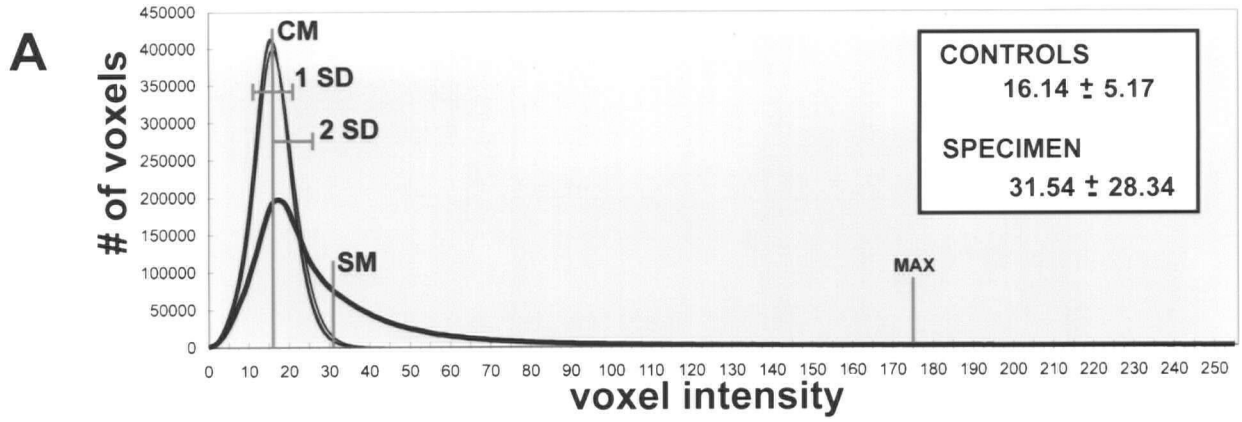
A
# of voxels
450000
400000
350000
300000
250000
200000
150000
100000
50000
0
CM
1 SD
2 SD
SM
MAX
CONTROLS
16.14 ± 5.17
SPECIMEN
31.54 ± 28.34
0 10 20 30 40 50 60 70 80 90 100 110 120 130 140 150 160 170 180 190 200 210 220 230 240 250
voxel intensity

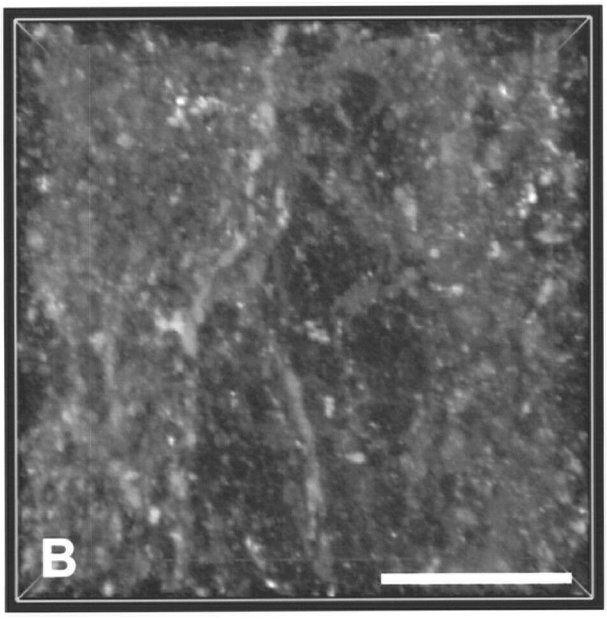
B

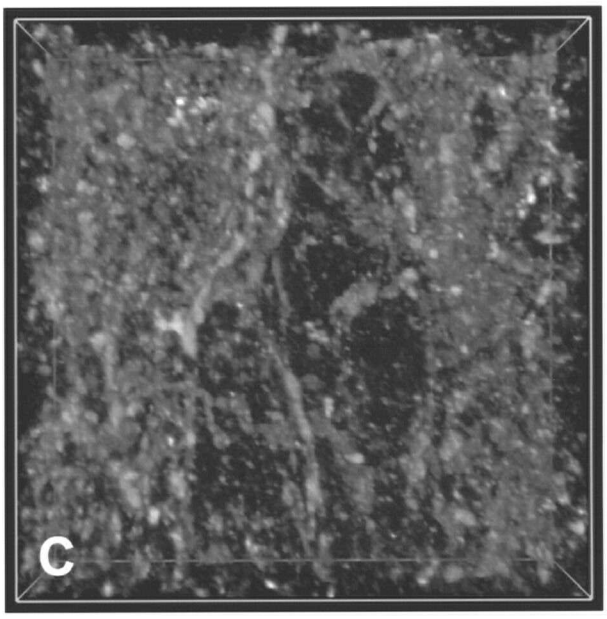
C

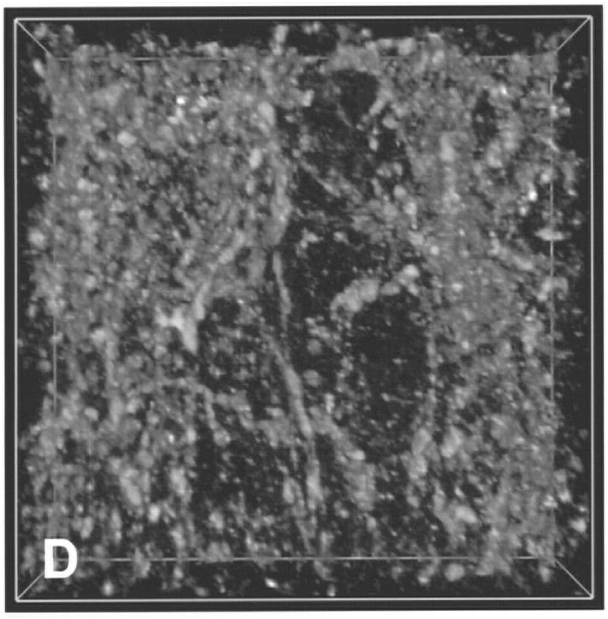
D

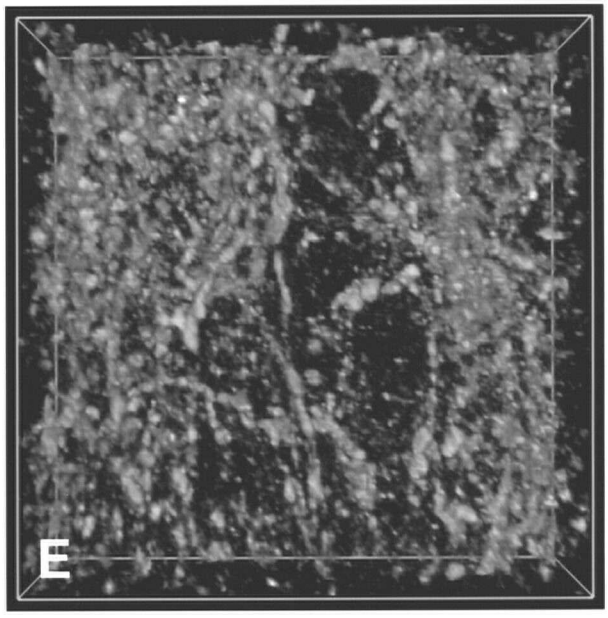
E

The histograms of control and actual specimens was initially analyzed by loading these datasets into Adobe PhotoShop as "raw" images and using the histogram tool. Numerical values representing the histogram data for each fluorophore in each of the control stacks and specimens was generated separately using a custom algorithm which measured the frequency of each 8-bit intensity value within each stack and output these values to a file. These files were then loaded into Microsoft Excel statistical/graphing software on a IBM-PC compatible computer and graphs were generated. The mean intensity and standard deviation for each histogram were calculated. The mean intensity ± 2 standard deviation units was used as the "range" when the lower threshold for the test data set was to be determined interactively (Figure 22; see also section 3.2.4).

Montage images of the rostral pole of the left DMV were created from 4 MIP images generated for overlapping fields of view captured from a horizontal section labelled with NK-1r (Cy2) and CT-B (Cy5). The set of MIP images corresponding to each fluorophore was loaded separately into Adobe PhotoShop software where they were cropped and composited into a seamless montage image. Since the acquisition parameters (e.g. black level and gain) were kept constant when acquiring the separate fields of view, only minor adjustments to the brightness and contrast of the overlapping maximum intensity images were required. The separate montage images generated for NK-1r and CT-B were merged into a combined RGB image (NK-1r assigned to the green channel, CT-B assigned to the blue channel) using PhotoShop so that both could be observed simultaneously.

A sample (N=4) of identified gastric efferent neurons that were labelled with CT-B and co-labelled with NK-1r-IR were extracted from individual stacks comprising

the montage data for 3-D reconstruction. Individual neurons were isolated in a given stack by stepping through optical sections (i.e. Z-planes) using the "IMOD" package (software for 3-D reconstruction from serial sections, obtained from the 3-D Fine Structure Laboratory, University of Colorado). Once a co-labelled neuron was located (exhibiting NK-1r-IR on its membrane and CT-B in its cytoplasm), its processes were followed from section to section (both above and below the plane of original identification) until they could no longer be traced reliably. Maximum intensity projections were created for the selective range of optical sections that confined each neuron and its processes, and these were used as masks to extract the neurons as described in chapter 3. The binary masks for each neuron that were generated in the "X-Y" plane were loaded into PhotoShop and used to create "outline" images of the neurons. These were then composited onto the combined montage view to label the positions from which the neurons were extracted.

Counts of labelled somata within the 4 overlapping fields of the horizontal section used for the montage images were also performed. Each corresponding pair of stacks (NK-1r-IR and CT-B) was interleaved to form a single merged stack using a custom algorithm. This interleaving scheme was used rather than merging the stacks on a 1:1 basis (e.g. using different colour channels, as described above), as this method made it easier to detect the presence of co-localization. Using the IMOD software, images representing the different fluorophores acquired from the same optical section could be displayed in succession and alternated between (via manual control) at the same location on a computer screen, enabling the detection of co-labelled neurons.

In addition to allowing the user to step through a series of optical section images, the IMOD software also permits the embedding of geometric objects at any Z-plane. When counting neuronal somata, spheres were used for this latter purpose. Since the approximate diameter of each DMV neuron was approx. 20 μm, this value was selected for the spheres that were embedded (by the appropriate conversion of pixels into microns). For each neuron, the upper and lower sections were determined by stepping through the image stack (as described above for isolation of individual neurons) and the middle section was determined. A sphere was embedded at this level, in the center of the nucleus of the identified neuron. Since cross sections of an embedded sphere could be observed when within the range of Z-sections of the a marked neuron, this would ensure that no neuron was counted twice. Different coloured spheres were used to label either gastric efferents both with and without NK-1r-IR colocalization, as well as neurons with NK-1r-IR, but containing no retrograde tracer (i.e. non-gastric efferents), and the software kept track of the numbers of the various spheres that were placed. This counting procedure was performed separately for each of the 4 image stacks. Overlapping regions between the 4 stacks were masked such that neurons in these areas would only be counted once. After all counts had been completed, all of the embedded sphere data from the separate stacks were merged into a single 3-D scatter plot.

The distance between the SP-IR nerves and NK-1r-IR was determined using the known voxel sizes, as described in chapter 3 for measuring the distance between CGRP-IR nerve fibres and identified gastric efferents labelled with FG-IR. Rather than attempting to count all SP-IR fibres that were present, a comparison was made between the proportion of fibres that directly abutted on the cell membrane of neurons labelled

with NK-1r-IR versus those that surrounded these neurons without making apparent contact. For this comparison, only the SP-IR fibres that were closest to the membrane without making contact were examined, and the remaining fibres were said to be further away from the membrane than these. Simple animations consisting of rotations around an axis were also generated, which aided the visualization process, as per the methods outlined in chapter 3.

4.3. Results

4.3.1. Mapping the Distribution of SP-IR, NK-1r-IR and Identified Gastric Efferent Neurons in the DMV of the Rat

4.3.1.1. Controls

Substance P staining was abolished when the antibody was pre-absorbed with SP, but was unaffected by pre-adsorption with either NK-B or bombesin. No staining was observed in sections developed with immunofluorescence or avidin-biotin-peroxidase if the primary antibody was omitted.

Fluoro-Gold labelling was not observed in either the AP or NA, and was only present in the DMV. These findings would suggest that there was minimal leakage of FG from the injection site into either the blood stream or abdominal cavity, and that the labelled neurons observed projected specifically to the stomach. The extent of retrograde

labelling was consistent between animals and no difference in distribution of labelled neurons was observed whether sagittal or coronal sections were examined.

4.3.1.2. Retrograde Labelling

Injection of FG along the greater curvature of the stomach (corpus) produced a distinct pattern of labelled neurons within the DMV (Figure 23, 24). Fluoro-Gold-labelled neurons were observed bilaterally, and had a distribution that closely resembled that described in Chapter 3. Although one or two retrogradely-labelled neurons could be detected in brainstem sections as far caudally as -2.8 mm and rostrally to +2.2 mm in some cases, the majority of labelled neurons consistently spanned the region of -1.0 mm to +1.5 mm between rats. Therefore, counts of neurons were taken from within and immediately surrounding these brainstem levels. In the region that was assessed in greater detail in 3 rats (-1.35 mm to +2.00 mm), a total of 1016±26 FG-labelled neurons (Figure 25a, Table 5). The greatest number of FG-labelled cell bodies were observed at and adjacent to the level of the obex, with fewer FG-labelled cell bodies at the rostral and caudal ends of the DMV. The distribution and number of FG-labelled cell bodies were identical on both sides of the DMV (Table 4).

4.3.1.3. Location of NK-1r/SP in the DVC

The majority of NK-1r labelling in the DVC was observed as a mesh of fine fibres in the DMV that extended into the overlying NTS. In the sagittal plane, the NK-1r-labelled fibres extended from +2.2 mm to -0.1 mm at the middle of the DMV in close association with FG-labelled neurons (Figure 26). The highest density of fibres was seen

within the DMV and at the interface of the DMV and NTS. In the coronal plane, the majority of the NK-1r-labelled fibres were observed along the lateral edges of the DMV and immediately overlying regions of the NTS. A low density of NK-1r labelling was observed in the ventral AP. The region of the DMV which exhibited the highest NK-1r density was below the medial division of the NTS.

A total of 205±5 cell bodies were labelled with NK-1r (Figure 25b, Table 5). As with the FG-labelled neurons, the distribution and number of NK-1r-labelled cell bodies located on each side of the DMV was identical (Table 4). The greatest number of NK-1r-labelled cell bodies were observed rostral to the obex, with fewer NK-1r-labelled cell bodies seen at either end of the DMV. Although no preferential distribution of NK-1r-labelled fibres was observed rostral to the obex, NK-1r-labelled cell bodies appeared to cluster in this region (Figure 25b). Analysis of the distribution of NK-1r-labelled cell bodies revealed that 60% were located in the range of +0.15 mm to +0.95 mm.

A total of 68±3 cell bodies were co-labelled with FG+NK-1r (Figure 25c, Table 5). The majority of these co-labelled neurons were observed rostral to the obex, with few observed caudal to -1.35 mm or rostral to +1.45 mm. This corresponded to the region with the highest number of NK-1r positive cell bodies. Of all NK-1r-labelled cell bodies counted, 33% were co-labelled with FG, representing 7% of the FG-labelled cell bodies. Caudal to the obex, 68% (76/111) of NK-1r-labelled neurons were also co-labelled with FG.

Substance P-IR appeared as a dense punctate staining of fibres within the DMV and NTS with no SP-IR cell bodies being observed. A high density of SP-IR was seen immediately below the AP and directly above the central canal. The SP-IR detected within the DMV was in close association with the FG-labelled neurons along the entire length of the nucleus. Substance P-IR within the DMV/NTS was observed to start at the same rostral position as NK-1r, but extended the full length of the DMV. The greatest association of SP/NK-1r labelling was observed within mid- to rostral regions of the DMV and NTS.

Table 4. Quantification of neurons labelled with FG and NK-1r-IR in the DMV.

RAT #	#FG LEFT	#NK-1r LEFT	#FG+NK-1r LEFT	#FG RIGHT	#NK-1r RIGHT	#FG+NK-1r RIGHT
1	396±18	96±4	31±2	444±22	96±3	29±2
2	509±28	104±5	41±3	465±29	118±6	22±1
3	617±27	100±6	43±3	618±28	102±5	37±2

Table 5. Percentage of neurons that were co-labelled with FG and NK-1r-IR in the DMV.

RAT #	TOTAL # FG	TOTAL # NK-1r	TOTAL # NK-1r+FG	% FG w/NK-1r	% NK-1r w/FG
1	840±20	192±3	60±2	7	31
2	974±29	222±5	63±2	6	28
3	1235±28	202±6	80±3	6	40
ALL	**1016±26**	**205±5**	**68±3**	**7**	**33**

Figure 23. Schematic illustration of FG-labelled neurons compared to NK-1r-labelled fibres in coronal sections at various rostrocaudal levels of the DVC. The left side of each image represents the distribution of FG-labelled gastric efferent neurons in the DMV. The right side represents the distribution and density of NK-1r-labelled fibres in the DVC. Hatching indicates the relative density of the NK-1r immunoreactivity. HYP = hypoglossal nucleus; CC = central canal.

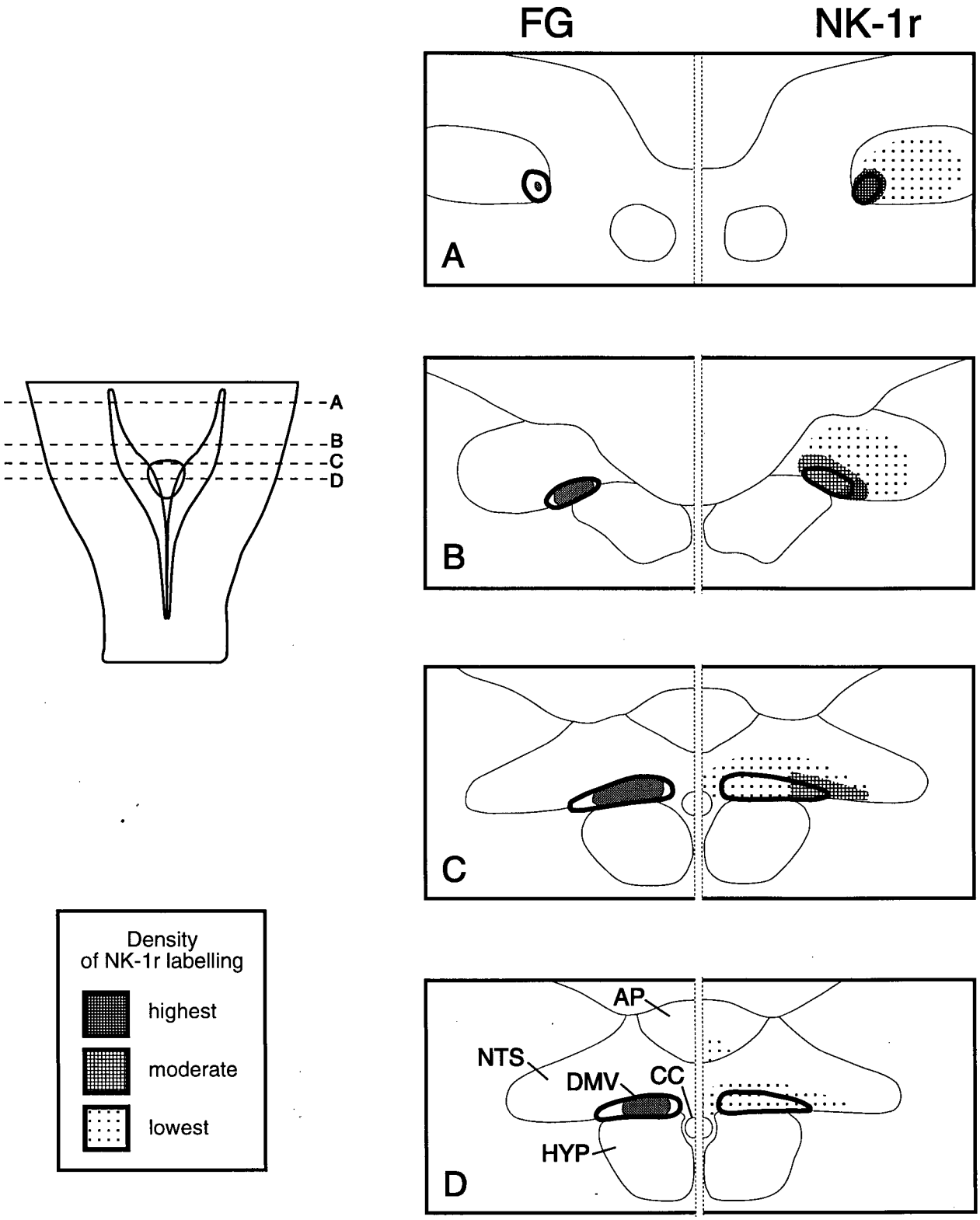
FG
NK-1r
A
B
C
D
Density
of NK-1r labelling
highest
moderate
lowest
AP
NTS
DMV
CC
HYP

Figure 24. Schematic illustration of FG-labelled neurons compared to NK-1r-labelled fibre distribution in sagittal sections at various rostrocaudal levels of the DVC. The area outlined by the thick black line represents the distribution of FG-labelled gastric efferent neurons in the DMV. The shaded areas represent the distribution and density of NK-1r-labelled fibres in the DVC. HYP = hypoglossal nucleus.

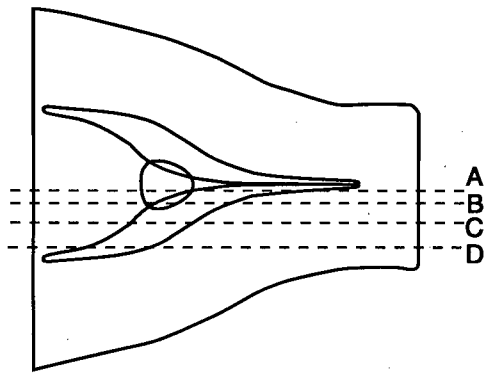
A
B
C
D

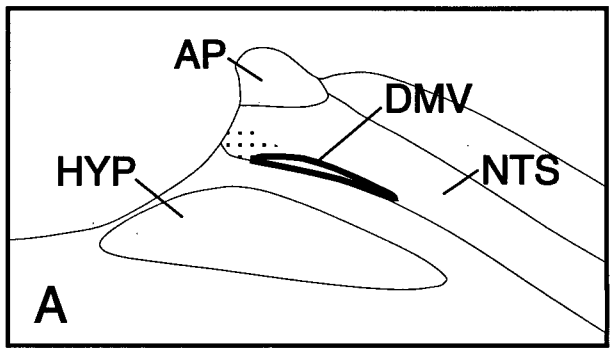
AP
DMV
HYP
NTS
A

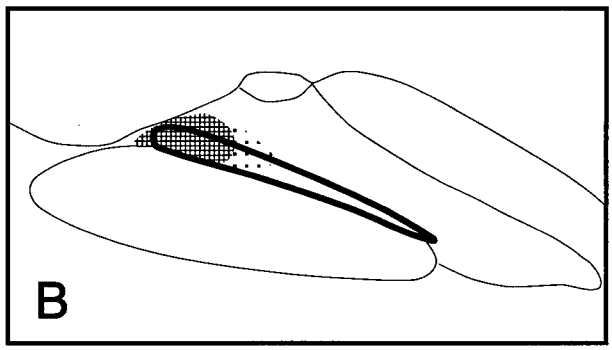
B

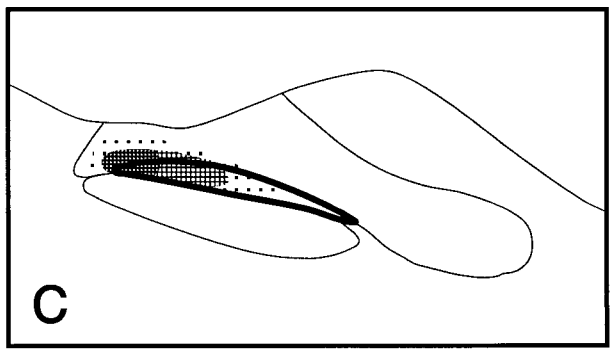
C

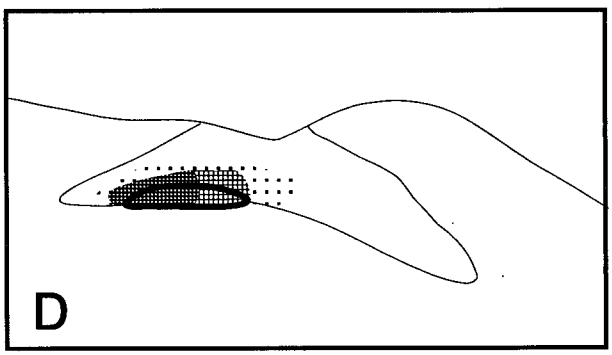
D

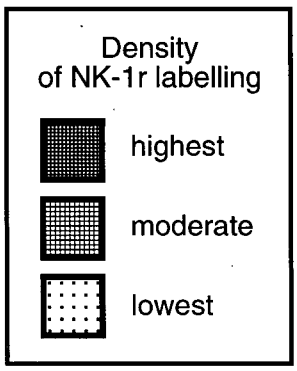
Density
of NK-1r labelling
highest
moderate
lowest

Figure 25. Bar charts representing the distribution of (A) FG-, (B) NK-1r- and (C) NK-1r+FG-labelled cell bodies in the DMV.

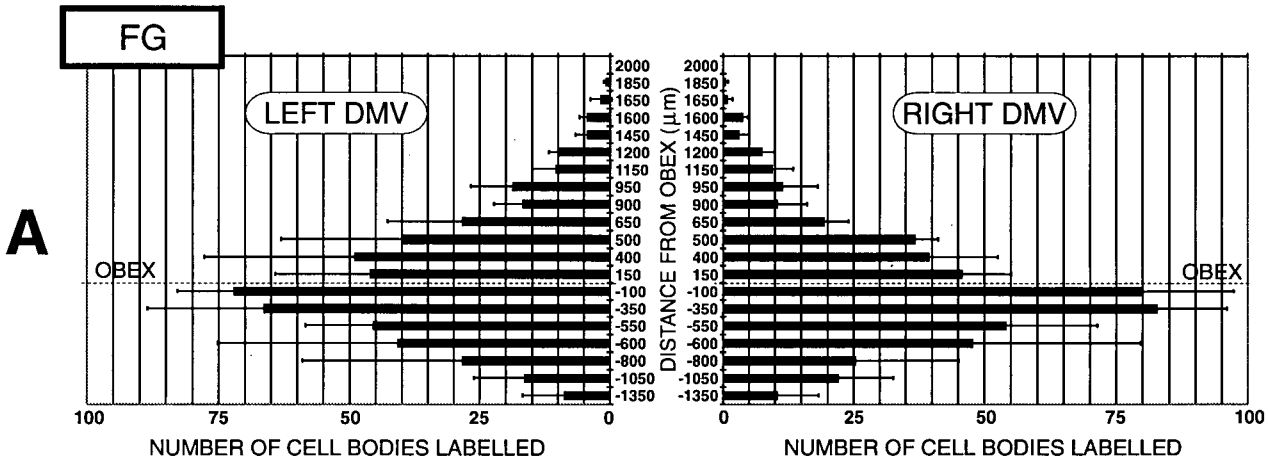
A
FG
LEFT DMV
RIGHT DMV
OBEX
OBEX
DISTANCE FROM OBEX (µm)
2000
1850
1650
1600
1450
1200
1150
950
900
650
500
400
150
-100
-350
-550
-600
-800
-1050
-1350
100
75
50
25
0
NUMBER OF CELL BODIES LABELLED
NUMBER OF CELL BODIES LABELLED

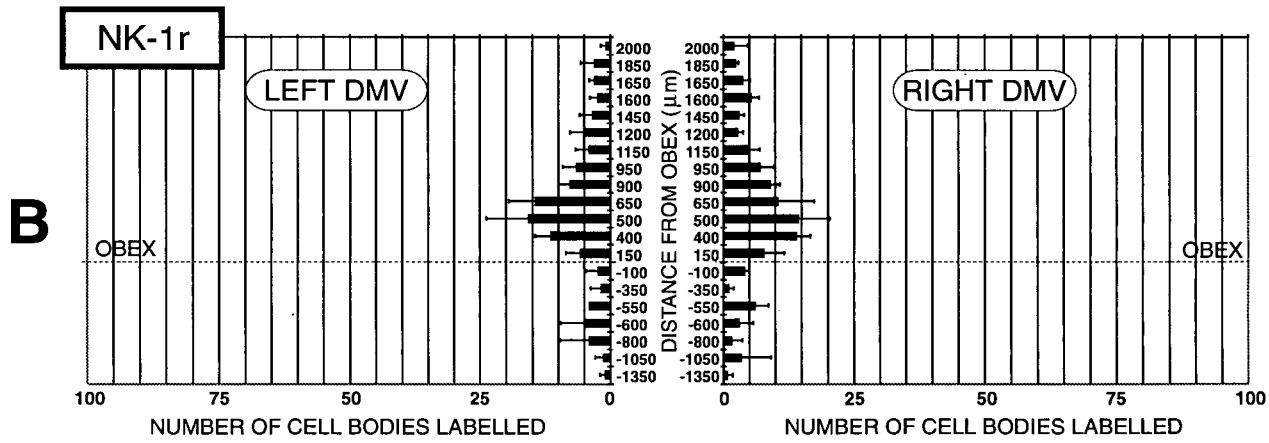
B
NK-1r
LEFT DMV
RIGHT DMV
OBEX
OBEX
DISTANCE FROM OBEX (µm)
2000
1850
1650
1600
1450
1200
1150
950
900
650
500
400
150
-100
-350
-550
-600
-800
-1050
-1350
100
75
50
25
0
NUMBER OF CELL BODIES LABELLED
NUMBER OF CELL BODIES LABELLED

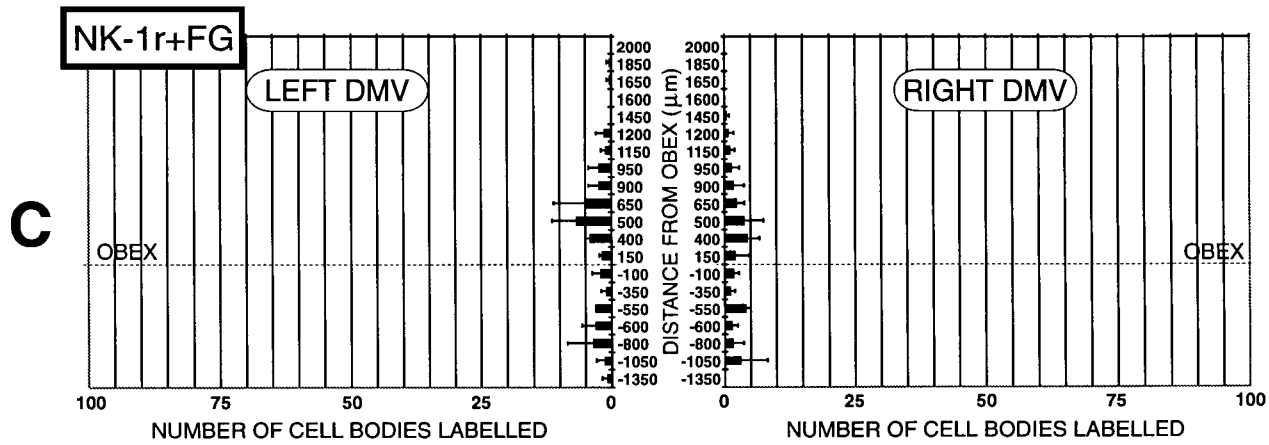
C
NK-1r+FG
LEFT DMV
RIGHT DMV
OBEX
OBEX
DISTANCE FROM OBEX (µm)
2000
1850
1650
1600
1450
1200
1150
950
900
650
500
400
150
-100
-350
-550
-600
-800
-1050
-1350
100
75
50
25
0
NUMBER OF CELL BODIES LABELLED
NUMBER OF CELL BODIES LABELLED

Figure 26. A sagittal section through the DVC illustrating NK-1r distribution using the avidin-biotin-peroxidase technique. (A) Note that the highest density of NK-1r-IR is at the rostral pole of the DVC. IV=fourth ventricle. Scale bar = 200 μm. (B) A detail of labelling observed in a coronal section of the DVC illustrating both cell bodies (arrows) and fibres. Scale bar = 150 μm.

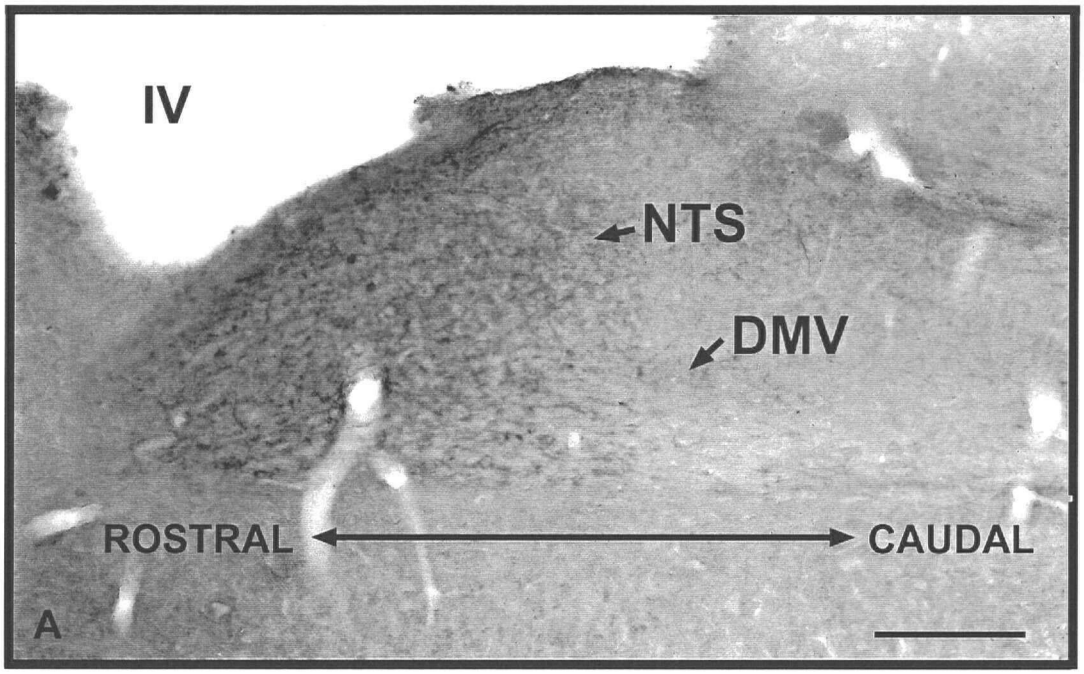
IV
NTS
DMV
ROSTRAL
CAUDAL
A

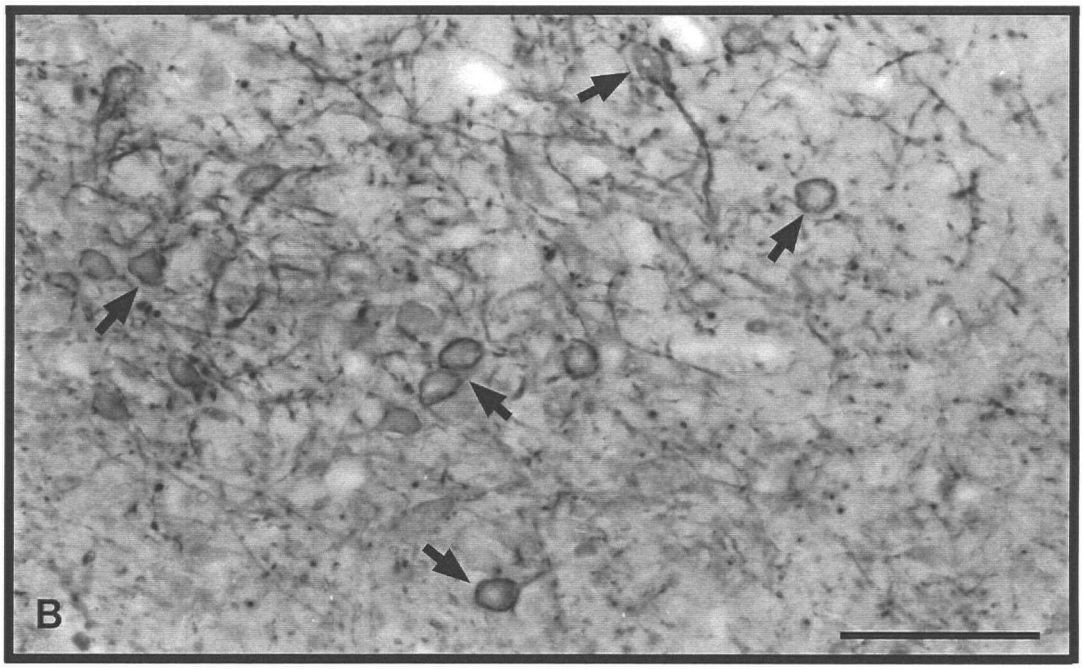
B

Figure 27. Demonstration of a FG+NK-1r co-labelled cell body associated with SP-IR fibres within the DMV as viewed with a conventional epifluorescence microscope at high magnification. (A) FG-labelled cell body (arrow). (B) the same neuron seen in (A) and an adjacent neuron with NK-1r-IR on the plasma membrane (arrows). (C) both neurons seen in (B) are surrounded by SP-IR nerve terminals. Scale bar = 25 μm.

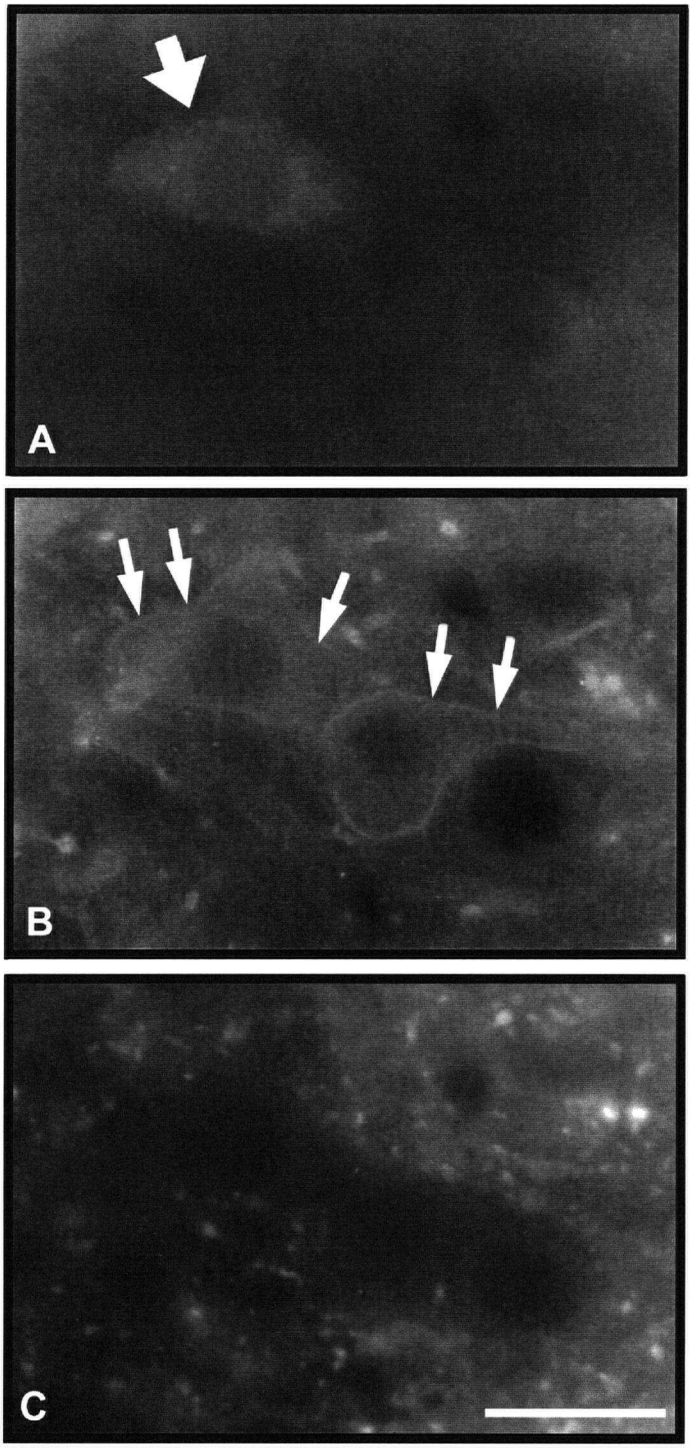
A
B
C

4.3.2. Examination of SP, NK-1r and Identified Gastric Efferent Neurons in the DMV using 3-D Reconstruction Techniques

Since SP-IR was observed in high density throughout the DMV, the initial focus was to obtain a high resolution map of NK-1r in relation to identified gastric efferents in this brainstem nucleus. In particular, the mid-to-rostral regions of this nucleus which contain the highest density of NK-1r-IR (as revealed by the preliminary mapping studies described in section 4.3) were of primary interest.

Initially, MIP images generated from coronal sections that were scanned with a confocal microscope for NK-1r alone. At levels caudal to the obex, the NK-1r-IR density was found to be very low, and was almost completely localized to nerve fibres (Figure 28a, b). Rostral to the obex, particularly in the region extending from approximately +300 to +1200 μm, a high density of NK-1r-IR was observed (Figure 28c, d). While this was also mainly localized to nerve fibres, NK-1r-IR was also observed on the somatic membrane of a subpopulation of neurons.

These observations were further clarified when horizontal sections stained for both NK-1r-IR and CT-B-IR were scanned by confocal microscopy. A montage of four overlapping fields covering the rostral to DMV was prepared from MIP images (Figure 29a, b). From these images, it can be appreciated that the intensity of NK-1r-IR was greatest at the rostral pole of this nucleus, with the density of receptor labelling decreasing towards caudal regions.

Figure 28. Maximum intensity projections of NK-1r-IR generated from coronal sections at various rostrocaudal levels of the DVC (relative to the obex). (A) A brainstem section at position -600 μm. (B) A section at -100 μm. (C) A section at +450 μm. (D) A section at +900 μm. Note that minimal NK-1r-IR is present in the sections caudal to the level of the obex (A and B), whereas an increased density of receptor labelling is seen at more rostral levels (C and D). Scalebar = 100 μm.

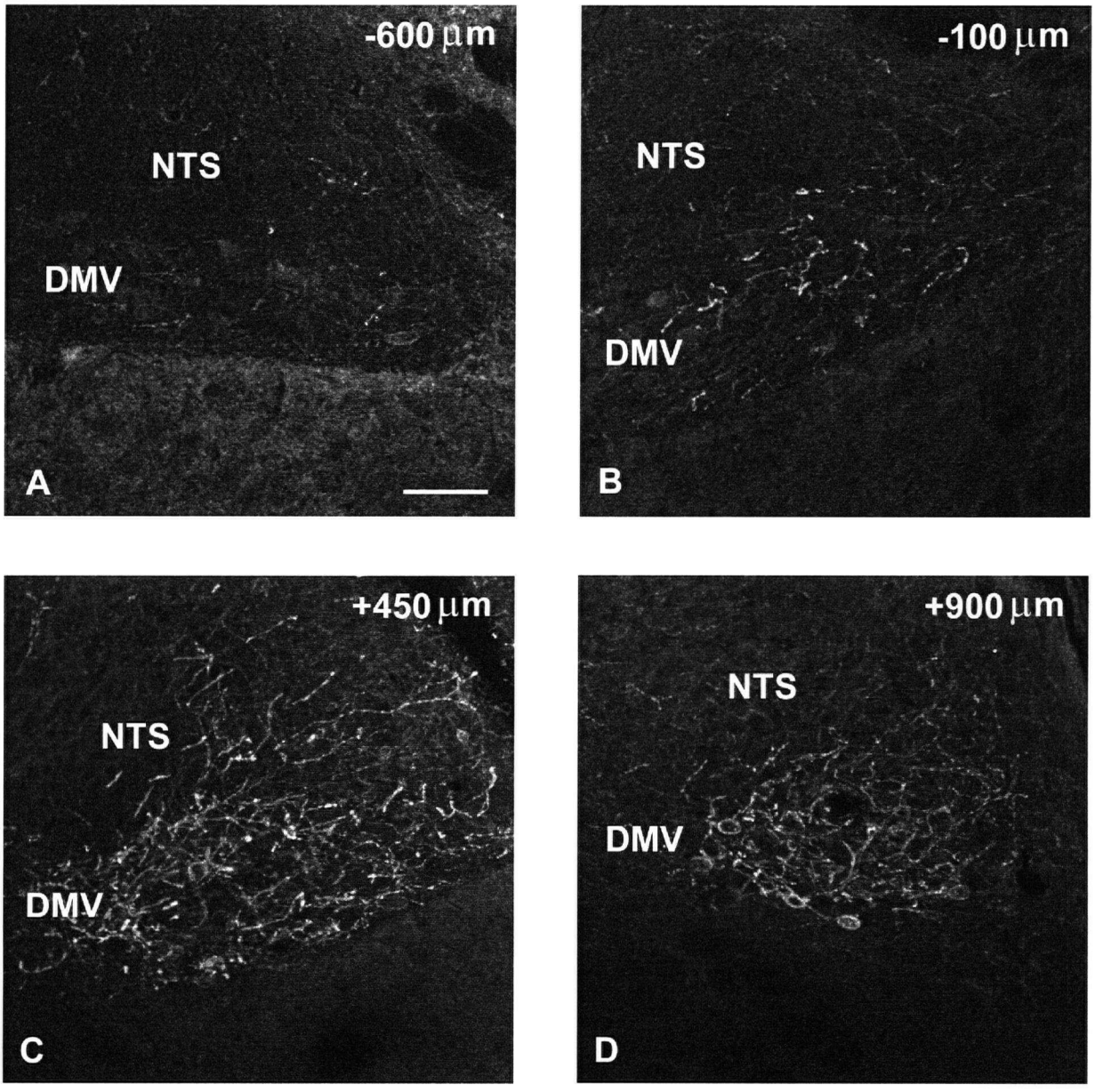
-600 μm
NTS
DMV
A
-100 μm
NTS
DMV
B
+450 μm
NTS
DMV
C
+900 μm
NTS
DMV
D

Figure 29. Montage of 4 overlapping maximum intensity projection images in a horizontal section through the DMV showing NK-1r-IR (A) and gastric efferent neurons labelled with CT-B (B) in this region. The inset in (A) shows the approximate location of the region of the DMV that is represented by the montage. C. A 3-D scatter plot of identified neurons in the montage: somata labelled with CT-B only (white), CT-B and NK-1r-IR (black) and NK-1r-IR only (grey). Scale bars = 500μm.

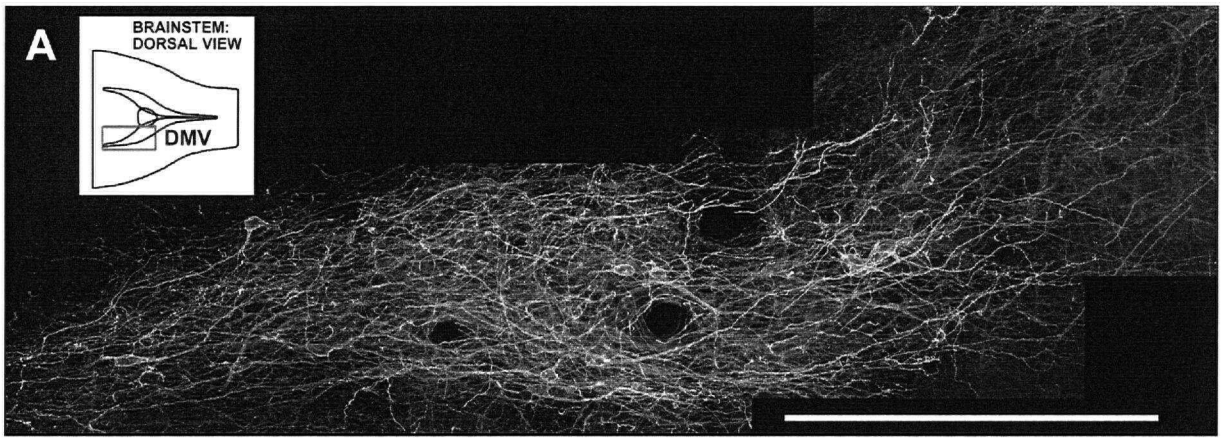
A
BRAINSTEM:
DORSAL VIEW
DMV

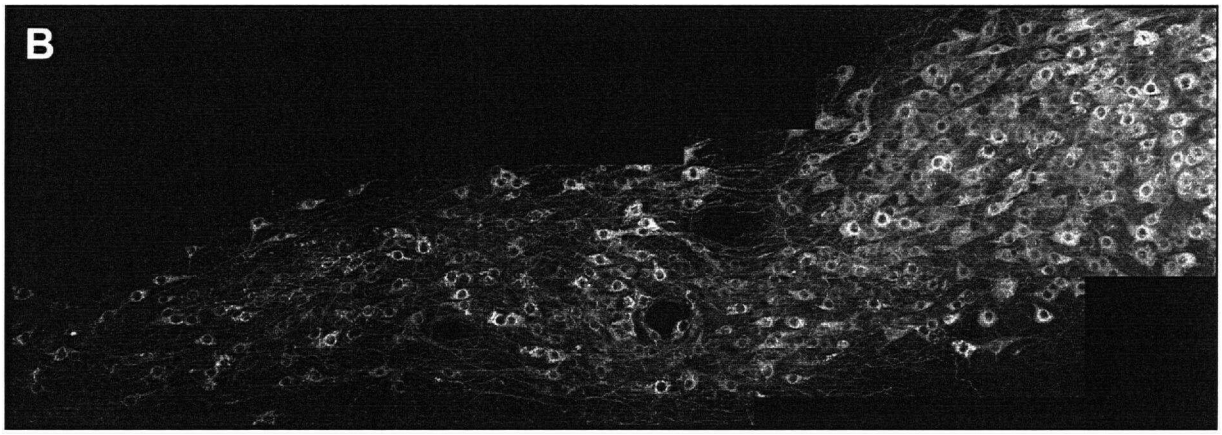
B

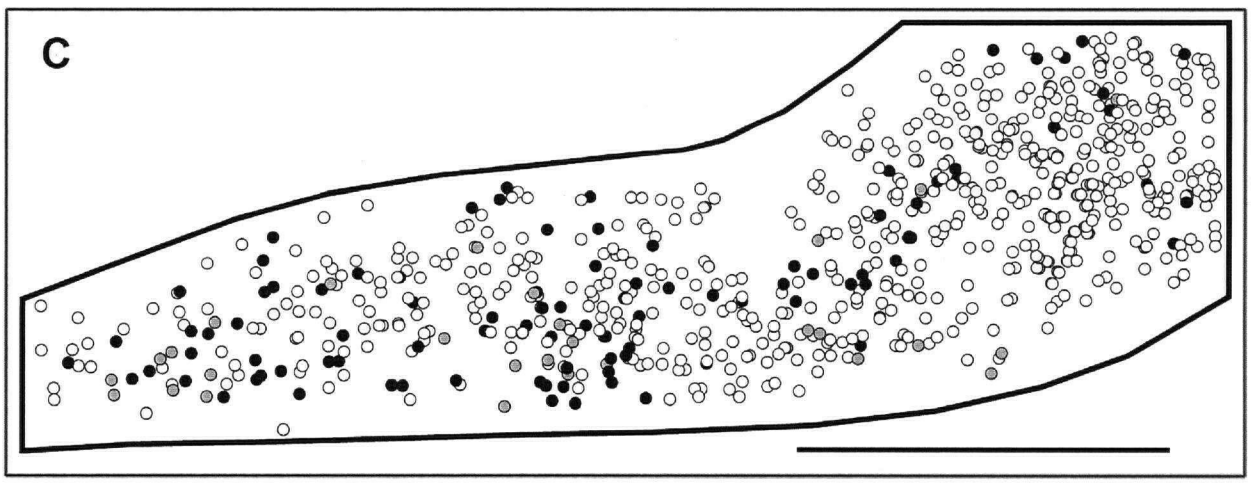
C

Figure 30. A combined montage view of NK-1r (green) and CT-B (blue) in a horizontal brainstem section generated using Figure 29a,b. The neurons outlined in white (A - D) are co-labelled for both CT-B and NK-1r and were extracted from the volume to produce 3-D reconstructions (see Figure 31). Scalebar = 500 μm.

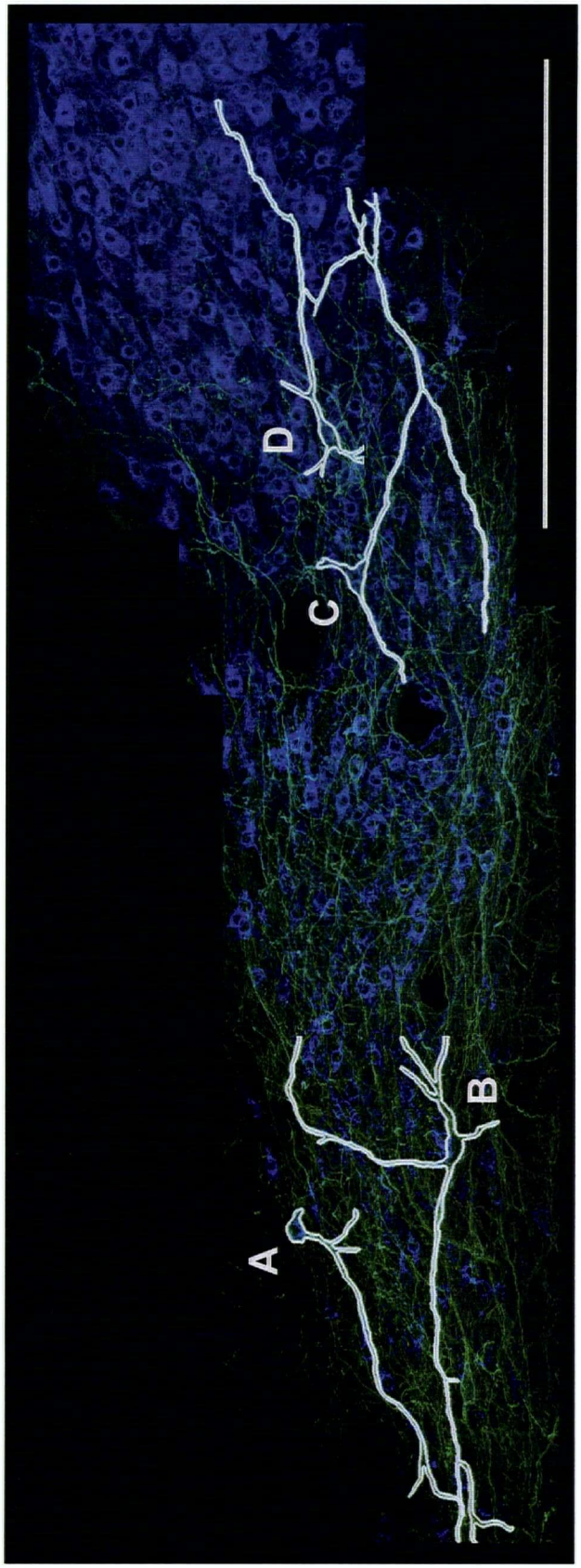
A
B
C
D

Figure 31. Volume renderings of NK-1r-IR on the cell membrane of selected gastric efferent neurons that were extracted from the volumes represented by the montage view in Figure 30. For each neuron, the "front" view is shown on the left, and a tilted view is shown on the right. Note that NK-1r-IR covers most of the cell membrane (both soma and dendrites) of these neurons, and that the dendrites are oriented in parallel to the rostrocaudal axis. Scalebar = 100 μm.

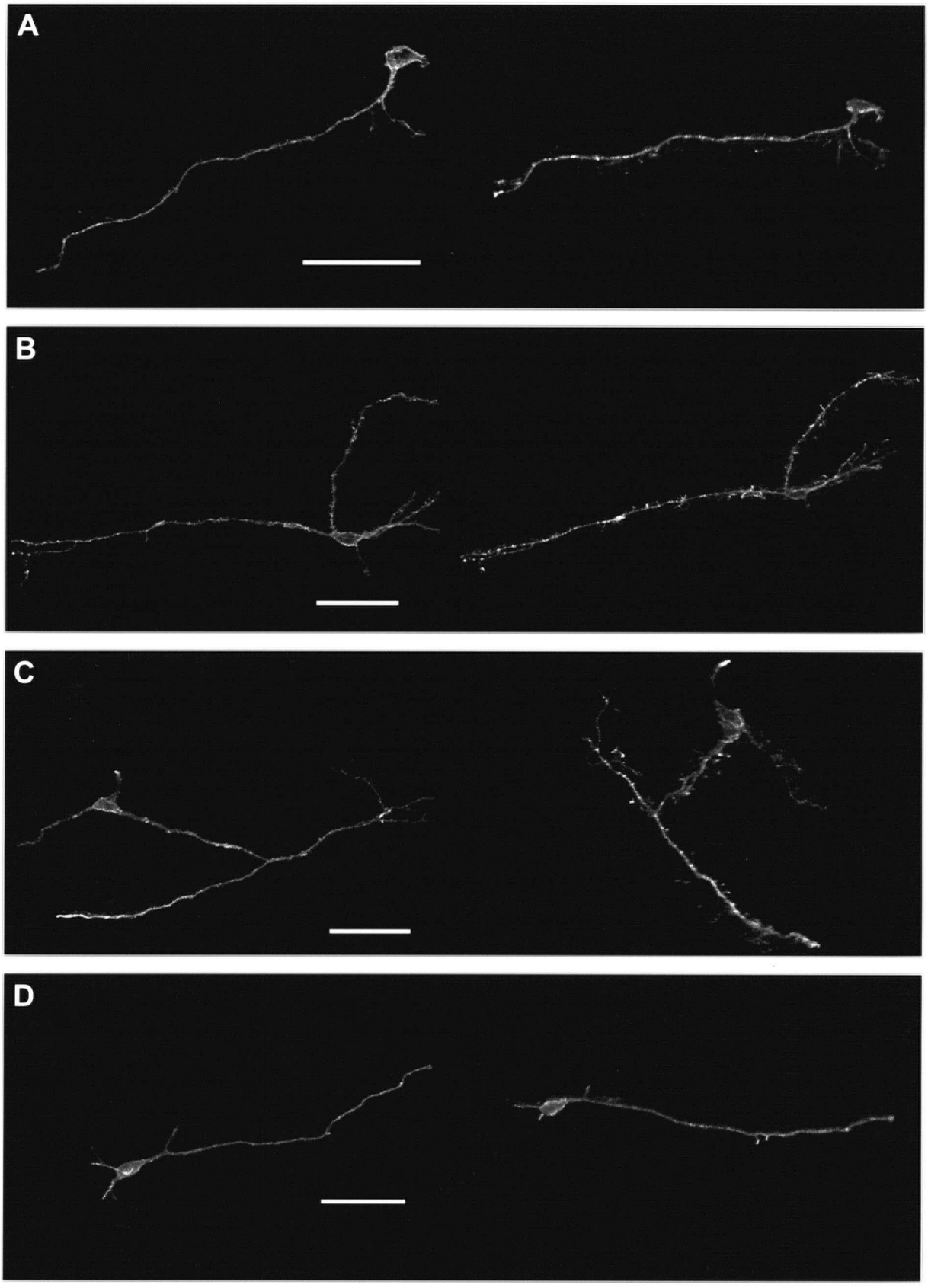
A
B
C
D

Figure 32. Volume rendering of a gastric efferent neuron (labelled with CT-B, blue) that is co-labelled with NK-1r-IR that was extracted from a horizontal brainstem section through the DMV. (A) front view, (B) oblique view, (C-F) cross sections through neuron demonstrating greater density of NK-1r-IR localized to dendrites of the neuron (arrows). Scalebars = 20 μm.

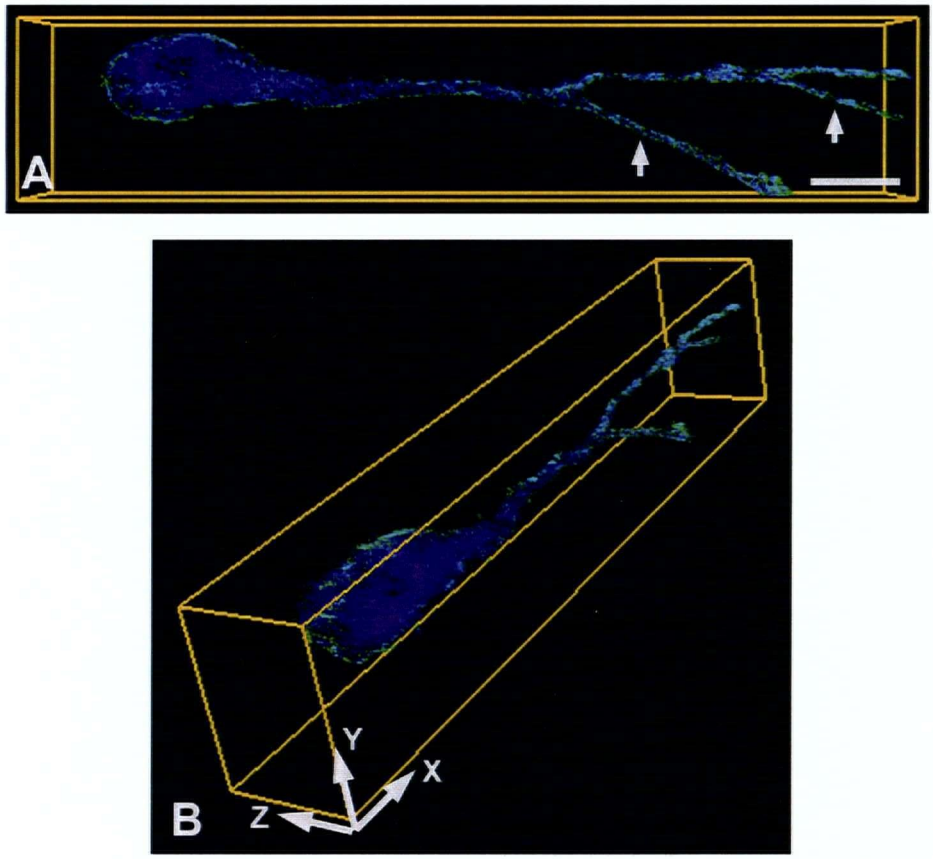
A
B
Y
X
Z
C
D
E
F

The precise number of co-labelled gastric efferents in the montage was determined by a 3-D counting procedure. The greatest number of co-labelled neurons were clustered at the rostral pole (Figure 29c). Of the identified neurons, 617 contained CT-B-IR only, 96 were co-labelled with CT-B-IR and NK-1r-IR and 28 were labelled with NK-1r-IR only. Thus, approximately 13% (96/[617+96]) of the identified gastric efferents in this montage series were co-labelled with receptor. These results are consistent with the counts obtained from coronal brainstem slices (i.e. approx. 7%) that were described in section 4.3. However, the proportion of the total number of NK-1r-IR neurons that were co-labelled with retrograde tracer (77%; 96/[96+28]) was significantly greater than observed previously (i.e. approx. 33%). In contrast to the counting method used for the coronal sections, the current technique provided the 3-D spatial arrangement of neurons within the depth of a brain slice. However, neither counting method could quantify the number of gastric efferents that possessed NK-1r-IR on their dendrites alone.

It is evident from these experiments that a large proportion of NK-1r-IR on fibres within the DMV corresponds to the dendrites of identified gastric efferent neurons. Dendritic labelling of NK-1r-IR on individual gastric efferent neurons could be demonstrated by extracting neurons from the montage and performing 3-D reconstructions (Figure 30, 31). Consistent with previous reports (Shapiro and Miselis, 1985; Altschuler et al., 1992), the dendrites of all extracted neurons projected parallel to the rostrocaudal axis of the DMV. This could be appreciated when the reconstructed neuron was rotated through 360 degrees using volume rendering software. The nerve fibres of the extracted neurons that were labelled with NK-1r were classified as dendrites

rather than axons, since the latter exit the DMV perpendicular to the rostrocaudal axis (see Altschuler et al., 1992).

The 3-D reconstructions of NK-1r on neurons isolated from the montage also demonstrate that the receptor is distributed over almost the entire surface of the cell membrane, including that of both soma and dendrites (Figure 31). Analysis of 3-D reconstructions generated using a higher magnification objective lens (63x) revealed that the highest density of NK-1r is localized to the dendrites, with less receptor on the soma of the neuron (Figure 32).

4.3.2.1. Association of SP and NK-1r at the single neuron level

The initial 3-D reconstructions demonstrating the spatial relationship between SP and NK-1r on identified gastric efferent neurons were generated from confocal images acquired from coronal brainstem sections. In contrast to the punctate appearance of SP-IR as visualized with a conventional epifluorescence microscope, the neuropeptide was clearly localized to nerve fibres running in a preferentially rostrocaudal orientation (i.e. perpendicular to the plane of sectioning) (Figure 33). However, as illustrated in this figure, most of the gastric efferent neurons that were co-labelled with NK-1r-IR within these coronal sections were truncated such that only the cell soma could be observed. Furthermore, in both of these figures, part of the neuron was physically removed during cryosectioning. The preliminary 3-D reconstructions of NK-1r-IR in coronal sections revealed that the receptor had a patchy distribution on the somatic membrane of identified neurons.

Figure 33. Volume rendering of a gastric efferent neuron labelled with CT-B (blue) that is co-labelled with NK-1r-IR (green) and surrounded by SP-IR nerve terminals (red.) (A) front view, (B) tilted view. Note that part of the neuron was removed during cryosectioning of the brainstem. (C-E) Cross sections through this neuron demonstrate that few SP-IR nerve terminals make contact with the cell membrane of the neuron (arrows), and that NK-1r-IR has a patchy appearance. The neuron was extracted from a coronal brainstem section at position +600 μm relative to the obex. Scalebar = 5 μm.

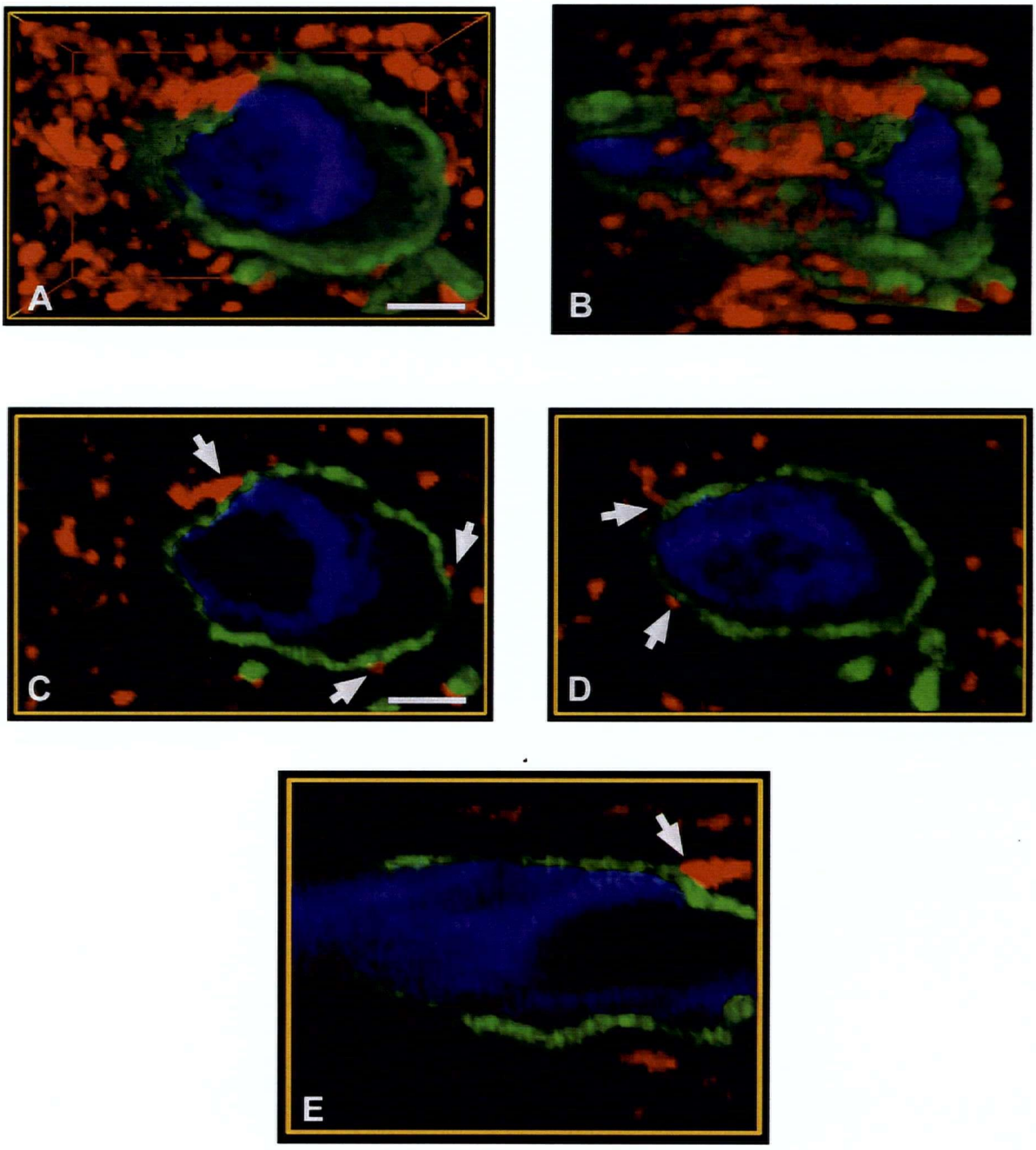
A
B
C
D
E

As compared to coronal sections, 3-D reconstructions obtained using confocal images of horizontal sections revealed fewer truncated neurons, and permitted observation of dendrites.

Once the NK-1 receptor distribution within the DMV had been elucidated, triple labelled sections containing gastric efferent neurons co-labelled with NK-1r-IR and surrounded by SP-IR fibres were examined in greater detail. Three dimensional reconstructions of selected neurons were generated (Figure 34). In contrast to the punctate appearance of SP-IR as visualized with a conventional epifluorescence microscope, the neuropeptide was clearly localized to nerve fibres running in all directions through the DMV. The SP-IR fibres surrounded both the soma and primary dendrites of the neurons, and was in close spatial arrangement with NK-1r-IR regions. Note that the side views of the neuron shown in Figure 34c,d appear slightly blurred compared to the front and back views depicted in Figure 34a,b. This is due to the fact that the axial resolution (i.e. resolution in the Z-plane) is worse than the lateral resolution for a confocal microscope (Wilson and Sheppard, 1984). As a result, 3-D reconstructions can appear fuzzy when observed from perspectives perpendicular to the plane of acquisition.

By taking cross-sections through the neuron, the spatial relationship of SP-IR fibres to the NK-1r-IR could be appreciated (Figure 35). Note that although there were several locations in which SP-containing varicosities directly abut NK-1r-IR on the membrane of the neuron (similar to the "presumptive termination sites" described for CGRP in section 3.3.5), there were numerous regions (on both the soma and dendrites) where NK-1r-IR was not associated with SP-IR. Since a very high density of SP-IR

fibres were present surrounding all surfaces of neurons isolated for 3-D reconstruction, a count of the total number of fibres was not attempted due to the difficulty associated with identifying individual fibres (e.g. several varicosites could constitute part of the same SP-IR fibre). Instead, a comparison of the SP-IR fibres that directly abutted on the cell membrane versus those that merely surrounded the neuron was performed. It was found that the majority of SP-IR nerve fibres were >5 μm away from the closest NK-1r-IR on the surface of the identified neuron.

Figure 34. Volume rendering of SP-IR (red) and NK-1r-IR (green) in relation to an isolated gastric efferent neuron (labelled with CT-B, blue) generated from a horizontal brainstem section through the DMV. (A) front view, (B) back view, (C) right view, (D) left view. Scalebars = 20 μm.

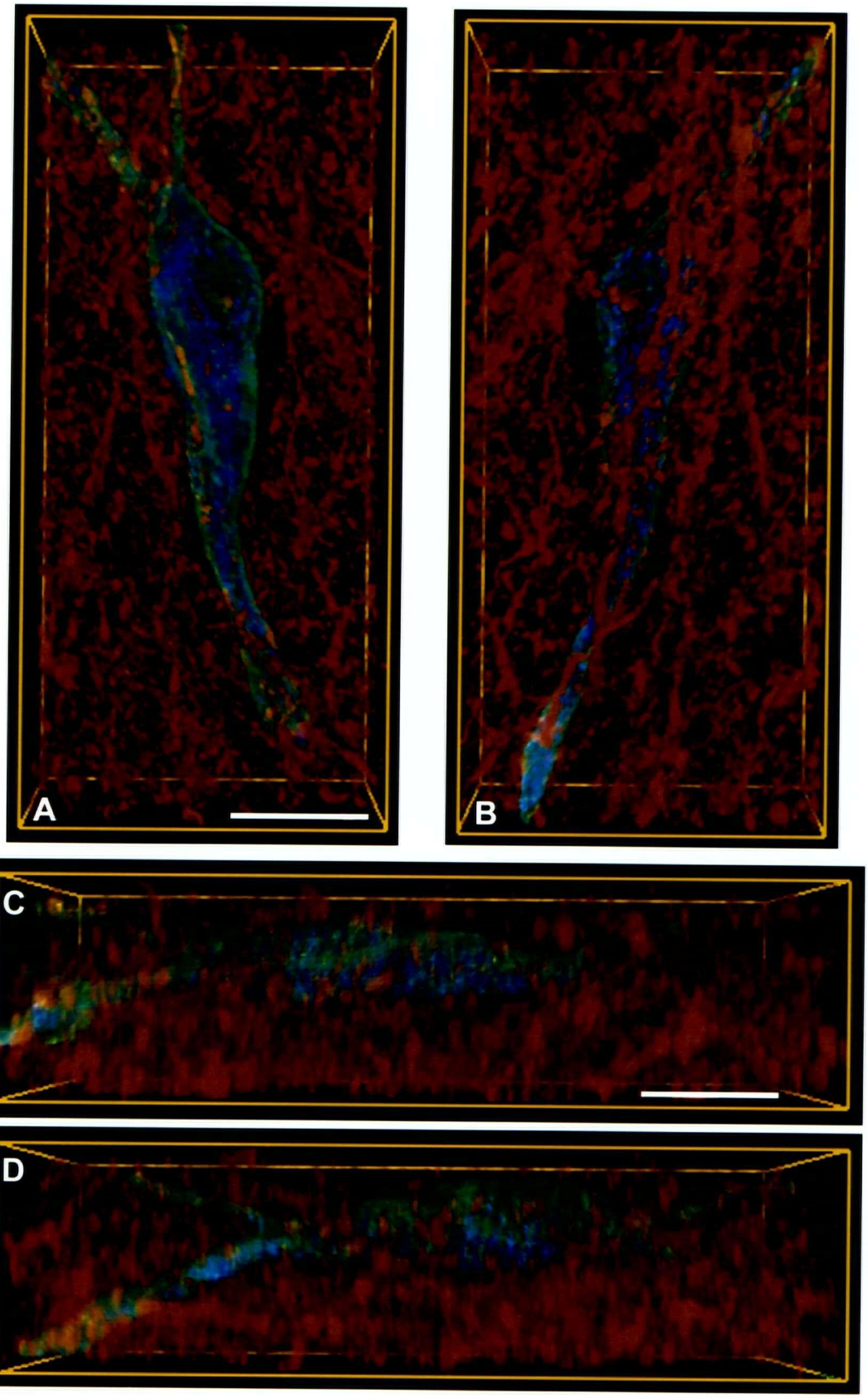
A
B
C
D

Figure 35. (A-D) Cross sections through the volume shown in Figure 34 demonstrating the relationship between SP-IR nerve fibres and NK-1r-IR on the cell membrane of the gastric efferent neuron. Note that few SP-IR nerve fibres come into direct contact with NK-1r-IR (arrows); most fibres are located >5 μm away from the receptor. The asterisks in (A) represent the position of DMV neurons that were not labelled with either CT-B or NK-1r-IR. Scalebars = 10 μm.

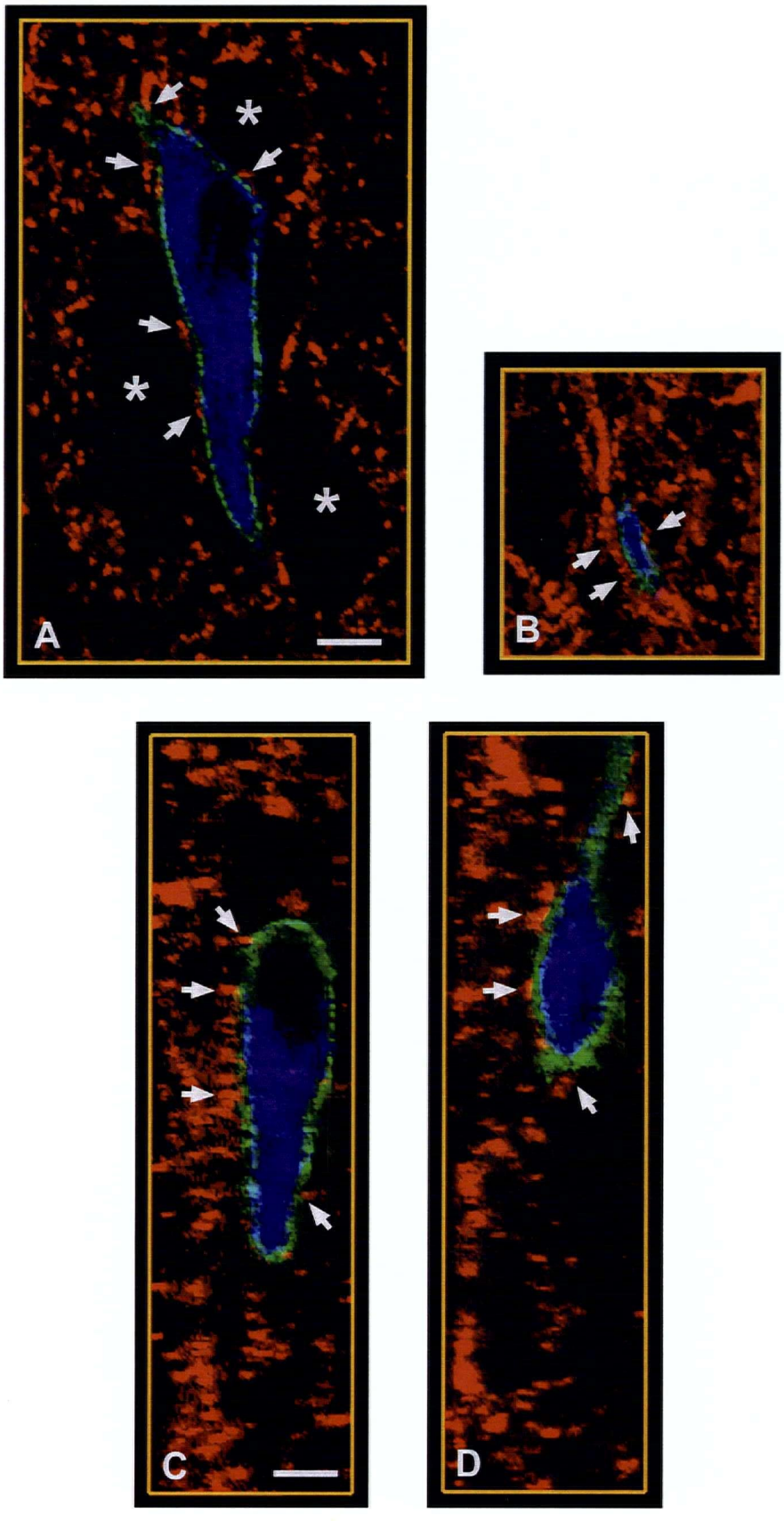
A
B
C
D

4.4. Discussion

By combining retrograde tracing with immunocytochemistry, data providing an anatomical basis for the role of SP in vagal gastric reflexes were obtained. Both SP- and NK-1r-IR were observed in association with retrogradely-labelled gastric efferent neurons.

The initial studies which employed FG as the retrograde tracer established the gross distribution of NK-1r-IR with respect to identified gastric efferent neurons in the DMV. The results revealed that while the greatest number of labelled gastric efferent neurons were observed around the level of the obex (Figure 25a), the majority of NK-1r-IR somata (Figure 25b) and nerve fibres were observed rostral to this position. Furthermore, the largest number of neurons that were co-labelled with both NK-1r-IR and FG were localized rostral to the obex. These results were confirmed in later studies when CT-B was used as the neuronal tracer (Figure 29, 30). The fact that the co-labelled neurons were observed in small clusters at locations rostral to the obex (Figure 25c and Figure 29c) would suggest that SP may regulate a specific sub-population of gastric efferent neurons within the DMV.

The distribution of NK-1r-IR was similar to that reported previously using either autoradiography (Manaker and Rizio, 1989; Maeno et al., 1993; Helke et al., 1984) or *in situ* hybridization (Elde et al., 1990; Kiyama et al., 1993; Maeno et al., 1993). An interesting finding was the concentration of NK-1r-IR in the boundaries between the DMV and NTS and DMV and hypoglossal nuclei which has not been previously reported. The advantage of the present studies was the ability to undertake multiple labelling experiments to identify individual gastric efferent neurons.

Counts obtained from coronal brainstem slices examined with epifluorescence microscopy revealed that 33% of the NK-1r-labelled cell bodies detected in a representative sample of sections along the length of the DMV were co-labelled with FG. However, these represented only 7% of all retrogradely labelled neurons projecting to the greater curvature of the stomach. A 3-D counting procedure applied to a montage series of a representative 50μm thick horizontal section through the DMV that was acquired by confocal microscopy yielded similar results. For this specimen, although 77% of all NK-1r-IR neurons were co-labelled with retrograde tracer, these constituted only 13% of all gastric efferent neurons observed. Furthermore, the co-labelled neurons in the horizontal section exhibited a similar distribution in the rostrocaudal plane to those gathered from multiple coronal sections (i.e. compare Figure 25c and Figure 29c). The discrepancies in the numerical results obtained using the different counting procedures could reflect regional variations in the distribution of NK-1r-IR labelled somata that were observed, since only a single section from one animal was used for the 3-D counting procedure whereas many more sections were used from animals (N=3) for the counts performed using the epifluorescence microscope.

Although the initial neuron counting results revealed that NK-1r-IR was clearly localized to the somata of a subpopulation of neurons within the DMV, the greatest concentration of NK-1r-IR was observed on fibres in both the DMV and NTS. The later studies which used CT-B as the neuronal tracer identified a large proportion of these fibres as dendrites of gastric efferent neurons (Figure 29Figure 32). Three-dimensional reconstructions of NK-1r-IR on the surface of gastric efferent neurons clearly illustrate that the receptor is distributed over the entire neuronal membrane (Figure 31).

Reconstructions generated using data captured with the 63x objective revealed that the highest density of receptor was localized to the dendrites of the neurons (Figure 32). These data suggest that the regulation of neuronal function in the DMV by SP may involve differential effects on somatic and dendritic structures.

The observation that NK-1r-Ir was localized to the dendrites of identified gastric efferent neurons projecting from the DMV is in opposition to the findings of a study that used application of the neurotoxin ricin to vagal nerves sectioned below the level of the nodose ganglion (Helke et al., 1985) to identify the sources of SP binding sites in the DVC. This procedure resulted in the selective destruction of the cell bodies of vagal afferents in the nodose ganglion and vagal efferents in the DMV. In these experiments, although SP binding sites were reduced by 30% in the DMV, no reduction of binding sites was observed in the NTS. These results suggested that only a minor proportion of the SP binding sites in the DMV and none in the NTS were present on vagal efferent or afferent neurons. While the 30% reduction in SP binding sites observed in the DMV could correspond to the NK-1r-IR cell bodies and fibres that we observed in this region, this former study did not identify the origin of the other 70% of SP binding sites within the DMV. Although it is possible that NK-1r-IR on interneurons within the NTS could contribute to some of these binding sites (since transynaptic transfer of ricin does not occur, Dumas et al., 1979), this does not explain the high density of fibres within the NTS which were co-labelled with CT-B and NK-1r.

Unlike NK-1r-IR, SP-IR was observed throughout the DVC in close association with the retrogradely labelled gastric efferent neurons, as well as throughout the entire NTS and AP, confirming previous studies completed in our laboratory (Buchan et al.,

1991). Substance P labelling within the DVC was more extensive than NK-1r, and a mismatch between peptide and receptor distribution was apparent, especially at locations caudal to the obex.

This finding is consistent with the distribution of SP in relation to NK-1r at several other sites within the rat CNS (Liu et al., 1994; see also section 1.13). Thus, unlike "classical" neurotransmitters where receptors immediately appose the site of neurotransmitter storage and release, neuropeptides may act in a diffuse, non-synaptic manner. Another possible explanation for the observed mismatch between SP and NK-1r distribution is that in regions where NK-1r-IR was low or absent, SP may be binding to one of the other tachykinin receptors (i.e. NK-2, NK-3) which have been reported within the DVC (Carpentier and Baude, 1996; Martini-Luccarini et al., 1996). Finally, low levels of NK-1r may be present that are below the level of detection using immunocytochemistry.

The results from this study demonstrated that a novel antibody directed against the NK-1r protein (NK-1) can be used to identify the distribution of this receptor and to localize it to discrete structures within the DVC. The NK-1r antibody can also be used in conjunction with an antibody to SP to observe the comparative distribution of receptor and ligand. The combination of retrograde tracing and SP/NK-1r immunocytochemistry indicated that SP has a direct effect on a subpopulation of efferent neurons within the DMV that project to the greater curvature of the rodent stomach.

5. COMPARISON OF THE SPATIAL DISTRIBUTION OF ENDOPEPTIDASE-24.11 WITH SUBSTANCE P, SUBSTANCE P RECEPTOR (NK-1r) AND GASTRIC EFFERENT NEURONS IN THE DORSAL VAGAL COMPLEX OF THE RAT

5.1. Introduction

In Chapter 4, morphological evidence was presented to suggest that SP may activate NK-1 receptors on the cell membrane of gastric efferent neurons within the rat DVC via a volume transmission mechanism. If SP diffuses through the extracellular fluid to interact with the NK-1 receptor, endopeptidases may be capable of degrading the peptide prior to binding. Although many enzymes can cleave SP (Table 6), neutral endopeptidase 24.11 has been implicated as the principal active enzyme responsible for this action within the CNS (Matsus et al., 1984; Sakurada et al., 1985; Hall et al., 1989).

Neutral endopeptidase 24.11 (EC 3.4.24.11, NEP) is a membrane-bound enzyme with its catalytic site on the extracellular portion of the protein (Matsus et al., 1983). Originally isolated from kidney brush border cells, NEP is now known to have wide distribution within many tissues, including lung, spleen, heart, pituitary, pancreas and brain (Kenny and Fulcher, 1983). Furthermore, NEP has a fairly broad substrate specificity related to -X-Y bonds, where Y is one of 7 hydrophobic amino acids (Matsus et al., 1984). The best substrates for NEP seem to be small peptides with little or no secondary structure.

In vitro, SP is the most rapidly degraded of the many neuropeptides that are cleaved by NEP (Matsus et al., 1984). When SP is incubated with crude brain homogenates or purified synaptic membranes, the cleavage products are those expected to result from digestion by NEP (Edwardson and McDermott, 1985; Matsus et al., 1984; Oblin et al., 1989). Furthermore, these cleavage products have been detected *in vivo* in both brain and spinal cord (Sakurada et al., 1985).

Cleavage of SP by NEP at any of the 3 peptide bonds depicted in Table 6 should lead to SP inactivation, based on the established structure-activity relationship for the biological effects of the peptide on smooth muscle (Bury and Mashford, 1976). The carboxy-terminal hexapeptide sequence of SP is both necessary and sufficient for full activity, whereas amino-terminal fragments lacking this region are inactive (Bury and Mashford, 1976; Hanley and Iversen, 1980).

However, the structure-activity relationship for the actions of SP in the CNS are controversial. It has been suggested that cleavage of SP by NEP may produce fragments with altered activity to the parent molecule (Hall et al., 1989). One study found that C- and N-terminal fragments of SP had opposite effects on blood pressure when these were injected into the caudal NTS in the rat (Hall et al., 1989). When phosphoramidon, an inhibitor of NEP, was injected into the caudal NTS prior to injection of SP, there was a complete block of the cardiovascular actions of SP. On the other hand, this inhibitor did not block the actions of the N-terminal fragment, SP(1-7). These results suggest that cleavage of SP by NEP may not lead to inactivation of the peptide, but rather might be a required step in mediating the effects attributed to intact SP in this region.

The possibility of N-terminal fragments of SP binding to and activating the NK-1r was previously examined by assessing the ligand-binding properties of the receptor using SP fragments (Ingi et al., 1991; Boyd et al., 1994). The minimum requirement for activation of the NK-1r is the C-terminal sequence SP(7-11). N-terminal fragments, including SP(1-7), do not show significant binding, although these amino acids are required for high-affinity binding of SP to the NK-1r. These findings indicate that N-terminal fragments of SP are activating a different receptor within the NTS.

A study by Okamoto et al., 1994 in which NK-1r and NEP were expressed in a mammalian cell line revealed that the enzyme was effective in degrading SP prior to receptor activation only if co-expressed in the same cell as the NK-1r, and not if the NK-1r and NEP were present on the surface of different, but adjacent, co-cultured cells (Okamoto et al., 1994). The requirement for co-expression can be explained by the fact that the affinity of the enzyme for SP is >10,000 fold lower than the receptor (Hershey and Krause, 1990; Matsus et al., 1983; Matsus et al., 1984). Therefore, close spatial proximity of the enzyme to NK-1r on a target cell is essential for effective hydrolysis of SP.

Previous studies employing immunocytochemistry (Lasher et al., 1990) and fluorescence histochemistry (Back and Gorenstein, 1990) have reported NEP-IR within the rat DVC. In these studies, NEP-IR was reported in the NTS, in fibres bordering the AP and in the AP itself. Only "light to moderate staining of cell bodies" has been reported in the DMV (Back and Gorenstein, 1990). Examination of the NTS at the ultrastructural level revealed NEP-IR associated with the cytoskeleton and plasma membrane of axons, dendrites and glial processes. Within this region, NEP-IR was found

in synaptic vesicles and plasma membranes in presynaptic terminals forming mainly axo-dendritic synapses. However, these studies localized the enzyme to caudal but not rostral levels of the DVC, and did not identify any relationship to NK-1r or identified gastric efferent neurons.

If a volume transmission mechanism is involved in the action of SP in the rostral DVC, the hypothesis that endopeptidase-24.11 is not localized in close proximity to NK-1r on the cell membrane of identified gastric efferent neurons within this region must be validated. This was investigated using a combination of retrograde tracing and immunocytochemistry techniques which examined the spatial relationship of this enzyme with respect to SP-IR, NK-1r-IR and retrogradely-labelled gastric efferent neurons in the DVC.

Table 6. Sites of SP hydrolysis by a variety of enzymatic activities. The arrows represent cleavage sites. Modified from Krause, 1985 (see this source to obtain references for enzymes 1-7 listed in this table).

	← N-terminal 1 2 3 4 5 6 7 8 9 10 11 Arg-Pro-Lys-Pro-Gln-Gln-Phe-Phe-Gly-Leu-Met-NH_2 → C-terminal
1. Dipeptidyl peptidase B	↑ ↑
2. Dipeptidyl peptidase IV	↑ ↑
3. Post Proline Cleaving Enzyme	↑ ↑
4. Serum Acetylcholinesterase	↑ ↑
5. Acid Proteinase	↑ ↑ ↑
6. **Endopeptidase-24.11**	↑ ↑ ↑
7. Substance P Endopeptidase	↑ ↑ ↑
8. Karlsson et al., 1996	↑ ↑ ↑
9. Endo et al., 1988	↑ ↑ ↑

5.2. Methods

Wistar rats (N=5) were anesthetized with pentobarbital and injected with 4% FG beneath the serosal surface of the stomach as described in chapter 2. After allowing time for retrograde transport of the tracer, the rats were perfused and fixed, and 25 μm thick serial sections were cut in the coronal plane using a cryostat. While cutting, the section at the position of the obex was noted and all other sections were referenced as being either rostral (+) or caudal (-) to this landmark. Distances between sections were expressed in microns.

Alternating serial sections spanning DVC levels from -500 to +1500 μm were stained with different protocols, either immunofluorescence or immunoperoxidase, as described in chapter 2. One set were incubated with guinea pig anti-SP at 1:1000 ("SP-6"; Dr. Kwok, Dept. of Physiology, UBC) and rabbit anti-NK-1r at 1:5000 (Dr. Vigna, Dept. of Medicine, Duke University), while the second set were incubated with mouse anti-NEP at 1:500 (a monoclonal antibody designated "172-3:17", provided by Dr. Lasher, Dept. of Cellular and Structural Biology, University of Colorado Medical School). Following incubation with the primary antisera, set 1 were developed with Texas Red-conjugated donkey anti-guinea pig IgG at 1:1000 and fluorescein-conjugated donkey anti-rabbit IgG at 1:500 for 1 hour. Set 2 were incubated with a biotinylated goat anti-mouse antibody for 1 hour and developed for immunoperoxidase. All sections were examined by transmitted light and epifluorescence microscopy.

The specificity of the primary antibodies against SP and NK-1r has been confirmed as reported in chapter 2. The antisera to NEP has also been characterized previously (Lasher et al., 1990). Briefly, Western blots of kidney proteins and

synaptosomal plasma membranes isolated from rat brain revealed that the anti-NEP reacted only to the band corresponding to purified NEP. Furthermore, when the anti-NEP was added to a Superose 12 column containing a preparation of solubilized NEP, the fraction containing enzyme activity was found to elute more rapidly than in the absence of the antibody (i.e. due to the increased weight of the antibody-NEP complex). Control sections for immunofluorescence and immunoperoxidase were developed using the general protocols outlined in chapter 2.

5.3. Results

Control sections for both immunofluorescence and immunoperoxidase revealed an absence of staining. No FG staining in the AP or NA was observed indicating minimal leakage of retrograde tracer and specific labelling of gastric efferents within the DMV.

Labelling for NEP was most intense below the level of the obex, and was largely confined to the border NTS and the AP (Figure 36 Figure 37). Light to moderate NEP-IR was observed immediately ventral to the AP, roughly corresponding to the commissural subnucleus of the NTS. At levels rostral to the obex, NEP-IR was localized to a narrow band in the dorsal NTS, immediately adjacent to the fourth ventricle on both sides of the brainstem. NEP-IR was also consistently found in the ependymal lining of central canal (and immediately around it), at the floor of the fourth ventricle and in endothelial cells of blood vessels in the DVC (Figure 38).

The results for SP-IR and NK-1r-IR were as reported in chapter 4. Briefly, dense SP-IR was observed throughout DVC, in close association with gastric efferents. The

NK-1r-IR was localized to cell bodies and fibres in the dorsal motor nucleus of the vagus (DMV) and NTS, with the greatest density of labelling observed rostral to the obex. The majority of gastric efferents co-labelled with NK-1r were located rostral to the obex. There was a discrepancy in the distribution of NEP staining with respect to SP and NK-1r in the DVC, rostral to the obex (Figure 36, 39). At a distance of 800 μm rostral to the obex, no NEP-IR was observed, although both SP-IR and NK-1r-IR were present.

Figure 36. Distribution of NEP-IR, SP-IR and NK-1r-IR at different rostrocaudal levels of the DVC. All distances are in microns; negative distances are below the level of the obex while positive distances are rostral to the obex. The relative labelling density observed at each level is shown.

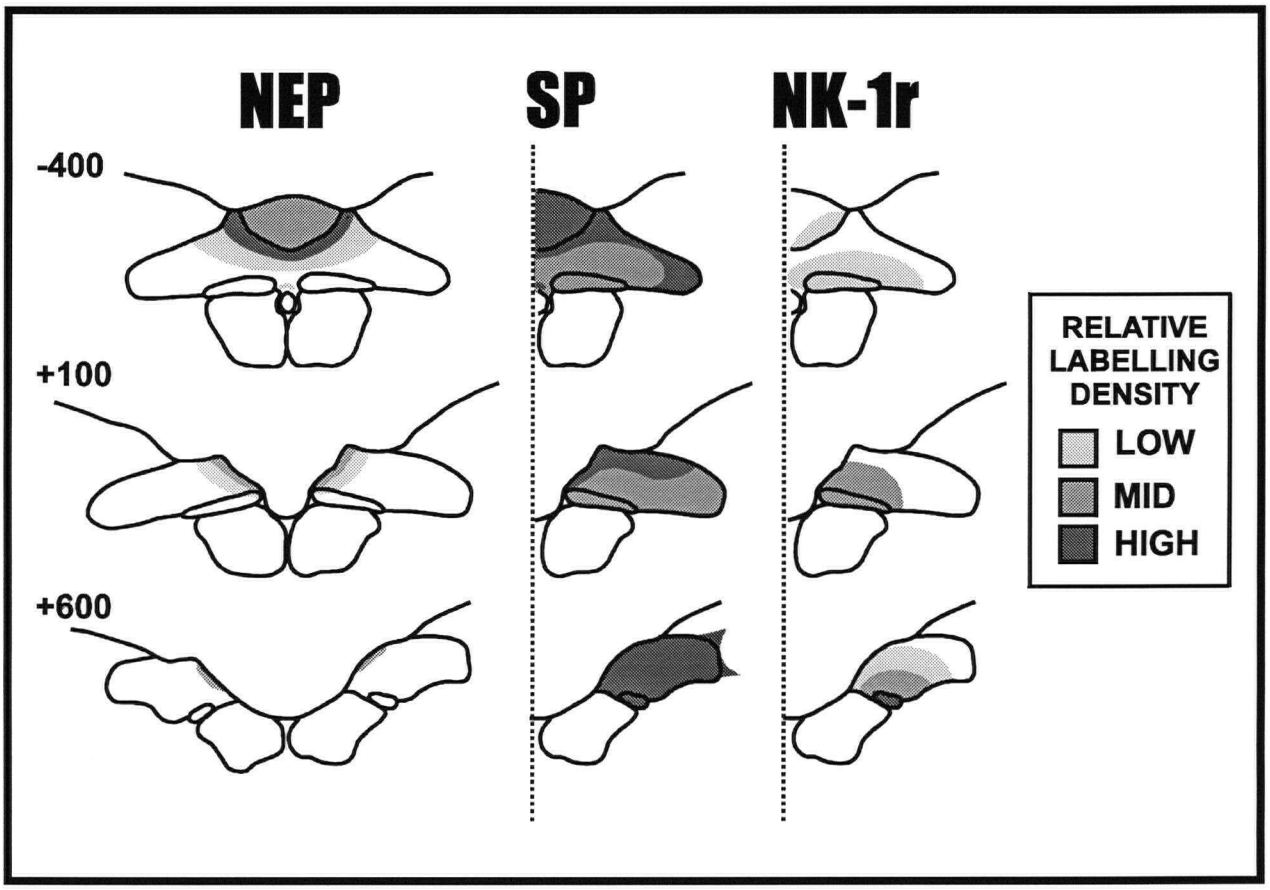
NEP
SP
NK-1r
-400
+100
+600
RELATIVE LABELLING DENSITY
LOW
MID
HIGH

Figure 37. Comparison of FG-labelled gastric efferent neurons (A) to NEP-IR (B) distribution in the DVC. Note the concentration of NEP-IR around the interface between the AP and NTS (arrow). A low density of NEP-IR was also observed in the NTS, immediately ventral to the AP. This section is at -300 μm relative to the obex. Scale bar=100 μm.

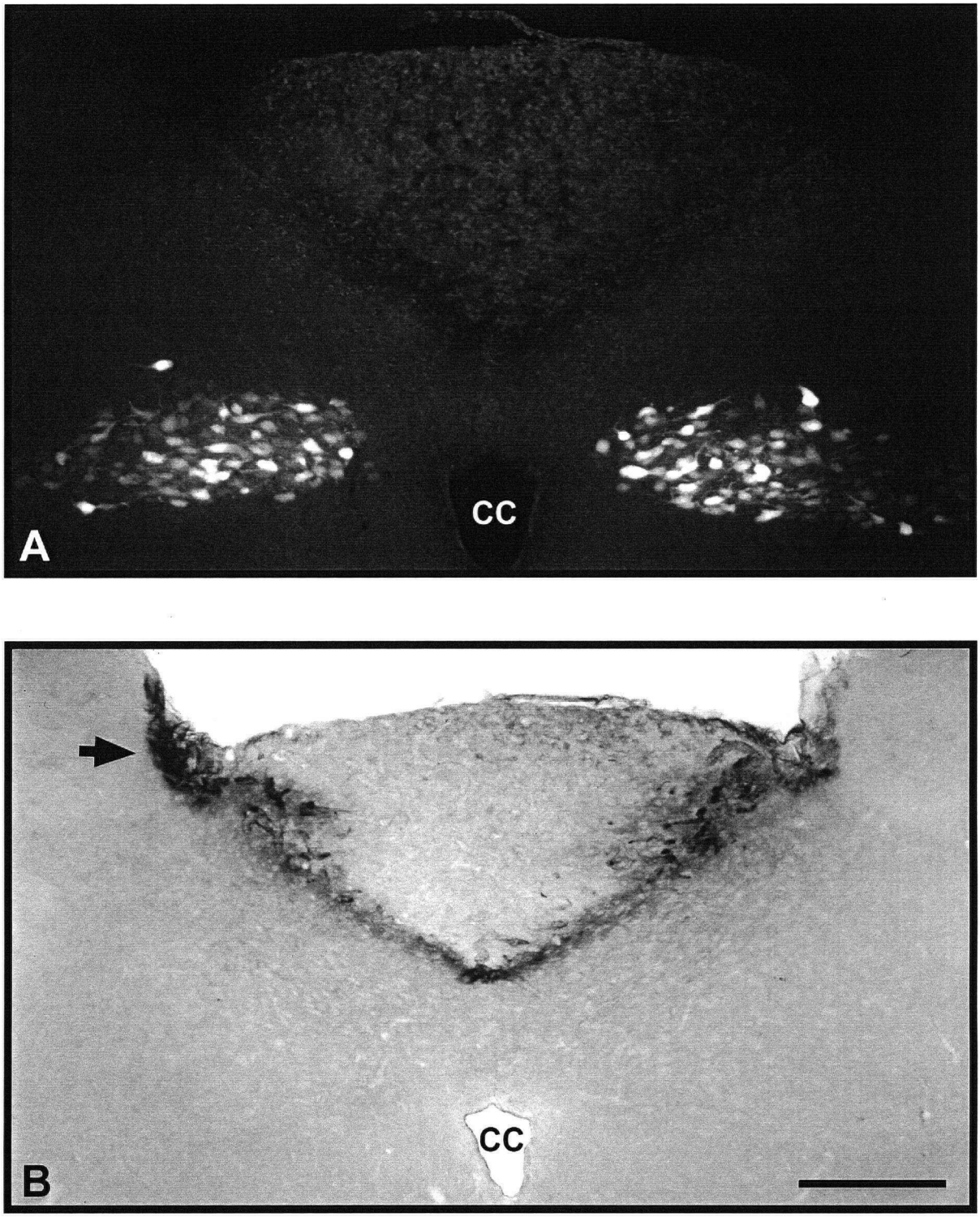
A
CC
B
CC

Figure 38. Demonstration of NEP-IR in (A) the ependymal lining of central canal (arrow), scalebar = 50 μm; and (B) endothelial cells of a blood vessel (BV; large arrows) as well as capillaries (small arrows) within the DVC (B). Scalebar = 20 μm.

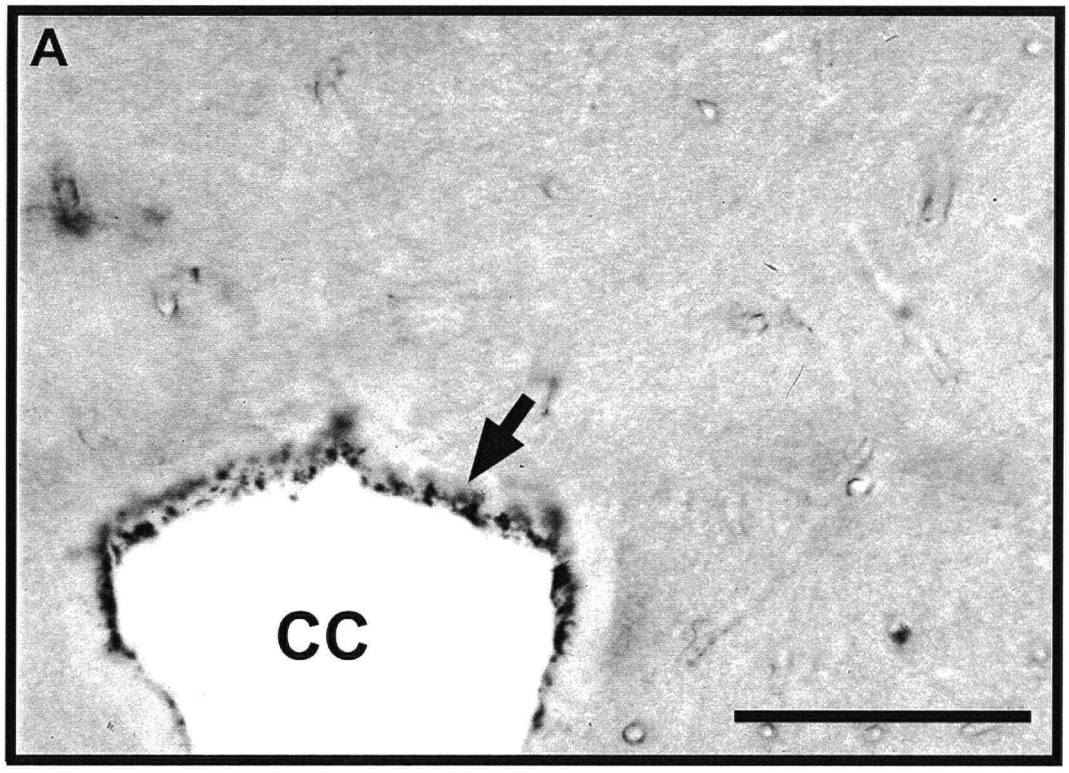
A
CC

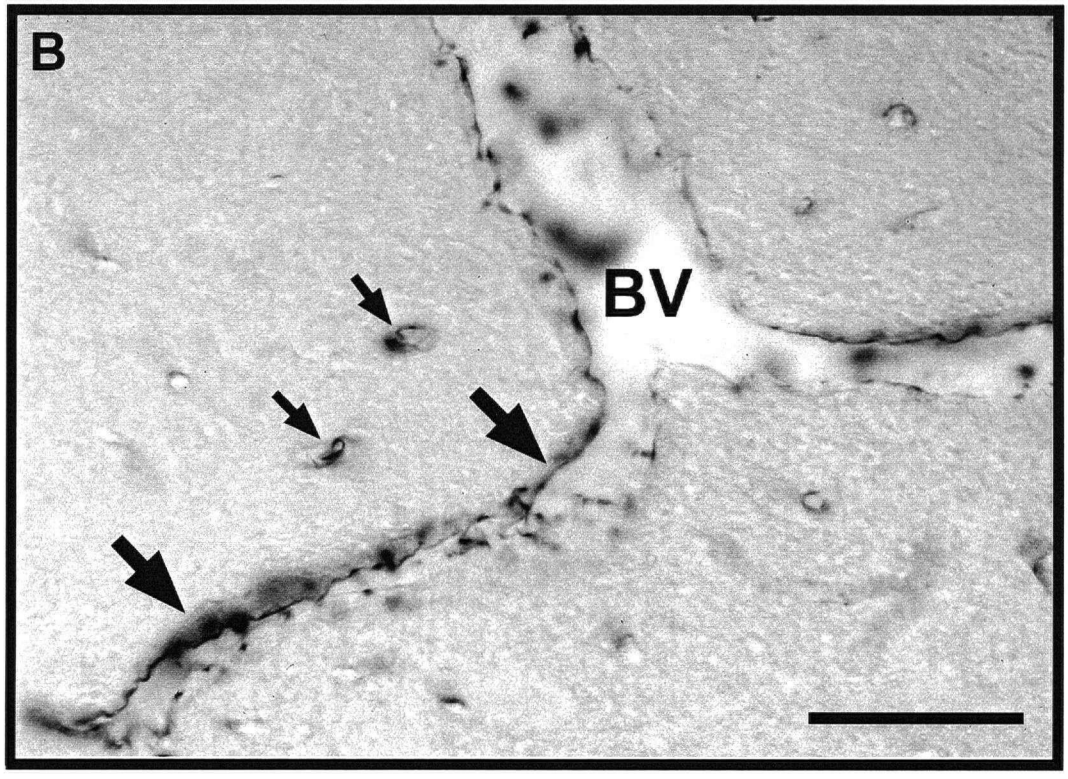
B
BV

Figure 39. The location of NEP-IR (A) compared to that of FG-labelled gastric efferent neurons (B), NK-1r-IR (C) and SP-IR (D) in a coronal brainstem section at +700 μm relative to the obex. The majority of NEP-IR is present in a narrow band at the edge of the IV ventricle (arrow). Scalebar=50 μm.

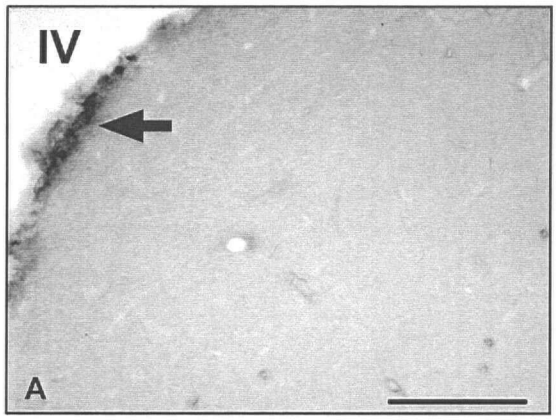
IV
A

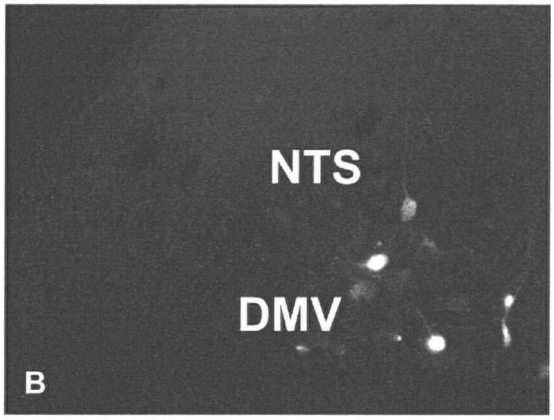
NTS
DMV
B

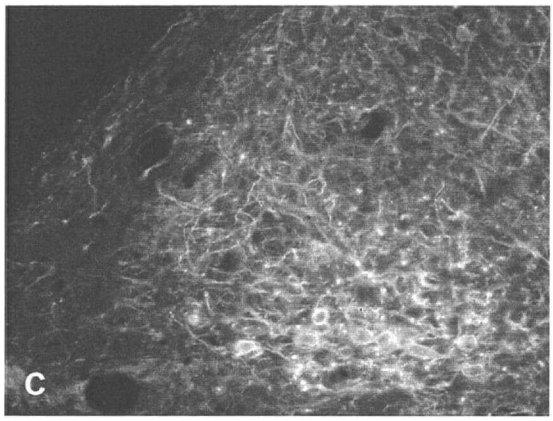
C

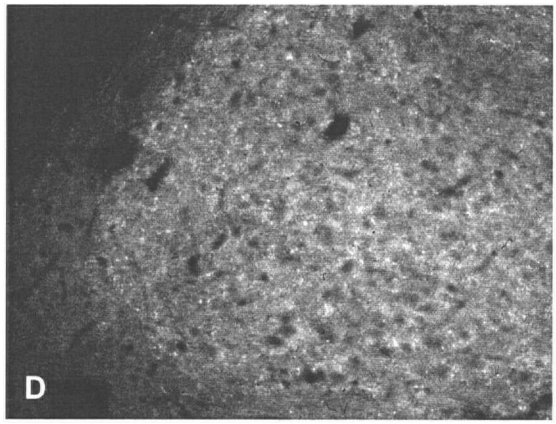
D

No NEP-IR was observed in association with the somata of retrogradely labelled gastric efferent neurons at all levels of the DMV that were examined (Figure 37, 39). The fact that FG labelling was limited to the proximal processes of identified gastric efferent neurons made it difficult to determine if NEP-IR was associated with NK-1r-IR on the dendrites of a subpopulation of these cells. At brainstem levels rostral to the obex, this relationship seemed unlikely since the minimal amount of NEP-IR detected within the NTS was not situated in the immediate vicinity of NK-1r-IR (Figure 39). Although a much higher density of NEP-IR was detected in the NTS caudal to the obex, little NK-1r-IR was observed in these regions, further supporting the lack of a relationship between the enzyme and NK-1r-IR on the dendrites of gastric efferent neurons.

5.4. Discussion

The fact that no NEP-IR was observed in association with NK-1r on a subpopulation of retrogradely labelled gastric efferent neurons in the DVC would suggest that the enzyme is not responsible for the inactivation or other processing associated with the action of SP on these cells. This finding would imply that SP released from nerve terminals in this region could diffuse for a considerable distance within the medulla without being degraded. It also supports the possibility that SP acts on gastric efferent neurons within the DVC via a non-synaptic volume transmission mechanism, due to the close association between this peptide and its receptor in the rostral DVC. However, the presence of other SP degrading enzymes (e.g. Endo et al., 1988; Karlsson et al., 1996) within this region cannot be excluded.

An alternative mechanism for inactivation of SP within the DVC involves internalization of the peptide after it binds to its receptor. Recently, the endocytotic pathway of SP and the NK-1 receptor has been delineated, both in cell culture (Grady et al., 1995) and *in vivo* in rat striatum (Mantyh et al., 1995). Briefly, these studies found that internalization is rapid, and is initiated immediately (within approximately 1 min.) after SP binds to its receptor. At this time, SP and NK-1r are internalized into the same clathrin-coated vesicle, and then are sorted into different endosomal compartments. The SP is degraded in lysosomal vesicles whereas the NK-1r recycles to the plasma membrane and is only rarely degraded. In *in vivo* experiments, it was demonstrated that the NK-1r located in both synaptic and non-synaptic regions are functional, since the receptor could undergo rapid internalization after binding SP at both sites (Mantyh et al., 1995).

Localization of NEP-IR to the AP, ependymal lining of the fourth ventricle and central canal, and to the endothelial cells of blood vessels within the DVC would suggest that the enzyme is actively involved in the degradation of circulating peptides, preventing their diffusion into the CSF. Particularly striking was the observation that the spatial distribution of NEP-IR within the DVC forms an effective "seal" around the AP and fourth ventricle. At levels caudal to the obex, this was seen in the form of dense staining at the interface between the AP and NTS which extended to narrow bands of immunoreactivity just ventral to the fourth ventricle at more rostral regions. Given the absence of a blood-brain barrier within the AP (see section 1.7.4), the strategic distribution of NEP may serve an important function in preventing neuropeptides from diffusing into the DVC where they might otherwise exert undesired effects.

In conclusion, the results of these experiments confirm the hypothesis that NEP is not localized in close proximity to NK-1r on the membranes of identified gastric efferent neurons within the DVC, supporting the contention that SP may act via a non-synaptic volume transmission mechanism in this region. The discrepancy between the distribution of NEP-IR compared to that of SP, NK-1r and identified gastric efferent neurons would imply that NEP is not involved in the enzymatic processing of SP in the vicinity of gastric efferent neurons. Inactivation of SP activity in this region may involve the action of other peptidases, or could result from internalization and degradation of SP and recycling of the NK-1 receptor.

6. GENERAL DISCUSSION

6.1. Differential Distribution of SP and CGRP within the DVC

The results obtained from Chapters 3 and 4 provide clear evidence that there is a differential distribution of SP-IR and CGRP-IR within the DVC of the rat. This finding is in contrast to the peripheral nervous system, where SP and CGRP are largely colocalized in primary sensory neurons, and would imply that their site of origin and function within the DVC are different.

In these studies, SP-IR was visualized in the form of a high density of punctate varicosities at all levels of the DVC that were examined, at locations rostral and caudal to the obex, in both the NTS and DMV. In contrast, CGRP-IR was visualized in the form of rope-like fibres that were confined mainly to the NTS, and these were located caudal to the obex. Furthermore, SP-IR was associated with both the soma and dendrites of identified neurons, whereas CGRP-IR appeared to be preferentially associated with dendrites of these neurons, with few somatic inputs observed. As confirmed by 3-D reconstructions, CGRP-IR nerve fibres had a lateral orientation within the DVC (i.e. perpendicular to the rostrocaudal axis) whereas SP fibres ran longitudinally (i.e. in parallel with the rostrocaudal axis).

In the periphery, CGRP and SP have been identified at the ultrastructural level within the same large, dense core vesicles in nerve endings of primary sensory neurons and in cell bodies in the dorsal root ganglia (Gulbenkian et al., 1986; Merighi et al., 1988). Taken together with the fact that the axonal transport rates of SP and CGRP in

visceral afferent nerves are quite similar (Gilbert et al., 1980), this data would suggest that after stimulation, both peptides are co-released simultaneously at peripheral nerve endings. Furthermore, it has been demonstrated that SP and CGRP have either complimentary or co-operative effects on peripheral targets. Both are potent vasoactive substances, and elicit vasodilation via an axon reflex mechanism whereby the peptides are released from sensory nerve endings (Brain et al., 1985). In the dorsal horn, there is evidence to suggest that CGRP may facilitate neural transmission by acting postsynaptically on dorsal horn neurons by facilitating the release of SP and excitatory amino acids and by inhibiting the breakdown of SP (Hökfelt et al, 1992). The increased SP levels may, in addition to exerting a postsynaptic effect, also enhance glutamate transmission in the dorsal horn (Hökfelt et al, 1992).

Unlike these effects in peripheral sensory neurons, there is evidence to suggest that the functions of SP and CGRP are different within the DVC. In addition to the differential distribution of both neuropeptides in this region, the distribution of corresponding receptors differs. As demonstrated in Chapter 5, the NK-1 receptor is localized to somata within the DMV and dendrites in the NTS, with the greatest density observed in the rostral DVC. While not observed in these studies, CGRP-binding sites have been preferentially localized to the NTS within the DVC and have a more caudal location, with the highest density observed below the level of the obex (Sexton et al., 1986, Inagaki et al., 1986). The localization of NK-1r-IR to both soma and dendrites of DMV neurons, and the high density of SP-IR varicosities surrounding both structures, indicates that SP may have different effects on each of these neuronal areas. In contrast, CGRP was most frequently seen in association with the proximal dendrites of identified

gastric efferent neurons, with the majority of CGRP-IR observed in the NTS. This finding, and the location of CGRP binding sites in the NTS, would indicate that this peptide is most likely acting only on dendrites within the NTS.

Also supporting differential effects for SP and CGRP within the DVC are the results of pharmacological experiments. With regard to gastric function, injection of SP into the cerebral ventricles or directly into the DVC results in increased gastric pressure and decreased gastric motility (Spencer and Talman, 1986), whereas injection of CGRP is associated with an inhibition of gastric secretion and an impairment of gastric transit (Taché et al., 1984; Taché et al., 1990.) Furthermore, direct superfusion of SP onto DMV neurons has been shown to induce either depolarization (majority) or hyperpolarization (minority) via a direct effect on the neuronal membrane (Plata-Salaman et al., 1989; Martini-Luccarini et al., 1996). While no similar studies with CGRP and DMV neurons have been conducted, evidence which examined the effect of CGRP on individual forebrain neurons revealed an inhibitory effect for this peptide (Twery and Moss, 1985).

Finally, the differences in the distribution of SP-IR and CGRP-IR fibres within the DVC would imply that each neuropeptide has a different point of origin. Although both peptides have been localized to vagal afferent cell bodies within the nodose ganglion (see section 3.4 for refs.), a study that combined neuroanatomical tracing to identify vagal afferents within the DVC with immunocytochemistry for SP and CGRP found that both peptides were represented in only a minority of vagal afferent fibres in this region (Sykes et al., 1994). Other studies that have used tracing, deafferentiation and neurochemical techniques have shown that up to 25% of SP content in the NTS originates from peripheral sensory fibres (Thor and Helke, 1987), indicating that central sources must

contribute to the majority of peptide in this region. One brain region that is emerging as a significant source of SP-IR projections to the DVC is the caudal raphe nuclei (Taché et al., 1995). Specifically, SP has been found colocalized with 5-HT in 50% of the NTS afferent neurons in the nucleus raphe pallidus and in 20% of similarly projecting neurons in the nucleus raphe obscurus (Thor and Helke, 1987; Thor and Helke, 1989). As described in section 1.8, there is pharmacological evidence to suggest that SP modulates the gastric response to raphe stimulation. Although no similar neuronal tracing and immunocytochemistry combination studies have been conducted to locate the origin of CGRP-IR nerve fibres within the DVC, CGRP-IR cell bodies have been identified in locations that are known to project to the NTS, including the petrosal and trigeminal ganglia (Helke and Hill, 1988) and the hypothalamus and amygdala (Kawai et al., 1985; Skofitsch and Jacobowitz, 1985).

In conclusion, SP-IR and CGRP-IR fibres within the DVC were observed to differ with respect to distribution, orientation and appearance. This is in contrast to the peripheral nervous system, where these peptides are colocalized in many primary sensory afferent neurons. Differences in the distribution of NK-1 receptor sites and CGRP binding sites within the DVC, together with the pharmacological data gathered from injection of SP and CGRP into the cerebral ventricles or directly into the DVC, would suggest different functions for each of these neuropeptides within the DVC. Finally, the differential distribution of SP-IR and CGRP-IR fibres within the DVC would imply that these inputs originate from different locations.

6.2. Evidence for Volume Transmission Within the DVC

The combination of confocal microscopy with 3-D reconstruction techniques permitted a detailed analysis of the spatial relationship of peptidergic nerve terminals in relation to identified neurons. Although the resolution provided by these techniques did not permit observation of synaptic connections between these nerve terminals and identified gastric efferent neurons, a distinction could be made between those fibres that came within a submicron distance of the neuronal membrane (classified as "putative" synaptic contacts) and those that were further away than this distance (which could be regarded as potential non-synaptic inputs). Furthermore, these techniques permitted the simultaneous observation of the spatial relationship between neuropeptide and an identified neuron (and the corresponding receptor in the case of SP) in 3-D, which is something that cannot be achieved using conventional microscopic techniques.

The 3-D reconstructions of SP-IR and CGRP-IR within the DVC illustrated that these peptides were localized to nerve fibres that were in most cases > 5 μm away from the closest neuron. In the case of CGRP, only a very small number of putative synaptic contacts were observed between CGRP-IR fibres and the proximal dendrites and somata of identified neurons in the DMV. In spite of this, the lack of antiserum to the CGRP receptor and the inability to observe distal dendrites of DMV neurons when these studies were conducted did not permit a detailed analysis a volume transmission mechanism in this scenario.

In contrast to CGRP, an anatomical basis for volume transmission in the case of SP was clearly established. The fact that NK-1r-IR almost completely covered the somatic and dendritic membrane of a subpopulation of neurons within the DVC indicates

that a significant proportion of the surface of these neurons is a potential target for SP. Since few SP-IR varicosities were observed to make putative synaptic contacts with NK-1r-IR on identified neurons, the vast majority of the receptor was considered to be extrasynaptic. In addition to the mismatch between peptide and receptor at the cellular level, there was an apparent mismatch between the gross-scale distribution of NK-1r-IR and SP-IR within the DVC. It was found that SP-IR was present at all levels (both rostral and caudal to the obex) whereas NK-1r-IR was preferentially located at levels rostral to the obex.

The possibility that SP can act upon NK-1r on almost any region of the neuronal membrane of a subpopulation of DMV neurons depends on the ability of SP to diffuse a considerable distance from its site of release. Studies by Duggan et al., 1990 have demonstrated that SP released from primary afferent neurons can diffuse several millimeters from its site of release in the substantia gelatinosa of the spinal cord (Duggan et al., 1990). Furthermore, the diffusion of SP within this region was dramatically enhanced when inhibitors of SP-degrading proteases were applied. Within the DVC, it has been shown that SP can diffuse through the CSF exert its effect on neurons within this region (e.g. Chan et al., 1995). The high density of SP-IR nerve fibres were observed surrounding all neurons throughout the DMV would suggest that peptide availability is not a limiting factor for NK-1r activation. These results, together with the finding that NEP was not associated with identified gastric efferent neurons, SP-IR or NK-1r-IR within the DVC, support the possibility that SP can diffuse from varicosities within the DMV and NTS to exert an effect on the subpopulation of these neurons which are co-labelled with NK-1r.

The fact that nonsynaptic localization of NK-1r has been previously observed in spinal cord, cortex and striatum (Liu et al., 1994), and now within the DVC, suggests that this property of the receptor is the rule, not the exception. The finding that most of the neuronal membrane contains NK-1r-IR, even when apposing presynaptic elements do not contain SP-IR, suggests that the insertion of the receptor is not directed to particular regions of the neuronal surface. An important question is whether the majority of receptors located at nonsynaptic regions are functional. Evidence to support this comes from studies that have examined the internalization of NK-1r after it has bound to SP in rat striatium (Mantyh et al., 1995). This study found that NK-1r which is present at both synaptic and non-synaptic sites on the membrane of neurons in this brain region can undergo rapid internalization after SP binding, suggesting that receptors at both of these locations are functional. Furthermore, the observed NK-1r internalization appeared to be due to receptor activation rather than simple ligand binding, since injection of RP-67,580, a specific antagonist which also binds to NK-1r, but at a different site than SP, produced no significant internalization of the NK-1r (Mantyh et al., 1995).

Although no data were presented in this thesis examining the spatial relationship of SP and NK-1r within the DVC using electron microscopy, a previous study examined this relationship in the dorsal horn of the rat spinal cord (Liu et al., 1994). This study revealed that in this location, over 90% of synaptic profiles containing large dense core vesicles that were SP-IR were located away from the synaptic junction. Additionally, although some SP-IR nerve terminals contacted NK-1r-IR on the postsynaptic membrane, no more than 15% of the NK-1r-IR membrane apposed synaptic terminals.

Studies that have examined the release of peptides from neurons also lend support to the possibility for SP acting via a volume transmission mechanism within the DVC. It has been observed that dense core vesicles which contain neuropeptides are usually located away from synaptic regions (De Biasi and Rustolini, 1988; Merighi et al., 1991). Furthermore, it has been demonstrated that the release of peptides from nerve terminals via exocytosis occurs preferentially at morphologically non-specialized sites that can be distant from the synaptic junction, even when synapses are present (Buma and Roubos, 1986; Zhu et al., 1986; Thureson-Klein et al., 1986). These results indicate that although few putative SP-IR synaptic contacts were observed on identified gastric efferent neurons that were co-labelled with NK-1r-IR, the peptide could still be released by surrounding (i.e. nonsynaptic) SP-IR nerve fibres to act on these neurons.

Pharmacological experiments also support the possibility of volume transmission for SP in the DMV. The time course of action for SP when injected into the rat NTS has a slow onset and a prolonged duration, with a maximal effect on gastric pressure observed approximately 8 minutes after injection (Spencer and Talman, 1986). Additionally, the depolarization or hyperpolarization of DMV neurons after direct superfusion of SP lasted for several minutes after the application of the peptide (Plata-Salaman et al., 1989). The time course of NK-1r internalization after SP binding also support the slower reaction kinetics that would be expected if SP diffused through the ECF to bind to its receptor. Following injection of SP into the rat striatum, up to 60% of NK-1r-IR neurons within the injection zone exhibited internalization within 1 minute (Mantyh et al., 1995). However, following application of the peptide, a relatively long period of tachyphylaxis (lasting from 2 to 60 min), where exposure to SP did not evoke receptor signaling, was observed.

Therefore, the sustained duration of SP effects seen after application of the peptide to DMV neurons could be due to the slow resensitization of the NK-1r after SP binding.

In conclusion, the results presented in this dissertation clearly demonstrated an anatomical basis for volume transmission involving SP and the NK-1r in the DVC of the rat. As revealed by 3-D reconstructions, a high density of SP-IR nerve fibres surrounded all surfaces of, and came in close spatial proximity to, a subpopulation of DMV neurons that were co-labelled with NK-1r-IR. Although few putative SP-IR synaptic contacts were observed, NK-1r-IR was detected on most of the somatic and dendritic membrane of these neurons. This would indicate that most of the surface of these neurons is a potential target for SP. The fact that NEP, the enzyme that has been implicated as being principally responsible for the inactivation of SP in other brain regions, was not found to be in association with SP, NK-1r or identified gastric efferent neurons in the DVC suggests that SP may diffuse a considerable distance from its site of release to bind to its receptor without being degraded.

6.3. Implications of Neutral Endopeptidase 24.11 Localization Within the DVC

The results from chapter 5 revealed that the spatial distribution of NEP-IR was distinct from that of SP, NK-1r and identified gastric efferent neurons within the DVC. This was especially evident in the rostral DMV/NTS, where the density of NK-1r was greatest. The absence of NEP-IR from the immediate vicinity of gastric efferent neurons that were co-labelled with NK-1r suggests that, excluding the presence of other degrading enzymes in the region, SP may diffuse over long distances to exert its effect.

The staining pattern observed for NEP in the medial to rostral DVC would suggest that it is strategically located to ensure the hydrolysis of circulating peptides within this region. The localization of NEP-IR to the area surrounding the AP and in the ependymal lining of the fourth ventricle and central canal would suggest that the enzyme may play a role in preventing peptides from entering the DVC from the CSF, where they could potentially interact with vagal afferents and efferents. Conversely, the enzyme could also prevent neuropeptides that are released via a volume transmission mechanism within the DVC from entering into the CSF where they could be transported to other areas of the brain and/or spinal cord. Detection of NEP-IR within endothelial cells lining blood vessels in the DVC is consistent with previous studies that have identified this enzyme within peripheral vascular structures (Kenny and Fulcher, 1983). At these locations, NEP is most likely involved with the degradation of vasoactive peptides (such as SP and CGRP).

In conclusion, the results obtained in Chapter 5 would suggest that although NEP is not involved the inactivation of SP within the DVC, it could play an important role in the inactivation/modification of peptides that enter the DVC from the CSF and/or prevent the outflow of peptides that are released in the DVC from entering into the CSF. Therefore, different mechanisms must be responsible for inactivation of neuropeptides that are released within the DVC versus those that enter this region from the CSF. These could involve the presence of other endopeptidases, or internalization of SP after binding to receptors, followed by internal peptide degradation and receptor recycling.

7. SUMMARY AND FUTURE DIRECTIONS

7.1. Summary

The hypothesis investigated by the studies described in this thesis was that SP and CGRP can act on gastric efferent neurons within the DVC via a nonsynaptic, volume transmission mechanism.

The major findings of this dissertation are as follows:

1. The combination of retrograde tracing and immunocytochemistry with confocal microscopy, image processing and volume rendering techniques permitted the 3-D reconstruction of identified neurons and surrounding nerve fibres in the brainstem of the rat.
2. Within the DVC, CGRP-IR nerve fibres were only associated with identified gastric efferent neurons around the level of the obex, predominantly at the border of the DMV and NTS. Few of these fibres formed putative synaptic contacts with the somata of identified gastric efferent neurons in the DMV.
3. Although SP-IR nerve fibres were detected surrounding all surfaces of identified gastric efferent neurons at all levels of the DVC, few putative synaptic contacts with these neurons were observed. NK-1r-IR was localized to the somata of a small subpopulation (7%) of identified gastric efferent neurons in the DMV. The highest density of NK-1r-IR was detected rostral to the obex and was confined to the DMV and NTS. NK-1r-IR covered almost the entire neuronal membrane of some DMV

neurons (including gastric efferents), with the highest density of receptor on the dendrites.

4. NEP-IR was not associated with SP-IR, NK-1r-IR or identified gastric efferent neurons in the DVC. The enzyme was localized to the AP, ependymal lining of the fourth ventricle and central canal and to endothelial cells of blood vessels in this region. The highest density of NEP-IR was observed around and caudal to the level of the obex.

These results support the hypothesis that neuropeptides within the DVC act via a non-synaptic, volume transmission mechanism.

7.2. Future Studies

In order to evaluate the possibility of a direct effect of CGRP on gastric efferent neurons within the DVC, the receptor for CGRP must be localized to the cell membrane of these neurons. Although many studies use either specific antisera or the binding of high affinity labelled peptide in an attempt to localize receptors, the former identifies the expressed receptor protein whereas the latter only identifies binding sites.

Although an association between CGRP-IR nerve fibres and the dendrites of identified gastric efferent neurons was implied in these studies, this could not be confirmed due to poor labelling of dendritic processes with the retrograde tracer that was used. This could be improved using a combination of microinjection with retrograde tracing, using a strategy similar to that of Fox and Powley, 1992. Briefly, this would involve injecting a fluorescent retrograde tracer into the stomach to identify gastric

efferent neurons and then filling these neurons with a fluorescent label such as Lucifer Yellow while observing thick brainstem slices using an epifluorescence microscope.

In order to strengthen the case for a volume transmission mechanism for CGRP within the DVC, the spatial relationship between the enzyme(s) responsible for the degradation of this peptide and receptors in this region must be identified. Although there is some evidence to suggest that NEP is involved in the degradation of CGRP (Katayama et al., 1991), the studies in Chapter 5 would need to be repeated in conjunction with an antibody to the CGRP receptor in order to verify this.

The origin of the CGRP-IR nerve fibres projecting to the DVC remains unclear. This could be resolved using a combination of retrograde tracing (tracer injected into the NTS/DMV) and immunocytochemistry (to detect CGRP-IR somata at the sites identified by the tracer). Pre-treatment of animals with colchicine may also be included in this procedure to enhance the detection of CGRP-IR within somata. Once the source(s) of CGRP projections to the DVC have been determined, neurons in these regions could be stimulated using electrical or chemical means, and the effect on gastric function observed.

As with CGRP, the source of SP inputs to the the DVC has not been clearly determined. Although the raphe nuclei provide a significant SP projection to the DVC and have been shown to participate in gastric regulation (Taché et al., 1995), it would be interesting to determine if the projections from this location are preferentially associated with the NK-1r-IR co-labelled gastric efferents that were observed in this study. This could be investigated by combining anterograde tracing (injected into the raphe) and retrograde tracing (injected into the stomach) with immunocytochemistry for NK-1r and

SP in the DVC. Other SP projections to the DVC could be determined as mentioned above for CGRP.

In Chapter 4 it was found that only a small subpopulation of gastric efferent neurons in the DMV that projected to the greater curvature of the rat stomach were co-labelled with NK-1r-IR. It would be interesting to determine if these neurons participate in a specific gastric function, such as distention. One way of testing this is to use the methods of Fogel et al., 1996 to identify distention-sensitive neurons (i.e. using microelectrode stimulation) in the rat DMV and fill these with a fluorescent intracellular label. Another way of investigating this would be to utilize a combination of Fos immunocytochemistry and retrograde tracing to identify those gastric efferent neurons that are activated by gastric distention. Several studies have demonstrated that the immediate-early gene c-fos is selectively induced in neurons during depolarization (see Sagar, 1988 for refs.). The protein product of this gene, Fos, can then be detected using immunocytochemistry to identify those neurons that were activated. In previous studies by Fraser and Davison (Fraser and Davison, 1994, 1995), it was demonstrated that physiological distention of the stomach using an intragastric balloon resulted in Fos expression in the DMV and NTS. These studies could be repeated with the addition of a retrograde tracer injected into the stomach and immunocytochemical processing of the resulting brainstem sections for both SP and NK-1r.

Some of the DMV neurons that were labelled with NK-1r-IR in Chapter 4 were not co-labelled with retrograde tracer. It remains unclear as to whether these neurons are also gastric efferent neurons, or if they project to one of the other abdominal viscera. In order to determine if these neurons project to the stomach, an increased number of

retrograde tracer injections into all areas of the stomach could be performed to label any remaining gastric efferent neurons in the DMV that were not labelled in the present studies. If this fails to produce co-labelling with all of the NK-1r-IR neurons that are observed, retrograde tracer injections into other abdominal viscera should be performed.

Although the studies described in this dissertation have presented neuroanatomical evidence for volume transmission within the DVC, the only functional data in support of this mechanism comes from pharmacological studies. In order to confirm that this non-synaptic activation of neurons occurs *in vivo*, it is necessary to demonstrate the release of a neuropeptide from nerve endings into the extracellular space in response to a physiological stimulus. One way of doing this is to use microdialysis combined with a sensitive radioimmunoassay (Lindefors et al., 1987). Microdialysis enables continuous monitoring of biochemical events in the extracellular tissue space. The technique involves the implantation of a semipermeable tubular membrane (microdialysis probes) into the brain region of interest, and perfusion of this membrane with a physiological solution. Molecules in the surrounding extracellular space diffuse into the perfusate and can be collected for determination.

While it is unlikely that NEP is involved in the inactivation of neuronally-released SP within the rostral DVC, the presence of other enzymes within this region that may be responsible for this was not investigated (see Table 6). The simplest way to determine if any of these enzymes were present would be to use antibodies raised against the enzymes in question. Additionally, a pharmacological approach could be used (e.g. analogous to a study by Hall et al., 1988) whereby a specific enzyme inhibitor could be microinjected

into the DVC prior to application of SP into this region and the effect on gastric motility observed.

It is possible that the inactivation of SP does not involve extracellular cleavage of the peptide, but rather is dependent on internalization of the peptide-receptor complex after binding, and subsequent recycling of the receptor. In order to test this, the endocytosis inhibitor phenylarsine oxide (e.g. Gibson et al., 1989) could be used in conjunction with electrophyisolological recording of DMV neurons. If the application of this inhibitor produces tonic depolarization (or hyperpolarization) of specific gastric DMV neurons after application of SP (e.g. by microinjection), this would support inactivation of SP by a receptor internalization mechanism.

Finally, a number of techniques could be applied to improve the resolution of 3-D reconstructions. Because the axial resolution (i.e. resolution in the Z-plane) is worse than the lateral resolution for a confocal microscope (Wilson and Sheppard, 1984), reconstructions can appear fuzzy when observed from perspectives perpendicular to the plane of acquisition. This loss of resolution can be improved by using newer microscope designs with improved optics, such as 4Pi and Theta confocal microscopy (Lindek et al., 1995) or by application of mathematical algorithms, such as deconvolution (see Shaw, 1994 for review) or superresolution (Carrington et al., 1995). Briefly, since axial resolution is inversely proportional to the square of the numerical aperture of the objective used (Inoué, 1995), the former techniques improve resolution by increasing the aperture angle using two opposing objective lenses that have a common focus (Lindek et al., 1995).

The latter techniques improve resolution by removing out of focus light that is present in each optical section, or by restoring desired signal that is present in out of focus light that is intentionally discarded using confocal microscopy. These mathematical approaches can be used in conjunction with either confocal or non-confocal microscopy (Shaw, 1994; Shaw, 1995).

REFERENCES

Abdel-Latif, A.A. Calcium-mobilizing receptors, polyphosphoinositides, and the generation of second messengers. *Pharmacol. Rev.* 38:227-272, 1986.

Altschuler, S.M., Ferenci, D.A., Lynn, R.B. and Miselis, R.R. Representation of the cecum in the lateral dorsal motor nucleus of the vagus nerve and commissural nucleus tractus solitarii in rat. *J. Comp. Neurol.* 304:261-274, 1991.

Altschuler, S.M., Rinaman, L. and Miselis, R.R. Viscerotopic representation of the alimentary tract in the dorsal and ventral vagal complexes in the rat. In: *Neuroanatomy and Physiology of Abdominal Vagal Afferents*, S. Ritter, R.C. Ritter and C.D. Barnes, Eds., CRC Press, Boca Raton, 1992, 23-53.

Amara, S.G., Jonas, V., Rosenfeld, M.G., Ong, S.E. and Evans, R.M. Alternative RNA processing in calcitonin gene expression generates mRNAs encoding different polypeptide products. *Nature.* 298:240-244, 1982.

Asala, S.A., Bower, A.J. An electron microscope study of vagus nerve composition in the ferret. *Anat. Embryol. (Berl).* 175:247-253, 1986.

Bach-y-Rita, P. and Smith, C.U.M. Comparative efficiency of volume and synaptic transmission in the coerulean system: relevance to neurologic rehabilitation. *Scand. J. Rehab. Med.* 25:3-5, 1993.

Bach-y-Rita, P. In: *Nonsynaptic Diffusion Neurotransmission and Late Brain Reorganization*, Demos Publications, New York, 1995.

Bach-y-Rita, P. Neurotransmission in the brain by diffusion in the extracellular fluid: a review. *NeuroReport.* 4:343-350, 1993.

Back, S.A. and Gorenstein, C. Fluorescent histochemical localization of neutral endopeptidase-24.11 in the rat brainstem. *J. Comp. Neurol.* 296:130-158, 1990.

Barraco, R., El-Ridi, M., Ergene, E., Parizon, M. and Bradley, D. An atlas of the rat subpostremal nucleus tractus solitarius. *Brain Res. Bull.* 29:703-765, 1992.

Baude, A., Couraud, J.Y., Puizillout, J.J. Fine distribution of substance P-like immunoreactivity in the dorsal nucleus of the vagus nerve in cats. *J. Chem. Neuroanat.* 5:263-274, 1992.

Baude, A., Lanoir, J., Vernier, P. and Puizillout, J.J. Substance P-immunoreactivity in the dorsal medial region of the medulla in the cat: effects of nodosectomy. *J. Chem. Neuroanat.* 2:67-81, 1989.

Bentivoglio, M. and Chen, S. Retrograde neuronal tracing combined with immunocytochemistry. In: *Immunohistochemistry II: IBRO Handbook Series: Methods in the Neurosciences*, A.C. Cuello, Ed., John Wiley & Sons, New York, NY, 1993, 301-328.

Berk, M.L., Smith, S.E. and Karten HJ Nucleus of the solitary tract and dorsal motor nucleus of the vagus nerve of the pigeon: localization of peptide and 5-hydroxytryptamine immunoreactive fibers. *J. Comp. Neurol.* 338:521-548, 1993.

Berthoud, H-.R. and Powley, T.L. Vagal afferent innervation of the rat fundic stomach: Morphological characterization of the gastric tension receptor. *J. Comp. Neurol.* 319:261-276, 1992.

Berthoud, H.-R., Carlson, N.R. and Powley, T.L. Topography of efferent vagal innervation of the rat gastrointestinal tract. *Am. J. Physiol. Regul. Integr. Comp. Physiol.* 260:R200-R207, 1991b.

Berthoud, H-.R., Fox, E.A. and Powley, T.L. Abdominal pathways of central origin of rat vagal fibers that stimulate gastric acid. *Gastroenterology.* 100:627-637, 1991.

Berthoud, H-.R., Jedrzejewska, A. and Powley, T.L. Simultaneous labeling of vagal innervation of the gut and afferent projections from the visceral forebrain with Dil injected into the dorsal vagal complex in the rat. *J. Comp. Neurol.* 301:65-79, 1990.

Blackshaw, L.A. and Grundy, D. Responses of vagal efferent fibres to stimulation of gastric mechano- and chemoreceptors in the anaesthetized ferret. *J. Autonom. Nerv. Sys.* 27:39-45, 1989.

Blackshaw, LA., Grundy D. and Scratcherd, T. Involvement of gastrointestinal mechano- and intestinal chemoreceptors in vagal reflexes: an electrophysiological study. . *J. Autonom. Nerv. Sys.* 18:225-234, 1987.

Block, C.H., Barnes, K.L. and Ferarrio, C.M. The distribution of substance P in the canine dorsomedial medulla. *J. Cardiovasc. Pharmacol.* 10:S230-S234, 1987.

Bobillier, P., Seguin, S., Petitjean, F., Salvert, D., Touret, M. and Jouvet, M. The raphe nuclei of cat brainstem: a topographical atlas of their efferent projections as revealed by autoradiography. *Brain Res.* 113:449-486, 1976.

Boyd, N.D., Kage, R.K. and Leeman, S.E. Characterization of the NK-1 receptor using photoaffinity probes. In: *The Tachykinin Receptors*, S.H. Buck, Ed., Humana Press, Totowa, NJ, 1994, 219-236.

Boyer, P.A., Trembleau, A., Leviel, V. and Arluison, M. Effects of intranigral injections of colchicine on the expression of some neuropeptides in the rat forebrain: an immunohistochemical and in situ hybridization study. *Brain Research Bulletin.* 33:541-560, 1994.

Brain, S.D., Williams, T.J., Tippins, J.R., Morris, H.R. and MacIntyre, I. Calcitonin gene-related peptide is a potent vasodilator. *Nature.* 313:54-56, 1985.

Buchan, A.M.J., Kwok, Y.N. and Pederson, R.A. Anatomical relationship between neuropeptide-containing fibers and efferent vagal neurons projecting to the rat corpus. *Regul. Pept.* 34:1-12, 1991.

Buma, P. and Roubos, E.W. Ultrastructural demonstration of nonsynaptic release sites in the central nervous system of the snail Lymnaea stagnalis, the insect Periplaneta americana, and the rat. *Neuroscience.* 17:867-879, 1986.

Burcher, E., Mussap, C.J., Geraghty, D.P., McClure-Sharp, J.M. and Watkins, D.J. Concepts in characterization of tachykinin receptors. In: *Calcitonin Gene-Related Peptide: The First Decade of a Novel Pleiotropic Neuropeptide*, Y. Taché, P. Holzer and M.G. Rosenfeld, Eds., New York Academy of Sciences, New York, 1992, 123-136.

Burcher, E., Mussap, C.J., Geraghty, D.P., McClure-Sharp, J.M. and Watkins, D.J. Concepts in characterization of tachykinin receptors. In: *Substance P and Related Peptides: Cellular and Molecular Physiology*, S.E. Leeman, J.E. Krause and F. Lembeck, Eds., New York Academy of Sciences, New York, 1991, 123-136.

Bury, R. and Mashford, M. Biological activity of C-terminal partial sequences of substance P. *J. Med. Chem.* 19:854-856, 1976.

Carpentier, C. and Baude, A. Immunocytochemical localization of NK-3 receptors in the dorsal vagal complex of rat. *Brain Res.* 734:327-331, 1996.

Carrington, W.A., Lynch, R.M., Moore, E.D.W., Isenberg, G., Fogarty, K.E. and Fay, F.S. Superresolution three-dimensional images of fluorescence in cells with minimal light exposure. *Science.* 268:1483-1486, 1995.

Chan, J. Y., Tsou, M. Y., Len, W.B., Lee, T. Y., and Chan, S. H. Participation of noradrenergic neurotransmission in the enhancement of baroreceptor reflex response by substance P at the nucleus tractus solitarii of the rat: a reverse microdialysis study.. *J. Neurochem.* 64:2644-2652, 1995.

Chen, S., Aston-Jones, G. Evidence that cholera toxin B subunit (CTb) can be avidly taken up and transported by fibers of passage. *Brain Res.* 674:107-111, 1995.

Chiba, T. and Murata, Y. Substance P-like immunoreactive axon varicosities with synaptic junctions in the nucleus tractus soliarius of the rat. *Brain Res.* 251:160-163, 1982.

Christopoulos, G., Paxinos, G., Huang, X.F., Beaumont, K., Toga, A.W. and Sexton, P.M. Comparative distribution of receptors for amylin and the related peptides calcitonin gene related peptide and calcitonin in rat and monkey brain. *Can. J. Physiol. Pharmacol.* 73:1037-1041, 1995.

Cooper, J.R., Bloom, F.E. and Roth, R.H. In: *The Biochemical Basis of Neuropharmacology*, Oxford University Press, New York, 1986.

Craigmyle, M.B.L. The Vagus Nerve. In: *Mixed Cranial Nerves*, J. Wiley and Sons, Chichester, 1985, 74-84.

Cuello, A.C. and Kanazaw, I. The distribution of substance P immunoreactive fibres in the rat central nervous system. *J. Comp. Neurol.* 178:129-156, 1978.

Czyzyk-Krzeska, M.F., Bayliss, D.A., Seroogy, K.B. and Millhorn, D.E. Gene expression for peptides in neurons of the petrosal and nodose ganglia in rat. *Exp. Brain Res.* 83:411-418, 1991.

Dado, R.J., Burstein, R., Cliffer, K.D. and Giesler, G.J. Evidence that Fluoro-Gold can be transported avidly through fibers of passage. *Brain Res.* 533:329-333, 1990.

Dam, T.V., Escher, E. and Quirion, R. Evidence for the existence of three classes of neurokinin receptors in brain.. *Brain Res.* 453:372-376, 1988.

Dana, C., Vial, M., Leonard, K., Beauregard, A., Kitabgi, P., Vincent, J.P., Rostene, W. and Beaudet, A. Electron microscopic localization of neurotensin binding sites in the midbrain tegmentum of the rat. I. Ventral tegmental area and the interfasciular nucleus. *J. Neurosci.* 9:2247-2257, 1989.

Davenport, H.W. Reflex control of gastric secretion. In: *A History of Gastric Secretion and Digestion*, Oxford University Press, New York, 1992, 134-152.

Davison, J.S. and Grundy, D. Modulation of single vagal efferent fibre discharge by gastrointestinal afferents in the rat. *J. Physiol. (Lond.)* 284:6-82, 1978.

De Biasi, S. and Rustioni, A. Glutamate and substance P coexist in primary afferent terminals in the superficial laminae of spinal cord. *Proc. Natl. Acad. Sci. U.S.A.* 85:7820-7824, 1988.

Diamant, N.E., Hall, K.E., Mui, H. and El Sharkway, T.Y. Vagal control of feeding motor pattern in the lower esophageal sphincter, stomach and small intestine of dog. In: *Gastrointestinal Motility*, J. Chrstenson, Ed., Raven Press, New York, 1980, 365-390.

Diz, D.I., Barnes, K.L. and Ferrario, C.M. Functional characteristics of neuropeptides in the dorsal medulla oblongata and vagus nerve. *Federation Proc.* 46:30-35, 1987.

Donahue, P.E., Yoshida, J., Polley, E.H. and Nyhus, L.M. Preganglionic vagus nerve fibers also enter the greater curvature of the stomach in rats and ferrets. *Gastroenterology* 94:1292-1299, 1988.

Duggan, A.W., Hope, P.J., Jarrott, B., Schaible, H.G. andFleetwood-Walker, S.M. Release, spread and persistence of immunoreactive neurokinin A in the dorsal horn of the cat following noxious cutaneous stimulation. Studies with antibody microprobes. *Neuroscience.* 35:195-202, 1990.

Dumas, M., Schwab, M.E. and Thoenen, H. Retrograde axonal transport of specific macromolecules as a tool for characterizing nerve terminal membranes. *J. Neurobiol.* 10:179-197, 1979.

Edwardson, J.A. and McDermott, J.R. Metabolism of neuropeptides at brain and pituitary sites. *Biochem. Soc. Trans.* 13:50-53, 1985.

Elde, R., Schalling, M., Ceccatelli, S., Nakanishi, S. and Hökfelt, T. Localization of neuropeptide receptor mRNA in rat brain: initial observations using probes for neurotensin and substance P receptors. *Neurosci. Letts.* 120:134-138, 1990.

Endo, S., Yokosawa, H. and Ishii, S-.I. Purification and characterization of a substance P-degrading endopeptidase from rat brain. *J. Biochem.* 104:999-1006, 1988.

Ericson, H. and Blomqvist, A. Tracing of neuronal connections with cholera toxin subunit B: Light and electron microscopic immunohistochemistry using monoclonal antibodies. *J. Neurosci. Methods* 24:225-235, 1988.

Ericson, H., Westman, J. and Blomqvist, H. Labelling of neuronal connections with monoclonal antibodies against cholera toxin subunit B. *Neurosci. Lett. [Suppl.]* 22:204, 1985.

Finger, T.E. Comparative anatomy of medullary vagal nerve nuclei. In: *Neuroanatomy and Physiology of Abdominal Vagal Afferents*, S. Ritter, R.C. Ritter and C.D. Barnes, Eds., CRC Press, Boca Raton, 1992, 2-19.

Florey, E. Modulation of neuronal function: A not so new concept. *Behav. Brain Sci.* 2:424-425, 1979.

Fodor, M., Pammer, C., Gorcs, T. and Palkovits, M. Neuropeptides in the human dorsal vagal complex: an immunohistochemical study. *Chem. Neuroanat.* 3:141-157, 1994.

Fogel, R., Zhang, X. and Renehan, W.E. Relationships between the morphology and function of gastric and intestinal distention-sensitive neurons in the dorsal motor nucleus of the vagus. *J. Comp. Neurol.* 364:78-91, 1996.

Fox, E.A. and Powley, T.L. False-positive artifacts of tracer strategies distort autonomic connectivity maps. *Brain Res. Rev.* 14:53-77, 1989.

Fox, E.A. and Powley, T.L. Longitudinal columnar organization within the dorsal motor nucleus represents separate branches of the abdominal vagus. *Brain Res.* 341:269-282, 1985.

Fox, E.A. and Powley, T.L. Morphology of identified preganglionic neurons in the dorsal motor nucleus of the vagus. *J. Comp. Neurol.* 322:79-98, 1992.

Fox, E.A. and Powley, T.L. Tracer diffusion has exaggerated CNS maps of direct preganglionic innervation of pancreas. *J. Autonom. Nerv. Sys.* 15:55-69, 1986.

Fraser, K.A. and Davison, J.S. Gastric distention induces c-fos immunoreactivity in the rat brain. *Ann. New York Acad. Sci.* 713:164-166, 1994.

Fraser, K.A., Raizada, E. and Davison J.S. Oral-pharyngeal-esophageal and gastric cues contribute to meal-induced c-fos expression. *American Journal of Physiology.* 268:R223-230, 1995.

Freedman, L.J. and Yi, H. Confocal imaging of the retrograde tracer Fluoro-Gold using a non-ultraviolet laser. *Brain Res. Bull.* 31:749-751, 1993.

Furness, J.B. and Costa, M. The Enteric Nervous System. Churchill Livingstone, Edinburgh, 1987.

Fuxe, K. and Agnati, L.F. Two principal modes of electrochemical communication in the brain: volume versus wiring transmission. In: *Volume Transmission in the Brain: Novel Mechanisms for Neural Transmission*, K. Fuxe and L.F. Agnati, Eds., Raven Press, New York, 1991, 1-9.

Ganong, W.F. In: *Review of Medical Physiology*, Appleton and Lange, Norwalk, 1989.

Gervautz, M. and Purgathofer, W. A simple method for color quantization: Octree Quantization. In: *New Trends in Computer Graphics.*, N. Magnenat-Thalmann and D. Thalmann, Eds., Springer-Verlag, New York, NY, 1988, 219-231.

Gibson, A.E., Noel, R.J., Herlihy, J.T. and Ward, W.F. Phenylarsine oxide inhibition of endocytosis: effects on asialofetuin internalization. *Am. J. Physiol.* 257:C182-C184, 1989.

Gilbert, R.F.T., Emson, P.C., Fahrenkrug, J., Lee, C.M., Penman, A. and Wass, J. Axonal transport of neuropeptides in the cervical vagus nerve of the rat. *J. Neurochem.* 34:105-113, 1980.

Gillis, R.A., Quest, J.A., Pagani, F.D. and Norman, W.P. Control centers in the central nervous system for regulating gastrointestinal motility. In: *Handbook of Physiology*, J.D. Wood, Ed., American Physiological Society, Bethesda, MD, 1988.

Golding, D.W. A pattern confirmed and refined. Synaptic, nonsynaptic and parasynaptic exocytosis. *Bioessays.* 16:503-508, 1994.

Gonatas, N.K., Stieber, A., Gonatas, J., Mommoi, T., Fishman, P.H. Endocytosis of exogenous GM1 ganglioside and cholera toxin by neuroblastoma cells. *Mol. Cell Biol.* 3:91-101, 1983.

Goodman, E.C. and Iversen, L.L. Calcitonin gene-related peptide: Novel neuropeptide. *Life Sci.* 38:2169-2178, 1986.

Goto, Y., Taché, Y., Debas, H. and Novin, D. Gastric acid and vagus nerve response to GABA agonist baclofen. *Life Sci.* 36:2471-2475, 1985.

Grady, E.F., Garland, A.M., Gamp, P.D., Lovett, M., Payan, D.G. and Bunnett N.W. Delineation of the endocytic pathway of substance P and its seven-transmembrane domain NK1 receptor. *Mol. Biol. Cell.* 6:509-524, 1995.

Green, T. and Dockray, G.J. Calcitonin gene-related peptide and substance P in afferents to the upper gastrointestinal tract in the rat. *Neurosci. Lett.* 76:151-156, 1987.

Gulbenkian, S., Merighi, A., Wharton, J., Varndell, I.M. and Polak JM Ultrastructural evidence for the coexistence of calcitonin gene-related peptide and substance P in secretory vesicles of peripheral nerves in the guinea pig. *J. Neurocytol.* 15:535-542, 1986.

Hall, M.E., Miley, F. and Stewart, J.M. The role of enzymatic processing in the biological actions of substance P. *Peptides.* 10:895-901, 1989.

Hanley, M. and Iversen, L. Substance P receptors. In: *Neurotransmitter Receptors*, S.J. Enna and H.I. Yamamura, Eds., Chapman and Hall, London, 1980, 72-103.

Hartig, W., Bruckner, G., Brauer, K., Seeger, G. and Bigl, V. Triple immunofluorescence labelling of parvalbumin, calbindin-D28k and calretinin in rat and monkey brain.. *J. Neurosci. Meth.* 67:89-95, 1996.

Helke, C.J. and Hill, K.M. Immunohistochemical study of neuropeptides in vagal and glossopharyngeal neurons in the rat. *Neuroscience* 26:539-551, 1988.

Helke, C.J., Charlton, C.G. and Wiley, R.G. Suicide transport of ricin demonstrates the presence of substance P receptors on medullary somatic and autonomic motor neurons. *Brain Res.* 328:190-195, 1985.

Helke, C.J., Shults, C.W., Chase, T.N. and O'Donohue, T.L. Autoradiographic localization of substance P receptors in rat medulla: effect of vagotomy and nodose ganglionectomy. *Neuroscience.* 12:215-223, 1984.

Helton, W.S., Mulholland, M.M., Bunnett, N.W. and Debas, H.T. Inhibition of gastric and pancreatic secretion in dogs by CGRP: role of somatostatin. *Am. J. Physiol.* 256:G145-G149, 1989.

Herkenham, M. and McLean, S. Mismatches between receptor and transmitter localizations in the brain. In: *Quantitative Receptor Autoradiography*, C.A. Boast and E.W. Snowhill, Eds., Liss, New York, 1986, 137-171.

Hersh, L.B., Smith, T.E. and McKelvy, J.F. Cleavage of endorphins to des-tyr endorphins by homogenous bovine brain aminopeptidase. *Nature* 286:160-162, 1980.

Hershey, A.D. and Krause, J.E. Molecular characterization of a functional cDNA encoding the rat substance P receptor. *Science.* 247:958-962, 1990.

Hershey, A.D., Polenzani, L., Woodward, R.M., Miledi, R. and Krause, J.E. Molecular and genetic characterization, functional expression, and mRNA expression patterns of a rat substance P receptor. In: *Substance P and Related Peptides: Cellular and Molecular Physiology*, S.E. Leeman, J.E. Krause and F. Lembeck, Eds. New York Academy of Sciences, New York, 1991, 63-78.

Hökfelt, T., Arvidsson, U., Ceccatelli, S., Cortes, R. and Cullheim, S. Calcitonin gene-related peptide in the brain, spinal cord and some peripheral systems. In: *Calcitonin Gene-Related Peptide: The First Decade of a Novel Pleiotropic Neuropeptide*, Y. Taché, P. Holzer and M.G. Rosenfeld, Eds., New York Academy of Sciences, New York, 1992, 119-134.

Hopkins, D.A., Bieger, D., de Vente, J. and Steinbusch, W.M. Vagal efferent projections: viscerotopy, neurochemistry and effects of vagotomy. *Prog. Brain Res.* 107:79-96, 1996.

Hrapchak, R.J. Immunohistochemistry. In: *Theory and practice of histotechnology, 2nd Edition*, D.C. Sheehan and B.B. Hrapchak, Eds., The C.V. Mosby Company, St. Louis, 1980, 310-327.

Huang, F.L., Zhuo, H., Sinclair, C., Goldstein, M.E., McCabe, J.T., Helke, C.J. Peripheral deafferentation alters calcitonin gene-related peptide mRNA expression in visceral sensory neurons of the nodose and petrosal ganglia. *Brain Res. Mol. Brain Res.* 22:290-298, 1994.

Huang, X-.F., Paxinos, G., Halasz, P., McRitchie, D. and Tork, I. Substance P- and tyrosine hydroxylase-containing neurons in the human dorsal motor nucleus of the vagus nerve. *J. Compar. Neurol.* 335:109-122, 1993.

Hui, K.S., Wang, Y.J. and Lajtha, A. Purification and characterization of an enkephalin aminopeptidase from rat brain membranes. *Biochemisrty.* 22:1062-1067, 1983.

Inagaki, S., Kito, S., Kubota, Y., Girgis, S., Hillyard, C.J. and MacIntyre, I. Autoradiographic localization of calcitonin gene-related peptide binding sites in human and rat brains. *Brain Res.* 374:287-298, 1986.

Ingi, T., Kitajima, Y., Minamitake, Y. and Nakanishi, S. Characterization of ligand-binding properties and selectivities of three rat tachykinin receptors by transfection and functional expression of their cloned cDNAs in mammalian cells.. *J. Pharm. Exper. Ther.* 259:969-975, 1991.

Inoué, S. Foundations of confocal scanned imaging in light microscopy. In: *Handbook of Biological Confocal Microscopy, 2nd Edition*, J.B. Pawley, Ed., Plenum Press, New York, 1995, 1-17.

Ishikawa, T. and Taché, Y. *Dig. Dis. Sci.* 34:979, 1989.

Ito, S. Functional gastric morphology. In: *Physiology of the Gastrointestinal Tract*, L.R. Johnson, Ed., Raven Press, New York, 1981, 517-550.

Jass, J.R. Anatomy of the gastrointestinal tract in relation to motiltiy and secretion. In: *Mechanisms of Gastrointesinal Motility and Secretion*, A. Bennett and G. Velo, Eds., Plenum Press, New York, 1983, 1-11.

Johnson, G.D., Davidson, R.S., McNamee, K.C., Russell, G., Goodwin, D. and Holborow, E.J. Fading of immunofluorescence during microscopy: a study of the phenomenon and its remedy. *J. Immunol. Meth.* 55:231-242, 1982.

Kage, R., McGregor, G.P., Thim, L. and Conlon, J.L. Neuropeptide gamma: a peptide isolated from rabbit intestine that is derived from gamma-preprotachykinin. *J. Neurochem.* 50:1412-1417, 1988.

Kalia, M. and Mesulam, M.-M. Brainstem projections of sensory and motor complex in the cat. II. Laryngeal, tracheobronchial, pulmonary, cardiac and gastrointestinal branches. *J. Comp. Neurol.* 193:467-508, 1980.

Kalia, M., Fuxe, K., Hökfelt, T., Johansson, O., Lang, R., Ganten, D., Cuello, C. and Terenius, L. Distribution of neuropeptide immunoreactive nerve terminals within the subnuclei of the nucleus of the tractus solitarius of the rat. *J. Comp. Neurol.* 222:409-444, 1984.

Karlsson, K., Eriksson, U., Andren, P. and Nyberg, F. Recovery and characterization of substance P endopeptidase activity in the rat spinal cord. *Reg. Peptides.* 64:86, 1996.

Katayama, M., Nadel, J.A., Bunnett, N.W., Di Maria, G.U., Haxhiu, M. and Borson, D.B. Catabolism of calcitonin gene-related peptide and substance P by neutral endopeptidase. *Peptides.* 12:563-567, 1991.

Katz, D.M. and Karten, H.J. Substance P in the vagal sensory ganglia: localization in cell bodies and pericellular arborizations. *J. Comp. Neurol.* 193:549-564, 1980.

Kaufman, A. Introduction to volume visualization. In: *Volume Visualization*, A. Kaufman, Ed., IEEE Computer Society Press, Los Alamitos, 1990, 1-22.

Kawai, Y., Takami, K., Shiosaka, P., Emson, C.P. Hillyard, C.J., Girgis, S., MacIntyre, I. and Tohyama, M., Topographic localization of calcitonin gene-related peptide in the rat brain: An immunohistochemical analysis. *Neuroscience* 15:747-763, 1985.

Kawano, H. and Chiba, T. Distribution of substance P immunoreactive nerve terminals within the nucleus tractus solitarius of the rat. *Neurosci. Letts.* 45:175-179, 1984.

Kenny, A.J., Fulcher, I.S. Microvillar endopeptidase, an enzyme with special topological features and a wide distribution. *Ciba Found. Symp.* 95:12-33, 1983.

Kirchgessner, A.L. and Gershon, M.D. Identification of vagal efferent fibres and putative target neurons in the enteric nervous system of the rat. *J. Comp. Neurol.* 285:38-53, 1989.

Kiyama, H., Maeno, H. and Tohyama, M. Substance P receptor (NK-1) in the central nervous system: possible functions from a morphological aspect. *Regul. Pept.* 46:114-123, 1993.

Koizumi, K. and Brooks, C.M. The autonomic nervous system and its role in controlling body functions. In: *Medical Physiology*, V.B. Mountcastle, Ed., C.V. Mosby Company, St. Louis, 1980, 893-922.

Konishi, S., Okamoto, T. and Otsuka, M. Substance P as a neurotransmitter released from peripheral branches of primary afferent neurones producing slow synaptic excitation in autonomic ganglion cells. In: *Substance P: Metabolism and Biological Actions*, C.C. Jordan and P. Oehme, Eds., Taylor and Francis, London, 1985, 121-136.

Kotani, H., Hoshimaru, M., Nawa, H. and Nakanishi, S. Structure and gene organization of bovine neuromedin K precursor. *Proc. Natl. Acad. Sci. U.S.A.* 83:7074-7078, 1986.

Krause, J.E. On the physiological metabolism of substance P. In: *Substance P: Metabolism and Biological Actions*, C.C. Jordan and P. Oehme, Eds., Taylor and Francis, London, 1985, 13-31.

Krause, J.E., Chirgwin, J.M., Carter, M.S., Xu, Z.S. and Hershey, A.D. Three rat preprotachykinin mRNAs encode the neuropeptides substance P and neurokinin A. *Proc. Natl. Acad. Sci. U.S.A.* 84:881-885, 1987.

Krenik, K.D., Kephart, G.M., Offord, K.P., Dunnette, S.L. and Gleich. G.J. Comparison of antifading agents used in immunofluorescence. *J. Immunol. Meth.* 117:91-97, 1989.

Ladic, L.A. The use of Internet graphics software for the processing and display of digital microscopy data. *Cell Biology: A Laboratory Handbook, 2nd Edition*, J. Celis, Ed., Academic Press, San Diego, 1997 (in press).

Lasher, R.S., Lutz, E.M., Mulholland, F., Sanderson, R., Stewart, J.M. and Bublitz, C. Immunocytochemical localization of endopeptidase-24.11 in the nucleus tractus solitarius of the rat brain. *Neurosci. Letts.* 117:43-49, 1990.

Laughton, W.B. and Powley, T.L. Localization of efferent function in the dorsal motor nucleus of the vagus. *Am. J. Physiol.* 252:R13-R25, 1987.

Le Greves, P., Nyberg, F., Terenius, L. and Hökfelt, T. Calcitonin gene-related peptide is a potent inhibitor of substance P degradation. *Euro. J. Pharmacol.* 115:309-311, 1985.

Leeman, S.E. In: *Substance P and Related Peptides: Cellular and Molecular Physiology*, S.E. Leeman, J.E. Krause and F. Lembeck, Eds., New York Academy of Sciences, New York, 1991.

Lenz, H.J., Mortrud, M.T., Rivier, J.E. and Brown, M.R. Central nervous system actions of calcitonin gene-related peptide on gasrtic acid secretion in the rat. *Gastroenterology.* 88:539-544, 1985.

Lenz, H.J., Mortrud, M.T., Vale, W.W., Rivier, J.E. and Brown, M.R. Calcitonin gene-related peptide acts within the central nervous system to inhibit gastric acid secretion. *Reg. Peptides.* 9:271-277, 1984.

Leslie, R.A Neuroactive substances in the dorsal vagal complex of the medulla oblongata: nucleus of the tractus solitarius, area postrema and dorsal motor nucleus of the vagus. *Neurochem. Int.* 7:191-211, 1985.

Leslie, R.A., Reynolds, D.J.M. and Lawes, I.N.C. Central connections of the nuclei of the vagus nerve. In: *Neuroanatomy and Physiology of Abdominal Vagal Afferents*, S. Ritter, R.C. Ritter and C.D. Barnes, Eds., CRC Press, Boca Raton, 1992, 82-98.

Lewis, P.R., Scott, J.A. and Navaratnam, V. Localization in the dorsal motor nucleus of the vagus in the rat. *J. Anat.* 107:197-208, 1970.

Lindefors, N., Brodin, E. and Ungerstedt, U. Microdialysis combined with a sensitive radioimmunoassay: A technique for studying in vivo release of neuropeptides. *J. Pharmacol. Meth.* 17:305-312, 1987.

Lindek, S., Stelzer, E.H.K. and Hell, S.W. Two new high-resolution confocal fluorescence microscopies (4Pi, Theta) with one- and two- photon excitation. In: *Handbook of Biological Confocal Microscopy, 2nd Edition*, J.B. Pawley, Ed., Plenum Press, New York, 1995, 417-430.

Liu, H., Brown, J.L., Jasmin, L., Maggio, J.E., Vigna, S.R., Mantyh, P.W. and Bausbaum, A.I. Synaptic relationship between substance P and the substance P receptor: light and electron microscopic characterization of the mismatch between neuropeptides and their receptors. *Proc. Natl. Acad. Sci. USA.* 91:1009-1013, 1994.

Ljungdahl, A., Hokfelt, T. and Nilsson, G. Distribution of substance P-like immunoreactivity in the central nervous system of the rat. I. Cell bodies and nerve terminals. *Neuroscience* 3:861-943, 1978.

Llewellyn-Smith, I.J., Minson, J.B., Wright, A.P. and Hodgson, A.J. Cholera toxin B-gold, a retrograde tracer that can be used in light and electron microscopic immunocytochemical studies. *J. Compar. Neurol.* 294:179-191, 1990.

Loh, Y.P., Brownstein, M.J. and Gainer, H. Proteolysis in neuropeptide processing and other neural functions. *Ann. Rev. Neurosci.* 7:189-222, 1984.

Lundberg, J.M. Volume transmission by coreleased peptides in the autonomic nervous system. In: *Volume Transmission in the Brain: Novel Mechanisms for Neural Transmission*, K. Fuxe and L.F. Agnati, Eds., Raven Press, New York, 1991, 425-432.

Lundberg, J.M., Hökfelt, T., Nilsson, G., Terenius, L., Rehfeld, J., Elde, R. and Said, S. Peptide neurons in the vagus, splanchnic and sciatic nerves. *Acta Physiol. Scand.* 104:499-501, 1978.

Luppi, P-.H., Fort, P. and Jouvet, M. Iontophoretic application of unconjugated cholera toxin B subunit (CTb) combined with immunohistochemistry of neurochemical substances: a method for transmitter identification of retrogradely labeled neurons. *Brain Res.* 534:209-224, 1990.

MacDonald, S.G., Dumas, J.J. and Boyd, N.D. Chemical cross-linking of the substance P (NK-1) receptor to the alpha subunits of the G proteins Gq and G11. *Biochemistry.* 35:2909-2916, 1996.

Maeno, H., Kiyama, H. and Tohyama, M. Distribution of the substance P receptor (NK-1 receptor) in the central nervous system. *Molec. Brain Res.* 18:43-58, 1993.

Maggi, C.A., Giuliani, S., Santicioli, P., Regoli, D. and Meli, A. Peripheral effects of neurokinins: functional evidence for the existence of multiple receptors. *J. Autonom. Pharmacol.* 7:11-32, 1987.

Maggio, J.E. and Hunter, J.C. Regional distribution of kassinin-like immunoreactivity in rat central and peripheral tissues and the effect of capsaicin. *Brain Res.* 307:370-373, 1984.

Maggio, J.E. Tachykinins. *Ann. Rev. Neurosci.* 11:13-28, 1988.

Manaker, S. and Rizio, G. Autoradiographic localization of thyrotropin-releasing hormone and substance P receptors in the rat dorsal vagal complex. *J. Comp. Neurol.* 290:526-526, 1989.

Manaker, S. and Zucchi, P.C. Effects of vagotomy on neurotransmitter receptors in the rat dorsal vagal complex. *Neuroscience.* 52:427-441, 1993.

Mantyh, P.W., Allen, C.J., Ghilardi, J.R., Rogers, S.D., Mantyh, C.R., Liu, H., Basbaum, A.I., Vigna, S.R. and Maggio, J.E. Rapid endocytosis of a G protein-coupled receptor: substance P evoked internalization of its receptor in the rat striatum in vivo. *Proc. Natl. Acad. Sci. USA.* 92:2622-2626, 1995.

Mantyh, P.W., Hunt, S.P. and Maggio, J.E. Substance P receptors: Localization by light microscopic autoradiography using 3H-SP as the radioligand. *Brain Res.* 307:147-166, 1984.

Martini-Luccarini, F., Reynaud, J-.C. and Puizillout, J-.J. Effects of tachykinins on identified dorsal vagal neurons: and electrophysiological study in vitro. *Neuroscience.* 71:119-131, 1996.

Matsus, R., Fulcher, I.S., Kenny, A.J. and Turner, A.J. Substance P and [Leu]enkephalin are hydrolyzed by an enzyme in pig caudate synaptic membranes that is identical with the endopeptidase of kidney microvilli. *Proc. Natl. Acad. Sci. USA.* 80:3111-3115, 1983.

Matsus, R., Kenny, A.J. and Turner, A.J. The metabolism of neuropeptides: The hydrolysis of peptides, including enkephalins, tachykinins and their analogues, by endopeptidase-24.11. *Biochem. J.* 223:433-440, 1984.

Matteoli, M., Reetz, A.T. and De Camilli, P. Small synaptic vesicles and large dense-core vesicles: secretory organelles involved in two modes of neuronal signalling. In: *Volume Transmission in the Brain: Novel Mechanisms for Neural Transmission*, K. Fuxe and L.F. Agnati, Eds., Raven Press, New York, 1991.

McCann, M., Hermann, G.E. and Rogers, R.C Nucleus raphe obscurus (nRO) influences vagal control of gastric motility in rats. *Brain Res.* 486:181-184, 1989.

McCann, M.J., Hermann, G.E. and Rogers, R.C. Thyrotropin-releasing hormone (TRH) potentiates the gastric responses evoked by drosal medullary serotinin (5HT). *J. Autonom. Nerv. Sys.* 25:35-40, 1988.

McKelvy, J.F. and Blumberg, S. Inactivation and metabolism of peptides. *Ann. Rev. Neurosci.* 9:415-434, 1986.

Merighi, A., Polak, J.M., Gibson, S.J., Gulbenkian, S., Valentino, K.L. and Peirone, S.M. Ultrastructural studies on calcitonin gene-related peptide-, tachykinins- and somatostatin-immunoreactive neurones in rat dorsal root ganglia: evidence for the colocalization of different peptides in single secretory granules. *Cell Tiss. Res.* 254:101-109, 1988.

Merighi, A., Polak, J.M., Theodosis, D.T. Ultrastructural visualization of glutamate and aspartate immunoreactivities in the rat dorsal horn, with special reference to the co-localization of glutamate, substance P and calcitonin-gene related peptide. *Neuroscience.* 40:67-80, 1991.

Mesulam, M-.M. and Brushart, T.M. Transganglionic and anterograde transport of horseradish peroxidase across dorsal root ganglia: A tetramethylbenzidine method for tracing central sensory connections of muscles and peripheral nerves. *Neuroscience.* 4:1107-1117, 1979.

Mesulam, M-.M. Principles of horseradish peroxidase neurohistochemistry and their applications for tracing neural pathways: Axonal transport, enzyme histochemistry and light microscopic analysis. In: *Tracing Neural Connections with Horseradish Peroxidase*, M-.M. Mesulam, Ed., John Wiley, New York, NY, 1982, 1-151.

Minamino, N., Masuda, H., Kanagawa, K. and Matsuo, H. Neuromedin L: a novel mammalian tachykinin identified in porcine spinal cord. *Neuropeptides.* 4:157-166, 1984.

Mitchell, G.A.G. and Warwick, R. The dorsal vagal nucleus. *Acta. Anat.* 25:371-395, 1955.

Mussap, C.J., Geraghty, D.P. and Burcher, E. Tachykinin recpetors: a radioligand binding perspective. *J. Neurochem.* 60:1987-2009, 1993.

Nawa, H., Doteuchi, M., Igano, K., Inouye, K and Nakanishi, S. Substance K: A novel mammalian tachykinin that differs from substance P in its pharmacological profile. *Life Sci.* 34:1153-1160, 1984.

Neuhuber, W.L. and Sandoz, P.A. Vagal primary afferent terminals in the dorsal motor nucleus of the rat: Are they making monosynaptic contacts on preganglionic efferent neurons?. *Neurosci. Letts.* 69:126-130, 1986.

Nicholl, R.A. Neurotransmitter regulated ion channels. *Science.* 241:545-555, 1988.

Norgren, R. and Smith, G.P. Central distribution of subdiaphragmatic vagal branches in the rat. *J. Comp. Neurol.* 273:207-223, 1988.

Oblin, A., Danse, M.J. and Zivkovic, B. Metalloendopeptidase (EC 3.4.24.11) but not angiotensin converting enzyme is involved in the inactivation of substance P by synaptic membranes of the rat substantia nigra. *Life Sci.* 44:1467-1474, 1989.

Ohkubo, H. and Nakanashi, S. Molecular characterization of the three tachykinin receptors. In: *Substance P and Related Peptides: Cellular and Molecular Physiology*, S.E. Leeman, J.E. Krause and F. Lembeck, Eds. New York Academy of Sciences, New York, 1991, 53-62.

Okamoto, A., Lovett, M., Payan, D.G. and Bunnett, N.W. Interactions between neutral endopeptidase (EC 3.4.24.11) and the substance P (NK1) receptor expressed in mammalian cells. *Biochem. J.* 299:683-693, 1994.

Okumura, T. and Namiki, M. Vagal motor neurons innervating the stomach are site-specifically organized in the dorsal motor nucleus of the vagus nerve in rats. *J. Autonom. Nerv. Sys.* 29:157-162, 1990.

Otsuka, M. and Yoshioka, K. Neurotransmitter functions of mammalian tachykinins. *Physiol. Rev.* 73:229-309, 1993.

Palkovits, M., Kiss, J.Z., Beinfield, M.C. and Williams, T.H. Cholecystokinin in the nucleus of the solitary tract of the rat: evidence for its vagal origin. *Brain Res.* 252:386-390, 1982.

Paxinos, G. and Watson, G. In: *The rat brain in stereotaxic coordinates, 2nd Ed.*, Academic Press, Sydney, 1986.

Pernow, B. Substance P. [Review]. *Pharmacol. Rev.* 35:85-141, 1983.

Plata-Salaman, C.R., Fukuda, A., Minami, T. and Oomura, Y. Substance P effects on the dorsal motor nucleus of the vagus. *Brain Res. Bull.* 23:149-153, 1989.

Powley, T.L., Fox, E.A., Baronowsky, E., Keller, D.L. and Berthoud, H.-R. Longitudinal column of gastric branch neurons in the dorsal motor nucleus of the vagus is composed of subcolumns corresponding to distal divisions of gastric branch. *Soc. Neurosci. Abstr.* 13:386, 1987.

Powley, T.L., Berthoud, H.-R., Fox, E.A. and Laughton, W. The dorsal vagal complex forms a sensory-motor lattice: the circuitry of gastrointestinal reflexes. In: *Neuroanatomy and Physiology of Abdominal Vagal Afferents*, S. Ritter, R.C. Ritter and C.D. Barnes, Eds., CRC Press, Boca Raton, 1992, 57-79.

Powley, T.L., Holst, M-.C., Boyd, D.B. and Kelly, J.B. Three-dimensional reconstructions of autonomic projections to the gastrointestinal tract. *Microsc. Res. Tech.* 29:297-309, 1994.

Prechtl, J.C. and Powley, T.L. The fiber composition of the abdominal vagus of the rat. *Anat. Embryol. (Berl).* 181:101-115, 1990.

Price, J.L. Integrated systems of the CNS: I, hypothalamus, hippocampus, amygdala and retina. In: *Handbook of Chemical Neuroanatomy*, J.L. Price, Ed., Elsevier Scientific, Amsterdam, 1987, 1-79.

Quirion, R., Van Rossum, D., Dumont, Y., St-Pierre, S. and Fournier, A. Characterization of CGRP1 and CGRP2 receptor subtypes. In: *Calcitonin Gene-Related Peptide: The First Decade of a Novel Pleiotropic Neuropeptide*, Y. Taché, P. Holzer and M.G. Rosenfeld, Eds., New York Academy of Sciences, New York, 1992, 88-105.

Raybould, H.E. Vagal afferent innervation and the regulation of gastric motor function. In: *Neuroanatomy and Physiology of Abdominal Vagal Afferents*, S. Ritter, R.C. Ritter and C.D. Barnes, Eds., CRC Press, Boca Raton, 1992, 192-219.

Regoli, D., Drapeau, G., Dion, S. and D'Orleans-Juste, P. Pharmacological receptors for substance P and neurokinins. *Life Sci.* 40:109-117, 1987.

Ren, J. Young, R.L., Lassiter, D.C., Rings, M.C., Harty, R.F. Calcitonin gene-related peptide: mechanisms of modulation of antral endocrine cells and cholinergic neurons. *Am. J. Physiol.* 262:G732-G739, 1992.

Rethelyi, M., Mohapatra, N.K., Metz, C.B., Petrusz, P. and Lund, P.K. Colchicine enhances mRNAs encoding the precursor of calcitonin gene-related peptide in brainstem motoneurons. *Neuroscience.* 42:531-539, 1991.

Rikard-Bell, G.C., Tork, I., Sullivan, C. and Scheibner, T. Distribution of substance P-like immnoreactive fibres and terminals in the medulla oblongata of the human infant. *Neuroscience.* 34:133-148, 1990.

Rinaman, L., Card, J.P., Schwaber, J.S. and Miselis, R.R. Ultrastructural demonstration of a gastric monosynaptic vagal circuit in the nucleus of the solitary tract in rat. *J. Neurosci.* 9:1985-1996, 1989.

Robert, A. Proposed terminology for the anatomy of the rat stomach. *Gastroenterology.* 60:344-345, 1971.

Robertson, B. and Grant, G. Immunocytochemical evidence for the localisation of GM1 ganglioside in carbonic anhydrase-containing and RT-97-immunoreactive rat primary sensory neurons . *J. Neurocytol.* 18:77-86, 1989.

Rogers, R.C, McTigue, D.M. and Hermann, G.E. Vagal control of digestion: modulation by central neural and peripheral endocrine factors. *Neurosci. Biobehav. Rev.* 20:57-66, 1996.

Rogers, R.C. and Hermann, G.E. Central regulation of brainstem gastric vago-vagal control circuits. In: *Neuroanatomy and Physiology of Abdominal Vagal Afferents*, S. Ritter, R.C. Ritter and C.D. Barnes, Eds., CRC Press, Boca Raton, 1992, 99-134.

Rogers, R.C., McCann, M.J. and Hermann, G.E. TRH effects on physiologically-identified neurons in the dorsal vagal complex: In vivo and in vitro studies. *Neurosci. Abs.* 14:538, 1988.

Rosenfeld, M.G., Emeson, R.B., Yeakley, J.M., Merillat, N., Hedjran, F., Lenz, J. and Delsert, C. In: *Calcitonin Gene-Related Peptide: The First Decade of a Novel Pleiotropic Neuropeptide*, Y. Taché, P. Holzer and M.G. Rosenfeld, Eds., New York Academy of Sciences, New York, 1992, 1-17.

Rosenfeld, M.G., Mermod, J.-J., Amara, S.G., Swanson, L.W., Sawchenko, P.E., Rivier, J., Vale, W.W., Evans, R.M. Production of a novel neuropeptide encoded by the calcitonin gene via tissue-specific RNA processing. *Nature.* 304:129-135, 1983.

Sagar, S.M., Sharp, F.R. and Curran, T. Expression of c-fos protein in brain: metabolic mapping at the cellular level. *Science.* 240:1328-1331, 1988.

Sakurada, T., Greves, P., Stewart, J. and Terenius, L. Measurement of substance P metabolites in rat CNS. *J. Neurochem.* 44:718-722, 1985.

Sawchenko, P.E. and Gerfen, C.R. Plant lectins and bacterial toxins as tools for tracing neuronal connections. *Trends Neurosci.* 8:378-384, 1985.

Sawchenko, P.E. Central connections of the sensory and motor nuclei of the vagus nerve. *J. Autonom. Nerv. Syst.* 9:13-26, 1983.

Schmued, L.C. and Fallon, J.H. Fluoro-Gold: a new fluorescent retrograde axonal tracer with numerous unique properties. *Brain Research* 377:147-154, 1986.

Schults, C.W., Quirion, R., Chronwall, B., Chase, T.N. and O'Donohue, T.L. A comparison of the anatomical distribution of substance P and substance P receptors in the rat central nervous system. *Peptides.* 5:1097-1128, 1984.

Schwartz, J.-C., Bouthenet, M.-L., Giros, B., Gors, C., Llorens-Cortes, C. and Pollard, H. Neuropeptidases and neuropeptide inactivation in the brain. In: *Volume Transmission in the Brain: Novel Mechanisms for Neural Transmission*, K. Fuxe and L.F. Agnati, Eds., Raven Press, New York, 1991, 381-394.

Sexton, P.M., McKenzie, J.S., Mason, R.T., Moseley, J.M., Martin, T.J. and Mendelsohn, F.A. Localization of binding sites for calcitonin gene-related peptide in rat brain by in vitro autoradiography. *Neuroscience.* 19:1235-1245, 1986.

Shapiro, R.E. and Miselis, R.R. The central neural connections of the area postrema of the rat. *J. Comp. Neurol.* 234:344-364, 1985.

Shaw, P.J. Comparison of wide-field/deconvolution and confocal microscopy for 3D imaging. In: *Handbook of Biological Confocal Microscopy, 2nd Edition*, J.B. Pawley, Eds., Plenum Press, New York, 1995, 373-387.

Shaw, P.J. Deconvolution in 3-D optical microscopy. *Histochem. J.* 26:687-694, 1994.

Shigemoto, R., Nakaya, Y., Nomura, S., Ogawa-Meguro, R., Ohishi, H., Kaneko, T., Nakanishi, S. and Mizuno, N. Immunohistochemical localization of rat substance P receptor in the striatum. *Neurosci. Lett.* 153:157-160, 1993.

Skirboll, L.R., Thor, K., Helke, C., Hökfelt, T., Robertson, B. and Long, R. Use of retrograde fluorescent tracers in combination with immunohistochemical methods. In: *Neuroanatomical Tract-tracing Methods 2.*, Heimer, L. and Zaborszky, L., Eds., Plenum Press, New York, 1989, 5-16.

Skofitsch, G. and Jacobowitz, D.M. Calcitonin gene-related peptide: Detailed immunohistochemical distribution in the central nervous system. *Peptides.* 6:721-745, 1985.

Skofitsch, G. and Jacobowitz, D.M. Quantitative distribution of calcitonin gene-related peptide in the rat central nervous system. *Peptides* 6:1069-1073, 1985b.

Spencer, S.E. and Talman, W.T. Central modulation of gastric pressure by substance P: a comparison with glutamate and acetylcholine. *Brain Res.* 385:371-374, 1986.

Sternini, C. Vagal afferent innervation of the enteric nervous system. In: *Neuroanatomy and Physiology of Abdominal Vagal Afferents*, S. Ritter, R.C. Ritter and C.D. Barnes, Eds., CRC Press, Boca Raton, 1992, 135-156.

Sugitani, A., Yoshida, J., Nyhus, L.M. and Donahue, P.E. Viscerotopic representation of preganglionic efferent vagus nerve in the brainstem of the rat: A Fluoro-Gold study. *J. Autonom. Nerv. Sys.* 34:211-220, 1991.

Sugiya, H., Obie, J.F. and Putney, J.W. Jr. Two modes of regulation of the phospholipase C-linked substance-P receptor in rat parotid acinar cells. *Biochemi. J.* 253:459-466, 1994.

Sykes, R.M., Spyer, K.M. and Izzo, P.N. Central distribution of substance P, calcitonin gene-related peptide and 5-hydroxytryptamine in vagal sensory afferents in the rat dorsal medulla. *Neuroscience.* 59:195-210, 1994.

Taché, Y. Central nervous system regulation of gastric acid secretion. In: *Physiology of the Gastrointestinal Tract*, L.R. Johnson, Ed., Raven Press, New York, NY, 1987, 911-930.

Taché, Y. Inhibition of gastric acid secretion and ulcers by calcitonin gene-related peptide. In: *Calcitonin Gene-Related Peptide: The First Decade of a Novel Pleiotropic Neuropeptide*, Y. Taché, P. Holzer and M.G. Rosenfeld, Eds., New York Academy of Sciences, New York, 1992, 240-247.

Taché, Y., Garrick, T. and Raybould, H. Central nervous system action of peptides to influence gastrointestinal motor function. *Gastroenterol.* 98:517-528, 1990.

Taché, Y., Gunion, M., Lauffenberger, M. and Goto, Y. Inhibition of gastric acid secretion by intracerebral injection of calcitonin gene related peptide in rats. *Life Sci.* 35:871-878, 1984.

Taché, Y., Yang, H. and Kaneko, H. Caudal raphe-dorsal vagal complex peptidergic projections: role in gastric vagal control. *Peptides.* 16:431-435, 1995.

Tallaksen-Greene, S.J., Elde, R. and Wessendorf, M. W. Regional distribution of serotonin and substance P co-existing in nerve fibres and terminals in the brainstem of the rat. *Neuroscience.* 53:1127-1142, 1993.

Terenius, L. and Nyberg, F. Peptidases and proteases in cerebrospinal fluid, significance in volume transmission. In: *Volume Transmission in the Brain: Novel Mechanisms for Neural Transmission*, K. Fuxe and L.F. Agnati, Eds., Raven Press, New York, 1991, 415-424.

Thor, K.B. and Helke, C.J. Serotonin and substance P colocalization in medullary projections to the nucleus tractus solitarius: dual-colour immunohistochemistry combined with retrograde tracing. *J. Chem. Neuroanat.* 2:139-148, 1989.

Thor, K.B. and Helke, C.J. Serotonin- and substance P-containing projections to the nucleus tractus solitarii of the rat. *J. Comp. Neurol.* 265:275-293, 1987.

Thor, K.B., Hill, K.M., Harrod, C., Helke, C.J. Immunohistochemical and biochemical analysis of serotonin and substance P colocalization in the nucleus tractus solitarii and associated afferent ganglia of the rat. *Synapse.* 2:225-231, 1988.

Thureson-Klein, A., Klein, R.L. and Zhu, P.C. Exocytosis from large dense cored vesicles as a mechanism for neuropeptide release in the peripheral and central nervous system. *Scan. Electron. Microsc.* Pt 1:179-87, 1986.

Torrealba, F. Calcitonin gene-related peptide immunoreactivity in the nucleus of the tractus solitarius and the carotid receptors of the cat originates from peripheral afferents. *Neuroscience* 47:165-173, 1992.

Trojanowsky, J.Q., Gonatas, J.O. and Gonatas, N.K. Horseradish peroxidase (HRP) conjugates of cholera toxin and lectins are more sensitive retrogradely transported markers than free HRP. *Brain Res.* 231:33-50, 1982.

Trumpp-Kallmeyer, S., Hoflack, J. and Hibert, M. Modeling of G protein-coupled receptors. In: *The Tachykinin Receptors*, S.H. Buck, Ed. Humana Press, Totowa, NJ, 1994, 237-255.

Turner, A.J. Processing and metabolism of neuropeptides. *Ess. Biochem.* 22:69-119, 1986.

Twery, M.J. and Moss, R.L. Calcitonin and calcitonin gene-related peptide alter the excitability of neurons in rat forebrain. *Peptides.* 6:373-378, 1985.

Vigna, S.R., Bowden, J.J., McDonald, D.M., Fisher, J., Okamoto, A., McVey, D.C., Payan, D.G., Bunnett, N.W. Characterization of antibodies to the rat substance P (NK-1) receptor and to a chimeric substance P receptor expressed in mammalian cells. *J. Neuroscience.* 14:834-845, 1994.

Vizi, E.S. In: *Non-Synaptic Interactions Between Neurons: Modulation of Neurochemical Transmission*, E.S. Vizi, Ed., John Wiley and Sons, Chichester, 1984.

Wang, F.B., Holst, M-.C., Powley, T.M. The ratio of pre- to postganglionic neurons and related issues in the autonomic nervous system. *Brain Res. Rev.* 21:93-115, 1995.

Wei, J.Y. and Taché, Y. *Gastroenterol.* 98:A531, 1990.

Wessendorf, M.W. Fluoro-Gold: composition, and mechanism of uptake. *Brain Res.* 553:135-148, 1991.

White, N. Visualization systems for multidimensional CLSM images. In: *Handbook of Biological Confocal Microscopy, 2nd Edition*, J.B. Pawley, Ed., Plenum Press, New York, 1995, 211-254.

Wilson, T. and Sheppard, C.J.R. In: *Theory and Practice of Scanning Optical Microscopy*, Academic Press, London, 1984.

Wood, J.D. Physiology of the enteric nervous system. In: *Physiology of the Gastrointestinal Tract*, L.R. Johnson, Ed., Raven Press, New York, 1981, 67-109.

Yang, H. and Taché, Y. Effect of microinjection of TRH, serotonin (5HT) and substance P analog into the medullary raphe pallidus on gastric acid secretion. *Dig. Dis. Sci.* 37:981, 1992.

Yang, H. Ohning, G. and Taché, Y. TRH in dorsal vagal comples mediates acid response to excitation of raphe pallidus neurons in rats. *Am. J. Physiol.* 265:G880-G886, 1993.

Yoshida, J., Polley, E.H., Nyhus, L.M. and Donahue, P.E. Brain stem topography of vagus nerve to the greater curvature of the stomach. *J. Surg. Res.* 46:60-69, 1989.

Yoshida, J., Polley, E.H., Nyhus, L.M. and Donahue, P.E. Labelling of nerve cells in the dorsal motor nucleus of the vagus of rats by retrograde transport of Fluoro-Gold. *Brain Res.* 455:1-8, 1988a.

Yoshida, J., Polley, E.H., Nyhus, L.M. and Donahue, P.E. Pyloroplasty divides vagus nerve fibers to the greater curvature of the stomach. An axonal tracing study. *Ann. Surg.* 208:708-713, 1988b.

Zhang, X., Fogel, R. and Renehan, W.E. Physiology and morphology of neurons in the dorsal motor nucleus of the vagus and the nucleus of the solitary tract are sensitive to distention of the small intestine. *J. Comp. Neurol.* 323:432-448, 1992.

Zhu, P.C., Thureson-Klein, A. and Klein, R.L. Exocytosis from large dense cored vesicles outside the active synaptic zones of terminals within the trigeminal subnucleus caudalis: a possible mechanism for neuropeptide release. *Neuroscience.* 19:43-54, 1986.

Zoli, M. and Agnati, L.F. Wiring and volume transmission in the central nervous system: the concept of closed and open synapses. *Prog. Neurobiol.* 49:363-380, 1996.

APPENDIX I

Absorption and emission spectra of different fluorophore-conjugated, affinity purified antibodies. These figures demonstrate the relative shape and position of each peak. Peak heights should not be compared quantitatively. The peak absorption/emission is shown in brackets below each fluorophore. FITC = fluorescein isothiocyanate; TXRD = Texas Red. *Source*: **Jackson ImmunoReasearch Laboratories Inc., 1993, 1996.**

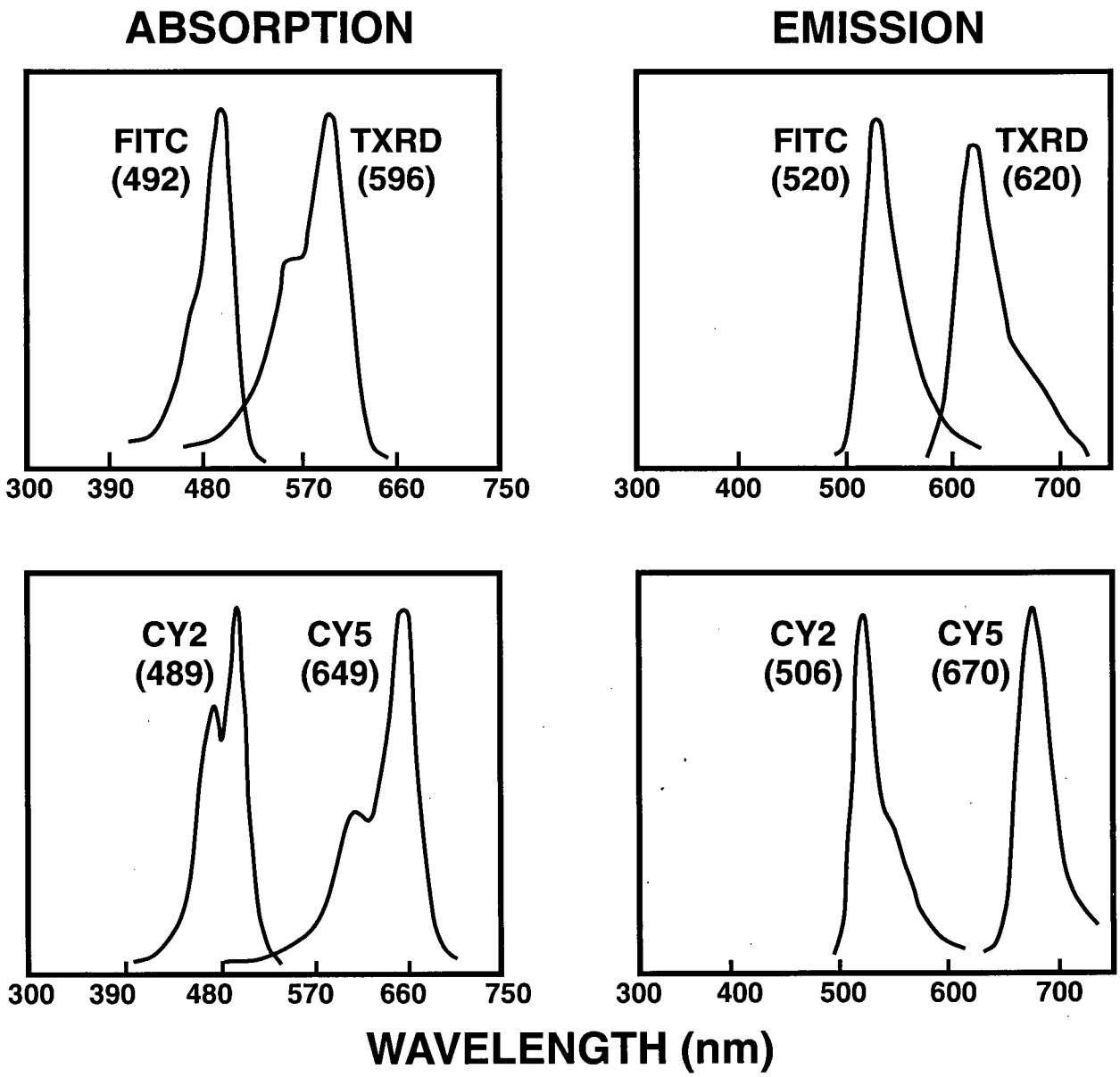

APPENDIX II

The following diagrams depict the spectral characteristics of the filter blocks and light path used with the Bio-Rad MRC 600 Confocal Microscope.
Source: Bio-Rad MRC-600 Confocal Microscope Manual, Bio-Rad Laboratories, Inc., 1993.

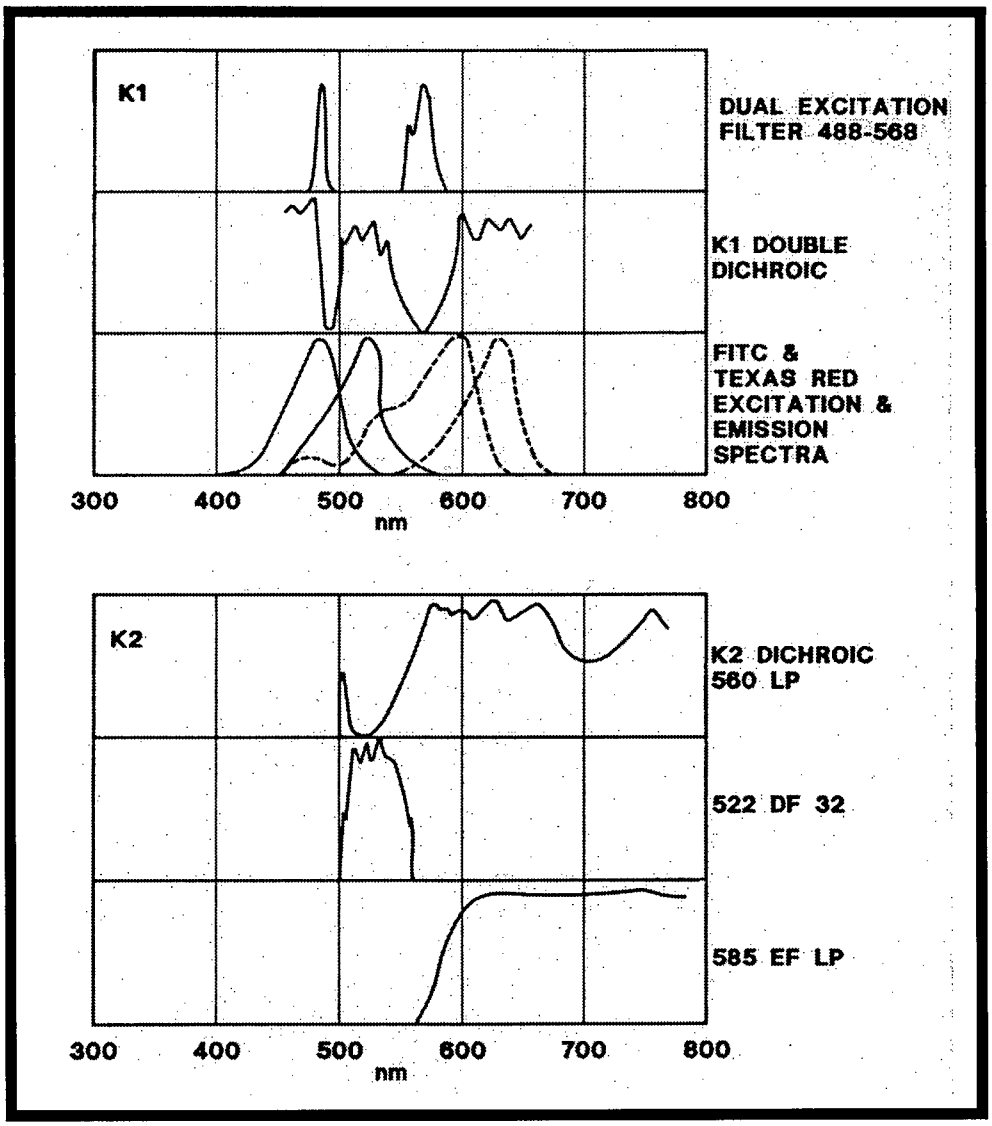

SPECTRA OF COMPONENTS OF FILTER BLOCKS K1 & K2

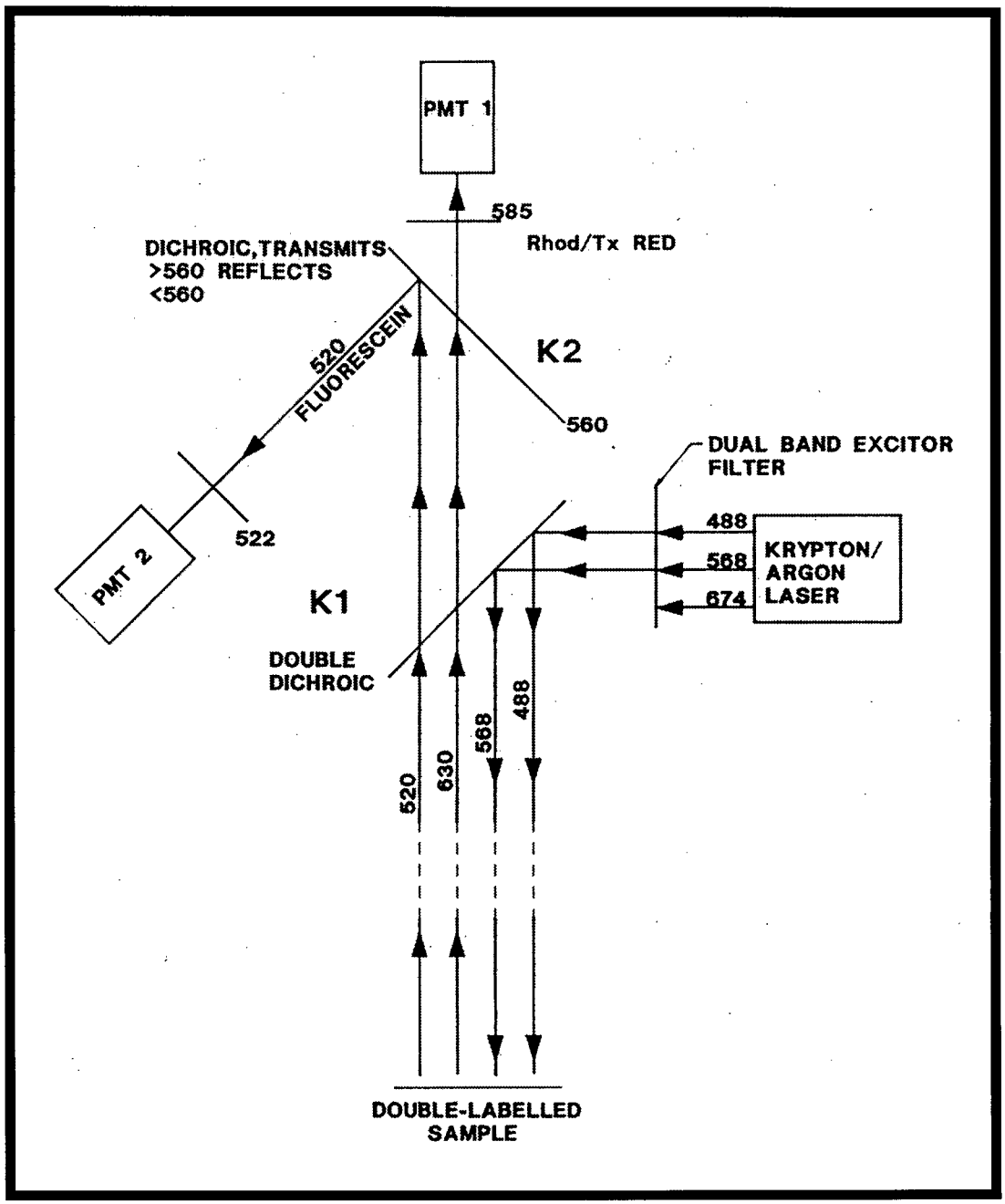

CHARACTERISTICS OF LIGHT PATH USING K1 & K2 BLOCKS

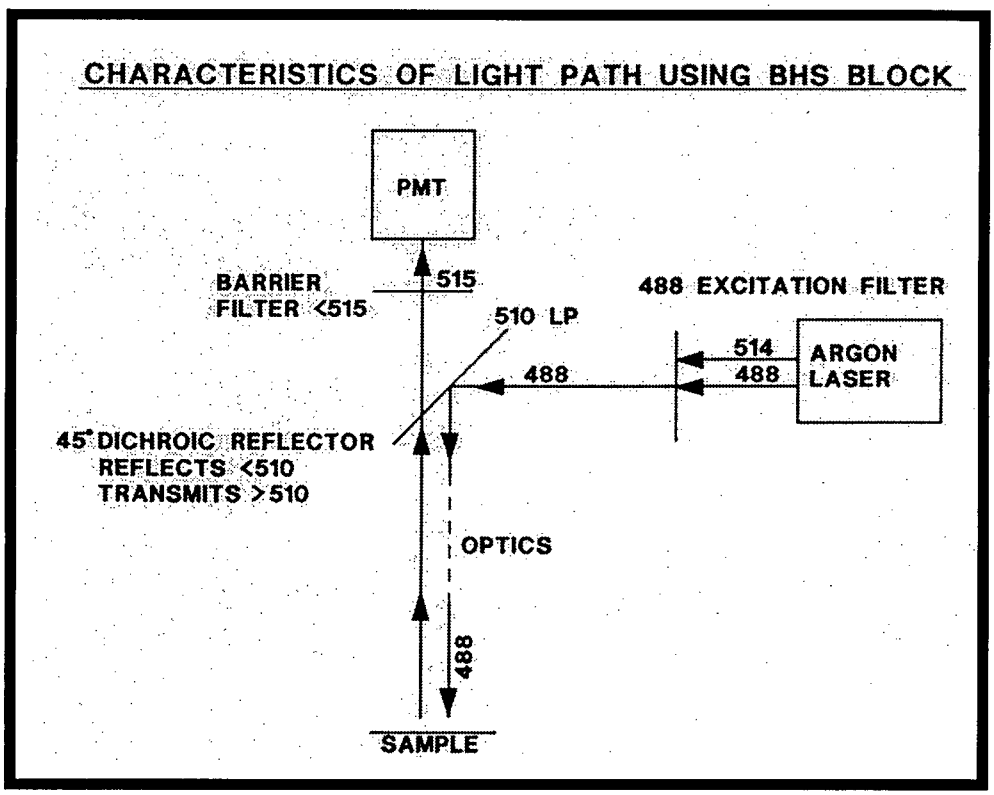
CHARACTERISTICS OF LIGHT PATH USING BHS BLOCK
PMT
BARRIER FILTER <515
515
488 EXCITATION FILTER
510 LP
514
488
ARGON LASER
488
45° DICHROIC REFLECTOR
REFLECTS <510
TRANSMITS >510
OPTICS
488
SAMPLE

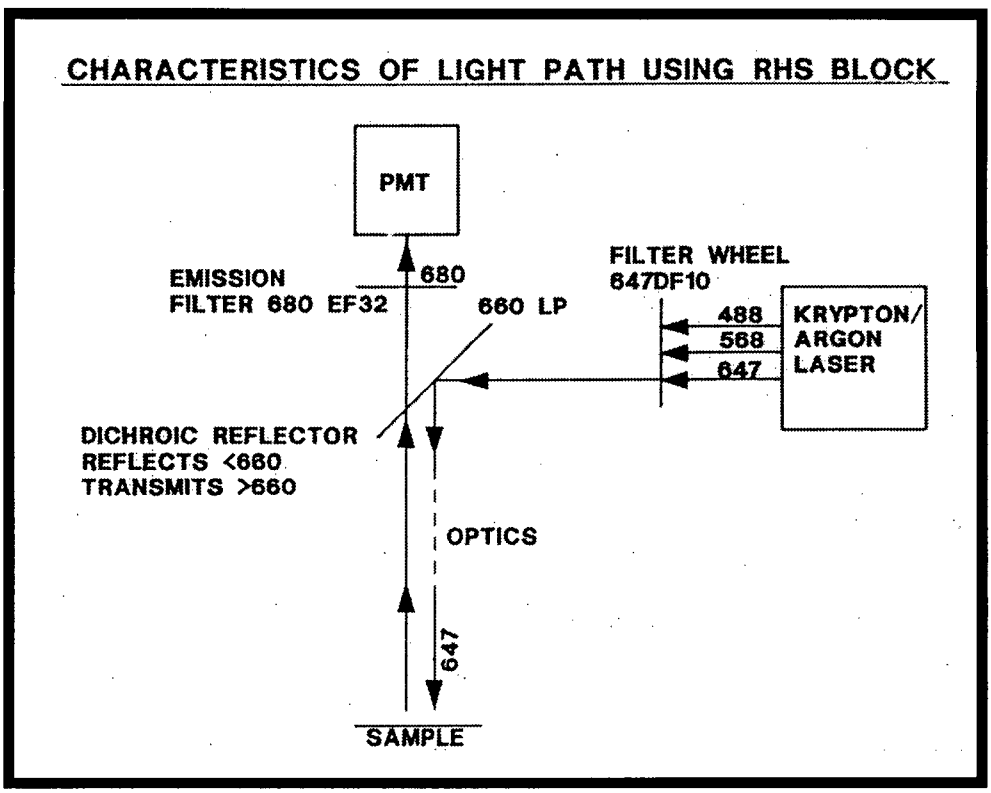
CHARACTERISTICS OF LIGHT PATH USING RHS BLOCK
PMT
EMISSION FILTER 680 EF32
680
FILTER WHEEL 647DF10
660 LP
488
568
647
KRYPTON/ ARGON LASER
DICHROIC REFLECTOR
REFLECTS <660
TRANSMITS >660
OPTICS
647
SAMPLE

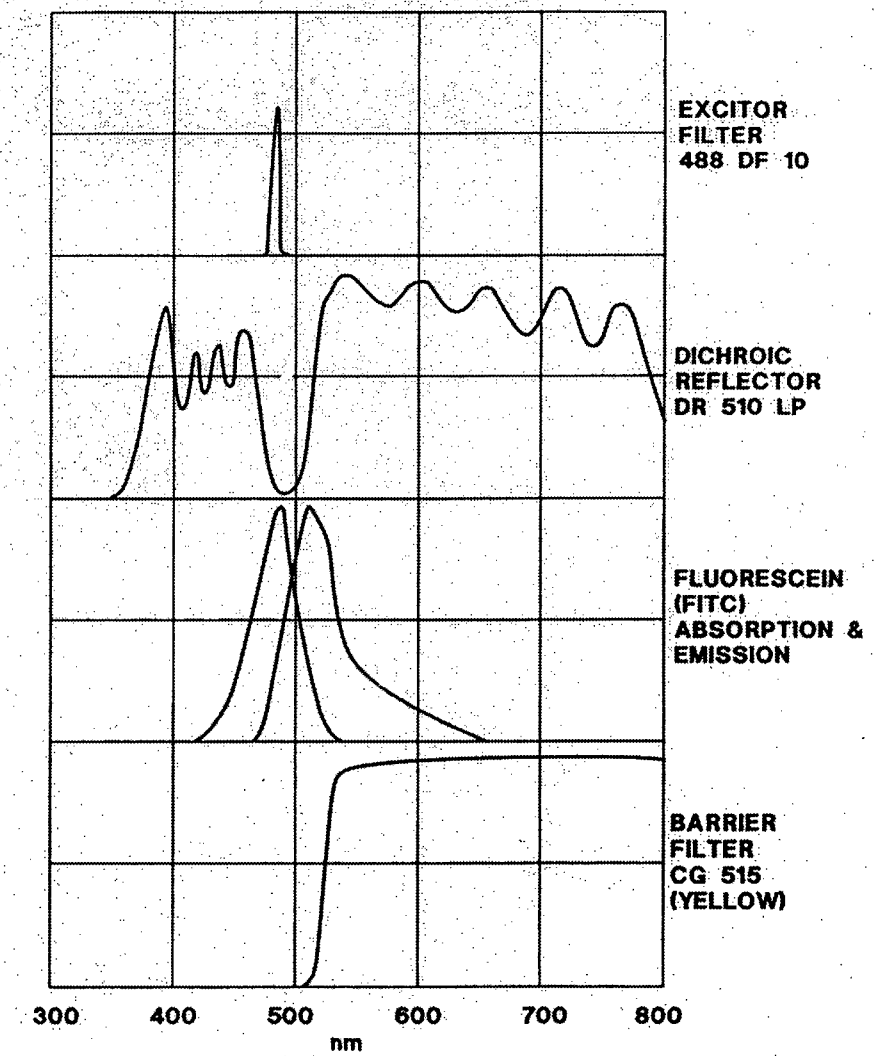

BHS FILTER BLOCK

SPECTRA ARE PLOTTED AS TRANSMISSISION CURVES ON A LINEAR SCALE. FULL SCALE IS 0% TO 100%

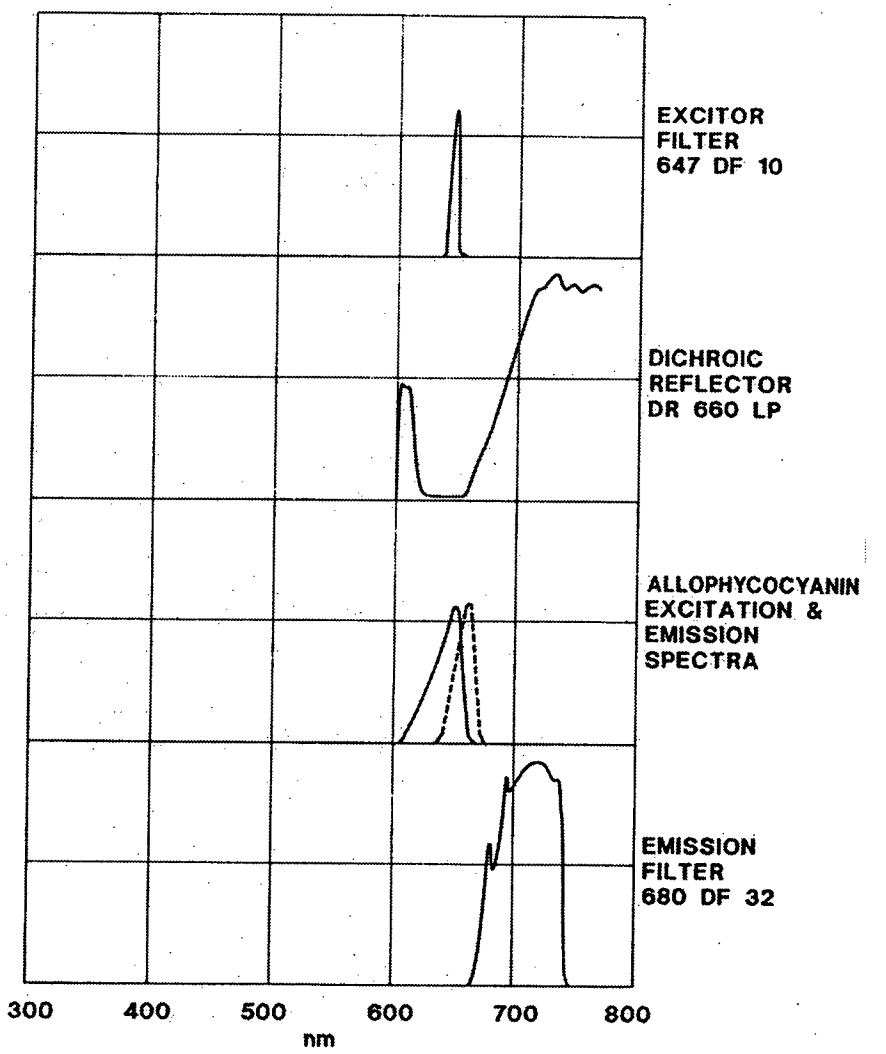

RHS FILTER BLOCK

SPECTRA ARE PLOTTED AS TRANSMISSISION CURVES ON A LINEAR SCALE. FULL SCALE IS 0% TO 100%